

# Distributed Signal Processing for Binaural Hearing Aids

THÈSE N° 4220 (2008)

PRÉSENTÉE LE 31 OCTOBRE 2008

À LA FACULTE INFORMATIQUE ET COMMUNICATIONS  
LABORATOIRE DE COMMUNICATIONS AUDIOVISUELLES 1  
PROGRAMME DOCTORAL EN INFORMATIQUE, COMMUNICATIONS ET INFORMATION

ÉCOLE POLYTECHNIQUE FÉDÉRALE DE LAUSANNE

POUR L'OBTENTION DU GRADE DE DOCTEUR ÈS SCIENCES

PAR

Olivier ROY

ingénieur en systèmes de communication diplômé EPF  
de nationalité suisse et originaire de Epauvillers (JU)

acceptée sur proposition du jury:

Prof. M. Hasler, président du jury  
Prof. M. Vetterli, directeur de thèse  
Prof. D. Jones, rapporteur  
Prof. M. Moonen, rapporteur  
Prof. B. Rimoldi, rapporteur



ÉCOLE POLYTECHNIQUE  
FÉDÉRALE DE LAUSANNE

Suisse  
2008



# Contents

<b>Abstract</b>	<b>v</b>
<b>Résumé</b>	<b>vii</b>
<b>Acknowledgments</b>	<b>ix</b>
<b>Glossary</b>	<b>xi</b>
<b>1 Introduction</b>	<b>1</b>
1.1 A Brief History of Hearing Aids . . . . .	1
1.2 Challenges . . . . .	4
1.3 Motivations . . . . .	5
1.4 Thesis Outline and Contributions . . . . .	6
<b>2 Binaural Noise Reduction as a Source Coding Problem</b>	<b>11</b>
2.1 Introduction . . . . .	11
2.2 Information Sources . . . . .	11
2.3 Centralized Source Coding . . . . .	13
2.3.1 Lossless Case . . . . .	13
2.3.2 Lossy Case . . . . .	14
2.4 Distributed Source Coding . . . . .	19
2.4.1 Lossless Case . . . . .	19
2.4.2 Lossy Case . . . . .	22
2.5 Binaural Hearing Aids . . . . .	26
2.5.1 Problem Statement . . . . .	26
2.5.2 Validity of the Assumptions . . . . .	29
2.6 Summary . . . . .	31
<b>3 Distributed Estimation under Communication Constraints</b>	<b>33</b>
3.1 Introduction . . . . .	33
3.2 Distributed Estimation . . . . .	34
3.2.1 Linear Approximation . . . . .	34
3.2.2 Compression . . . . .	35
3.3 Local Optimality for Memoryless Vector Sources . . . . .	36
3.3.1 Linear Approximation . . . . .	36
3.3.2 Compression . . . . .	38
3.4 Local Optimality for Discrete-Time Sources with Memory . . . . .	41
3.4.1 Linear Approximation . . . . .	41
3.4.2 Compression . . . . .	45

---

3.5	Case Study: First-order Autoregressive Process . . . . .	46
3.5.1	Centralized Scenario . . . . .	47
3.5.2	Perfect Side Information Scenario . . . . .	49
3.5.3	Partial Observation Scenario . . . . .	50
3.5.4	General Scenario . . . . .	52
3.6	Summary . . . . .	55
3.A	Proofs . . . . .	57
<b>4</b>	<b>Gain-rate Optimality</b>	<b>71</b>
4.1	Introduction . . . . .	71
4.2	Coding Strategies . . . . .	71
4.2.1	Side Information Aware Coding . . . . .	72
4.2.2	Side Information Unaware Coding . . . . .	73
4.3	Monaural Gain-rate Trade-offs . . . . .	74
4.4	Binaural Gain-rate Trade-offs . . . . .	78
4.5	Simulation Results . . . . .	83
4.5.1	Setup . . . . .	83
4.5.2	Coding Strategies . . . . .	84
4.5.3	Spatial Extent . . . . .	86
4.5.4	Rate Allocation . . . . .	86
4.6	Summary . . . . .	87
4.A	Proofs . . . . .	89
<b>5</b>	<b>Multichannel Filtering in the Weighted Overlap-Add Domain</b>	<b>91</b>
5.1	Introduction . . . . .	91
5.2	Monaural Filtering . . . . .	91
5.2.1	Processing Architecture . . . . .	92
5.2.2	Frame-Based Optimality Criterion . . . . .	97
5.2.3	Suboptimal Strategies . . . . .	100
5.2.4	Recursive Algorithms . . . . .	103
5.2.5	Practical Considerations . . . . .	105
5.3	Binaural Filtering . . . . .	108
5.3.1	Processing Architecture . . . . .	108
5.3.2	Binaural Optimality . . . . .	110
5.3.3	Practical Considerations . . . . .	111
5.4	Simulation Results . . . . .	112
5.4.1	Annihilating Power . . . . .	113
5.4.2	Signal-to-Noise Ratio Improvement and Speech Distortion . . . . .	114
5.5	Summary . . . . .	114
<b>6</b>	<b>Distributed Source Coding of Binaural Innovation</b>	<b>119</b>
6.1	Introduction . . . . .	119
6.2	Model Based on Auditory Cues . . . . .	119
6.2.1	Model Description . . . . .	119
6.2.2	Distributed Source Coding of Binaural Cues . . . . .	121
6.3	Model Based on Sparsity Principles . . . . .	124
6.3.1	Model Description . . . . .	124
6.3.2	Distributed Source Coding of the Binaural Filter . . . . .	124
6.3.3	Robustness to Model Mismatch . . . . .	126
6.4	Application: Distributed Spatial Audio Coding . . . . .	128

<b>Contents</b>	<b>iii</b>
<hr/>	
6.4.1 Model Based on Auditory Cues . . . . .	129
6.4.2 Model Based on Sparsity Principles . . . . .	131
6.5 Summary . . . . .	131
<b>7 Conclusions</b>	<b>135</b>
7.1 Thesis Summary . . . . .	135
7.2 Future Research . . . . .	136
<b>A Weighted Mean Squared Linear Estimation</b>	<b>139</b>
A.1 General Transform Matrix . . . . .	139
A.2 Diagonal Transform Matrix . . . . .	142
<b>Bibliography</b>	<b>143</b>
<b>Curriculum Vitae</b>	<b>155</b>



# Abstract

Over the last centuries, hearing aids have evolved from crude and bulky horn-shaped instruments to lightweight and almost invisible digital signal processing devices. While most of the research has focused on the design of monaural apparatus, the use of a wireless link has been recently advocated to enable data transfer between hearing aids such as to obtain a binaural system. The availability of a wireless link offers brand new perspectives but also poses great technical challenges. It requires the design of novel signal processing schemes that address the restricted communication bitrates, processing delays and power consumption limitations imposed by wireless hearing aids.

The goal of this dissertation is to address these issues at both a theoretical and a practical level. We start by taking a distributed source coding view on the problem of binaural noise reduction. The proposed analysis allows deriving mean square optimal coding strategies, and to quantify the noise reduction enabled by a wireless link as a function of the communication bitrate. The problem of rate allocation between the hearing aids is also studied. In a more general setting, these findings are used to design algorithms for distributed estimation in sensor networks, under both a linear approximation and a compression constraint. The potential of our approach in this context is illustrated by means of a simple case study based on a first-order autoregressive model. Two important practical aspects of binaural noise reduction are then investigated. The first issue pertains to multichannel filtering in the transformed domain using a weighted overlap-add filter bank. We propose three subband filtering strategies together with recursive algorithms for the computation of the filter coefficients. Some numerical methods to reduce their computational complexity are also discussed. The second problem concerns the estimation of binaural characteristics using the wireless link. These characteristics are modeled in two different ways. The first approach is based on binaural cues. A source coding method to estimate these cues in a distributed fashion is proposed. It takes advantage of the particularities of the recording setup to reduce the transmission bitrate. The second approach involves a filter that is sparse in the time domain. This sparsity allows for the design of a novel distributed scheme based on annihilating filters. Finally, application of these methods to the distributed coding of spatial audio is presented.

**Keywords:** binaural hearing aids, distributed source coding, wireless communication link.





# Résumé

Durant les dernières décennies, les aides auditives ont évolué de manière significative, passant d'instruments en forme de cor, à la fois rudimentaires et volumineux, à des appareils de traitement numérique du signal légers et quasi invisibles. Alors que la majeure partie de la recherche s'est focalisée sur la conception de dispositifs monauraux, l'utilisation d'un lien de communication sans fil a récemment été préconisée afin de permettre la transmission de données entre aides auditives et ainsi d'obtenir un système binaural. L'accès à la technologie sans fil offre de nouvelles perspectives mais pose également d'énormes défis techniques. Elle nécessite le développement de nouvelles méthodes de traitement du signal qui prennent en compte les limites imposées par les aides auditives sans fil en termes de débits de communication, de délais de traitement et de consommation énergétique.

L'objectif de cette thèse est d'aborder ces problèmes sous un angle théorique et pratique. Nous considérons, en premier lieu, le problème de la réduction de bruit binaurale en adoptant un point de vue de codage source distribué. Notre analyse permet d'obtenir des stratégies de codage optimales au sens des moindres carrés, et de quantifier la réduction de bruit obtenue grâce à un lien sans fil en fonction du débit de communication. Le problème de l'allocation du débit entre les deux aides auditives est également étudié. Plus généralement, ces résultats nous permettent de concevoir des algorithmes d'estimation distribués pour des réseaux de capteurs, en considérant une contrainte de communication basée soit sur l'approximation linéaire, soit sur la compression. Dans ce contexte, le potentiel de notre approche est mis en évidence par une étude de cas simple basée sur un modèle autorégressif du premier ordre. Deux aspects importants de la réduction de bruit binaurale sont ensuite considérés. Le premier problème est lié au filtrage multicanal dans le domaine transformé en utilisant un banc de filtres de type addition-recouvrement pondéré. Nous proposons trois stratégies de filtrage sous-bandes ainsi que des algorithmes récursifs pour le calcul des coefficients de filtre. Quelques méthodes numériques permettant d'en réduire leur complexité sont également discutées. Le deuxième sujet d'investigation concerne l'estimation de caractéristiques binaurales à l'aide du lien de communication sans fil. Ces caractéristiques sont modélisées de deux manières différentes. La première est basée sur l'utilisation de repères binauraux. Une technique de codage source pour estimer ces repères de manière distribuée est proposée. Elle exploite les particularités du système d'acquisition de manière à réduire le débit de transmission. La seconde approche comprend un filtre parcimonieux dans le domaine temporel. Cette parcimonie permet la conception d'un nouvel algorithme distribué basé sur l'utilisation de filtres

---

annihilant. Finalement, l'application de ces méthodes au codage distribué de contenu audio spatial est présentée.

**Mots clés:** aides auditives binaurales, codage source distribué, lien de communication sans fil.

# Acknowledgments

It has been a pleasure to work with Prof. Martin Vetterli. I have always felt very lucky and proud to have an advisor like Martin. His extraordinary human qualities, endless enthusiasm and great sense of humour made these few research years both enjoyable and fun. Martin is a great teacher and an outstanding scientist with a broad knowledge of many research fields. I have been particularly impressed by his faculty to state problems in such a way that they capture the big picture, while remaining simple enough to be analytically tractable. Martin, thanks for your scientific guidance and for making my graduate studies a memorable experience.

It was an honor to have as thesis committee members, Prof. Martin Hasler, Prof. Douglas L. Jones, Prof. Marc Moonen and Prof. Bixio Rimoldi. I would like to thank them for accepting to read this thesis and for providing valuable comments.

An important acknowledgment goes to Prof. Emre Telatar for the interesting discussions we have had throughout the past few years, either in Lausanne, or in some of Barcelona's best restaurants.

I am grateful to Dr. Peter Derleth and Dr. Sascha Korl for giving me the opportunity to do a summer internship at Phonak, and for supervising me during this period. This experience in industry was invaluable as it provided me with a better understanding of the processing constraints of digital hearing aids.

My thanks also go to Jocelyne Plantefol and Jacqueline Aeberhard for administrating the lab in such a professional manner, as well as to Simon Hiscox for taking care of the computer infrastructure.

Several colleagues and friends have also contributed to this work. In particular, I would like to thank Andrea, Christof, Florence, Luciano, Michael, Patrick, Thibaut and Yue for enlightening interactions. A special thanks to my officemate Bob for our technical discussions and, above all, for the nights spent clubbing in Lausanne, Fribourg and Florence, enjoying the sweet taste of a "White Russian". A big thank you to Ali for all the laughs we shared, and for our fruitful collaboration, together with Yue, on the distributed sensing project.

I would also like to thank my friends Jeanne, Damien and Sanjay, for all the great time we had, whether in Switzerland or on trips abroad, and for their subtle way to make me understand that signal processing is not necessarily a topic covered at primary school.

A very special thanks to Ivana, who has accompanied me through all the ups and downs of research, always providing me with a listening ear. Ivana,

thank you for all the beautiful moments we have spent together, which have made these last few years so special to me.

Last but not least, I am grateful to my parents Janine and Yvan, as well as to my brother Nicolas, for their love and unconditional support in all my endeavors.

# Glossary

## Mathematical Notation

### Variables & Operators

$a$	scalar $a$
$\mathbf{a}$	vector $\mathbf{a}$
$\mathbf{A}$	matrix $\mathbf{A}$ or discrete Fourier transform of vector $\mathbf{a}$
$a[n], \mathbf{a}[n], \mathbf{A}[n]$	discrete-time scalar, vector, matrix sequence
$\mathbf{a}^N$	vector with elements $a[0], a[1], \dots, a[N-1]$
$\hat{a}, \hat{\mathbf{a}}, \hat{\mathbf{A}}$	reconstructed value of scalar $a$ , vector $\mathbf{a}$ , matrix $\mathbf{A}$
$a^s, \mathbf{a}^s, \mathbf{A}^s$	speech component of scalar $a$ , vector $\mathbf{a}$ , matrix $\mathbf{A}$
$a^n, \mathbf{a}^n, \mathbf{A}^n$	noise component of scalar $a$ , vector $\mathbf{a}$ , matrix $\mathbf{A}$
$A(\omega), \mathbf{A}(\omega)$	discrete-time Fourier transform of scalar sequence $a[n]$ , of vector sequence $\mathbf{a}[n]$
$\mathcal{A}$	set $\mathcal{A}$
$\mathcal{A}^N$	$N$ -fold Cartesian product of set $\mathcal{A}$
$\angle a$	phase of scalar $a$
$ a $	modulus of scalar $a$
$a^*$	complex conjugate of scalar $a$
$\lfloor a \rfloor$	largest integer smaller than or equal to (real) scalar $a$
$\lceil a \rceil$	smallest integer greater than or equal to (real) scalar $a$
$\mathbf{A}^T$	transpose of matrix $\mathbf{A}$
$\mathbf{A}^H$	Hermitian transpose of matrix $\mathbf{A}$
$\mathbf{A}^{-1}$	inverse of matrix $\mathbf{A}$
$\mathbf{A}^\dagger$	pseudoinverse of matrix $\mathbf{A}$
$\text{tr}(\mathbf{A})$	trace of matrix $\mathbf{A}$
$\det(\mathbf{A})$	determinant of matrix $\mathbf{A}$
$\ \mathbf{A}\ $	Frobenius norm of matrix $\mathbf{A}$
$\mathcal{A}_0$	interior set of set $\mathcal{A}$
$\mathcal{A}^c$	complementary set of set $\mathcal{A}$
$1_{\mathcal{A}}(x)$	indicator function on set $\mathcal{A}$

---

$p_a(x)$	probability distribution of random variable $a$
$P_a(\omega)$	power spectral density of discrete-time sequence $a[n]$
$P_{ab}(\omega)$	cross power spectral density between $a[n]$ and $b[n]$
$P_{a b}(\omega)$	power spectral density of the prediction error of $a[n]$ using $b[n]$
$\mathbf{C}_a$	circulant matrix with vector $\mathbf{a}$ as first column
$\mathbf{D}_a$ or $\text{diag}(\mathbf{a})$	diagonal matrix with vector $\mathbf{a}$ as diagonal elements
$\mathbf{R}_a$	covariance matrix of random vector $\mathbf{a}$
$\mathbf{R}_{ab}$	cross covariance matrix between $\mathbf{a}$ and $\mathbf{b}$
$\mathbf{R}_{a b}$	covariance matrix of the prediction error of $\mathbf{a}$ using $\mathbf{b}$
$\mathbf{T}_N(P)$	Toeplitz matrix of size $N \times N$ generated from power spectral density $P(\omega)$
$\Phi_a(\omega)$	power spectral density matrix of discrete-time vector sequence $\mathbf{a}[n]$
$\Phi_{ab}(\omega)$	cross power spectral density matrix between $\mathbf{a}[n]$ and $\mathbf{b}[n]$
$\Phi_{a b}(\omega)$	power spectral density matrix of the prediction error of $\mathbf{a}[n]$ using $\mathbf{b}[n]$
$\mathcal{E}\{\cdot\}, \mathcal{E}\{\cdot \cdot\}$	expectation, conditional expectation
$H(\cdot), H(\cdot \cdot)$	entropy, conditional entropy
$I(\cdot, \cdot), I(\cdot, \cdot \cdot)$	mutual information, conditional mutual information
$\odot$	element-wise product
$\otimes$	Kronecker product
$*$	convolution
$\circledast$	circular convolution
$\times$	Cartesian product
$\approx$	approximately equal

## Symbols

$c$	speed of sound
$d(x, \hat{x})$	distortion function
$e[n]$	discrete-time error sequence
$f$	frequency
$f_s$	sampling frequency
$f_M$	encoding function
$g_M$	decoding function
$j$	imaginary unit
$k$	frequency bin index ( $k = 0, 1, \dots, K - 1$ )
$m$	frame index ( $m = 0, 1, \dots, M - 1$ )
$n$	time sample index ( $n = 0, 1, \dots, N - 1$ )
$D$	distortion
$R$	rate

---

<b>F</b>	discrete Fourier transform matrix
$\mathbf{I}_N$	identity matrix of size $N \times N$
$\mathbf{O}_{M \times N}$	all-zero matrix of size $M \times N$
<b>W</b>	filter weight matrix
$T_{60}$	reverberation time
$T_\lambda$	time-averaging constant
$\alpha$	fraction of retained transformed coefficients
$\gamma$	signal-to-noise ratio
$\delta[n]$	Dirac impulse
$\eta$	weight update step size
$\theta$	reverse “water-filling” parameter
$\lambda$	exponential forgetting factor
$\lambda_n$	$n$ th eigenvalue
$\mu$	speech distortion parameter
$\rho$	correlation parameter
$\sigma$	standard deviation
$\omega$	normalized frequency
$\mathbb{C}$	set of complex numbers
$\mathbb{R}$	set of real numbers
$\mathcal{B}$	frequency band
$\mathcal{O}(N)$	order $N$
$\mathcal{R}$	rate region
$\mathcal{S}$	source alphabet
$\mathcal{T}$	description alphabet
$\mathcal{X}$	observation alphabet

## Abbreviations & Acronyms

e.g.	exempli gratia (for example)
et al.	et alia (and others)
i.e.	id est (that is)
i.i.d.	independent and identically distributed
s.t.	subject to
DFT	discrete Fourier transform
ERB	equivalent rectangular bandwidth
HRIR	head-related impulse response
HRTF	head-related transfer function
ICLD	inter channel level difference
ICTD	inter channel time difference
KLT	Karhunen-Loève transform
MSE	mean squared error

---

MWF	multichannel Wiener filter
SIA	side information aware
SIU	side information unaware
SNR	signal-to-noise ratio
WOLA	weighted overlap-add



# Chapter 1

## Introduction

### 1.1 A Brief History of Hearing Aids

Hearing aids have a long history, starting from large, horn-shaped devices to lightweight and almost invisible digital signal processing instruments. The following is a brief account of this rich history. For a more in-depth coverage of the subject, the interested reader is referred to [10, 11, 120] and to the excellent online resources [26, 119].

More than three centuries ago, ear trumpets, such as elongated tubes with funnel-shaped end (see Figure 1.1(a)), were used to direct the sound into the ear to provide basic passive sound amplification. These instruments were useful to sailors to communicate over long distances. Eventually, they would help people afflicted with hearing loss. Such devices were commented on in the work of Francis Bacon published in 1627 [5], but versions of the ear trumpet have most likely been used by humans for thousands of years. These instruments were heavy, cumbersome and might have been more useful for self-defense than to really improve hearing quality. While these ear trumpets would gradually taper into thin tubes and possibly be made less conspicuous by means of ingenious camouflages (see Figure 1.2), their functionality would essentially remain the same.

It is only starting from the late 19th century that the development of modern hearing aid technology has been made possible thanks to two major technical breakthroughs: the electrical amplification system used in Alexander Graham Bell's telephone invented in 1876 [9], and the invention of the "carbon-transmitter" by Thomas Alva Edison in 1878 [41], which allows translating sound into electric signals. The carbon-transmitter was the basis for the first commercial hearing aid produced by the Dictograph Company in 1898. A year later, the Akouphone Company manufactured what may be the first electrical hearing device. It used a carbon microphone and a battery and was as large as a desk radio.

At the turn of the 20th century, smaller body-worn electrical hearing aids were produced. These early models basically worked as ear trumpets but provided a wider frequency range. In the meanwhile, a few hearing aids company were established in Europe and in the United States. Oticon of Danemark, in 1904, and the Global Ear-Phone Company of Boston, in 1907, are two exam-

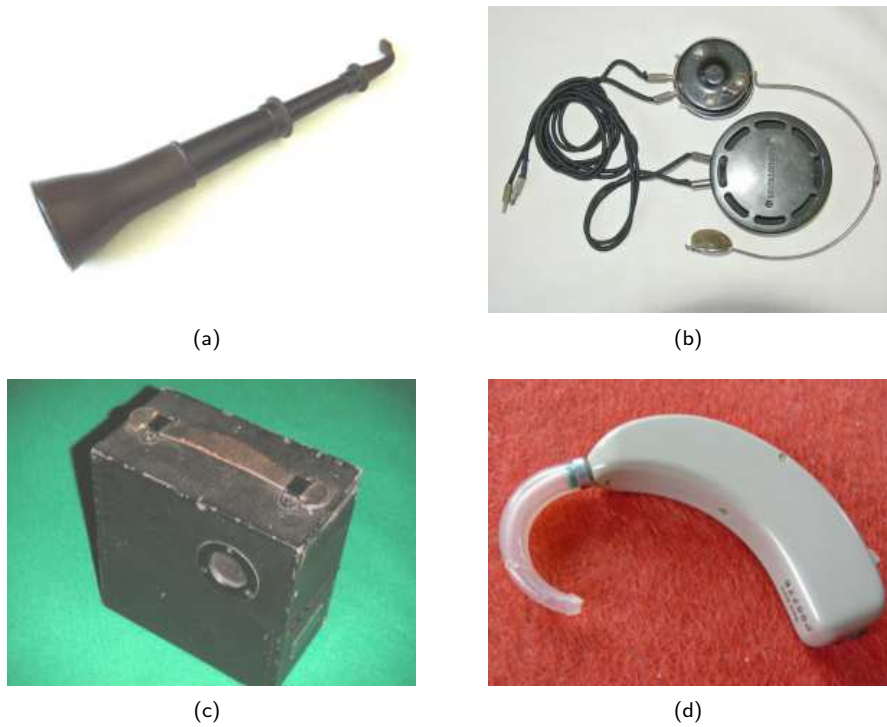


**Figure 1.1:** Hearing aids through the 19th and 20th centuries. (a) Acoustic era: hard rubber ear trumpet. (b) Carbon transmitter era: the Acousticon Model A. (c) Vacuum tube era: the Vactuphone. (d) Transistor era: a behind-the-ear hearing aid.

Source: <http://www.hearingaidmuseum.com>. Copyright: the Hugh Hetherington On-line Hearing Aid Museum. Used by permission.

ples. This latter introduced the first volume control, for an electrical hearing aid, in 1912. In 1920, Earl Charles Hansen invented the “Vactuphone” [64] (see Figure 1.1(c)), the first hearing aid that incorporated the use of vacuum tubes. It was manufactured by the Western Electric Company and distributed by the Global Ear-Phone Company in 1921. While amplification efficiency was greatly improved, this hearing instrument was far too unwieldy to be carried around easily. In this context, the miniaturization of batteries and vacuum tubes played an important role in making these devices portable. In the mid 1930’s, the first wearable vacuum tube hearing aids were produced in England. Similar models were then released in the United States, first using vacuum tubes imported from Europe, then using U.S.-made vacuum tubes, for which the Raytheon Company was the predominant supplier.

In 1947, the advent of the transistor, invented at the Bell Telephone Laboratories by William Shockley, John Bardeen and Walter Brattain [6, 125], marked a clear departure from technologies based on vacuum tubes. In the early 1950’s, transistors started to replace vacuum tubes in hearing aids. Their smaller size and lower energy requirement allowed for a dramatic miniaturization in hearing

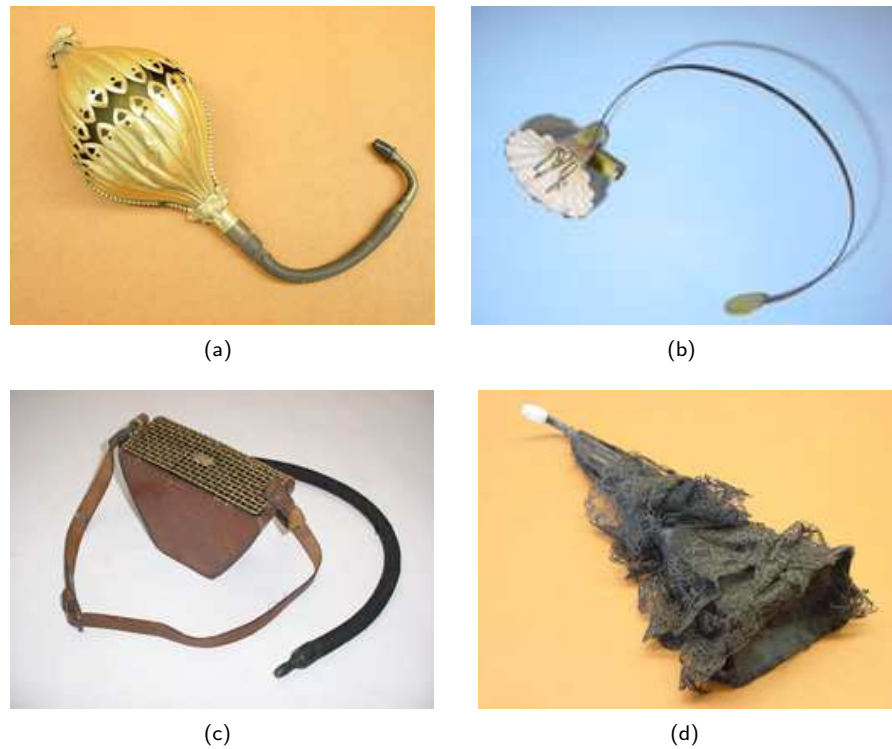


**Figure 1.2:** Deafness in disguise: concealed devices of the 19th century. (a) The bouquet holder. (b) The floral Aurolese phone. (c) The ear trumpet disguised as a water canteen. (d) The mourning ear trumpet.

Source: <http://beckerexhibits.wustl1.edu/did>. Copyright: Bernard Becker Medical Library. Used by permission.

devices and permitted novel styles of hearing aids to be developed, such as the behind-the-ear model still used today (see Figure 1.1(d)). In 1952, Sonotone released the first hybrid hearing aids that included both transistors and vacuum tubes. One year later, the first all-transistor hearing aid was introduced by Microtone. Within months, vacuum tube hearing aids became obsolete. Transistors were further miniaturized which ultimately yielded the first integrated circuit, developed in 1958 by Jack St. Clair Kilby of Texas Instruments [83]. By the end of the 1960's, hearing aids included integrated circuits and additional features, such as directional microphones. Forerunners of today's radio-based assistive listening device (e.g., remote microphone) started to appear. Smaller microphones and receivers along with the invention of the zinc-air battery, in 1977, propelled the development of in-the-ear hearing aids.

During the 1980's, the hearing devices started to go digital. The first experimental form of digital hearing aid was made by Audiotone in 1983. The same year, in-the-canal hearing aids were introduced. In 1987, digitally programmable devices hit the market. Some of them also featured a user-operated remote control to program and adjust the instrument. In the early 1990's,

---

the use of microprocessors in hearing aids allowed to incorporate digital signal processing algorithms, such as feedback suppression. In 1993, completely-in-the-canal hearing devices were introduced and the first fully digital hearing aid was commercialized by Widex in 1996. One year later, Siemens released the first dual microphone hearing instrument.

The last decade has witnessed the replacement of the analog technology by its digital counterpart in almost all hearing aid fittings. Innovations in the field of digital signal processing have permitted to significantly improve speech intelligibility in adverse listening scenarios by means of dynamic compression techniques, scene classification methods, feedback cancellation algorithms and noise reduction schemes. The use of wireless technologies (e.g., FM, Bluetooth) has allowed to connect hearing aids with remote assistive listening devices (e.g., lecturer's microphone) or customary electronic devices (e.g., cell phones, televisions) such as to provide audio signals subject to less interferences.

## 1.2 Challenges

Despite the significant progress achieved during the 19th and 20th centuries, correcting hearing loss using hearing aids remains a challenging task. While the present work is concerned about technological aspects, it is important to put the engineering perspective into a broader context and to look at the associated challenges.

From a *sociological standpoint*, first, major efforts have to be made to promote the availability and use of hearing aids by hearing impaired people. According to the United Nations World Health Organization's estimation for 2005 [150], approximately 278 million people suffer from a moderate to profound hearing loss in both ears. Among them, only 10% benefit from a hearing device. This gap is even more apparent in developing countries, where fewer than 1 in 40 people has a needed hearing aid. This is of significant concern as hearing impairment is a serious disability that can impose a heavy social and economic burden on individuals and families. Children with hearing impairment often experience delayed development of speech, language and cognitive skills, and adults have difficulties to obtain, perform and keep employment. As a result, both children and adults may suffer from social stigmatization and isolation. While hearing impairment may be significantly reduced by means of appropriate preventive measures [38], availability of affordable, suitable and properly fitted hearing aids must also be encouraged. Beyond the financial aspect, the stigma associated with the wearing of hearing instruments may preclude the necessary commitment of customers to use their hearing aids. Making hearing instruments fashionable will thus play a pivotal role in improving the quality of lives for millions of people who have access to the technology, but are ashamed to use it.

From a *fitting perspective*, then, the methodology must be improved. In fact, hearing aids are not as easily adaptable by an audiologist as glasses are by an optician. They need to be programmed according to the user's hearing characteristics, which are often difficult to measure with precision despite many advanced fitting protocols [24, 27, 96]. While fitting software and tools have been developed in order to increase the patient satisfaction, the rates of hearing instrument returns has not lowered significantly over the past few years [76].

---

Hearing devices are also more complicated to use, especially for the elderly. It is interesting, but somewhat disappointing, to observe that, while engineers strive to solve difficult problems in the most innovative way, their efforts are made useless by a consumer that simply forgets to change the batteries of his or her hearing device. Therefore, successful hearing aid fitting will only be guaranteed through the establishment of a more collaborative process between the involved parties, namely, the manufacturer, the audiologist and the consumer.

From a *technical point of view*, finally, the development of improved hearing aids requires innovation in a number of engineering fields. Progress has to be made in electronics to address low power requirements as well as the limited space available for chip area. Typically, current hearing aids consume less than 1 mA, operate at 1 V and use less than 10 mm<sup>2</sup> of silicon area. Components that are more energy efficient must thus be devised. As power consumption is probably the most limiting factor, longer lasting batteries have to be developed, while keeping their size to a bare minimum [103]. In particular, rechargeable batteries should be drastically improved in order to be viable for hearing aid applications. The choice of the materials composing the hearing device is also crucial. For example, ear molds in behind-the-ear hearing aids should be flexible enough while ensuring robustness, excellent acoustic sealing properties and bio-compatibility with patients that suffer from allergy or sensitivity problems [105]. The hearing aid body should also be made of a material that reduces the problem of acoustic feedback, which occurs when the amplified loudspeaker signal recycles into the microphones and provokes a strident whistling that is particularly unpleasant. Digital signal processing, on which the interest of this thesis is focused, is another important field of investigation [62]. For example, the problem of acoustic feedback mentioned previously cannot be solved completely using appropriate ear molds. This is even more true with open ear fittings, namely fittings that do not completely block the ear canal. Acoustic feedback thus also needs to be addressed from an algorithmic standpoint [47, 80, 94, 129]. Making feedback cancellation algorithms work under rapidly changing conditions is a challenging task which requires further research efforts. More efficient algorithms must also be designed to improve speech intelligibility in adverse listening scenarios. This can be achieved, for example, using advanced multi-band compression strategies that allow adapting the output signal to the user's dynamic range of hearing [81, 128]. Speech understanding can also be improved by means of noise reduction schemes, possibly using multiple microphone inputs [34, 36, 42, 75, 89, 92, 138]. These methods often require knowledge about the spatio-temporal characteristics of the acoustic environment (e.g., localization of sources, detection of speech and noise periods) and thus entail the use of reliable auditory scene analysis algorithms [21, 23]. All the aforementioned problems are particularly challenging considering the stringent processing delay requirements imposed by digital hearing aids, typically around 15 ms with closed ear fittings [132] and 5 ms with open ear fittings [133].

### 1.3 Motivations

During the past few decades, most of the research has focused on *monaural* hearing aids. One historical reason is that, before the availability of behind-

the-ear hearing aids, it was simply not convenient to wear two hearing devices. As hearing instruments became less bulky, *bilateral* hearing aids gained in popularity, despite the fact that there was little objective evidence attesting to the superiority of bilateral versus monaural amplification. In fact, this question remains rather controversial [67, 86, 137]. A major issue is that, in a bilateral fitting, the two hearing aids work independently of each other, each introducing its own processing delay, using its own compression method and having independent noise reduction schemes [137]. In other words, there is a lack of synchronization.

Recently, the use of a wireless link between the two devices has been advocated to allow information sharing in order to form a *binaural* system [17]. The availability of a wireless communication link offers brand new perspectives but also poses great technical challenges. At the simplest level, it allows synchronizing hearing aid controls (e.g., volume) and to transmit useful parameters as a means to coordinate processing strategies at both hearing aids [44]. At a more advanced level, increased data rates (of the order of tens of kilobits per second) permit the exchange of coded audio signals. In terms of noise reduction, this collaborative mechanism has the potential to offer substantial improvements over monaural noise reduction schemes. In fact, limited by obvious design considerations, each hearing aid is generally equipped with only two or three closely separated microphones (typically 1 cm apart). This restriction will be even more apparent in the future as miniaturization plays an important role in the acceptance of such devices by hearing impaired people. To overcome this limitation, a substantial body of research has focused on the development of larger microphone arrays [82], possibly mounted on glasses [91], or in the shape of a necklace [87, 146, 147]. However, these designs are cumbersome and, in light of the stigma associated with the wearing of hearing aids, are unlikely to be widely accepted. By contrast, a wireless link allows using the microphones directly available at both hearing aids to form a microphone array with larger spatial extent. Various binaural noise reduction schemes have been proposed in the literature [31, 35, 85, 145]. Moreover, strategies that reduce the number of transmitted signals have been investigated to address the bandwidth limitation of the wireless link [37]. However, the rate-constrained nature of the communication medium has, to the best of our knowledge, never been taken into account in previous studies.

The driving motivation behind our work is to address such wireless transmission constraints, at both a *theoretical* and a *practical* level. From a theoretical standpoint, we wish to study the fundamental trade-off between the communication bitrate and the associated noise reduction gain. From a practical perspective, our goal is to design signal processing methods and coding schemes that take into account the characteristics of the setup and the processing limitations imposed by digital hearing aids.

## 1.4 Thesis Outline and Contributions

We first give a quick overview of the structure of the dissertation. Chapter 2 reviews some background material and states the problem of noise reduction with binaural hearing aids. Chapters 3 and 4 investigate the problem from an information-theoretic standpoint. This theoretical analysis suggests that

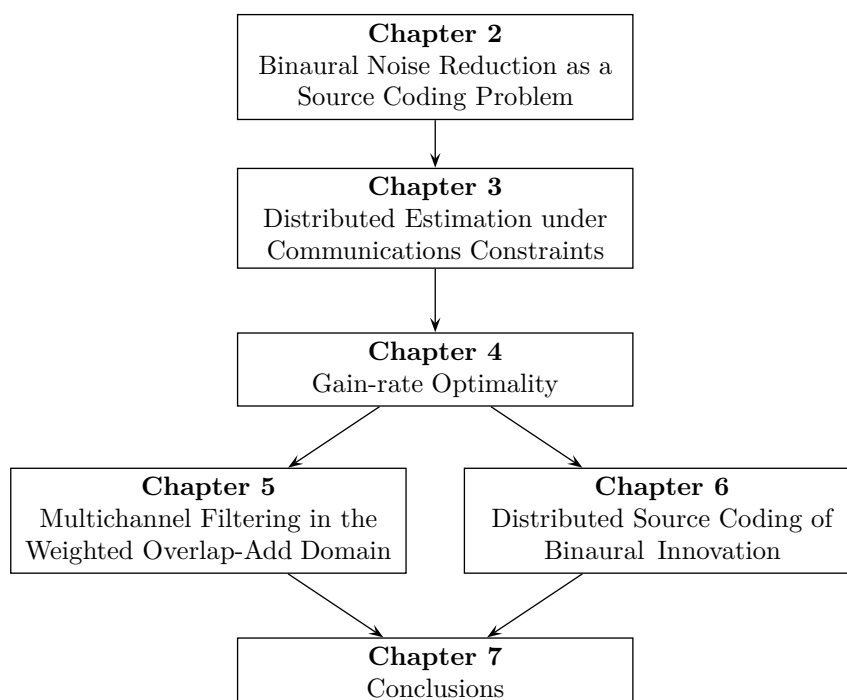


**Figure 1.3:** Schematic overview of the thesis.

two main types of problems should be addressed from a practical viewpoint: multichannel filtering and distributed source coding of binaural content. These two subjects are investigated in Chapters 5 and 6, respectively. Chapter 7 concludes the dissertation. A schematic overview of the thesis is depicted in Figure 1.3.

Let us now describe the content of the thesis in more detail. In **Chapter 2**, we identify the problem of noise reduction with binaural hearing aids as a distributed source coding task. More precisely, we show that it corresponds to a remote source coding problem with side information at the decoder. A large portion of the exposition is thus devoted to the review of fundamental results in lossless and lossy source coding, in both a centralized and a distributed setup. First, we recall the concept of information source. We then state Shannon's fundamental theorem of lossless data compression<sup>1</sup>. Lossy source coding is reviewed and the concept of rate-distortion function is presented. A particular emphasis is put on the remote source coding problem, in which the source of interest is not directly observed at the encoder. Our attention then shifts to distributed infrastructures, studied in the seminal work of Slepian and Wolf, and Wyner and Ziv. We provide a review of both theoretical and practical distributed source coding results in order to put our contribution into perspec-

<sup>1</sup>Throughout this discussion, the term compression is used as a synonym to source coding. It should not be mistaken with hearing aid compression techniques, mentioned above, which merely adjust frequency powers to match the user's dynamic range of hearing.

---

tive. Again, a distinction between direct and remote source coding is made. We then formally state the problem of noise reduction with binaural hearing aids. We describe the considered distortion criteria and comment on their practical relevance. More specifically, we discuss the effect of the chosen error measures on important perceptual characteristics of binaural hearing. We also argue about the feasibility of distributed source coding in the context of binaural hearing aids. In particular, we comment on some strong assumptions pertaining to the knowledge of signal statistics, as well as processing complexity and coding delays.

The theoretical results needed to study the problem under consideration are derived in **Chapter 3**. Actually, we investigate a more general setup of distributed estimation under communication constraints. It involves a set of terminals (or sensors) observing jointly Gaussian processes correlated with a remote source of interest. These terminals provide a fusion center with a representation of their observation. Based on the received data, the fusion center estimates the desired source with minimum mean squared error. We first address the case of random vector processes. Two types of communication constraints are considered: *linear approximation* and *compression*. In the former case, each terminal provides the fusion center with a low-dimensional approximation of its vector observation by means of a linear transform. In the latter scenario, each sensor generates a bit stream that appears at a prescribed communication rate. In both cases, the goal is to find mean square optimal processing strategies. While the associated optimization problems appear to be analytically intractable, we derive locally optimal solutions at one terminal assuming all else is fixed. We demonstrate that, similarly to the centralized scenario, the locally optimal compression architecture can be given a transform coding interpretation using the corresponding locally optimal linear transform. Based on these constructions, we propose iterative algorithms which are proved to converge to local optimums that are either local minimums or saddle points of the overall cost functions. The possible suboptimality of the proposed schemes is exemplified with a simple correlation model. Similar optimality results are then obtained for discrete-time random processes by letting the size of the input vectors go to infinity. In particular, we derive the locally optimal trade-off between the distortion and the fraction of retained coefficients (linear approximation), and that between the distortion and the communication bitrate (compression). The associated optimal processing architectures are also described. Finally, we show through a simple case study, how our findings allow for the computation of analytical distortion formulas, in both the linear approximation and compression frameworks. We consider a first-order autoregressive correlation model and derive optimal trade-offs for various limiting scenarios of practical interest.

The aim of **Chapter 4** is to apply the obtained results to the study of binaural hearing aids. We first rewrite the optimal rate-distortion trade-off derived in Chapter 3 using a weighted mean squared error criterion. This allows for the use of perceptually motivated weighting operators. As the optimal processing strategy involves statistics which might be difficult to compute in a practical setting, we also consider a suboptimal scheme where the encoder neglects the presence of correlated side information at the decoder. These two coding methods are respectively referred to as *side information aware* and



---

*side information unaware*. For these strategies, we compute optimal trade-offs between the bitrate sustainable by the wireless link and the resulting noise reduction gain. In order to derive analytical formulas, we consider a simplified, yet insightful, acoustic scenario. We first address the problem from the perspective of one hearing device (monaural setup). We compute analytical gain-rate functions and comment on the optimal allocation of the bitrate across the frequency band. We then consider bi-directional communication between the hearing instruments (binaural setup) and compute similar gain-rate trade-offs. More importantly, we provide the exact characterization of the rate allocation between the two hearing aids. Finally, we present simulation results obtained from real measurements recorded in a reverberant room using a two-microphone behind-the-ear hearing aid. These results are compared with the simple model considered previously. In particular, it is shown that the loss associated with side information unaware coding strategies vanishes in the presence of multiple interfering point sources.

The processing architectures described in Chapter 4 involves a mean square optimal multichannel filter. For complexity reasons, filtering is often performed in the frequency domain. The goal of **Chapter 5** is to study the optimality of multichannel filtering in the transformed domain using a weighted overlap-add filter bank. This filter bank is particularly appealing from a computational point of view and is thus often considered in practice. Similarly to Chapter 4, we address the problem from both a monaural and a binaural perspective. We first describe the monaural filtering architecture and define the associated frame-based optimality criterion. The corresponding optimization problem is deemed intractable due to the strong interdependency introduced by the filter bank between consecutive frames. We thus resort to three suboptimal strategies, respectively referred to as *non-weighted*, *weighted* and *iterative*, for which conclusive results can be found. We derive associated recursive algorithms for the computation of the weights. Practical considerations are then discussed, in particular related to the complexity of the proposed filtering methods. We then turn our attention to the problem of binaural filtering. The corresponding processing architecture is explained and binaural optimality is discussed, for both the side information aware and the side information unaware strategies. We also comment on important practical considerations associated with the use of a wireless link in this context. Finally, some simulations results comparing the proposed filtering schemes are presented.

The exchange of data over a wireless communication link allows the hearing aids to estimate important binaural characteristics which can be subsequently used, for example, in scene analysis algorithms. In **Chapter 6**, these characteristics are modeled in two different ways. The first approach involves auditory cues. Our goal is to estimate these cues in a distributed fashion while keeping the amount of transmitted data at a bare minimum. To this end, we propose a distributed source coding scheme that benefits from the correlation induced by the recording setup to achieve low bitrates, while keeping complexity and delay at an affordable level. Under some assumptions, we prove its optimality by comparing it to the case where the binaural signals could be processed jointly. In the second strategy, binaural characteristics are modeled using a sparse filtering operation. We propose a source coding method to estimate this filter in a distributed manner. The proposed scheme builds upon the recent concept of

---

compressive sampling and involves the use of annihilating filters. It has a reasonable complexity and can be made robust to noise and model mismatch. The details of the method are described and its reconstruction accuracy is assessed in a simple scenario. Finally, we show how the above techniques can be applied to the distributed coding of spatial audio. We propose two algorithms and evaluate their accuracy through information listening experiments. We discuss the strengths of our approach in this context together with its limitations.

**Chapter 7** concludes the dissertation and suggests further directions of research.

## Chapter 2

# Binaural Noise Reduction as a Source Coding Problem

### 2.1 Introduction

This chapter serves two purposes: reviewing the theory of distributed source coding and identifying the problem of binaural noise reduction as a distributed source coding task.

Section 2.2 first recalls the concept of information sources introduced by Shannon in its landmark paper on communication theory [123]. We then provide an overview of the main results of centralized and distributed source coding as they pertain to both fundamental performance bounds and practical algorithms. In the *centralized* case, studied in Section 2.3, the source is measured at a single encoder. By contrast, the *distributed* case, investigated in Section 2.4, involves multiple encoders each observing a part of the source. In these two scenarios, we address both *lossless* and *lossy* source coding. In the former, the goal is to retrieve the original source perfectly while, in the latter, reconstruction is achieved only to within some accuracy. In the lossy case, we further make a distinction between *direct* and *remote* problems, depending whether the source can be directly observed at the encoder(s) or only through noisy measurements. In all the above scenarios, a particular emphasis is put on the Gaussian case, for which analytical formulas can be derived. In Section 2.5, we describe the setup of binaural hearing aids. The binaural noise reduction problem is then formally stated by identifying it as a distributed source coding task. We then examine the underlying assumptions and discuss their validity in a practical setting. In particular, we comment on the relevance of the chosen distortion criterion as well as some assumptions that relate to coding delay and processing complexity. Section 2.6 provides some concluding remarks.

### 2.2 Information Sources

A source of information can be modeled as a random process, that is, a sequence of random variables taking values in a set  $\mathcal{S}$ . The source is said to be *continuous-time* if the parameter used to index this sequence can take any

possible real value. If the parameter only takes discrete values, we speak about a *discrete-time* source. Similarly, we distinguish between a *discrete-amplitude* (or simply *discrete*) source and a *continuous-amplitude* (or simply *continuous*) source depending whether the set  $\mathcal{S}$  is countable or not. Finally, we speak about a *memoryless* source if the random variables are independent and identically distributed (i.i.d.). Otherwise, the source is said to have *memory*. Note that we use the same notation to denote deterministic and random quantities. Their nature should be clear from the context. Moreover, bandlimited continuous-time sources can be equivalently represented by discrete-time sequences of uniformly spaced samples, by invoking the sampling theorem [102, Sec. 3.2]. We will thus work exclusively in the discrete-time domain.

In the memoryless case, the source is completely described by the distribution of one of its samples. We denote this random variable by  $s$  and its distribution by  $p_s(u)$ . If the set  $\mathcal{S}$  is countable, the *entropy* of the random variable  $s$  is defined as [29, Sec. 2.1]

$$H(s) = - \sum_{u \in \mathcal{S}} p_s(u) \log_2 p_s(u) .$$

The base of the logarithm can be chosen according to the desired unit. The entropy is usually computed in nats (base  $e$ ) or in bits (base 2). Throughout this thesis, we will use bits as a measure of information. The entropy can be interpreted as a measure of uncertainty of the random variable  $s$ . Similarly, the *joint entropy* of two random variables  $s_1$  and  $s_2$  taking values in the finite sets  $\mathcal{S}_1$  and  $\mathcal{S}_2$ , respectively, is defined as [29, Sec. 2.2]

$$H(s_1, s_2) = - \sum_{u_1 \in \mathcal{S}_1} \sum_{u_2 \in \mathcal{S}_2} p_{s_1, s_2}(u_1, u_2) \log_2 p_{s_1, s_2}(u_1, u_2) ,$$

where  $p_{s_1, s_2}(u_1, u_2)$  denotes the joint distribution. The *conditional entropy* of the random variable  $s_1$  given  $s_2$  is defined as

$$H(s_1|s_2) = - \sum_{u_1 \in \mathcal{S}_1} \sum_{u_2 \in \mathcal{S}_2} p_{s_1|s_2}(u_1|u_2) \log_2 p_{s_1|s_2}(u_1|u_2) ,$$

where  $p_{s_1|s_2}(u_1|u_2)$  denotes the conditional distribution. The conditional entropy is a measure of the uncertainty of  $s_1$  provided that  $s_2$  is available. Therefore, it is natural to compute the reduction in uncertainty of the random variable  $s_1$  due to  $s_2$ . This quantity is referred to as *mutual information* and is defined as [29, Sec. 2.3]

$$I(s_1; s_2) = H(s_1) - H(s_1|s_2) = \sum_{u_1 \in \mathcal{S}_1} \sum_{u_2 \in \mathcal{S}_2} p_{s_1, s_2}(u_1, u_2) \log_2 \frac{p_{s_1, s_2}(u_1, u_2)}{p_{s_1}(u_1) p_{s_2}(u_2)} .$$

Properties of the above quantities and variations thereof can be found in [29, Chap. 2]. For continuous-amplitude memoryless sources, similar definitions can be stated using the concept of differential entropy [29, Chap. 9].

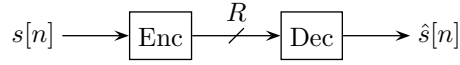


Figure 2.1: The centralized source coding problem.

## 2.3 Centralized Source Coding

### 2.3.1 Lossless Case

As depicted in Figure 2.1, the lossless source coding problem for the source  $s[n]$  consists of an encoder, which maps a vector of  $M$  consecutive samples to one of a finite set of possible messages, and a decoder, that reconstructs the input vector based on the chosen message. More specifically, the encoder maps the input vector  $\mathbf{s}^M \in \mathcal{S}^M$ , defined as

$$\mathbf{s}^M = [s[0], s[1], \dots, s[M-1]]^T,$$

to a description  $T_M \in \mathcal{T}_M$  by means of an *encoding function*

$$f_M : \mathcal{S}^M \rightarrow \mathcal{T}_M,$$

where  $\mathcal{T}_M = \{1, 2, \dots, 2^{MR}\}$  and  $\mathcal{S}^M$  denotes the  $M$ -fold Cartesian product of the set  $\mathcal{S}$ . In the above notation, the superscript  $T$  denotes the transpose operation. The message  $T_M$  can hence be described using  $R$  bits per sample. Based on  $T_M$ , the decoder reconstructs the vector  $\hat{\mathbf{s}}^M \in \hat{\mathcal{S}}^M$ , defined as

$$\hat{\mathbf{s}}^M = [\hat{s}[0], \hat{s}[1], \dots, \hat{s}[M-1]]^T,$$

by means of a *decoding function*

$$g_M : \mathcal{T}_M \rightarrow \hat{\mathcal{S}}^M.$$

The reconstructed value follows as

$$\hat{\mathbf{s}}^M = g_M (f_M (\mathbf{s}^M)).$$

The design of a lossless source code thus amounts to choosing encoding and decoding functions that allow for the perfect reconstruction of the source. More precisely, a lossless source code with parameters  $(M, R, \delta)$  consists of an encoding function  $f_M : \mathcal{S}^M \rightarrow \mathcal{T}_M$  and a decoding function  $g_M : \mathcal{T}_M \rightarrow \hat{\mathcal{S}}^M$  such that

$$P(\mathbf{s}^M \neq g_M (f_M (\mathbf{s}^M))) \leq \delta, \quad (2.1)$$

where  $\mathcal{T}_M = \{1, 2, \dots, 2^{MR}\}$ . It thus guarantees perfect reconstruction with a probability larger than  $1 - \delta$ . An important problem is the determination of the achievable rates with lossless source codes. A rate  $R$  is said to be *achievable* if the probability of error (2.1) can be made arbitrarily small as  $M$  tends to infinity. More formally, for any  $\delta > 0$ , there must exist an integer  $M_0$  such that, for all  $M \geq M_0$ , we can build a lossless source code with parameters

$(M, R_M, \delta)$  satisfying  $R_M \leq R + \delta$ . The central result of lossless source coding is the characterization of the set of achievable rates and is given by the following theorem.

**Theorem 2.1.** Given a discrete memoryless source  $s[n]$ , the rate  $R$  is achievable without loss if  $R > H(s)$ . Conversely,  $R < H(s)$  is not achievable without loss.

A rate  $R$  equal to the entropy (and not only arbitrarily close) may be achieved in some special cases, but not always. Note that Theorem 2.1 still holds for sources with memory that are ergodic. In this case, the entropy rate must be considered in lieu of the entropy [29, Sec. 4.2]. Theorem 2.1 was obtained by Shannon for memoryless sources and Markov sources [123]. A proof of the general case can be found in [63].

The above definition of achievable rate does not impose any complexity or delay constraints on the chosen coding method. A lossless source code that approaches the lower bound given by Theorem 2.1 may thus be computationally prohibitive. Moreover, it assumes that the encoder has access to the entire source sequence and knows its distribution. Nevertheless, the above theorem remains of great practical relevance as it allows benchmarking the compression efficiency of implementable methods. From a practical standpoint, a large number of lossless source coding schemes have been proposed, including Huffman codes [72], Golomb codes [53], arithmetic codes [110] and Lempel-Ziv codes [88, 144].

### 2.3.2 Lossy Case

In most scenarios of practical interest, the source is a real-valued physical quantity (e.g., audio signals) and cannot be perfectly described by a finite number of bits. Instead, the available bitrate is used to provide a description of the source to within the minimum possible *average* distortion. The distortion is measured using a distortion function

$$d : \mathcal{S} \times \hat{\mathcal{S}} \rightarrow [0, \infty),$$

namely, a mapping which assigns a non-negative real number to each pair formed by a sample and its reconstruction. The notation  $\times$  stands for the Cartesian product. The choice of a distortion function depends on the application at hand, but should provide an acceptable trade-off between model accuracy and mathematical tractability. Given a source  $s[n]$ , a lossy source code with parameters  $(M, R, D)$  is defined as an encoding function  $f_M : \mathcal{S}^M \rightarrow \mathcal{T}_M$  and a decoding function  $g_M : \mathcal{T}_M \rightarrow \hat{\mathcal{S}}^M$  such that

$$\frac{1}{M} \sum_{m=0}^{M-1} \mathcal{E} \{d(s[m], \hat{s}[m])\} \leq D,$$

where  $\mathcal{T}_M = \{1, 2, \dots, 2^{MR}\}$  and  $\hat{s}[m]$  is the  $m$ th element of the reconstructed vector

$$\hat{\mathbf{s}}^M = g_M (f_M (\mathbf{s}^M)).$$

The notation  $\mathcal{E} \{ \cdot \}$  stands for the expectation operator. With the above definition, a rate  $R$  is said to be *achievable* with distortion  $D$  if the rate-distortion

pair  $(R, D)$  can be approached arbitrarily closely using lossy source codes. More formally, for all  $\delta > 0$ , there must exist an integer  $M_0$ , such that for all  $M \geq M_0$ , we can design a lossy source code with parameters  $(M, R_M, D_M)$  satisfying  $R_M \leq R + \delta$  and  $D_M \leq D + \delta$ . The fundamental problem is the determination of the set of achievable rates for a given distortion. For memoryless sources, it is given by the following result.

**Theorem 2.2.** Given a memoryless source  $s[n]$  and a distortion measure  $d : \mathcal{S} \times \hat{\mathcal{S}} \rightarrow [0, \infty)$ , a rate  $R$  is achievable with distortion  $D$  if  $R > R(D)$ , where

$$R(D) = \min_{p_{s|\hat{s}}(\hat{u}|u): \mathcal{E}\{d(s, \hat{s})\} \leq D} I(s; \hat{s}) .$$

Conversely,  $R < R(D)$  is not achievable with distortion  $D$ .

The function  $R(D)$  characterizes the optimal trade-off between rate and distortion for a memoryless source and is referred to as the *rate-distortion function*. This trade-off can be equivalently expressed by a *distortion-rate function*  $D(R)$ . While the literature has mostly adopted the former formulation, the latter is more relevant from a practical point of view, since a communication system is constrained in terms of rate and not in terms of distortion. This discussion is mostly concerned with the mean squared error (MSE) distortion, that is,  $d(s, \hat{s}) = |s - \hat{s}|^2$ . Unless otherwise stated, the rate-distortion functions are expressed in terms of this criterion and are referred to as *quadratic rate-distortion functions*.

From a practical perspective, the encoding of a scalar source can be split into a quantizer followed by an entropy coder (e.g., Huffman). For complexity reasons, quantization and entropy coding is usually performed on a sample-by-sample basis. This incurs a loss compared to the rate-distortion function obtained by assuming that all the source samples can be processed jointly. For a discussion on optimality in this context, we refer to the exposition in [54].

The computation of the rate-distortion function using Theorem 2.2 involves an optimization problem which can only be solved for specific distributions and distortion measures. The most prominent example is that of a memoryless Gaussian source and a MSE distortion. In this case, the rate-distortion function evaluates as follows [29, Th. 13.3.2].

**Theorem 2.3.** The quadratic rate-distortion function of a memoryless Gaussian source with mean zero and variance  $\sigma^2$  is given by

$$R(D) = \max \left\{ \frac{1}{2} \log_2 \frac{\sigma^2}{D}, 0 \right\} ,$$

where  $R(D)$  is expressed in bits per sample.

Figure 2.2 plots the rate-distortion function obtained for different values of  $\sigma$ . When the minimization task in Theorem 2.2 cannot be solved analytically, numerical optimization methods, such as the Blahut-Arimoto algorithm [3, 15], can be used.

Theorem 2.2 applies to memoryless sources. To compute optimal rate-distortion trade-offs for sources with memory, one can use the vector extension of the rate-distortion function of Theorem 2.2 and consider the limit, as the

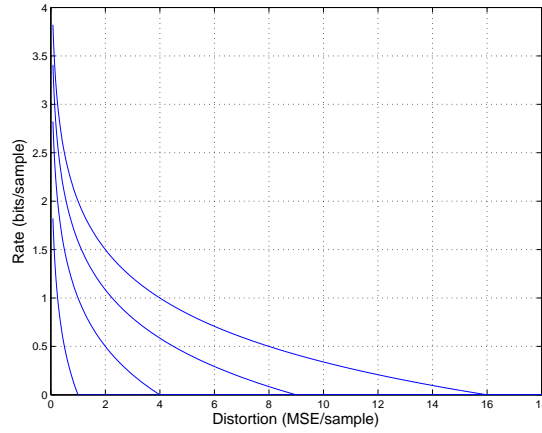


**Figure 2.2:** Quadratic rate-distortion function of a memoryless Gaussian source with mean zero and variance  $\sigma^2$ . The different curves correspond to  $\sigma = 1, 2, 3, 4$  (left to right).

size  $N$  of the vectors goes to infinity. For general sources, this task is difficult and one must resort to bounds (see, e.g., [12, Th. 4.3.3]). For the Gaussian scenario considered previously, however, conclusive results can be found. Let us first compute the quadratic rate-distortion function for a memoryless Gaussian vector source. It is given by the following theorem [29, Th. 13.3.3].

**Theorem 2.4.** The quadratic rate-distortion function of a memoryless source of Gaussian vectors of size  $N$  with mean zero and covariance matrix  $\mathbf{R} \in \mathbb{R}^{N \times N}$  is given by

$$D_N(\theta) = \sum_{k=1}^N \min\{\theta, \lambda_k\},$$

$$R_N(\theta) = \sum_{k=1}^N \max\left\{0, \frac{1}{2} \log_2 \frac{\lambda_k}{\theta}\right\},$$

with  $\theta \in (0, \max_k \lambda_k]$ , where  $\lambda_k$  denote the eigenvalues of the matrix  $\mathbf{R}$ .  $R_N(\theta)$  is expressed in bits per vector and  $D_N(\theta)$  in MSE per vector.

The above rate-distortion function corresponds to that of  $N$  independent Gaussian sources with variances  $\lambda_k$  ( $k = 1, 2, \dots, N$ ). It can be checked that an optimal architecture amounts to decorrelating the Gaussian vectors, and to code each transformed component sequence independently. This process is commonly referred to as *transform coding* [54]. The rate allocation across components is obtained by means of a reverse “water-filling” strategy, as illustrated in Figure 2.3. In this case, the decorrelating transform is known as the Karhunen-Loève transform (KLT) [79], or Hotelling transform [70]. In other words, the KLT diagonalizes the covariance matrix. Moreover, by only keeping the  $K$  transform coefficients with largest variance, we obtain the optimal linear estimate of the vector  $\mathbf{s}$  in a subspace of dimension  $K$  [73, Sec. 6.1.2]. This approximation method is usually referred to as principal component analysis



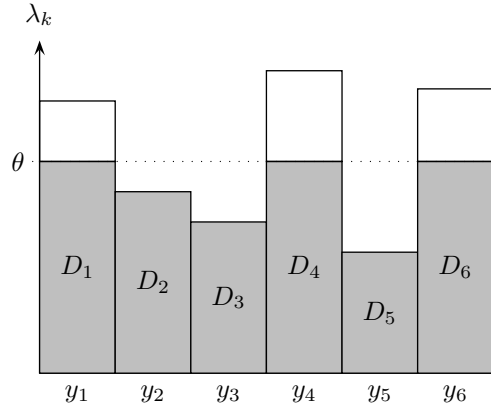


**Figure 2.3:** Illustration of the reverse water-filling rate allocation strategy [29, Fig. 13.7]. A vector of size  $N = 6$  is considered. We encode the transformed coefficients  $y_k$  whose variance  $\lambda_k$  is above the threshold  $\theta$  ( $k = 1, 2, \dots, 6$ ). The other components are discarded. The total distortion corresponds to the shaded area.

(PCA) [104]. The KLT is thus also the optimal transform in this linear approximation framework. In Chapter 3, we show that a similar optimality result holds in a distributed infrastructure. From a practical standpoint, the transform coding approach is appealing in that it allows reducing a vector source coding problem to  $N$  independent scalar source coding tasks. Variations on this model have also been considered (see, e.g., [55]).

Based on the above result, the rate-distortion function for a source with memory can be derived as

$$D(\theta) = \lim_{N \rightarrow \infty} \frac{1}{N} D_N(\theta), \quad (2.2)$$

$$R(\theta) = \lim_{N \rightarrow \infty} \frac{1}{N} R_N(\theta), \quad (2.3)$$

provided that the above limits exist. For a general source, the limits (2.2) and (2.3) are difficult to compute. However, for a (wide-sense) stationary Gaussian source with mean zero and a power spectral density  $P(\omega)$ , they can be computed using the Toeplitz distribution theorem of Grenander and Szegő [61, Sec. 5.2] (see also [58, 59]). The result is given in the form of the following theorem [12, Th. 4.5.3].

**Theorem 2.5.** The quadratic rate-distortion function of a stationary Gaussian source with mean zero and power spectral density  $P(\omega)$  is given by

$$D(\theta) = \frac{1}{2\pi} \int_0^{2\pi} \min\{\theta, P(\omega)\} d\omega,$$

$$R(\theta) = \frac{1}{4\pi} \int_0^{2\pi} \max\left\{0, \log_2 \frac{P(\omega)}{\theta}\right\} d\omega,$$

with  $\theta \in (0, \text{ess sup}_\omega P(\omega)]$ .  $R(\theta)$  is expressed in bits per sample and  $D(\theta)$  in

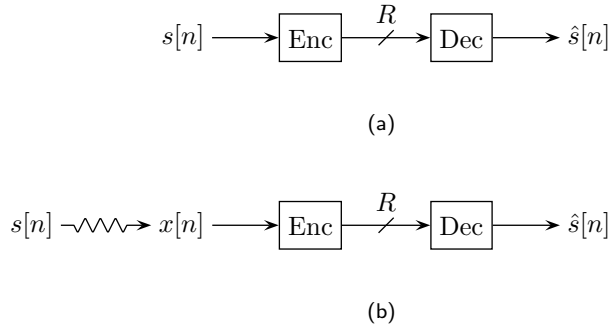


**Figure 2.4:** Direct and remote source coding. (a) The source of interest  $s[n]$  is directly observed at the encoder. (b) Only a noisy version  $x[n]$  of the source is available at the encoder.

MSE per sample.

In the above theorem,  $\text{ess sup}_\omega P(\omega)$  denotes the essential supremum of the function  $P(\omega)$ . When a process is stationary, its covariance matrix is of Toeplitz form and can be asymptotically diagonalized by a discrete Fourier transform (DFT) matrix. By strict analogy to the vector case, the optimal architecture thus amounts to taking a discrete-time Fourier transform of the source and to allocating the bitrate across the frequency band by reverse water-filling on the power spectral density.

Often, the source of interest  $s[n]$  is not directly observed at the sensing device. Instead, only a noisy version  $x[n]$  of the source can be measured. We will refer to this noisy version as the *observation*. As an example, assume that we record a concert using a microphone and that we are only interested to encode the violin part. The other instruments are considered as noise and should not be reconstructed. This problem is referred to as a *remote*, noisy or indirect source coding problem and is illustrated in Figure 2.4(b). It was originally addressed by Dobrushin and Tsybakov [32]. More generally, Witsenhausen [148] elegantly demonstrated how certain classes of remote rate-distortion problems can be reduced to direct ones, unifying earlier results by Sakrison [118] and Wolf and Ziv [149]. In our setting, the remote rate-distortion function can be readily obtained from the direct one by considering a modified distortion measure. In particular, under the above assumptions of Gaussianity and stationarity, we can state the following theorem [12, Sec. 4.5.4].

**Theorem 2.6.** Consider a source and an observation that are jointly stationary Gaussian with mean-zero and power spectral density  $P_s(\omega)$  and  $P_x(\omega)$ , respectively. The cross power spectral density is denoted by  $P_{sx}(\omega)$ . The quadratic remote rate-distortion function is given by

$$D(\theta) = \frac{1}{2\pi} \int_0^{2\pi} P_{s|x}(\omega) d\omega + \frac{1}{2\pi} \int_0^{2\pi} \min\{\theta, P_s(\omega) - P_{s|x}(\omega)\} d\omega,$$

$$R(\theta) = \frac{1}{4\pi} \int_0^{2\pi} \max\left\{0, \log_2 \frac{P_s(\omega) - P_{s|x}(\omega)}{\theta}\right\} d\omega,$$

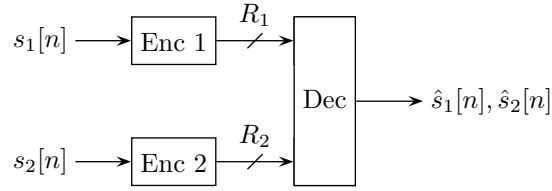


**Figure 2.5:** The distributed source coding problem with two encoders.

with  $\theta \in (0, \text{ess sup}_\omega P_s(\omega) - P_{s|x}(\omega)]$ .  $R(\theta)$  is expressed in bits per sample and  $D(\theta)$  in MSE per sample.

In the above theorem,  $P_{s|x}(\omega)$  denotes the power spectral density of the Wiener estimate of the source given the observation. It can be computed as

$$P_{s|x}(\omega) = P_s(\omega) - P_{sx}(\omega) P_x^{-1}(\omega) P_{sx}^*(\omega),$$

where the superscript  $*$  denotes the complex conjugate. The important fact about the remote rate-distortion function derived in Theorem 2.6 is that an optimal encoding architecture amounts to first computing the Wiener estimate of the source using the observation, and then encoding this estimate as if it were the source of interest. As a consequence, the minimum achievable distortion corresponds to the error incurred at the Wiener estimation stage.

## 2.4 Distributed Source Coding

### 2.4.1 Lossless Case

As illustrated in Figure 2.5, the distributed source coding problem consists of multiple encoders (or terminals), each observing a different source. In the lossless scenario, the goal of the decoder is to reconstruct perfectly all the sources. Since the sources are correlated, the distributed source coding problem does not simply reduce to multiple independent centralized source coding tasks. For simplicity of exposure, we will concentrate on a two-terminal setup. More precisely, we consider two sources,  $s_1[n]$  and  $s_2[n]$ , taking values in the sets  $\mathcal{S}_1$  and  $\mathcal{S}_2$ , respectively. The two encoders respectively map the input vectors  $\mathbf{s}_1^M \in \mathcal{S}_1^M$  and  $\mathbf{s}_2^M \in \mathcal{S}_2^M$ , defined as

$$\mathbf{s}_1^M = [s_1[0], s_1[1], \dots, s_1[M-1]]^T \quad \text{and} \quad \mathbf{s}_2^M = [s_2[0], s_2[1], \dots, s_2[M-1]]^T,$$

to descriptions  $T_{1,M} \in \mathcal{T}_{1,M}$  and  $T_{2,M} \in \mathcal{T}_{2,M}$ . This is achieved by means of *encoding functions*

$$f_{1,M} : \mathcal{S}_1^M \rightarrow \mathcal{T}_{1,M} \quad \text{and} \quad f_{2,M} : \mathcal{S}_2^M \rightarrow \mathcal{T}_{2,M},$$

where  $\mathcal{T}_{1,M} = \{1, 2, \dots, 2^{MR_1}\}$  and  $\mathcal{T}_{2,M} = \{1, 2, \dots, 2^{MR_2}\}$ . The message of the first encoder thus appears at a rate of  $R_1$  bits per sample. The one of the second encoder requires  $R_2$  bits per sample. Using  $T_{1,M}$  and  $T_{2,M}$ , the decoder

reconstructs the vectors  $\hat{\mathbf{s}}_1^M \in \hat{\mathcal{S}}_1^M$  and  $\hat{\mathbf{s}}_2^M \in \hat{\mathcal{S}}_2^M$ , defined as

$$\hat{\mathbf{s}}_1^M = [\hat{s}_1[0], \hat{s}_1[1], \dots, \hat{s}_1[M-1]]^T \quad \text{and} \quad \hat{\mathbf{s}}_2^M = [\hat{s}_2[0], \hat{s}_2[1], \dots, \hat{s}_2[M-1]]^T,$$

by means of a *decoding function*

$$g_M : \mathcal{T}_{1,M} \times \mathcal{T}_{2,M} \rightarrow \hat{\mathcal{S}}_1^M \times \hat{\mathcal{S}}_2^M.$$

The reconstruction follows as

$$(\hat{\mathbf{s}}_1^M, \hat{\mathbf{s}}_2^M) = g_M(f_{1,M}(\mathbf{s}_1^M), f_{2,M}(\mathbf{s}_2^M)).$$

The encoding and decoding functions should be chosen such that the original sources can be perfectly reconstructed. More specifically, a two-terminal lossless source code with parameters  $(M, R_1, R_2, \delta)$  consists of encoding functions  $f_{1,M} : \mathcal{S}_1^M \rightarrow \mathcal{T}_{1,M}$  and  $f_{2,M} : \mathcal{S}_2^M \rightarrow \mathcal{T}_{2,M}$  as well as a decoding function  $g_M : \mathcal{T}_{1,M} \times \mathcal{T}_{2,M} \rightarrow \hat{\mathcal{S}}_1^M \times \hat{\mathcal{S}}_2^M$  such that

$$P((\hat{\mathbf{s}}_1^M, \hat{\mathbf{s}}_2^M) \neq g_M(f_{1,M}(\mathbf{s}_1^M), f_{2,M}(\mathbf{s}_2^M))) \leq \delta, \quad (2.4)$$

where  $\mathcal{T}_{1,M} = \{1, 2, \dots, 2^{MR_1}\}$  and  $\mathcal{T}_{2,M} = \{1, 2, \dots, 2^{MR_2}\}$ . As in the centralized scenario, the fundamental problem is the determination of the achievable rates  $R_1$  and  $R_2$ . A rate pair  $(R_1, R_2)$  is said to be *achievable* if we can find a sequence of two-terminal lossless source codes such that the error probability (2.4) vanishes as  $M$  becomes large. More precisely, for any  $\delta > 0$ , we must find an integer  $M_0$  such that, for all  $M \geq M_0$ , we can design a two-terminal lossless source code with parameters  $(M, R_{1,M}, R_{2,M}, \delta)$  satisfying  $R_{1,M} \leq R_1 + \delta$  and  $R_{2,M} \leq R_2 + \delta$ . The complete characterization of the achievable rate region was obtained by Slepian and Wolf in [126] and is given by the following theorem.

**Theorem 2.7.** Given discrete memoryless sources  $s_1[n]$  and  $s_2[n]$ , the rate pair  $(R_1, R_2)$  is achievable without loss if it satisfies

$$\begin{aligned} R_1 &> H(s_1|s_2), \\ R_2 &> H(s_2|s_1) \quad \text{and} \\ R_1 + R_2 &> H(s_1, s_2). \end{aligned}$$

Conversely, a rate pair  $(R_1, R_2)$  satisfying  $R_1 < H(s_1|s_2)$ ,  $R_2 < H(s_2|s_1)$  or  $R_1 + R_2 < H(s_1, s_2)$  cannot be achieved.

A rate pair  $(R_1, R_2)$  meeting the above lower bounds with equality may be achievable, but not always. The rate region is depicted in Figure 2.6. Note that Theorem 2.7 can be extended to ergodic sources with memory by considering entropy rates [28]. The Slepian-Wolf theorem proves that the minimum achievable sum rate  $R_1 + R_2$  is the joint entropy, that is, the minimum achievable rate when the sources can be processed centrally. In other words, there is no rate loss in coding the two sources separately. An important special case of the general two-terminal setup is obtained when one of the sources (say  $s_2[n]$ ) is perfectly available at the decoder. The source  $s_1[n]$  can then be encoded at a rate of  $H(s_1|s_2)$  bits per source sample. This strategy can be applied part of the time in turn at each terminal (time-sharing) to obtain any point on

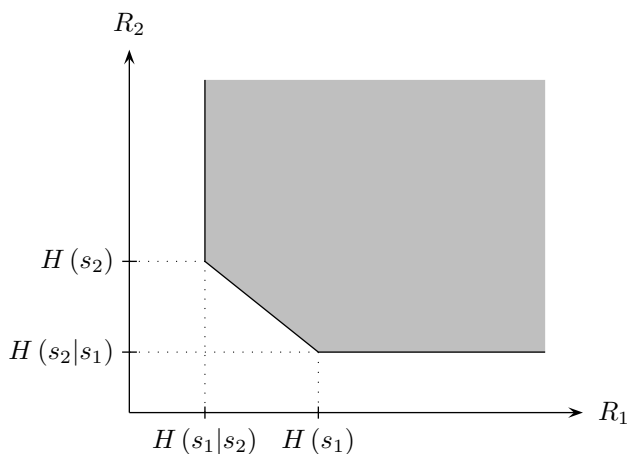


**Figure 2.6:** Achievable rate region for the two-terminal lossless source coding problem.

the boundary of the achievable rate region. We now give a simple illustrative example of distributed lossless source coding.

**Example 2.1.** Assume that  $s_1[n]$  is a memoryless source taking values in the set  $\mathcal{S}_1 = \{0, 1, 2, 3\}$  with equal probabilities  $1/4$ . The source  $s_2[n]$  is a memoryless source taking values in the same set ( $\mathcal{S}_2 = \mathcal{S}_1$ ). The joint probabilities  $p_{s_1, s_2}(u_1, u_2)$  and the conditional probabilities  $p_{s_1|s_2}(u_1|u_2)$  are given in the following tables:

$p_{s_1, s_2}$	0	1	2	3	$p_{s_1 s_2}$	0	1	2	3
0	0.25	0	0.25	0	0	0.5	0	0.5	0
1	0	0.25	0	0.25	1	0	0.5	0	0.5
2	0.25	0	0.25	0	2	0.5	0	0.5	0
3	0	0.25	0	0.25	3	0	0.5	0	0.5

It is easily checked that  $H(s_1) = H(s_2) = 2$  bits per sample. Independent coding of the two sources thus requires 4 bits per sample. However, the Slepian-Wolf theorem says that a sum rate of only  $H(s_1, s_2) = 3$  bits per sample is needed. How can this be achieved?

The gain of 1 bit per sample is obtained by realizing that the random variables  $s_1$  and  $s_2$  are not independent. More precisely, they have the same parity. For example, if the value of  $s_2$  is 0, then the only possible values for  $s_1$  are 0 and 2. Assume that each value of  $s_2[n]$  is encoded using its binary representation (two bits). The required bitrate to encode  $s_2[n]$  is 2 bits per sample. Knowing the value of  $s_2[n]$ , the decoder also knows the parity of  $s_1[n]$ , that is, its least significant bit. The first encoder thus only needs to provide the decoder with the most significant bit of  $s_1[n]$ . This coding scheme achieves a sum rate of 3 bits per sample and is therefore optimal.  $\square$

The key observation in the above example is that, while  $s_1$  and  $s_2$  can each take four possible values, knowing the value of  $s_2$  reduces the uncertainty about

$s_1$  to only two possible values. The above coding method is a simple version of a strategy known as binning, which can be applied to prove the achievability of the rate region defined in Theorem 2.7 (see, e.g., [29, Sec. 14.4.1]). A couple of important remarks are however at hand. First, knowledge of the joint statistics is assumed. These statistics are easily computable in a centralized scenario since the sources can be observed jointly. However, this task is significantly more involved in a distributed setup. Depending on the application at hand, this assumption may turn out to be unrealistic. The second remark pertains to coding complexity. While no rate loss is incurred in the limit of large block lengths, the coding delays and processing complexity of a distributed source code approaching optimality may be much higher than those of a centralized source code. This fact might preclude its use in a practical setting.

While the theoretical foundations of distributed lossless source coding have been laid by the pioneering work of Slepian and Wolf in the early 1970's [126], practical coding schemes based on these principles have only been proposed recently (see, e.g., [130]). A constructive practical framework for the source coding problem with side information at the decoder has been proposed by Pradhan and Ramchandran [108]. The key idea is to consider the side information to be a noisy version of the source as if the source had passed through a noisy channel. The encoder then only needs to provide the decoder with the minimum amount of information required to correct the errors introduced by this fictitious channel. The use of different error correcting schemes have been used in this context, such as Hamming codes [51], turbo codes [48] or low-density parity-check codes [90].

### 2.4.2 Lossy Case

As in the centralized scenario, it is natural to study the lossy version of the distributed source coding problem. In this case, the reconstruction of the sources  $s_1[n]$  and  $s_2[n]$  is achieved only to within some distortions  $D_1$  and  $D_2$ , respectively. These distortions are computed using distortion measures

$$d_1 : \mathcal{S}_1 \times \hat{\mathcal{S}}_2 \rightarrow [0, \infty) \quad \text{and} \quad d_2 : \mathcal{S}_2 \times \hat{\mathcal{S}}_1 \rightarrow [0, \infty).$$

Given the sources  $s_1[n]$  and  $s_2[n]$ , a two-terminal lossy source code with parameters  $(M, R_1, R_2, D_1, D_2, \delta)$  consists of encoding functions  $f_{1,M} : \mathcal{S}_1^M \rightarrow \mathcal{T}_{1,M}$  and  $f_{2,M} : \mathcal{S}_2^M \rightarrow \mathcal{T}_{2,M}$  as well as decoding functions  $g_{1,M} : \mathcal{T}_{1,M} \times \mathcal{T}_{2,M} \rightarrow \hat{\mathcal{S}}_1^M$  and  $g_{2,M} : \mathcal{T}_{1,M} \times \mathcal{T}_{2,M} \rightarrow \hat{\mathcal{S}}_2^M$  such that

$$\frac{1}{M} \sum_{m=0}^{M-1} \mathcal{E} \{d_1(s_1[m], \hat{s}_1[m])\} \leq D_1 \quad \text{and} \quad \frac{1}{M} \sum_{m=0}^{M-1} \mathcal{E} \{d_2(s_2[m], \hat{s}_2[m])\} \leq D_2,$$

where  $\mathcal{T}_{1,M} = \{1, 2, \dots, 2^{MR_1}\}$  and  $\mathcal{T}_{2,M} = \{1, 2, \dots, 2^{MR_2}\}$ . The random variables  $\hat{s}_1[m]$  and  $\hat{s}_2[m]$  correspond the  $m$ th element of the reconstructed vectors

$$\hat{\mathbf{s}}_1^M = g_{1,M}(f_{1,M}(\mathbf{s}_1^M), f_{2,M}(\mathbf{s}_2^M)) \quad \text{and} \quad \hat{\mathbf{s}}_2^M = g_{2,M}(f_{1,M}(\mathbf{s}_1^M), f_{2,M}(\mathbf{s}_2^M)),$$

respectively. Again, a rate pair  $(R_1, R_2)$  is said to be *achievable* with distortion pair  $(D_1, D_2)$  the rate-distortion tuple  $(R_1, R_2, D_1, D_2)$  can be approached ar-

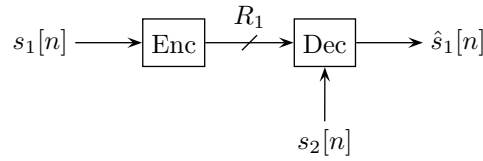


**Figure 2.7:** Source coding with side information at the decoder.

bitrarily closely using two-terminal lossy source codes. More formally, for all  $\delta > 0$ , there must exist an integer  $M_0$ , such that for all  $M \geq M_0$ , we can build a two-terminal lossy source code with parameters  $(R_{1,M}, R_{2,M}, D_{1,M}, D_{2,M}, \delta)$  such that  $R_{1,M} \leq R_1 + \delta$ ,  $R_{2,M} \leq R_2 + \delta$ ,  $D_{1,M} \leq D_1 + \delta$  and  $D_{2,M} \leq D_2 + \delta$ .

Unfortunately, the achievable rate region for the distributed lossy source coding problem is unknown to date. The important special case of source coding with *side information at the decoder* was solved by Wyner and Ziv [151]. This scenario assumes that one of the sources is directly available at the decoder, as depicted in Figure 2.7. A peculiarity of this setup is that, in the jointly Gaussian case, the rate-distortion function would remain the same if the encoder also had access to the side information (i.e., as in a *conditional* rate-distortion problem [57]). For other statistics, however, there is a penalty for the absence of the side information at the encoder [153]. Another important special case is obtained by assuming that the observations are *independently corrupted* versions of the source. This problem is often referred to as the CEO problem [14] and its rate-distortion function was derived by Oohama in [101]. Other conclusive results can be found for the case of high-resolution [154], or for certain special distortion measures [100] (not including MSE). For the general multiterminal scenario, an achievable strategy was proposed by Berger and Tung [13, 135] and Housewright and Omura [71]. Their approach combines quantization of the sources at each encoder, as in the centralized lossy source coding problem, and binning of the quantization indexes, as in the distributed lossless case. The optimality of this strategy in a two-encoder setup is still unknown. The only example for which it is known to be optimal is the quadratic Gaussian case derived by Wagner *et al.* [143]. Their result is summarized in the following theorem.

**Theorem 2.8.** Consider two memoryless sources  $s_1[n]$  and  $s_2[n]$  that are jointly Gaussian with mean zero and covariance matrix

$$\mathbf{R} = \begin{bmatrix} \sigma_1^2 & \rho\sigma_1\sigma_2 \\ \rho\sigma_1\sigma_2 & \sigma_2^2 \end{bmatrix}.$$

Define the set  $\mathcal{R}(D_1, D_2)$  of rate pairs  $(R_1, R_2)$  satisfying

$$\begin{aligned} R_1 &\geq \max \left\{ \frac{1}{2} \log_2 \frac{(1 - \rho^2 + \rho^2 2^{-2R_2}) \sigma_1^2}{D_1}, 0 \right\}, \\ R_2 &\geq \max \left\{ \frac{1}{2} \log_2 \frac{(1 - \rho^2 + \rho^2 2^{-2R_1}) \sigma_2^2}{D_2}, 0 \right\} \quad \text{and} \end{aligned}$$

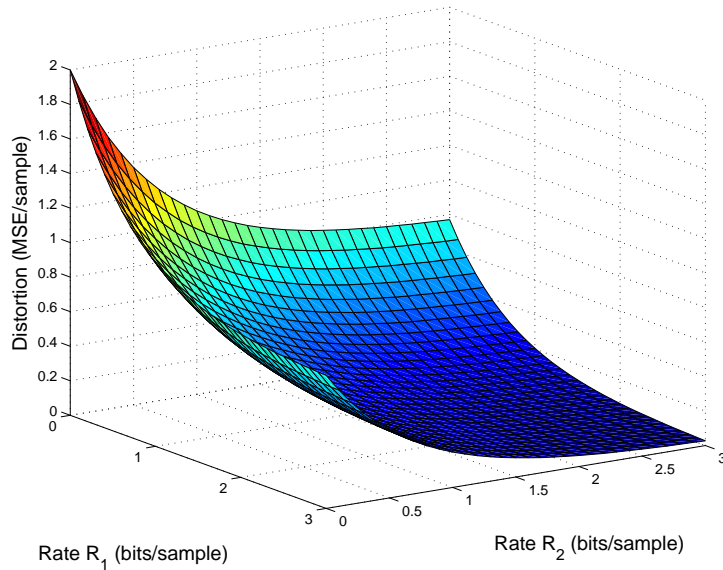


**Figure 2.8:** Two-terminal quadratic rate-distortion function of memoryless jointly Gaussian sources. The variances are  $\sigma_1^2 = \sigma_2^2 = 1$  and the correlation parameter is  $\rho = 0.5$ .

$$R_1 + R_2 \geq \max \left\{ \frac{1}{2} \log_2 \frac{(1 - \rho^2) \sigma_1^2 \sigma_2^2 \beta(D_1, D_2)}{2D_1 D_2}, 0 \right\},$$

where

$$\beta(D_1, D_2) = 1 + \sqrt{1 + \frac{4\rho^2 D_1 D_2}{(1 - \rho^2)^2 \sigma_1^2 \sigma_2^2}}$$

with MSE distortions  $D_1, D_2 > 0$ . Let  $\mathcal{R}_0$  be the interior of the set  $\mathcal{R}$ . A rate pair  $(R_1, R_2)$  is achievable with MSE distortion pair  $(D_1, D_2)$  if it satisfies  $(R_1, R_2) \in \mathcal{R}_0$ . Conversely,  $(R_1, R_2) \notin \mathcal{R}_0$  cannot be achieved with MSE distortion pair  $(D_1, D_2)$ .

The parameter  $\rho$  allows changing the correlation between the two sources. When  $\rho = 0$ , the sources are uncorrelated and the rate-distortion function of Theorem 2.3 applies to both sources. Conversely, when  $\rho \rightarrow 1$ , the two sources are essentially the same and the sum rate constraint is always satisfied. A consequence of the result in [143] is that vector quantization of each source followed by Slepian-Wolf encoding of the quantized indices is optimal. However, unlike the lossless scenario, there is a rate loss compared to centralized encoding. In the sequel, we will be mostly interested in minimizing the sum distortion  $D = D_1 + D_2$  instead of each term separately. In this case, a distortion-rate surface  $D(R_1, R_2)$  can be obtained from Theorem 2.8. An example is depicted in Figure 2.8.

In the case of memoryless jointly Gaussian vector sources, the above result cannot be easily extended. In particular, it is not known whether a transform coding approach, similar to the centralized case, could be optimal. Suboptimal solutions have thus been investigated. In [50], Gastpar *et al.* derived the mean



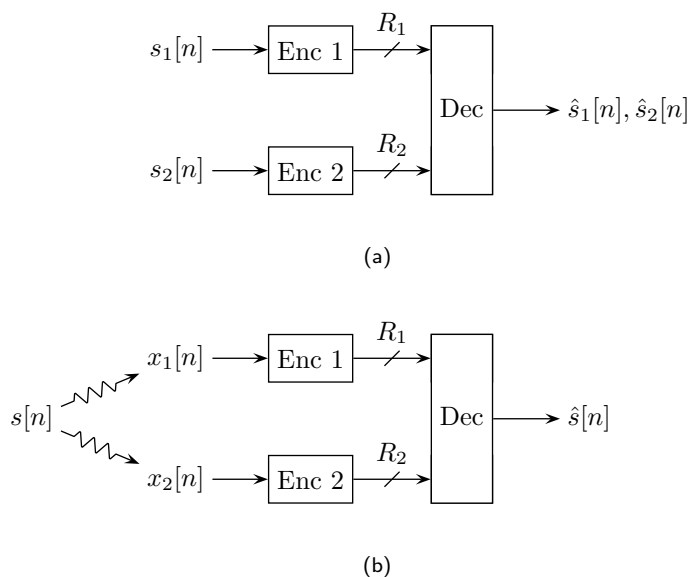


**Figure 2.9:** Direct and remote distributed source coding with two encoders.

square optimal coding strategy at one terminal assuming all else is fixed. They showed that this local perspective can be given a transform coding interpretation. They proposed a suboptimal distributed architecture which consists of applying this local optimization step in turn at each terminal. Several other authors have looked at transform-based distributed architectures, from both a linear approximation [99, 122, 155] and compression [107, 109] standpoint. Some of the aforementioned references can be rather straightforwardly extended to the case of stationary jointly Gaussian sources. In fact, as in Theorem 2.5, the Toeplitz distribution theorem can be invoked to derive optimality results in this context.

Let us turn our attention to the remote version of the lossy distributed source coding problem. In this case, the two encoders only observe noisy versions  $x_1[n]$  and  $x_2[n]$  of the signals of interest, that is,  $s_1[n]$  and  $s_2[n]$ . Without loss of generality, we can assume that  $x_1[n]$  and  $x_2[n]$  can be obtained from a single source that we denote by  $s[n]$ . This setup corresponds to a rate-constrained distributed estimation problem [74] and is depicted in Figure 2.9(b). In the centralized case, we mentioned that the remote source coding problem can be seen as a direct one with a modified distortion criterion. Similarly, the distributed remote source coding problem can be stated as a direct one using a modified distortion measure. As pointed out in [43], it is simply a matter of adding an additional encoder with direct access to the source  $s[n]$  and setting its rate to zero. The distortion is then computed in terms of the signal observed at this new encoder and its reconstruction. One contribution of this thesis [112, 117] is to extend the iterative approach derived in [50] to this remote scenario, for both memoryless vector sources and discrete-time sources with memory. In this case, the optimal solution at each step corresponds to a *remote source coding problem with side information at*

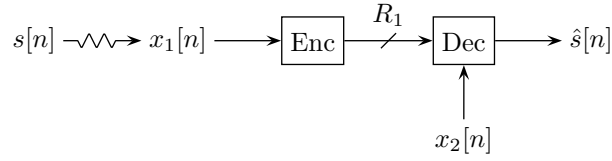


**Figure 2.10:** Remote source coding with side information at the decoder.

the decoder. It is illustrated in Figure 2.10 and is also referred to as a remote, noisy or indirect Wyner-Ziv problem. As argued in the next section, the remote Wyner-Ziv rate-distortion function is the key element to study the binaural noise reduction problem. Its characterization as a minimization problem was obtained by Yamamoto and Itoh [152]. Our aim will be to evaluate it for the case of jointly Gaussian sources that are either memoryless vector sources or discrete-time sources with memory. Note that the remote Wyner-Ziv problem has already been addressed by various other researchers in the scalar case (see, e.g., [39, 40, 46]). The extension to vector sources was investigated in [109] in the context of high-rate quantization. Recently, and in parallel to our work, Schizas *et al.* [121, 122] have considered some extensions of the results in [50] to a remote scenario with non-ideal communication links (fading and noise).

## 2.5 Binaural Hearing Aids

### 2.5.1 Problem Statement

The binaural configuration is schematically depicted in Figure 2.11. A user carries two hearing aids, both comprising a set of microphones, a processing unit with wireless communication capabilities and a loudspeaker. Hearing aid 1 comprises  $L_1$  microphones. The discrete-time signals recorded by these microphones can each be expressed as

$$x_{1,l}[n] = x_{1,l}^s[n] + x_{1,l}^n[n] \quad \text{for } l = 0, 1, \dots, L_1 - 1, \quad (2.5)$$

where  $x_{1,l}^s[n]$  denotes the (desired) speech component and  $x_{1,l}^n[n]$  the (undesired) noise component. Similarly, the signals recorded at the  $L_2$  microphones of hearing aid 2 can be written as  $x_{2,l}[n] = x_{2,l}^s[n] + x_{2,l}^n[n]$  for  $l = 0, 1, \dots, L_2 - 1$ . Typically, the speech components  $x_{1,l}^s[n]$  and  $x_{2,l}^s[n]$  correspond to the speech sources of interest, as recorded by hearing aid 1 and 2, respectively (see Figure 2.11(a)). The distinction between desired and undesired signals is generally achieved by means of a voice activity detection mechanism, which discriminates whether the sources of interest are active or not. Note that each microphone records a different version of the involved sources, owing to different propagation delays and different attenuations. For convenience, we will write the input signals in vector form as

$$\mathbf{x}_t[n] = [x_{t,0}[n], x_{t,1}[n], \dots, x_{t,L_t-1}[n]]^T \quad \text{for } t = 1, 2,$$

where  $\mathbf{x}_t[n] = \mathbf{x}_t^s[n] + \mathbf{x}_t^n[n]$  with  $\mathbf{x}_t^s[n]$  and  $\mathbf{x}_t^n[n]$  defined similarly as  $\mathbf{x}_t[n]$ . The speech vector  $\mathbf{x}_t^s[n]$  and the noise vector  $\mathbf{x}_t^n[n]$  are modeled as independent

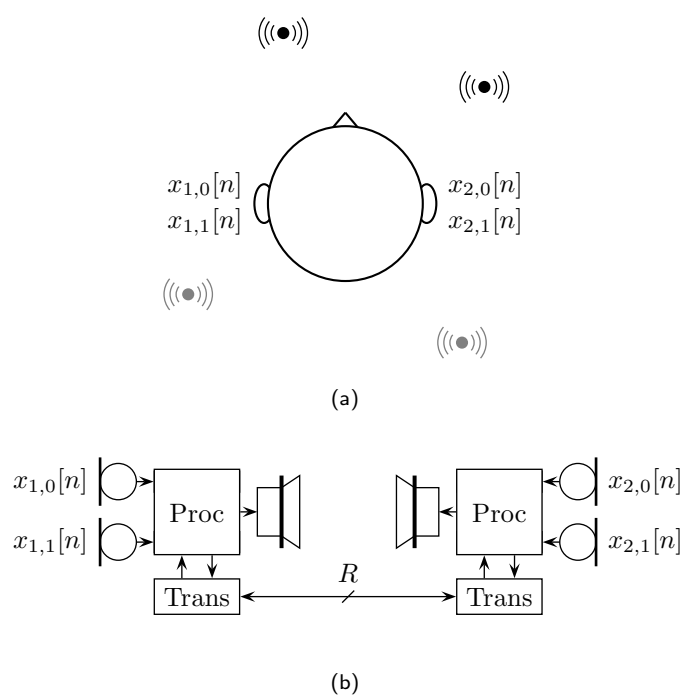


**Figure 2.11:** Binaural hearing aids with  $L_1 = L_2 = 2$  microphones. (a) Typical acoustic scene. The two sources in the front (black) are the (desired) speech sources, whereas the two sources in the back (gray) are the (undesired) noise sources. (b) Collaboration using a rate-constrained wireless link.

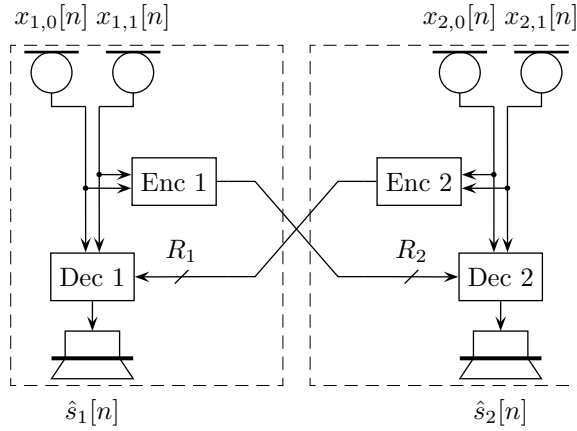


**Figure 2.12:** Binaural hearing aids with  $L_1 = L_2 = 2$  microphones.

stationary Gaussian vector sources with mean zero and power spectral density matrices  $\Phi_{x_t^s}(\omega)$  and  $\Phi_{x_t^n}(\omega)$ , respectively. The power spectral density matrix of the vector source  $\mathbf{x}_t[n]$  hence follows as  $\Phi_{x_t}(\omega) = \Phi_{x_t^s}(\omega) + \Phi_{x_t^n}(\omega)$ . Similarly, we can define the binaural input  $\mathbf{x}[n]$  as

$$\mathbf{x}[n] = [\mathbf{x}_1^T[n], \mathbf{x}_2^T[n]]^T.$$

It has mean zero and power spectral density matrix  $\Phi_x(\omega)$ . It can be decomposed as  $\mathbf{x}[n] = \mathbf{x}^s[n] + \mathbf{x}^n[n]$ , where the binaural speech component  $\mathbf{x}^s[n]$  and the binaural noise component  $\mathbf{x}^n[n]$  are defined similarly as  $\mathbf{x}[n]$ . Their power spectral density matrices are denoted by  $\Phi_{x^s}(\omega)$  and  $\Phi_{x^n}(\omega)$ , respectively.

The goal of each hearing instrument is to recover the speech component of its reference microphone (say microphone 0) with minimum (weighted) MSE distortion. In other words, each hearing aid aims at estimating the contribution of the speech sources in the signal recorded by its reference microphone. These components, referred to as the *desired* sources, thus correspond to  $x_{1,0}^s[n]$  and  $x_{2,0}^s[n]$ . For ease of notation, we will denote them by  $s_1[n]$  and  $s_2[n]$ , respectively. To make matters clearer, let us adopt the perspective of hearing aid 1. Its goal is to estimate the signal  $s_1[n]$  with minimum distortion based on its own observations  $\mathbf{x}_1[n]$  and a compressed version of the signals  $\mathbf{x}_2[n]$  recorded at the microphones of hearing aid 2. The key is to realize that this setup corresponds to the remote source coding problem with side information at the decoder described in Section 2.4. More specifically, we wish to encode the vector observation  $\mathbf{x}_2[n]$  with rate  $R_1$  such as to minimize the distortion between the remote source  $s_1[n]$  and its reconstruction  $\hat{s}_1[n]$ , taking into account the presence of the side information  $\mathbf{x}_1[n]$  at the decoder. Equivalently, the problem can be viewed as a two-terminal remote source coding problem of the source  $s_1[n]$ , where the observation  $\mathbf{x}_1[n]$  of the first terminal is directly available at the decoder. This procedure is illustrated for the two devices in Figure 2.12. The *monaural* gain achieved at hearing aid  $t$  is defined as

$$G_t(R_t) = \frac{D_t(0)}{D_t(R_t)} \quad \text{for } t = 1, 2, \quad (2.6)$$

where  $D_t(R_t)$  denotes the corresponding optimal distortion rate trade-off,  $D_t(0)$  being the distortion incurred when there is no help from the contralateral device ( $R_t = 0$ ). Note that  $R_t$  refers to the rate at which data is delivered to hearing aid  $t$ . The quantity  $G_t(R_t)$  actually corresponds to the signal-to-distortion improvement enabled by the wireless link when it operates at rate  $R_t$ . The *binaural* gain can thus be obtained as

$$G(R) = \frac{D(0)}{D(R)}, \quad (2.7)$$

where  $D(R)$  refers to the optimal trade-off between the sum distortion  $D = D_1 + D_2$  and the total (bidirectional) transmission rate  $R = R_1 + R_2$ . Our main concern is the study of the above optimal gain-rate trade-offs, from both a theoretical and a practical standpoint [113–115]. Before we proceed, let us look more carefully at the main assumptions of the considered model.

### 2.5.2 Validity of the Assumptions

In the binaural noise reduction problem stated above, there are a number of implicit assumptions that we would like to discuss in more detail.

#### Setup

The first assumption pertains to the use of a wireless link between hearing aids. The main postulate is that the transmission of audio signals is possible despite the stringent power and delay constraints. State-of-the-art wireless hearing aids are able to exchange only low data rate content in the form of synchronization parameters [44]. However, in view of the progress made in the field of low power electronics and in the development of longer-lasting batteries, we believe that the exchange of audio signals will be possible in the near future. Moreover, binaural processing has a great potential in terms of speech intelligibility improvement. Hence, it will be worth using resources for the purpose of ear-to-ear communication.

#### Signal Model

The considered signal model assumes that the involved sources are stationary and Gaussian. While stationarity cannot be guaranteed over long time periods, it is reasonable to assume that this property holds over small durations. The Gaussian assumption is mostly motivated by its mathematical tractability. Nevertheless, it has been successfully applied in a plethora of signal processing fields, including audio. Regarding the noise component, it is assumed to be both additive and uncorrelated with the speech component. The former assumption is motivated by the laws of physics, more precisely, by the wave equation in free space [97, Sec. 7.1]. In this case, the wave field induced by a point source is obtained as the convolution of the source by a linear and space-time invariant filter, whose impulse response is referred to as the Green's function [97, Sec. 7.1]. The sound field induced by multiple sources can thus be computed as the

sum of each individual contribution. The assumption of uncorrelated speech and noise components is reasonable since, in the envisioned application, the noise typically consists of interferers producing sound that is independent from the desired source. This assumption would be clearly flawed in a dereverberation context, for example, since reflections are strongly correlated with the underlying clean signal.

### Distortion Criterion

In the monaural setup, the choice of a minimum weighted MSE distortion is partly motivated by the fact that the optimality of the MSE processor extends to various other criteria with minor modifications [138, Sec. 6.2]. While some of the characteristics of the human ear can be taken into account using an appropriate weighting, it is important to point out that the weighted MSE does not take into consideration other important factors related to speech intelligibility in noise. More relevant speech intelligibility measures can be found in the literature (see, e.g., [60]), but are usually not amenable to closed-form optimization. More generally, an accurate distortion measure seems rather elusive owing to the complexity of human hearing. In this context, the MSE criterion is appealing in that it captures the general features of speech in noise while being simple enough to derive optimal processing strategies.

In terms of binaural noise reduction, a sum distortion appears to be the most natural choice considering the inherent symmetry of the human hearing system. Different weighting operators may be used at the left and right ear to take into account unequal characteristics. However, the MSE distortion does not fully capture the complexity of binaural hearing, a topic which is currently matter of substantial research efforts (see, e.g., [65]). In particular, it preserves the spatial characteristics of the speech source, but modifies those of the noise component [33, 136]. The overall auditory image is thus modified by the noise reduction scheme. This effect may be circumvented, for example, by adding a small fraction of the original binaural signal to the output [85]. This obviously increases the amount of noise but also introduces some of the original binaural cues. The basic assumption is that better speech intelligibility can be achieved due to an improved spatial rendering, even if more noise (in the mean square sense) is present. The MSE criterion thus still provides a useful means to design binaural noise reduction algorithms.

### Delays, Processing Complexity and Statistical Knowledge

A large part of our exposition is devoted to the information-theoretic analysis of the binaural hearing aid communication problem. As pointed out in Sections 2.3 and 2.4, optimal rate-distortion trade-offs are derived without taking into account coding delays or processing complexity constraints. In this context, is the information-theoretic analysis really meaningful? We believe it is indeed the case for two main reasons. First, it provides a limit to the best achievable noise reduction under processing constraints. It thus allows us to benchmark practical binaural noise reduction schemes that take into account limited communication bitrates. Second, it provides useful insights about the design of an optimal encoding architecture.

In this information-theoretic framework, the correlation statistics of the

---

input signals are assumed to be known at both hearing aids. These latter are functions of the audio sources as well as the characteristics of the recording setup. The statistics of the signals measured at one device may be estimated by means of a voice activity detection mechanism (see, e.g., [134]). However, the quantities involving signals from both hearing aids cannot be easily computed. An alternative would be to use a side channel for this purpose, but the success of this task is rather unclear. With this limitation in mind, Chapter 4 considers the best achievable trade-off obtained by a strategy which does not require the computation of such statistics. While correlation between input signals may be difficult to estimate, it is important to point out that the recording setup might induce dependencies that are known *a priori*. They thus do not need to be learned. We will explore this fact in more detail in Chapter 6.

## 2.6 Summary

This chapter demonstrated how the binaural noise reduction problem can be seen as a distributed source coding task. Towards this goal, we reviewed the fundamental concepts of distributed source coding and presented binaural noise reduction in light of these results.

We started by recalling the notion of information sources and described different types of sources. We reviewed important quantities used to quantify the information content of a source, in particular entropy and mutual information.

We then looked at the centralized source coding problem and presented the fundamental theorem of data compression, in both the lossless and lossy scenario. In the lossy case, we introduced the notion of rate-distortion function. rate-distortion functions were computed under Gaussian assumptions for different types of sources. In particular, we explained how a memoryless Gaussian vector source can be optimally encoded by means of a transform coding architecture. We then addressed the remote scenario, that is, when the source of interest is observed at the encoder in a noisy fashion.

Our attention then shifted to the distributed infrastructure, which is considerably more difficult to analyze. For simplicity of exposure, we concentrated on a two-terminal scenario. We reviewed the Slepian-Wolf theorem which characterizes the set of achievable rates with distributed lossless source coding. While the lossy counterpart to this theorem is unknown to date, we described some of the scenarios for which conclusive results are available in the literature. As in centralized source coding, we then looked at the remote case and explained what is the contribution of this thesis in this context.

The problem of binaural hearing aids was then formulated as a particular type of distributed source coding problem, namely, a remote source coding problem with side information at the decoder. Monaural and binaural gain-rate functions were defined. They characterize the optimal trade-off between the rate at which the wireless link operates and the noise reduction resulting from this data exchange. Finally, we detailed the main assumptions made in the considered model and discussed their validity in a practical setting. In particular, we argued for the usefulness of an information-theoretic approach to this problem.





## Chapter 3

# Distributed Estimation under Communication Constraints

### 3.1 Introduction

As pointed out in the previous chapter, the binaural noise reduction task corresponds to a two-terminal remote source coding problem. The aim of the present chapter is to study such a source coding problem for both memoryless vector sources and discrete-time sources with memory. Unfortunately, the latter appears to be intractable. We thus resort to suboptimal strategies for which conclusive results can be found. More precisely, we extend the iterative transform coding architecture presented in [50] to a remote scenario. From the perspective of the decoder, the problem can be viewed as a distributed estimation task under communication constraint. Two types of constraints are considered: *linear approximation* and *compression*. In the former, the terminals provide the decoder with a low-dimensional linear approximation of their observed vector. In the latter, the data they observe is described using a bit stream that appears at a prescribed bitrate. As in the centralized scenario, we will see that these two viewpoints are related to each other through transform coding.

In Section 3.2, we formally state the problem of mean square optimal distributed estimation, from both the linear approximation and compression standpoints. As the general solution seems difficult to derive, locally optimal strategies are investigated. We first consider memoryless vector sources, in Section 3.3, and then discrete-time sources with memory, in Section 3.4. In both cases, we borrow the iterative approach in [50] which consists in optimizing the description at one terminal assuming that the other is fixed. This local optimization strategy is then used as the step of an iterative algorithm whose optimality is discussed. Finally, we illustrate our findings with a simple correlation model in Section 3.5. A summary of this chapter is given in Section 3.6.

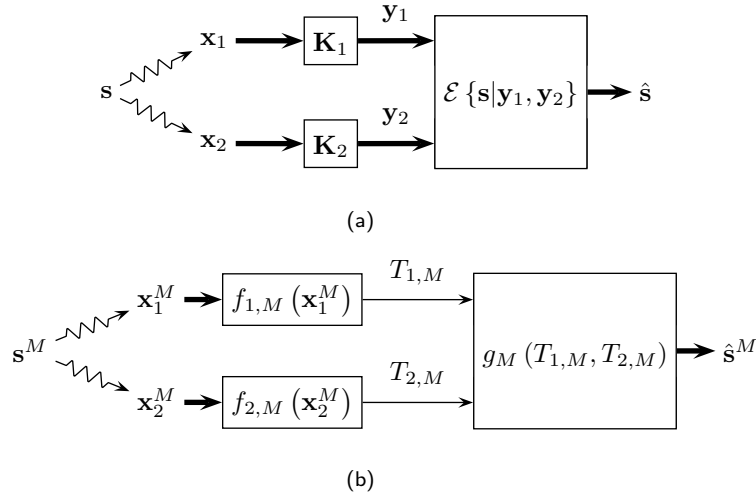


**Figure 3.1:** The distributed estimation problem under communication constraints. (a) Linear approximation. (b) Compression.

## 3.2 Distributed Estimation

### 3.2.1 Linear Approximation

The linear approximation problem is depicted in Figure 3.1(a). The two terminals observe the random vectors  $\mathbf{x}_1 \in \mathbb{C}^{N_1}$  and  $\mathbf{x}_2 \in \mathbb{C}^{N_2}$ , respectively. These vectors are correlated with a random vector  $\mathbf{s} \in \mathbb{C}^P$  of interest. For simplicity, we assume that  $N_1, N_2 \leq P$ . The terminals provide the decoder with low-dimensional linear approximations  $\mathbf{y}_1 \in \mathbb{C}^{K_1}$  and  $\mathbf{y}_2 \in \mathbb{C}^{K_2}$  computed as

$$\mathbf{y}_1 = \mathbf{K}_1 \mathbf{x}_1 \quad \text{and} \quad \mathbf{y}_2 = \mathbf{K}_2 \mathbf{x}_2,$$

where  $\mathbf{K}_1 \in \mathbb{C}^{K_1 \times N_1}$  and  $\mathbf{K}_2 \in \mathbb{C}^{K_2 \times N_2}$  denote the matrices applied at the first and second terminals, respectively. Equivalently, we can let  $N = N_1 + N_2$  and  $K = K_1 + K_2$  and define the stacked vectors  $\mathbf{x} \in \mathbb{C}^N$  and  $\mathbf{y} \in \mathbb{C}^K$  as

$$\mathbf{x} = [\mathbf{x}_1^T, \mathbf{x}_2^T]^T \quad \text{and} \quad \mathbf{y} = [\mathbf{y}_1^T, \mathbf{y}_2^T]^T.$$

The vector observed at the decoder can then be expressed as

$$\mathbf{y} = \mathbf{K} \mathbf{x},$$

with  $\mathbf{K} \in \mathbb{C}^{K \times N}$  the block diagonal matrix given by

$$\mathbf{K} = \begin{bmatrix} \mathbf{K}_1 & \mathbf{O}_{K_1 \times N_2} \\ \mathbf{O}_{K_2 \times N_1} & \mathbf{K}_2 \end{bmatrix}.$$

The decoder then computes the reconstruction  $\hat{\mathbf{s}} \in \mathbb{C}^P$  as a function of  $\mathbf{y}$  such as to minimize the MSE distortion. The optimal reconstruction  $\hat{\mathbf{s}}$  is given by the conditional expectation of  $\mathbf{s}$  given  $\mathbf{y}$  which, in the jointly Gaussian case,

reduces to the linear operation [78, Th. 3.2.1]

$$\hat{\mathbf{s}} = \mathbf{R}_{sy} \mathbf{R}_y^{-1} \mathbf{y} = \mathbf{R}_{sx} \mathbf{K}^H (\mathbf{K} \mathbf{R}_x \mathbf{K}^H)^{-1} \mathbf{K} \mathbf{x}.$$

In the above equation, the superscript  $H$  denotes the Hermitian (conjugate) transpose. The corresponding MSE distortion follows as [78, Th. 3.2.1]

$$\mathcal{E} \left\{ \|\mathbf{s} - \hat{\mathbf{s}}\|^2 \right\} = \text{tr} \left( \mathbf{R}_s - \mathbf{R}_{sx} \mathbf{K}^H (\mathbf{K} \mathbf{R}_x \mathbf{K}^H)^{-1} \mathbf{K} \mathbf{R}_{sx}^H \right), \quad (3.1)$$

where  $\|\cdot\|$  stands for the Frobenius norm and  $\text{tr}(\cdot)$  denotes the trace operator.

For fixed  $K_1$  and  $K_2$ , the linear approximation problem consists in finding the block diagonal approximation matrix  $\mathbf{K}$  that minimizes the MSE distortion (3.1). The solution seems difficult to derive since the approximation matrix  $\mathbf{K}$  is constrained to have a particular block diagonal structure that reflects the distributed nature of the setup. In Section 3.3.1, we will investigate a suboptimal strategy for which conclusive results can be found.

### 3.2.2 Compression

In the compression problem, depicted in Figure 3.1(b), we are interested in reconstructing  $M$  i.i.d. consecutive samples of the remote vector source  $\mathbf{s}[m]$ . We represent them in the form of a stacked vector, denoted by  $\mathbf{s}^M \in \mathbb{C}^{MP}$ , as

$$\mathbf{s}^M = [\mathbf{s}^T[0], \mathbf{s}^T[1], \dots, \mathbf{s}^T[M-1]]^T.$$

The two encoders respectively observe the input vectors  $\mathbf{x}_1^M \in \mathbb{C}^{MN_1}$  and  $\mathbf{x}_2^M \in \mathbb{C}^{MN_2}$  defined as

$$\mathbf{x}_1^M = [\mathbf{x}_1^T[0], \mathbf{x}_1^T[1], \dots, \mathbf{x}_1^T[M-1]]^T \text{ and } \mathbf{x}_2^M = [\mathbf{x}_2^T[0], \mathbf{x}_2^T[1], \dots, \mathbf{x}_2^T[M-1]]^T.$$

They provide the decoder with descriptions  $T_{1,M} \in \mathcal{T}_{1,M}$  and  $T_{2,M} \in \mathcal{T}_{2,M}$  by means of *encoding functions*

$$f_{1,M} : \mathbb{C}^{MN_1} \rightarrow \mathcal{T}_{1,M} \quad \text{and} \quad f_{2,M} : \mathbb{C}^{MN_2} \rightarrow \mathcal{T}_{2,M}, \quad (3.2)$$

where  $\mathcal{T}_{1,M} = \{1, 2, \dots, 2^{MR_1}\}$  and  $\mathcal{T}_{2,M} = \{1, 2, \dots, 2^{MR_2}\}$ . The descriptions provided by the first and the second terminal thus appear at a rate of  $R_1$  and  $R_2$  bits per vector, respectively. The decoder reconstructs, as a function of the descriptions  $T_{1,M}$  and  $T_{2,M}$ , the sequence  $\hat{\mathbf{s}}^M \in \mathbb{C}^{MP}$  given by

$$\hat{\mathbf{s}}^M = [\hat{\mathbf{s}}^T[0], \hat{\mathbf{s}}^T[1], \dots, \hat{\mathbf{s}}^T[M-1]]^T,$$

by means of a *decoding function*

$$g_M : \mathcal{T}_{1,M} \times \mathcal{T}_{2,M} \rightarrow \mathbb{C}^{MP}. \quad (3.3)$$

The reconstructed sequence thus follows as

$$\hat{\mathbf{s}}^M = g_M (f_{1,M}(\mathbf{x}_1^M), f_{2,M}(\mathbf{x}_2^M))$$

and the average mean squared error is given by

$$\mathcal{E} \left\{ \|\mathbf{s}^M - \hat{\mathbf{s}}^M\|^2 \right\} = \frac{1}{M} \sum_{m=0}^{M-1} \mathcal{E} \left\{ \|\mathbf{s}[m] - \hat{\mathbf{s}}[m]\|^2 \right\}. \quad (3.4)$$

The compression problem consists in finding the encoding functions (3.2) and the decoding function (3.3) that minimize the distortion (3.4) for fixed communications rates  $R_1, R_2$ , in the limit as  $M \rightarrow \infty$ . This optimization problem is difficult and the optimal processing strategy is unknown to date. In Section 3.3.2, we will propose an iterative method that allows obtaining suboptimal solutions.

### 3.3 Local Optimality for Memoryless Vector Sources

#### 3.3.1 Linear Approximation

Let us assume that one of the two terminals (say terminal 2) provides a fixed approximation  $\mathbf{y}_2$  of its local observation by means of a linear transform. Our goal is to find the optimal matrix  $\mathbf{K}_1 \in \mathbb{C}^{K_1 \times N_1}$  to apply at the first terminal. To this end, let us define the *local approximation transform*  $\mathbf{A}_1 \in \mathbb{C}^{N_1 \times N_1}$  as

$$\mathbf{A}_1 = \mathbf{U}_1^H \mathbf{R}_{s\bar{\mathbf{x}}_1} \mathbf{R}_{\bar{\mathbf{x}}_1}^{-1}, \quad (3.5)$$

where  $\bar{\mathbf{x}}_1$  is given by  $\bar{\mathbf{x}}_1 = \mathbf{x}_1 - \mathbf{R}_{x_1 y_2} \mathbf{R}_{y_2}^{-1} \mathbf{y}_2$  and  $\mathbf{U}_1 \in \mathbb{C}^{N_1 \times N_1}$  is the unitary matrix whose columns are the eigenvectors of  $\mathbf{R}_{s|y_2} - \mathbf{R}_{s|x_1, y_2}$  that correspond to the  $N_1$  largest eigenvalues arranged in decreasing order. The operational relevance of the local approximation transform stems from the following result.

**Theorem 3.1.** The optimal transform matrix  $\mathbf{K}_1 \in \mathbb{C}^{K_1 \times N_1}$  is given by the first  $K_1$  rows of the local approximation transform  $\mathbf{A}_1$ . The resulting mean squared distortion is given by

$$D_{N_1}(K_1) = \text{tr}(\mathbf{R}_{s|x_1, y_2}) + \sum_{k=K_1+1}^{N_1} \lambda_k, \quad (3.6)$$

where  $\lambda_k$  denote the  $N_1$  largest eigenvalues of  $\mathbf{R}_{s|y_2} - \mathbf{R}_{s|x_1, y_2}$  arranged in decreasing order.

**Proof:** See Appendix 3.A.1. ■

Note that the local approximation transform  $\mathbf{A}_1$  is not unique if the eigenvalues  $\lambda_k$  are not all distinct. Nevertheless, any local approximation transform allows obtaining the distortion (3.6).

The local approximation transform can be interpreted as follows. It is designed such that, if  $\bar{\mathbf{x}}_1$  were observable at the terminal (or equivalently the side information  $\mathbf{y}_2$ ), the product  $\mathbf{A}_1 \bar{\mathbf{x}}_1$  would be tantamount to (i) compute the mean square optimal estimation of  $\mathbf{s}$  given  $\bar{\mathbf{x}}_1$  and (ii) apply a KLT on this estimate. Less formally, the encoder would send the part of  $\mathbf{s}$  that can be predicted by  $\mathbf{x}_1$  but not by  $\mathbf{y}_2$ . Since  $\bar{\mathbf{x}}_1$  is not available in our scenario,  $\mathbf{A}_1$  is directly applied to  $\mathbf{x}_1$ . Nevertheless, it is seen in the proof of Theorem 3.1 that the availability of the side information vector  $\mathbf{y}_2$  at both the encoder

---

**Algorithm 3.1:** Linear approximation (memoryless vector sources)

---

**Input:** A fixed tolerance  $\epsilon$  and initial matrices  $\mathbf{K}_1^{(0)}$  and  $\mathbf{K}_2^{(0)}$  of size  $K_1 \times N_1$  and  $K_2 \times N_2$ , respectively.

**Output:** Approximation matrices  $\mathbf{K}_1$  and  $\mathbf{K}_2$  and resulting distortion  $D$ .

**Procedure:**

```

Set  $i = 1$ .
while true
  for  $t = 1, 2$  do
    Compute  $\mathbf{K}_t^{(i)}$  from Theorem 3.1.
  end for
  Compute  $D^{(i)}$  from Theorem 3.1.
  if  $|D^{(i)} - D^{(i-1)}| < \epsilon$  then
    return  $\mathbf{K}_1 = \mathbf{K}_1^{(i)}$ ,  $\mathbf{K}_2 = \mathbf{K}_2^{(i)}$  and  $D = D^{(i)}$ .
  end if
  Set  $i = i + 1$ .
end while

```

---

and decoder would result in the same approximation error. In particular, the minimum distortion  $\mathbf{tr}(\mathbf{R}_{\mathbf{s}|x_1, y_2})$  in (3.6) corresponds to the part of  $\mathbf{s}$  that can be estimated neither by  $\mathbf{x}_1$  nor by  $\mathbf{y}_2$ , while the sum corresponds to the subspace approximation error.

Similarly to the iterative algorithms developed in [50, 122, 155], the local perspective offered by Theorem 3.1 suggests an iterative approach to the quest of an optimal distributed architecture. Namely, the two terminals select arbitrary initial transform matrices of size  $K_1 \times N_1$  and  $K_2 \times N_2$ , respectively. In turn, each terminal then updates its transform following Theorem 3.1. Note that Theorem 3.1 is stated from the perspective of the first terminal. It should be clear that an optimal transform for the second terminal is obtained by simply exchanging the role of the two terminals. This strategy allows us to replace the original bi-dimensional block-component optimization problem by an iterative one-dimensional block-component minimization task for which conclusive results can be found. The method is summarized in Algorithm 3.1. As in [50, Th. 9], Algorithm 3.1 imposes no restriction on the matrix  $\mathbf{K}_t$  such that, at each iteration, the overall distortion cannot increase. The algorithm is thus guaranteed to converge. However, its outcome may not necessarily be a global minimum of the cost function, but just a stationary point that is either a local minimum or a saddle point. To illustrate this fact, we will now consider a simple numerical example.

**Example 3.1.** Suppose that the source  $\mathbf{s}$  is a Gaussian random vector with mean zero and covariance matrix

$$\mathbf{R}_s = \begin{bmatrix} 1 & \rho \\ \rho & 1 \end{bmatrix},$$

for some correlation parameter  $\rho \in (0, 1)$ . The observed vectors  $\mathbf{x}_1$  and  $\mathbf{x}_2$  are

noisy version of the source, that is

$$\mathbf{x}_1 = \mathbf{s} + \mathbf{n}_1 \quad \text{and} \quad \mathbf{x}_2 = \mathbf{s} + \mathbf{n}_2,$$

where  $\mathbf{n}_t$  is a Gaussian random vector with mean zero and covariance matrix  $\mathbf{R}_{n_t} = \sigma^2 \mathbf{I}_2$  for  $t = 1, 2$  with  $\mathbf{I}_2$  the identity matrix of size  $2 \times 2$ . The vectors  $\mathbf{s}$ ,  $\mathbf{n}_1$  and  $\mathbf{n}_2$  are assumed to be independent. Both terminals are required to provide a one-dimensional approximation of their observation. Since the performance is invariant under scaling, the transforms applied at the terminals may be parameterized as

$$\mathbf{K}_1 = [\cos \vartheta \quad \sin \vartheta] \quad \text{and} \quad \mathbf{K}_2 = [\cos \psi \quad \sin \psi],$$

for some scalar  $\vartheta$  and  $\psi$ . We plot in Figure 3.2(a) the distortion surface obtained for  $\rho = 0.5$  and  $\sigma = 1$ . A top view of a portion of the optimization surface is depicted in Figure 3.2(b). We observe that the point  $(\vartheta_0, \psi_0)$  corresponds to a local minimum along both (optimization) directions  $\vartheta$  and  $\psi$ , but only a saddle point of the overall cost function. Algorithm 3.1 will thus stop if it reaches this point, yielding a suboptimal solution in this case. Probabilistic methods, such as simulated annealing [84], may be used to increase the probability of reaching the global optimum. A thorough exposure of such techniques is however beyond the scope of this work.  $\square$

### 3.3.2 Compression

Let us now turn our attention to the compression problem. We assume that the compressed data provided by the second terminal to the decoder is fixed and that it can be modeled as a sequence of  $M$  i.i.d. random vectors. We represented it using the stacked vector  $\mathbf{y}_2^M \in \mathbb{C}^{MN_2}$  defined as

$$\mathbf{y}_2^M = [\mathbf{y}_2^T[0], \mathbf{y}_2^T[1], \dots, \mathbf{y}_2^T[M-1]]^T,$$

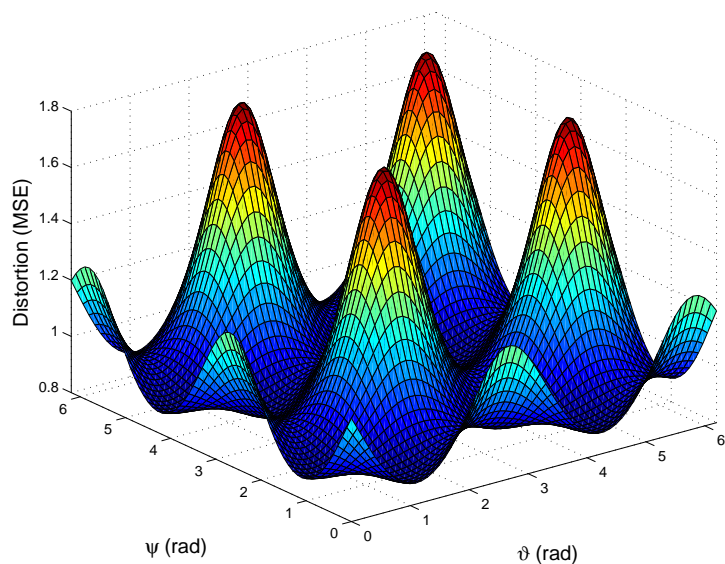
where  $\mathbf{y}_2[m] \in \mathbb{C}^{N_2}$  are Gaussian random vectors with mean zero and covariance matrix  $\mathbf{R}_{y_2}$ . Moreover,  $\mathbf{x}_2[m]$  and  $\mathbf{y}_2[m]$  are assumed to be jointly Gaussian. The above assumptions are verified, for example, if the second terminal optimally encodes its sequence disregarding the presence of the first terminal. The first terminal wants to encode the sequence  $\mathbf{x}_1^M$  using  $R_{N_1}$  bits per vector. We denote by  $D_{N_1}$  the minimum achievable MSE distortion in the limit of large  $M$ . The optimal rate-distortion trade-off is given by the remote Wyner-Ziv rate-distortion function which can be obtained by means of the minimization task [152, Th. 2]

$$D_{N_1} = \min_{\mathbf{y}_1 \in \mathcal{Y}_1} \mathcal{E} \left\{ \|\mathbf{s} - \mathcal{E} \{ \mathbf{s} | \mathbf{y}_1, \mathbf{y}_2 \} \|^2 \right\}, \quad (3.7)$$

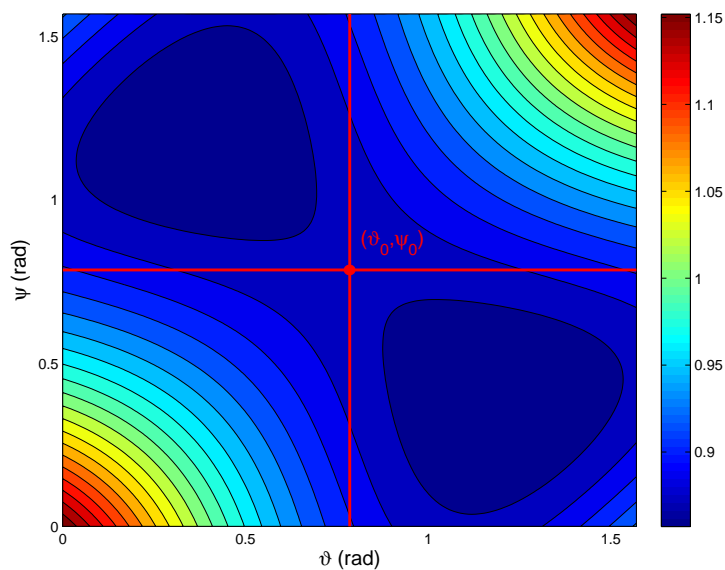
where  $\mathcal{Y}_1$  is the set of random vectors  $\mathbf{y}_1$  such that  $(\mathbf{s}, \mathbf{y}_2) \longrightarrow \mathbf{x}_1 \longrightarrow \mathbf{y}_1$  and

$$I(\mathbf{x}_1; \mathbf{y}_1 | \mathbf{y}_2) \leq R_{N_1}. \quad (3.8)$$

The notation  $\mathbf{x} \longrightarrow \mathbf{y} \longrightarrow \mathbf{z}$  means that the vectors  $\mathbf{x}$ ,  $\mathbf{y}$  and  $\mathbf{z}$  form a Markov chain, that is,  $\mathbf{x}$  and  $\mathbf{z}$  are independent conditionally on  $\mathbf{y}$ . Under our Gaus-



(a)



(b)

**Figure 3.2:** Distortion surface of Example 3.1 with  $\rho = 0.5$  and  $\sigma = 1$ . (a) Cost function to be minimized. (b) Top-view of a portion of the optimization surface. The point  $(\vartheta_0, \psi_0)$  is a local minimum along both the optimization directions  $\vartheta$  and  $\psi$  (indicated by the horizontal and vertical lines) but only to a saddle point of the overall cost function.

sian assumptions, the solution to the above minimization problem evaluates as follows.

**Theorem 3.2.** The quadratic remote Wyner-Ziv rate-distortion function for memoryless jointly Gaussian vector sources is given in parametric form by

$$D_{N_1}(\theta) = \mathbf{tr}(\mathbf{R}_{s|x_1, y_2}) + \sum_{k=1}^{N_1} \min\{\theta, \lambda_k\}, \quad (3.9)$$

$$R_{N_1}(\theta) = \sum_{k=1}^{N_1} \max\left\{0, \frac{1}{2} \log_2 \frac{\lambda_k}{\theta}\right\}, \quad (3.10)$$

with  $\theta \in (0, \max_k \lambda_k]$ , where  $\lambda_k$  denote the  $N_1$  largest eigenvalues of  $\mathbf{R}_{s|y_2} - \mathbf{R}_{s|x_1, y_2}$ .  $R_{N_1}(\theta)$  is expressed in bits per vector and  $D_{N_1}(\theta)$  in MSE per vector.

**Proof:** See Appendix 3.A.2. ■

It can be checked that an optimal encoding architecture consists in (i) applying the local approximation transform  $\mathbf{A}_1$  given by (3.5) to every vector of the sequence  $\mathbf{x}_1[m]$  and (ii) encode separately the components of the transformed sequence in a Wyner-Ziv optimal fashion. In other words, the local approximation transform allows reducing the remote rate-distortion problem for vector sources to  $N_1$  separate direct scalar source compression tasks. It thus plays the same role as the KLT in the centralized coding scenario. The rate allocation among the components is achieved by means of a reverse water-filling strategy (see Section 2.3). As a consequence of this fact, the vector  $\mathbf{y}_1$  solution to the optimization problem (3.7) follows as

$$\mathbf{y}_1 = \mathbf{K}_1 \mathbf{x}_1 + \mathbf{z}_1. \quad (3.11)$$

The matrix  $\mathbf{K}_1 \in \mathbb{C}^{K_1 \times N_1}$  contains the first  $K_1$  rows of the local approximation transform  $\mathbf{A}_1$ , where  $K_1$  is the largest integer satisfying  $\lambda_{K_1} > \theta$ . The additive quantization noise vector  $\mathbf{z}_1 \in \mathbb{C}^{K_1}$  is Gaussian, independent from  $\mathbf{x}_1$ , with mean zero and covariance matrix

$$\mathbf{R}_{z_1} = \text{diag}\left(\frac{\lambda_1 \theta}{\lambda_1 - \theta}, \frac{\lambda_2 \theta}{\lambda_2 - \theta}, \dots, \frac{\lambda_{K_1} \theta}{\lambda_{K_1} - \theta}\right).$$

The relation (3.11), sometimes referred to as the optimum forward test channel [29, Sec. 13.3.2], reveals that the vector  $\mathbf{y}_1$  is jointly Gaussian with  $\mathbf{x}_1$ , hence with  $\mathbf{x}_2$ . With appropriate initialization, the result of Theorem 3.2 can thus be used iteratively to obtain Algorithm 3.2. A few important remarks are however at hand. First, the update of the second terminal at iteration  $i$  should be such that condition (3.8) remains valid for the first terminal at iteration  $i + 1$ . A sufficient condition is to check that

$$I(\mathbf{x}_1; \mathbf{y}_1) \leq R_1[i + 1], \quad (3.12)$$

that is, without conditioning on  $\mathbf{y}_2$  as it is the case in (3.8). If  $R_1[i + 1]$  is not large enough, no update occurs. The same remark applies to terminal 1. It may hence happen that the rate targeted by the chosen rate schedule cannot be attained. However, since the rate schedules  $R_1[i]$  and  $R_2[i]$  are nondecreasing sequences, the solution at iteration  $i$  remains in the optimization space at



---

**Algorithm 3.2:** Compression (memoryless vector sources)

---

**Input:** Non-decreasing rate schedules  $R_t[i]$  with  $R_t[0] = 0$  and  $R_t[i] \leq R_t$ , for  $t = 1, 2$  and  $i = 1, 2, \dots, I$ .

**Output:** Forward test channels ( $\mathbf{K}_t$  and  $\mathbf{R}_{z_t}$  for  $t = 1, 2$ ) and resulting distortion  $D$ .

**Procedure:**

```

Set  $\mathbf{K}_t^{(0)} = \mathbf{O}_{1 \times N_t}$  and  $\mathbf{R}_{z_t}^{(0)} = \mathbf{O}_{1 \times 1}$  for  $t = 1, 2$ .
for  $i = 1, 2, \dots, I$  do
  for  $t = 1, 2$  do
    if condition (3.12) is satisfied then
      Compute  $\mathbf{K}_t^{(i)}$  and  $\mathbf{R}_{z_t}^{(i)}$  from (3.11).
    end if
  end for
  Compute  $D^{(i)}$  from Theorem 3.2.
end for
return  $\mathbf{K}_t = \mathbf{K}_t^{(I)}$ ,  $\mathbf{R}_{z_t} = \mathbf{R}_{z_t}^{(I)}$  and  $D = D^{(I)}$  for  $t = 1, 2$ .

```

---

iteration  $i + 1$ . This guarantees that the overall distortion cannot increase, hence the local convergence of Algorithm 3.2. Also, while the initial assumption of jointly Gaussian vectors allows us to apply Theorem 3.2 iteratively, it may not be the optimal choice. Finally, the forward test channels provided by the algorithm depend on the chosen rate schedules. In particular, if  $R_1[1] = R_1$  and  $R_2[1] = R_2$  (one iteration), only one terminal benefits from the data transmitted by the other terminal, that is, using distributed source coding principles. Rate schedules with multiple iterations promote more “balanced” scenarios, as it will be seen in Section 3.5.4.

## 3.4 Local Optimality for Discrete-Time Sources with Memory

### 3.4.1 Linear Approximation

In Section 3.3, we addressed the problem of distributed estimation of vector sources in both the linear approximation and compression frameworks. We now extend these results to the case of discrete-time sequences by letting the size of the vectors go to infinity. To this end, we assume that the desired vector  $\mathbf{s}$  and observed vectors  $\mathbf{x}_1$  and  $\mathbf{x}_2$  are of equal length  $N$ . In the limit of large  $N$ , these vectors are described by discrete-time sequences  $s[n]$ ,  $x_1[n]$  and  $x_2[n]$ , respectively. To obtain conclusive results, we assume that these random sequences are stationary jointly Gaussian processes with mean zero and power spectral densities  $P_s(\omega)$ ,  $P_{x_1}(\omega)$  and  $P_{x_2}(\omega)$ , respectively.

Under these asymptotic considerations, let us again adopt a local perspective to the approximation problem. The first terminal observes the sequence  $x_1[n]$  and provides the decoder with a description of size  $K_1 = \lfloor \alpha_1 N \rfloor$  with  $\alpha_1 \in [0, 1]$ , that is, only a fraction  $\alpha_1$  of transformed coefficients is kept, where  $\lfloor \cdot \rfloor$  denotes the floor operation. It is worth noting that both the size of the

observed and transformed vectors go to infinity whereas the ratio remains constant and is given by<sup>1</sup>  $\alpha_1 \sim K_1/N$ . The transformation is achieved by means of a linear and time-invariant filter  $k_1[n]$  with transfer function  $K_1(\omega)$ . By strict analogy to the vector case, we wish to find the optimal filter  $k_1[n]$  assuming that the process provided by the second terminal is fixed and is given by

$$y_2[n] = k_2[n] * x_2[n],$$

for some filter  $k_2[n]$ . Here,  $*$  denotes the convolution operator. To this end, let us define the power spectral density  $P_1(\omega)$  as

$$P_1(\omega) = P_{s|y_2}(\omega) - P_{s|x_1, y_2}.$$

We assume the set over which  $P_1(\omega)$  is constant to be of measure zero. This condition ensures the continuity of the limiting eigenvalue distribution  $p_1(u)$  given by [59, Cor. 4.1]

$$p_1(u) = \frac{1}{2\pi} \int_{\omega \in \mathcal{X}} d\omega,$$

where  $\mathcal{X} = \{\omega \in [0, 2\pi] : P_1(\omega) \leq u\}$ . We also define the set  $\mathcal{A}_1$  as

$$\mathcal{A}_1 = \{\omega \in [0, 2\pi] : P_1(\omega) > \theta\}, \quad (3.13)$$

where  $\theta$  satisfies  $p_1(\theta) = 1 - \alpha_1$ . The complementary set of  $\mathcal{A}_1$  in  $[0, 2\pi]$  is denoted by  $\mathcal{A}_1^c$ . Furthermore, we define the process  $\bar{x}_1[n]$  as

$$\bar{x}_1[n] = x_1[n] - h_2[n] * y_2[n],$$

where the transfer function of  $h_2[n]$  is given by  $H_2(\omega) = P_{x_1 y_2}(\omega) P_{y_2}^{-1}(\omega)$ . For simplicity, we assume that the involved power spectral densities are non-zero almost everywhere. Under our asymptotic considerations, the minimum achievable distortion is computed as

$$D_1(\alpha_1) = \lim_{N \rightarrow \infty} \frac{1}{N} D_N(K_1), \quad (3.14)$$

if the limit exists. The distortion  $D_N(K_1)$  follows from (3.6). The optimal filter at the first terminal can be characterized by means of the *linear approximation filter*  $a_1[n]$  whose transfer function  $A_1(\omega)$  is given by

$$A_1(\omega) = P_{s\bar{x}_1}(\omega) P_{\bar{x}_1}^{-1}(\omega).$$

Denoting by  $1_{\mathcal{A}_1}(\omega)$  the indicator function on the set  $\mathcal{A}_1$ , the optimal strategy can be described as follows.

**Theorem 3.3.** The transfer function  $K_1(\omega)$  of the optimal filter  $k_1[n]$  that retains only a fraction  $\alpha_1$  of transformed coefficients is obtained as

$$K_1(\omega) = A_1(\omega) 1_{\mathcal{A}_1}(\omega). \quad (3.15)$$

---

<sup>1</sup>The notation  $\alpha_1 \sim K_1/N$  means that  $\lim_{N \rightarrow \infty} K_1/N = \alpha_1$ .

The resulting distortion  $D_1(\alpha_1)$  follows as

$$D_1(\alpha_1) = \frac{1}{2\pi} \int_{\omega \in [0, 2\pi]} P_{s|x_1, y_2}(\omega) d\omega + \frac{1}{2\pi} \int_{\omega \in \mathcal{A}_1^c} P_{s|y_2}(\omega) - P_{s|x_1, y_2}(\omega) d\omega. \quad (3.16)$$

**Proof:** See Appendix 3.A.3. ■

The optimal strategy hence amounts to filtering the process  $x_1[n]$  by  $a_1[n]$  and to bandlimit the result such that the set of retained frequencies  $\mathcal{A}_1$  is of measure  $2\pi\alpha_1$ . The choice of these frequencies is given by  $P_1(\omega)$  which depends on the process  $y_2[n]$  provided by the second terminal. Actually, it is seen in the proof of Theorem 3.3 that the term  $A_1(\omega)$  is not needed for optimality as it is assumed to be non-zero almost everywhere. We provide it here by analogy to the finite dimensional case. Note also that, in a strictly analogous manner to (3.6), the distortion given by (3.16) is the sum of a first term that is not influenced by the first terminal, and a second term that amounts to integrating the frequency components of  $P_1(\omega)$  that are below an admissible threshold  $\theta$ . The relationship between  $\alpha_1$  and  $\theta$  is given by the limiting eigenvalue distribution  $p_1(u)$ . As  $\alpha_1$  ranges from 0 to 1,  $\theta$  scopes from the essential infimum to the essential supremum of  $P_1(\omega)$  as dictated by the relation

$$p_1(\theta) = 1 - \alpha_1. \quad (3.17)$$

This is illustrated in Figure 3.3(a). Analytical computations thus require finding  $\theta$  satisfying (3.17). This is generally difficult. However, if  $P_1(\omega)$  is symmetric and monotonic in  $[0, \pi]$ , then a simple geometrical argument reveals that the set  $\mathcal{A}_1$  in (3.13) can be expressed as

$$\mathcal{A}_1 = [0, \pi\alpha_1] \cup (2\pi - \pi\alpha_1, 2\pi], \quad (3.18)$$

if  $P_1(\omega)$  is *decreasing* in  $[0, \pi]$  (see Figure 3.3(b)), and

$$\mathcal{A}_1 = (\pi(1 - \alpha_1), \pi(1 + \alpha_1)),$$

if  $P_1(\omega)$  is *increasing* in  $[0, \pi]$ . Interestingly, under these restrictive assumptions, the knowledge of the limiting eigenvalue distribution is not required to compute the distortion. This will greatly simplify the derivation presented in Section 3.5.

As in the vector case, Theorem 3.3 can be used to describe the optimal step of the iterative procedure summarized in Algorithm 3.3. If the assumptions of the above theorem are satisfied at initialization, the consecutive steps simply amount to chose the optimal filters  $K_1^{(i)}(\omega)$  and  $K_2^{(i)}(\omega)$  as described by Theorem 3.3. In this case, the quest for optimality amounts to bandpass filtering, in turn at each terminal, the observed spectrum with respect to what is provided by the other terminal. The algorithm thus reduces to a “spectrum shaping game” whose outcome provides the necessary filters. Similarly to Section 3.3.1, it is important to point out that the particular initialization imposed by Theorem 3.3 may lead Algorithm 3.3 to a suboptimal solution. The design of an optimal distributed dimensionality reduction architecture thus remains a

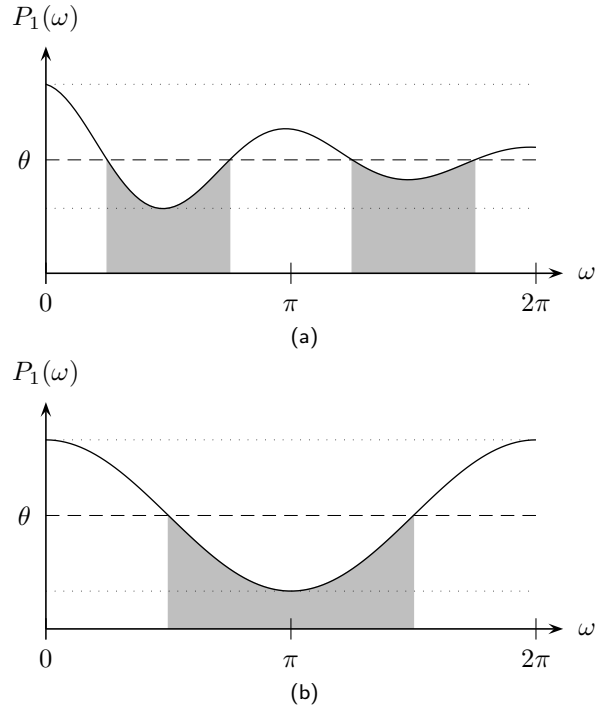


**Figure 3.3:** Integration as a function of the fraction of retained coefficients  $\alpha_1$ . (a)  $P_1(\omega)$  is arbitrary. (b)  $P_1(\omega)$  is symmetric around  $\pi$  and decreasing in  $[0, \pi]$ . As  $\alpha_1$  ranges from 0 to 1,  $\theta$  scopes from the essential infimum to the essential supremum of  $P_1(\omega)$  according to the relation  $p_1(\theta) = 1 - \alpha_1$ .

---

**Algorithm 3.3:** Linear approximation (discrete-time sources with memory)

---

**Input:** A fixed tolerance  $\epsilon$ , filters  $K_1^{(0)}(\omega)$  and  $K_2^{(0)}(\omega)$  such that the sets  $\mathcal{A}_1$  and  $\mathcal{A}_2$  are of measure  $2\pi\alpha_1$  and  $2\pi\alpha_2$ , respectively.

**Output:** Filters  $K_1(\omega)$  and  $K_2(\omega)$  and resulting distortion  $D$ .

**Procedure:**

```

Set  $i = 1$ .
while true
  for  $t = 1, 2$  do
    Compute  $K_t^{(i)}(\omega)$  from Theorem 3.3.
  end for
  Compute  $D^{(i)}$  from Theorem 3.3.
  if  $|D^{(i)} - D^{(i-1)}| < \epsilon$  then
    return  $K_1(\omega) = K_1^{(i)}(\omega)$ ,  $K_2(\omega) = K_2^{(i)}(\omega)$  and  $D = D^{(i)}$ .
  end if
  Set  $i = i + 1$ .
end while

```

---

challenging task.

### 3.4.2 Compression

Let us now turn to the compression problem. The first terminal observes the sequence  $x_1[n]$  and provides the decoder with a bit stream that appears at a rate of  $R_1$  bits per sample. We assume that the description provided by the second terminal is fixed and can be modeled as a discrete-time stationary Gaussian process  $y_2[n]$  with mean zero and power spectral density  $P_{y_2}(\omega)$ . As in the finite dimensional regime, we further assume that  $x_2[n]$  and  $y_2[n]$  are jointly Gaussian. The optimal rate-distortion trade-off is computed as

$$D_1(\theta) = \lim_{N \rightarrow \infty} \frac{1}{N} D_N(\theta) \quad \text{and} \quad R_1(\theta) = \lim_{N \rightarrow \infty} \frac{1}{N} R_N(\theta), \quad (3.19)$$

if the limits exist. The terms  $D_N(\theta)$  and  $R_N(\theta)$  follow from (3.9) and (3.10), respectively. These limits can be directly computed from Theorem 3.2 and the Toeplitz distribution theorem [59, Th. 4.2] as follows.

**Theorem 3.4.** The quadratic remote Wyner-Ziv rate-distortion function for jointly Gaussian discrete-time sources with memory is given in parametric form by

$$D_1(\theta) = \frac{1}{2\pi} \int_0^{2\pi} P_{s|x_1, y_2}(\omega) d\omega + \frac{1}{2\pi} \int_0^{2\pi} \min\{\theta, P_{s|y_2}(\omega) - P_{s|x_1, y_2}(\omega)\} d\omega, \quad (3.20)$$

$$R_1(\theta) = \frac{1}{4\pi} \int_0^{2\pi} \max\left\{0, \log_2 \frac{P_{s|y_2}(\omega) - P_{s|x_1, y_2}(\omega)}{\theta}\right\} d\omega, \quad (3.21)$$

with  $\theta \in (0, \text{ess sup}_\omega P_{s|y_2}(\omega) - P_{s|x_1, y_2}(\omega)]$ .  $R_1(\theta)$  is expressed in bits per sample and  $D_1(\theta)$  in MSE per sample.

**Proof:** See Appendix 3.A.4. ■

In an analogous manner to Theorem 3.2, the allocation of the rate is achieved by means of a reverse water-filling strategy on the power spectral density  $P_1(\omega) = P_{s|y_2}(\omega) - P_{s|x_1, y_2}(\omega)$ . Moreover, the compressed sequence  $y_1[n]$  provided by the first terminal is given by

$$y_1[n] = k_1[n] * x_1[n] + z_1[n]. \quad (3.22)$$

The filter  $k_1[n]$  is the optimal filter derived in Theorem 3.3 where the fraction of retained coefficients  $\alpha_1$  is chosen according to (3.17). The additive quantization noise  $z_1[n]$  is a Gaussian random process, independent from  $x_1[n]$ , with mean zero and power spectral density

$$P_{z_1}(\omega) = \frac{\theta P_1(\omega)}{P_1(\omega) - \theta} 1_{\mathcal{A}_1}(\omega),$$

where the set  $\mathcal{A}_1$  is defined in (3.13). For completeness, the iterative procedure obtained from Theorem 3.4 is summarized in Algorithm 3.4. Note that the

**Algorithm 3.4:** Compression (discrete-time sources with memory)

**Input:** Non-decreasing rate schedules  $R_t[i]$  with  $R_t[0] = 0$  and  $R_t[i] \leq R_t$  for  $t = 1, 2$  and  $i = 1, 2, \dots, I$ .

**Output:** Forward test channels ( $K_t(\omega)$  and  $P_{z_t}(\omega)$  for  $t = 1, 2$ ) and resulting distortion  $D$ .

**Procedure:**

```

Set  $K_t^{(0)}(\omega) = 0$  and  $P_{z_t}^{(0)}(\omega) = 0$  for  $t = 1, 2$ .
for  $i = 1, 2, \dots, I$  do
  for  $t = 1, 2$  do
    if condition (3.12) is satisfied then
      Compute  $K_t^{(i)}(\omega)$  and  $P_{z_t}^{(i)}(\omega)$  from (3.22).
    end if
  end for
  Compute  $D^{(i)}$  from Theorem 3.4.
end for
return  $K_t(\omega) = K_t^{(I)}(\omega)$ ,  $P_{z_t}(\omega) = P_{z_t}^{(I)}(\omega)$  and  $D = D^{(I)}$  for  $t = 1, 2$ .

```

comments of Section 3.3.2 regarding the choice of appropriate rate schedules also apply here.

### 3.5 Case Study: First-order Autoregressive Process

We apply the results obtained previously to a first-order autoregressive process. Owing to its simplicity, it allows for the derivation of distortion formulas for different scenarios of interest, in both the linear approximation and compression framework. More importantly, it is observed that, in this example, the asymptotic analysis provides an accurate estimation of the distortion incurred with vectors of small dimension. We then relate these analytical results to the general two-terminal achievable distortion surface obtained numerically using the proposed iterative algorithms.

A first-order autoregressive process  $x[n]$  is a random process that satisfies

$$x[n] = \rho x[n-1] + z[n],$$

where  $z[n]$  is white Gaussian noise with mean zero and power spectral density  $P_z(\omega) = 1 - \rho^2$ , and  $\rho \in (0, 1)$  is a correlation parameter<sup>2</sup>. We will consider the case where the first terminal samples the odd coefficients of  $x[n]$  and the second terminal observes the even ones, that is,  $s[n] = x[n]$ ,  $x_1[n] = x[2n+1]$  and  $x_2[n] = x[2n]$ . The sequences  $s[n]$ ,  $x_1[n]$  and  $x_2[n]$  are stationary random processes with mean zero and (cross) power spectral densities given by

$$P_s(\omega) = \frac{1 - \rho^2}{1 + \rho^2 - 2\rho \cos \omega}, \quad P_{x_1}(\omega) = P_{x_2}(\omega) = \frac{1 - \rho^4}{1 + \rho^4 - 2\rho^2 \cos \omega}$$

<sup>2</sup>The case  $\rho \in (-1, 0)$  follows immediately by considering  $|\rho|$ .

and

$$P_{x_1 x_2}(\omega) = \frac{\rho(1 - \rho^2)(1 + e^{-j\omega})}{1 + \rho^4 - 2\rho^2 \cos \omega}.$$

This setup could be motivated, for example, by super-resolution imaging problems [139]. Two sub-sampled versions of the same image are acquired by cheap sensing devices in order to build a higher resolution image. In this case, correlation (hence stationarity) is considered across space. The analysis of the distortion in this scenario allows for the computation of the gain achieved when a low-resolution image is used as perfect side information, that is, when one terminal entirely conveys its observed signal to the decoder. It also gives a useful characterization of the loss incurred due to the need of interpolating missing samples, that is, when one terminal does not transmit anything.

### 3.5.1 Centralized Scenario

We first consider the centralized scenario where the two terminals are allowed to process their observations jointly.

In the linear approximation framework, the observed process is  $s[n]$  and a fraction  $\alpha$  of transformed coefficients is kept. The resulting distortion, denoted by  $D_c(\alpha)$ , can be expressed as follows.

**Proposition 3.1.** In the centralized scenario, the distortion due to linear approximation is given by

$$D_c(\alpha) = 1 - \frac{2}{\pi} \arctan\left(\frac{1 + \rho}{1 - \rho} \tan\left(\frac{\pi\alpha}{2}\right)\right),$$

where  $\alpha \in [0, 1]$  denotes the retained fraction of source/observed coefficients.

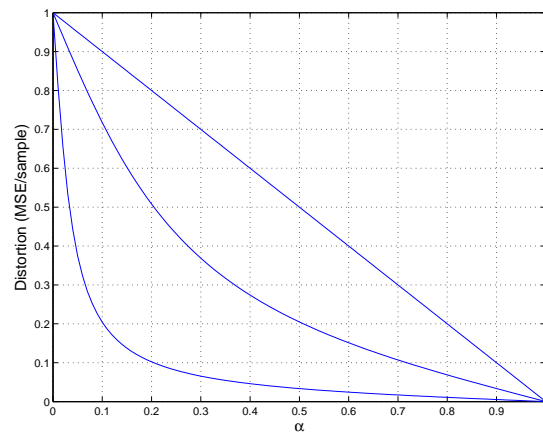
**Proof:** See Appendix 3.A.5. ■

We plot in Figure 3.4(a) the distortion obtained in Proposition 3.1 for different values of the correlation parameter  $\rho$ . Figure 3.4(b) shows how  $D_c(\alpha)$  is approximated for  $\rho = 0.6$  and a block length  $N = 12$ . We observe that even for small values of  $N$ , the proposed asymptotic analysis offers a very good approximation of the distortion in the finite dimensional regime. We also compute in Figure 3.4(c) the approximation error

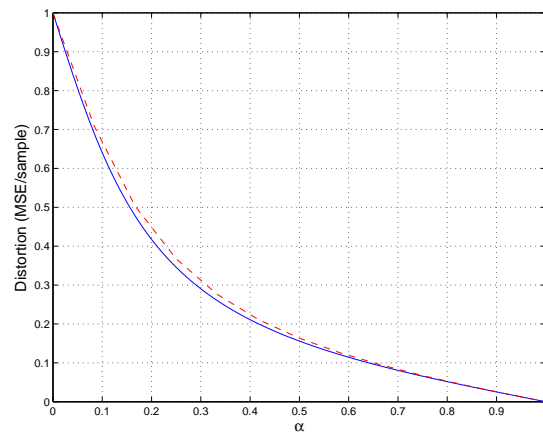
$$e[N] = \frac{1}{N} \sum_{K=0}^{N-1} |D_{c,N}(K) - D_c(K/N)|^2$$

to quantify the quality of the estimate as a function of the size of the vectors. The observed decay suggests that the results obtained by the asymptotic analysis approximate accurately the distortion we would compute with a finite number of measurements. This can be explained by the exponential decay of the correlation function in this particular example.

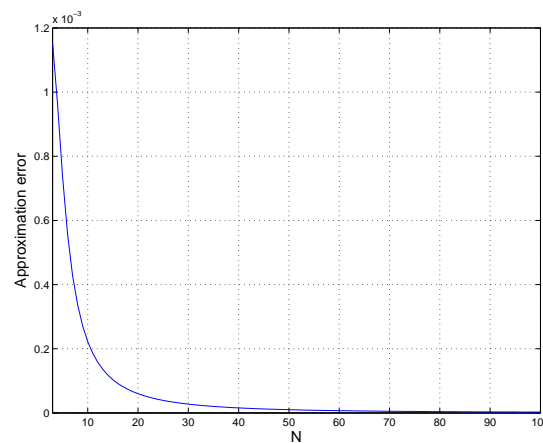
In the compression framework, the observed sequence  $s[n]$  is represented using a bit stream that appears at a rate of  $R$  bits per sample. The optimal distortion-rate trade-off in this case, denoted by  $D_c(R)$ , can be characterized as follows.



(a)



(b)



(c)

**Figure 3.4:** Distortion in the centralized scenario due to linear approximation. (a)  $D_c(\alpha)$  for  $\rho = 0, 0.5, 0.9$  (top to bottom). (b)  $D_c(\alpha)$  (solid) and its approximation (dashed) for  $\rho = 0.6$  and a block length  $N = 12$ . (c) Approximation error  $e[N]$  as a function of the size of the source vector for  $\rho = 0.6$ .



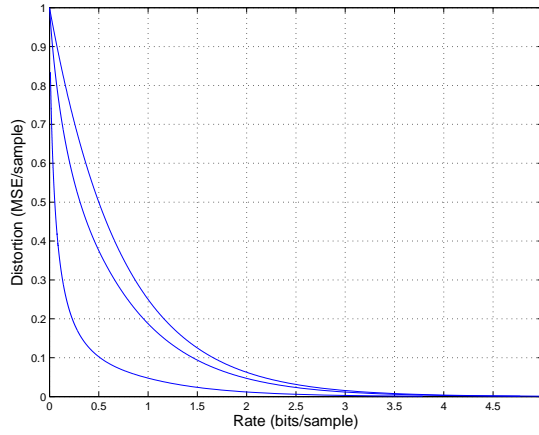


**Figure 3.5:** Distortion rate function in the centralized scenario for  $\rho = 0, 0.5, 0.9$  (top to bottom).

**Proposition 3.2.** In the centralized scenario, the distortion-rate function is given by

$$D_c(R) = (1 - \rho^2) 2^{-2R},$$

where  $R \geq \bar{R} = \log_2(1 + \rho)$  bits per source/observation sample.

**Proof:** See Appendix 3.A.6 or [12, Ex. 4.5.2.2]. ■

When  $R < \bar{R}$ , the function must be left in parameterized form. We plot in Figure 3.5 the distortion-rate function for different values of the correlation parameter  $\rho$ . Distortions for rates smaller than  $\bar{R}$  are obtained numerically.

### 3.5.2 Perfect Side Information Scenario

Let us now consider the case where the first terminal needs to describe the signal  $x_1[n]$  and that the process  $x_2[n]$  acts as side information, that is, is perfectly conveyed to the decoder.

In the linear approximation framework, the distortion, denoted by  $D_s(\alpha)$ , can be computed as follows.

**Proposition 3.3.** In the perfect side information scenario, the distortion due to linear approximation is given by

$$D_s(\alpha) = \frac{1 - \rho^2}{2(1 + \rho^2)} (1 - \alpha),$$

where  $\alpha \in [0, 1]$  denotes the retained fraction of observed coefficients.

**Proof:** See Appendix 3.A.7. ■

We depict the distortion  $D_s(\alpha)$  in Figure 3.6(a). It is seen in the proof of Proposition 3.3 that the prediction error of the odd coefficients by the even ones has uncorrelated components, that is, the error process is white. This explains the linear decrease in distortion. When  $x_2[n]$  is completely available at the decoder, the distortion of  $s[n]$  is equivalent to that of  $x_1[n]$  up to a scaling factor  $1/2$ . The above distortion is thus half the reconstruction error

of the process  $x_1[n]$  with  $x_2[n]$  as side information. Also, replacing  $\rho$  by  $\rho^2$  in Proposition 3.1 allows computing the distortion in the absence of side information at the decoder. We compare these two scenarios in Figure 3.6(b). We clearly see the decrease in distortion achieved by providing the decoder with some correlated side information. The exact value can be expressed using Propositions 3.1 and 3.3 with the aforementioned modifications. As  $\rho \rightarrow 0$ , the processes  $x_1[n]$  and  $x_2[n]$  become uncorrelated such that the side information does not allow for any gain. When  $\rho \rightarrow 1$ , the correlation among the components of  $x_1[n]$  allows us to perfectly recover the discarded coefficients without the need for  $x_2[n]$ . Between these two extreme cases, however, a substantial decrease in distortion is achieved by the use of noisy side information. This is illustrated in Figure 3.6(c).

In the compression framework, the optimal distortion-rate trade-off, denoted by  $D_s(R)$ , is given by the following proposition.

**Proposition 3.4.** In the perfect side information scenario, the distortion-rate function is given by

$$D_s(R) = \frac{1 - \rho^2}{2(1 + \rho^2)} 2^{-2R},$$

where  $R \geq 0$  bits per observation sample.

**Proof:** See Appendix 3.A.8. ■

Figure 3.7 depicts the above distortion-rate function for different values of the correlation parameter  $\rho$ .

### 3.5.3 Partial Observation Scenario

We treat now the case where the first terminal needs to represent  $x_1[n]$  taking into account that the process  $x_2[n]$  is completely discarded by the second terminal, that is, is not observable by the decoder.

In the linear approximation framework, the distortion, denoted by  $D_p(\alpha)$ , is given by the following result.

**Proposition 3.5.** In the partial observation scenario, the distortion due to linear approximation is given by

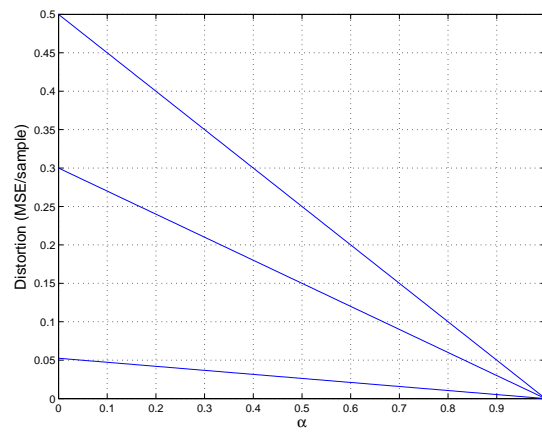
$$D_p(\alpha) = 1 + \frac{\alpha(1 - \rho^2)}{2(1 + \rho^2)} - \frac{2}{\pi} \arctan\left(\frac{1 + \rho^2}{1 - \rho^2} \tan\left(\frac{\pi\alpha}{2}\right)\right),$$

where  $\alpha \in [0, 1]$  denotes the retained fraction of observed coefficients.

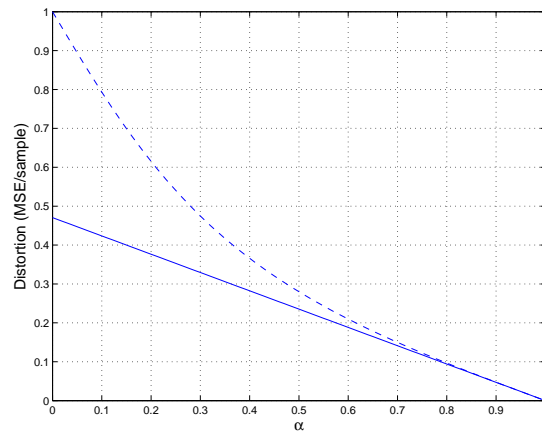
**Proof:** See Appendix 3.A.9. ■

The distortion obtained in Proposition 3.5 is depicted in Figure 3.8(a). We also compare in Figure 3.8(b) the distortion obtained with and without hidden part. We clearly see the increase in distortion incurred by having to reconstruct the missing information at the decoder. Furthermore, increasing  $\rho$  allows us to estimate the missing data with increasing accuracy, hence reducing the gap between the two distortions as shown in Figure 3.8(c). The exact value can be expressed from Proposition 3.5 and by replacing  $\rho$  by  $\rho^2$  and normalizing by a factor 2 the distortion obtained in Proposition 3.1.

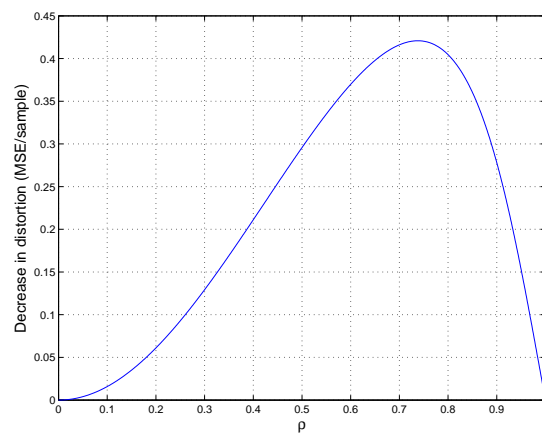
In the compression framework, the distortion-rate function, denoted by  $D_p(R)$ , can be evaluated as follows.



(a)



(b)



(c)

**Figure 3.6:** Distortion in the perfect side information scenario due to linear approximation (re-normalized by a factor  $1/2$ ). (a) Distortion for  $\rho = 0, 0.5, 0.9$  (top to bottom). (b) Distortion with (solid) and without (dashed) side information for  $\rho = 0.6$ . (c) Decrease in distortion due to side information as a function of  $\rho$  for  $\alpha = 0.1$ .

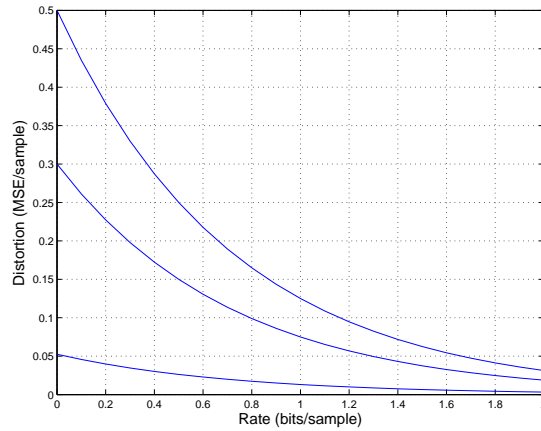


**Figure 3.7:** Distortion rate function in the perfect side information scenario for  $\rho = 0, 0.5, 0.9$  (top to bottom).

**Proposition 3.6.** In the partial observation scenario, the distortion-rate function is given by

$$D_p(R) = \frac{1 - \rho^2}{2(1 + \rho^2)} \left( 1 + \frac{1 + 4\rho^2 + \rho^4 + (1 + \rho^2) \sqrt{1 + 6\rho^2 + \rho^4}}{2} 2^{-2R} \right),$$

where  $R \geq \bar{R} = \frac{1}{2} \left( \log_2 \left( 1 + 4\rho^2 + \rho^4 + (1 + \rho^2) \sqrt{1 + 6\rho^2 + \rho^4} \right) - 1 \right)$  bits per observation sample.

**Proof:** See Appendix 3.A.10. ■

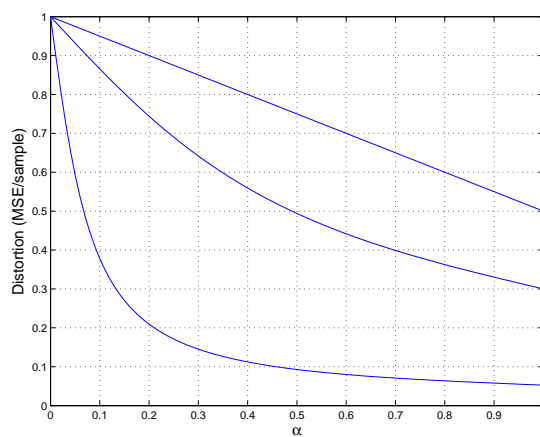
Note again that for rates smaller than  $\bar{R}$ , the function must be left in parametric form. Figure 3.9 depicts the above distortion-rate function for different values of  $\rho$ . Distortions for rates smaller than  $\bar{R}$  are computed numerically.

### 3.5.4 General Scenario

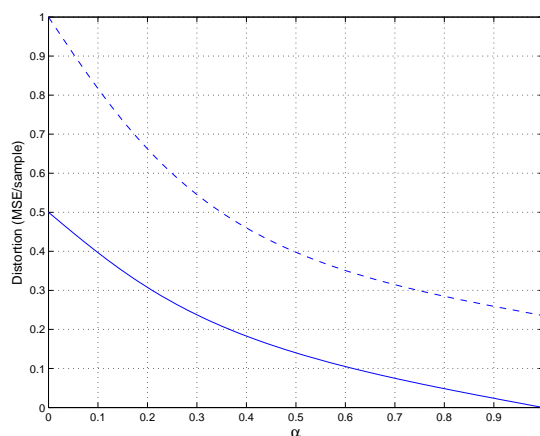
Let us now consider again the general two-terminal setup.

In the linear approximation framework, assume that terminal  $t$  only keeps a fraction  $\alpha_t$  of transformed coefficients. We can then conveniently represent the entire distortion surface as a function of  $\alpha_1$  and  $\alpha_2$ , both taking values in  $[0, 1]$ . This is shown in Figure 3.10 for  $\rho = 0.4$ . The inside of the distortion surface is obtained numerically using Algorithm 3.1 with a block length of size  $N = 20$ . This is an achievable performance, but not necessarily an optimal one. The borders can however be characterized analytically since they correspond to the distortion obtained for the partial observation scenario ( $\alpha_1 = 0$  or  $\alpha_2 = 0$ ) and the perfect side information scenario ( $\alpha_1 = 1$  or  $\alpha_2 = 1$ ). They respectively provide a lower bound and an upper bound to the minimum achievable distortion at the point  $(\alpha_1, \alpha_2)$ . The distortion surface owes its symmetry to the fact that  $P_{x_1}(\omega)$  and  $P_{x_2}(\omega)$  are equal.

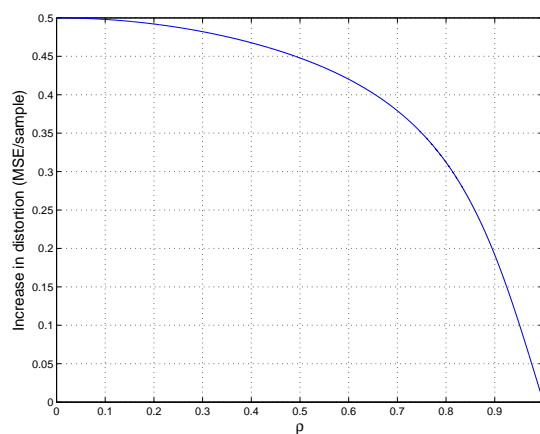
Similarly, Figure 3.11 depicts the distortion achieved in the compression framework as a function of the rates  $R_1$  and  $R_2$  available at the terminals. The



(a)



(b)



(c)

**Figure 3.8:** Distortion due to linear approximation in the partial-observation scenario. (a)  $D_p(\alpha)$  for  $\rho = 0, 0.5, 0.9$  (top to bottom). (b) Distortion with (dashed) and without (solid) hidden part for  $\rho = 0.6$ . (c) Increase in distortion due to the hidden part as a function of  $\rho$  for  $\alpha = 0.1$ .

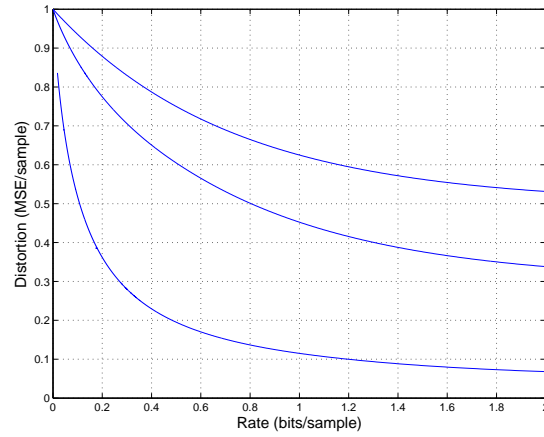


**Figure 3.9:** Distortion rate function in the partial observation scenario for  $\rho = 0, 0.5, 0.9$  (top to bottom).

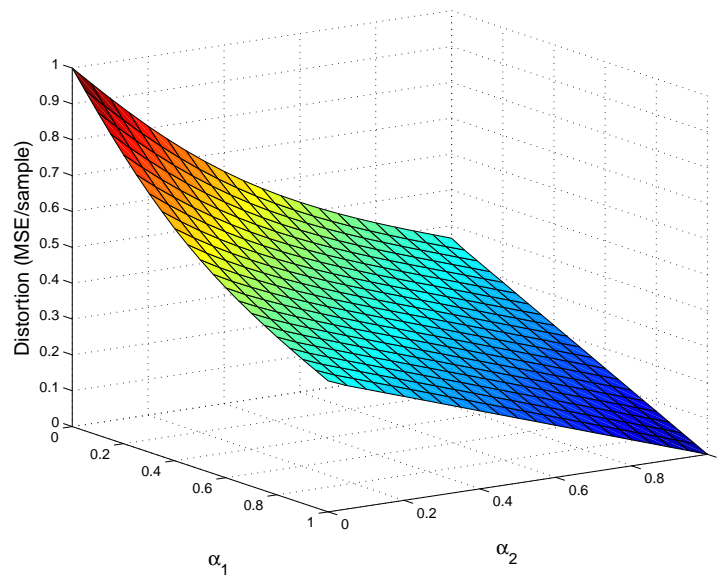


**Figure 3.10:** Achievable distortion due to linear approximation in the general scenario for  $\rho = 0.4$ . The inside of the distortion surface is obtained using Algorithm 3.1 and a block length  $N = 20$ .

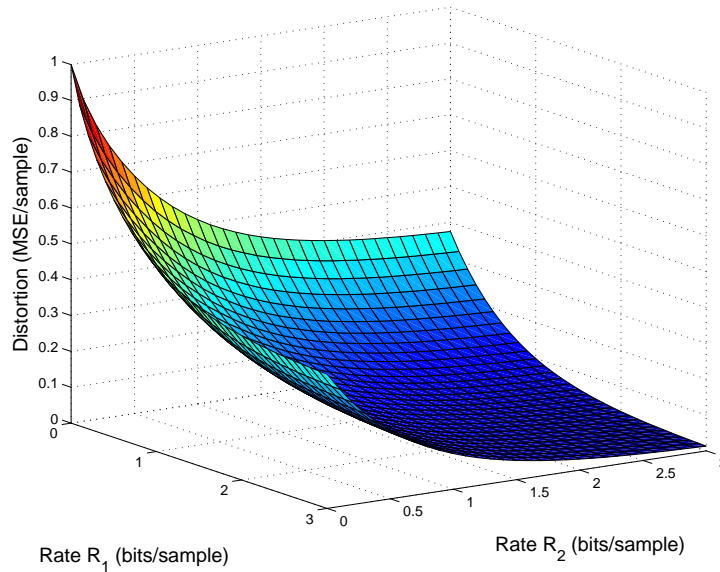


**Figure 3.11:** Achievable distortion-rate function in the general scenario for  $\rho = 0.4$ . The inside of the distortion surface is obtained using Algorithm 3.2 and a block length  $N = 20$ .

inside of the distortion surface is computed numerically using Algorithm 3.2. The achievable distortion for given rates  $R_1$  and  $R_2$  is computed as the minimum obtained over 1000 randomly generated rate schedules of 10 iterations. The borders correspond to the perfect side information scenario ( $R_1 \rightarrow \infty$  or  $R_2 \rightarrow \infty$ ) and the partial observation scenario ( $R_1 = 0$  or  $R_2 = 0$ ). Again, it is important to recall that global optimality is not guaranteed. The distortion surface depicted in Figure 3.11 is thus achievable but may not be optimal.

### 3.6 Summary

This chapter investigated the problem of distributed estimation under communication constraints. We addressed the problem from both a linear approximation and a compression point of view.

We started our analysis with memoryless vector sources. While the general solution is deemed intractable, a suboptimal strategy was presented. The approach consists in optimizing the descriptions provided by the two terminals in turn, instead of optimizing them jointly. The optimal solution at each step was derived. In the linear approximation framework, the optimal solution was referred to as the local approximation transform. Using this transform, the optimal strategy in the compression framework was shown to admit a transform coding interpretation. More precisely, the terminal applies a local approximation transform to the observed vector signal and then encodes each scalar transformed sequence separately. Based on this local optimization step, an iterative algorithm was presented and its optimality properties were discussed.

We then addressed the distributed estimation of discrete-time sources with

---

memory under additional stationarity requirements. To this end, we considered the results obtained for the vector case in the limit of large block lengths. Similar results were obtained in that regime. In particular, the optimal linear approximation step was achieved by means of a local approximation filter. Local optimality in the compression framework was obtained by filtering the input sequence with the local approximation filter. The frequency components of the filtered signal were then encoded separately. The corresponding iterative algorithms were also presented.

Finally, our findings were illustrated with a simple first-order autoregressive model. We derived distortion formulas for both the linear approximation and compression frameworks. Achievable distortion surfaces for the two-terminal scenario were obtained using the proposed iterative algorithms.



## 3.A Proofs

### 3.A.1 Proof of Theorem 3.1

The proof makes use of the following two lemmas.

**Lemma 3.1.** Let  $\mathbf{x}$ ,  $\mathbf{y}$  and  $\mathbf{z}$  be zero-mean jointly Gaussian random vectors. It holds that

$$\mathcal{E} \{ \mathbf{x} | \mathbf{y}, \mathbf{z} \} = \mathcal{E} \{ \mathbf{x} | \mathbf{y} \} + \mathcal{E} \{ \mathbf{x} | \bar{\mathbf{z}} \},$$

where  $\bar{\mathbf{z}} = \mathbf{z} - \mathcal{E} \{ \mathbf{z} | \mathbf{y} \}$ .

**Proof:** We can write

$$\begin{aligned} & \mathcal{E} \{ \mathbf{x} | \mathbf{y}, \mathbf{z} \} \\ & \stackrel{(a)}{=} [\mathbf{R}_{xy} \quad \mathbf{R}_{xz}] \begin{bmatrix} \mathbf{R}_y & \mathbf{R}_{yz} \\ \mathbf{R}_{yz}^H & \mathbf{R}_z \end{bmatrix}^{-1} \begin{bmatrix} \mathbf{y} \\ \mathbf{z} \end{bmatrix} \\ & \stackrel{(b)}{=} [\mathbf{R}_{xy} \quad \mathbf{R}_{xz}] \begin{bmatrix} (\mathbf{R}_y - \mathbf{R}_{yz} \mathbf{R}_z^{-1} \mathbf{R}_{yz}^H)^{-1} & -\mathbf{R}_y^{-1} \mathbf{R}_{yz} \mathbf{R}_z^{-1} \\ -\mathbf{R}_z^{-1} \mathbf{R}_{yz}^H \mathbf{R}_y^{-1} & \mathbf{R}_z^{-1} \end{bmatrix} \begin{bmatrix} \mathbf{y} \\ \mathbf{z} \end{bmatrix} \\ & \stackrel{(c)}{=} [\mathbf{R}_{xy} \quad \mathbf{R}_{xz}] \begin{bmatrix} \mathbf{R}_y^{-1} + \mathbf{R}_y^{-1} \mathbf{R}_{yz} \mathbf{R}_z^{-1} \mathbf{R}_{yz}^H \mathbf{R}_y^{-1} & -\mathbf{R}_y^{-1} \mathbf{R}_{yz} \mathbf{R}_z^{-1} \\ -\mathbf{R}_z^{-1} \mathbf{R}_{yz}^H \mathbf{R}_y^{-1} & \mathbf{R}_z^{-1} \end{bmatrix} \begin{bmatrix} \mathbf{y} \\ \mathbf{z} \end{bmatrix} \\ & = \mathbf{R}_{xy} \mathbf{R}_y^{-1} \mathbf{y} + (\mathbf{R}_{xz} - \mathbf{R}_{xy} \mathbf{R}_y^{-1} \mathbf{R}_{yz}) \mathbf{R}_z^{-1} (\mathbf{z} - \mathbf{R}_{yz}^H \mathbf{R}_y^{-1} \mathbf{y}) \\ & = \mathbf{R}_{xy} \mathbf{R}_y^{-1} \mathbf{y} + \mathbf{R}_{x\bar{z}} \mathbf{R}_{\bar{z}}^{-1} \bar{\mathbf{z}} \\ & = \mathcal{E} \{ \mathbf{x} | \mathbf{y} \} + \mathcal{E} \{ \mathbf{x} | \bar{\mathbf{z}} \}, \end{aligned}$$

where (a) follows from the expression of the conditional expectation in the jointly Gaussian case [106, Sec. IV.B], (b) from the inversion formula of a partitioned matrix [69, Sec. 0.7.3] and (c) from that of a small rank adjustment [69, Sec. 0.7.4].  $\blacksquare$

**Lemma 3.2.** Let  $\mathbf{x}$ ,  $\mathbf{y}$  and  $\mathbf{z}$  be zero-mean jointly Gaussian random vectors. It holds that

$$\mathbf{R}_x - \mathbf{R}_{x|\bar{z}} = \mathbf{R}_{x|\mathbf{y}} - \mathbf{R}_{x|\mathbf{y}, \mathbf{z}},$$

where  $\bar{\mathbf{z}} = \mathbf{z} - \mathcal{E} \{ \mathbf{z} | \mathbf{y} \}$ .

**Proof:** Using Lemma 3.1 we can write

$$\mathcal{E} \{ \mathbf{x} | \bar{\mathbf{z}} \} = \mathcal{E} \{ \mathbf{x} | \mathbf{y}, \mathbf{z} \} - \mathcal{E} \{ \mathbf{x} | \mathbf{y} \} = (\mathbf{x} - \mathcal{E} \{ \mathbf{x} | \mathbf{y} \}) - (\mathbf{x} - \mathcal{E} \{ \mathbf{x} | \mathbf{y}, \mathbf{z} \}). \quad (3.23)$$

From the definition of the conditional expectation [124, Def. 10.1.2],  $\mathcal{E} \{ \mathbf{x} | \bar{\mathbf{z}} \}$  is orthogonal to both  $\mathbf{y}$  and  $\mathbf{x} - \mathcal{E} \{ \mathbf{x} | \bar{\mathbf{z}} \}$  (orthogonality principle), hence to  $\mathbf{x} - \mathcal{E} \{ \mathbf{x} | \mathbf{y}, \mathbf{z} \}$ . It thus holds that

$$\begin{aligned} & \mathcal{E} \left\{ (\mathbf{x} - \mathcal{E} \{ \mathbf{x} | \mathbf{y} \}) (\mathbf{x} - \mathcal{E} \{ \mathbf{x} | \mathbf{y}, \mathbf{z} \})^H \right\} \\ & = \mathcal{E} \left\{ (\mathbf{x} - \mathcal{E} \{ \mathbf{x} | \mathbf{y} \} - \mathcal{E} \{ \mathbf{x} | \bar{\mathbf{z}} \}) (\mathbf{x} - \mathcal{E} \{ \mathbf{x} | \mathbf{y}, \mathbf{z} \})^H \right\} \\ & = \mathcal{E} \left\{ (\mathbf{x} - \mathcal{E} \{ \mathbf{x} | \mathbf{y}, \mathbf{z} \}) (\mathbf{x} - \mathcal{E} \{ \mathbf{x} | \mathbf{y}, \mathbf{z} \})^H \right\}. \end{aligned} \quad (3.24)$$

From (3.23) and (3.24) it follows that

$$\mathbf{R}_x - \mathbf{R}_{x|\bar{z}} = \mathcal{E} \left\{ \mathcal{E} \{ \mathbf{x} | \bar{z} \} \mathcal{E} \{ \mathbf{x} | \bar{z} \}^H \right\} = \mathbf{R}_{x|y} - \mathbf{R}_{x|y,z},$$

yielding the claimed equality.  $\blacksquare$

Let us now turn to the proof of Theorem 3.1. We first find the minimum achievable distortion (converse) and then show that the proposed transform achieves it (achievability).

*Converse:* The MSE can be expressed as

$$\begin{aligned} & \mathcal{E} \left\{ \|\mathbf{s} - \mathcal{E} \{ \mathbf{s} | \mathbf{y}_1, \mathbf{y}_2 \} \|^2 \right\} \\ &= \mathcal{E} \left\{ \|\mathbf{s} - \mathcal{E} \{ \mathbf{s} | \mathbf{K}_1 \mathbf{x}_1, \mathbf{y}_2 \} \|^2 \right\} \\ &\stackrel{(a)}{=} \mathcal{E} \left\{ \|\mathbf{s} - \mathcal{E} \{ \mathbf{s} | \mathbf{x}_1, \mathbf{y}_2 \} \|^2 \right\} + \mathcal{E} \left\{ \|\mathcal{E} \{ \mathbf{s} | \mathbf{x}_1, \mathbf{y}_2 \} - \mathcal{E} \{ \mathbf{s} | \mathbf{K}_1 \mathbf{x}_1, \mathbf{y}_2 \} \|^2 \right\} \\ &\stackrel{(b)}{=} \mathcal{E} \left\{ \|\mathbf{s} - \mathcal{E} \{ \mathbf{s} | \mathbf{x}_1, \mathbf{y}_2 \} \|^2 \right\} + \mathcal{E} \left\{ \|\mathcal{E} \{ \mathbf{s} | \bar{\mathbf{x}}_1 \} - \mathcal{E} \{ \mathbf{s} | \mathbf{K}_1 \bar{\mathbf{x}}_1 \} \|^2 \right\} \\ &\stackrel{(c)}{=} \mathcal{E} \left\{ \|\mathbf{s} - \mathcal{E} \{ \mathbf{s} | \mathbf{x}_1, \mathbf{y}_2 \} \|^2 \right\} + \mathcal{E} \left\{ \|\mathcal{E} \{ \mathbf{s} | \bar{\mathbf{x}}_1 \} - \mathcal{E} \{ \mathcal{E} \{ \mathbf{s} | \bar{\mathbf{x}}_1 \} | \mathbf{K}_1 \bar{\mathbf{x}}_1 \} \|^2 \right\} \\ &\stackrel{(d)}{=} \text{tr} \left( \mathbf{R}_{\mathbf{s} | \mathbf{x}_1, \mathbf{y}_2} \right) + \text{tr} \left( \mathbf{R}_{\mathbf{s} \bar{\mathbf{x}}_1} \mathbf{R}_{\bar{\mathbf{x}}_1}^{-1} \mathbf{R}_{\mathbf{s} \bar{\mathbf{x}}_1}^H \right) \\ &\quad - \text{tr} \left( \mathbf{R}_{\mathbf{s} \bar{\mathbf{x}}_1} \mathbf{K}_1^H \left( \mathbf{K}_1 \mathbf{R}_{\bar{\mathbf{x}}_1} \mathbf{K}_1^H \right)^{-1} \mathbf{K}_1 \mathbf{R}_{\mathbf{s} \bar{\mathbf{x}}_1}^H \right), \end{aligned} \quad (3.25)$$

where (a) follows from the orthogonality principle, (b) from Lemma 3.1, (c) from the successive conditioning property (or Tower property) of conditional expectation [124, Sec. 10.1.2] and (d) from the definition of the Frobenius norm and the fact that expectation and trace commute. Differentiating the above expression with respect to  $\mathbf{K}_1$  yields

$$\begin{aligned} & \frac{\partial}{\partial \mathbf{K}_1} \mathcal{E} \left\{ \|\mathbf{s} - \mathcal{E} \{ \mathbf{s} | \mathbf{K}_1 \mathbf{x}_1, \mathbf{y}_2 \} \|^2 \right\} \\ &= - \frac{\partial}{\partial \mathbf{K}_1} \text{tr} \left( \mathbf{K}_1 \mathbf{R}_{\mathbf{s} \bar{\mathbf{x}}_1}^H \mathbf{R}_{\mathbf{s} \bar{\mathbf{x}}_1} \mathbf{K}_1^H \left( \mathbf{K}_1 \mathbf{R}_{\bar{\mathbf{x}}_1} \mathbf{K}_1^H \right)^{-1} \right) \\ &= 2 \mathbf{R}_{\bar{\mathbf{x}}_1} \mathbf{K}_1^H \left( \mathbf{K}_1 \mathbf{R}_{\bar{\mathbf{x}}_1} \mathbf{K}_1^H \right)^{-1} \mathbf{K}_1 \mathbf{R}_{\mathbf{s} \bar{\mathbf{x}}_1}^H \mathbf{R}_{\mathbf{s} \bar{\mathbf{x}}_1} \mathbf{K}_1^H \left( \mathbf{K}_1 \mathbf{R}_{\bar{\mathbf{x}}_1} \mathbf{K}_1^H \right)^{-1} \\ &\quad - 2 \mathbf{R}_{\mathbf{s} \bar{\mathbf{x}}_1}^H \mathbf{R}_{\mathbf{s} \bar{\mathbf{x}}_1} \mathbf{K}_1^H \left( \mathbf{K}_1 \mathbf{R}_{\bar{\mathbf{x}}_1} \mathbf{K}_1^H \right)^{-1}, \end{aligned} \quad (3.26)$$

where the last equality follows from trace derivative formulas (see, e.g., [66]). The matrix  $\mathbf{K}_1 \mathbf{R}_{\bar{\mathbf{x}}_1} \mathbf{K}_1^H$  is (Hermitian) positive definite and  $\mathbf{K}_1 \mathbf{R}_{\mathbf{s} \bar{\mathbf{x}}_1}^H \mathbf{R}_{\mathbf{s} \bar{\mathbf{x}}_1} \mathbf{K}_1^H$  is (Hermitian) nonnegative definite. They can be simultaneously diagonalized by a non-singular matrix  $\mathbf{P}_1 \in \mathbb{C}^{K_1 \times K_1}$  as [4]

$$\mathbf{P}_1^H \mathbf{K}_1 \mathbf{R}_{\mathbf{s} \bar{\mathbf{x}}_1}^H \mathbf{R}_{\mathbf{s} \bar{\mathbf{x}}_1} \mathbf{K}_1^H \mathbf{P}_1 = \mathbf{D}_1, \quad (3.27)$$

$$\mathbf{P}_1^H \mathbf{K}_1 \mathbf{R}_{\bar{\mathbf{x}}_1} \mathbf{K}_1^H \mathbf{P}_1 = \mathbf{I}_K, \quad (3.28)$$

where  $\mathbf{D}_1 \in \mathbb{C}^{K_1 \times K_1}$  is a diagonal matrix with diagonal elements  $\mu_1, \mu_2, \dots, \mu_{K_1}$  arranged in decreasing order. Note that the matrix  $\mathbf{P}_1$  is not necessarily unitary. A necessary condition for optimality is obtained by setting the partial derivative (3.26) to zero. Using (3.27) and (3.28) in (3.26) reduces the problem

to that of finding the matrix  $\mathbf{Q}_1 \in \mathbb{C}^{N_1 \times K_1}$  that satisfies

$$\mathbf{R}_{\bar{x}_1}^{-1} \mathbf{R}_{s\bar{x}_1}^H \mathbf{R}_{s\bar{x}_1} \mathbf{Q}_1 = \mathbf{Q}_1 \mathbf{D}_1,$$

where  $\mathbf{Q}_1$  is defined as  $\mathbf{Q}_1 = \mathbf{K}_1^H \mathbf{P}_1$ . The above equations are the eigen-equations for the matrix  $\mathbf{R}_{\bar{x}_1}^{-1} \mathbf{R}_{s\bar{x}_1}^H \mathbf{R}_{s\bar{x}_1}$ . The columns of  $\mathbf{Q}_1$  are thus  $K_1$  eigenvectors and  $\mathbf{D}_1$  contains the corresponding eigenvalues. Denoting by  $\mathcal{K} \subset \{1, 2, \dots, N_1\}$  the set of  $K_1$  chosen indexes, the MSE evaluates as

$$\text{tr}(\mathbf{R}_{s|x_1, y_2}) + \text{tr}(\mathbf{R}_{s\bar{x}_1} \mathbf{R}_{\bar{x}_1}^{-1} \mathbf{R}_{s\bar{x}_1}^H) - \sum_{k \in \mathcal{K}} \mu_k.$$

The above expression is minimized by choosing the  $K_1$  largest eigenvalues, that is,  $\mathcal{K} = \{1, 2, \dots, K_1\}$ . The  $N_1$  eigenvalues  $\mu_k$  correspond to the  $N_1$  largest eigenvalues of the matrix  $\mathbf{R}_{s\bar{x}_1} \mathbf{R}_{\bar{x}_1}^{-1} \mathbf{R}_{s\bar{x}_1}^H$ , the  $P - N_1$  remaining ones being zero. Moreover, from Lemma 3.2,

$$\mathbf{R}_{s\bar{x}_1} \mathbf{R}_{\bar{x}_1}^{-1} \mathbf{R}_{s\bar{x}_1}^H = \mathbf{R}_s - \mathbf{R}_{s|\bar{x}_1} = \mathbf{R}_{s|y_2} - \mathbf{R}_{s|x_1, y_2}.$$

The minimum distortion can thus be equivalently expressed as

$$D_{N_1}(K_1) = \text{tr}(\mathbf{R}_{s|x_1, y_2}) + \sum_{k=K_1+1}^{N_1} \lambda_k,$$

where  $\lambda_k$  denote the  $N_1$  largest eigenvalues of the matrix  $\mathbf{R}_{s|y_2} - \mathbf{R}_{s|x_1, y_2}$  arranged in decreasing order.

*Achievability:* The optimality of the proposed transform is readily assessed by substituting it in (3.25) and verifying that it provides the minimum distortion.

Finally note that, in the jointly Gaussian case, Lemma 3.1 allows us to write  $\mathcal{E}\{\mathbf{s}|\mathbf{K}_1 \mathbf{x}_1, \mathbf{y}_2\} = \mathcal{E}\{\mathbf{s}|\mathbf{K}_1 \bar{\mathbf{x}}_1, \mathbf{y}_2\}$  such that the availability of  $\mathbf{y}_2$  at the encoder does not change the MSE. In this case, the optimal transform is still the same but the transmitted coefficients are different since the transform can be applied on  $\bar{\mathbf{x}}_1$  instead of  $\mathbf{x}_1$ .

### 3.A.2 Proof of Theorem 3.2

The rate-distortion function has been derived in [152, Th. 2]. Our goal is to evaluate it under our jointly Gaussian assumption. To this end, we proceed similarly to [50, Th. 3]. We first establish that no better rate-distortion trade-off can be hoped for (converse part) and then provide an encoding architecture that achieves it (achievability part).

*Converse:* The rate-distortion function follows as [152, Th. 2]

$$R_{N_1} = \min_{\mathbf{y}_1 \in \mathcal{Y}_1} I(\mathbf{x}_1; \mathbf{y}_1 | \mathbf{y}_2),$$

where  $\mathcal{Y}_1$  denotes the set of random vectors such that  $(\mathbf{s}, \mathbf{y}_2) \longleftrightarrow \mathbf{x}_1 \longleftrightarrow \mathbf{y}_1$  and

$$\mathcal{E}\left\{\|\mathbf{s} - \mathcal{E}\{\mathbf{s}|\mathbf{y}_1, \mathbf{y}_2\}\|^2\right\} \leq D_{N_1}.$$

It can be easily checked that a lower bound to the above minimization task is

obtained as

$$R_{N_1} = \min_{p_{\mathbf{y}_1|\mathbf{x}_1, \mathbf{y}_2}(\mathbf{v}_1|\mathbf{u}_1, \mathbf{v}_2)} I(\mathbf{x}_1; \mathbf{y}_1|\mathbf{y}_2),$$

and  $\mathcal{E} \left\{ \|\mathbf{s} - \mathbf{y}_1\|^2 \right\} \leq D_{N_1}$  where now the minimization is over all conditional distribution  $p_{\mathbf{y}_1|\mathbf{x}_1, \mathbf{y}_2}(\mathbf{v}_1|\mathbf{u}_1, \mathbf{v}_2)$ . We have that

$$I(\mathbf{x}_1; \mathbf{y}_1|\mathbf{y}_2) = I(\bar{\mathbf{x}}_1; \bar{\mathbf{y}}_1|\mathbf{y}_2) \geq I(\mathcal{E}\{\mathbf{s}|\bar{\mathbf{x}}_1\}; \bar{\mathbf{y}}_1|\mathbf{y}_2),$$

where  $\bar{\mathbf{x}}_1 = \mathbf{x}_1 - \mathcal{E}\{\mathbf{x}_1|\mathbf{y}_2\}$  and  $\bar{\mathbf{y}}_1 = \mathbf{y}_1 - \mathcal{E}\{\mathbf{s}|\mathbf{y}_2\}$ . Moreover, the distortion can be split as

$$\begin{aligned} \mathcal{E} \left\{ \|\mathbf{s} - \mathbf{y}_1\|^2 \right\} &\stackrel{(a)}{=} \mathcal{E} \left\{ \|\mathbf{s} - \mathcal{E}\{\mathbf{s}|\mathbf{x}_1, \mathbf{y}_2\}\|^2 \right\} + \mathcal{E} \left\{ \|\mathcal{E}\{\mathbf{s}|\mathbf{x}_1, \mathbf{y}_2\} - \mathbf{y}_1\|^2 \right\} \\ &\stackrel{(b)}{=} \mathcal{E} \left\{ \|\mathbf{s} - \mathcal{E}\{\mathbf{s}|\mathbf{x}_1, \mathbf{y}_2\}\|^2 \right\} + \mathcal{E} \left\{ \|\mathcal{E}\{\mathbf{s}|\bar{\mathbf{x}}_1\} - \bar{\mathbf{y}}_1\|^2 \right\}, \end{aligned}$$

where (a) follows from the orthogonality principle and the fact that  $\mathbf{y}_1$  is a function of  $\mathbf{x}_1$  and  $\mathbf{y}_2$  and (b) from the equality  $\mathcal{E}\{\mathbf{s}|\mathbf{x}_1, \mathbf{y}_2\} = \mathcal{E}\{\mathbf{s}|\mathbf{y}_2\} + \mathcal{E}\{\mathbf{s}|\bar{\mathbf{x}}_1\}$  in the jointly Gaussian case. A lower bound is thus obtained as

$$R_{N_1} = \min_{p_{\mathbf{y}_1|\mathbf{x}_1, \mathbf{y}_2}(\bar{\mathbf{v}}_1|\mathbf{u}_1, \mathbf{v}_2)} I(\mathcal{E}\{\mathbf{s}|\bar{\mathbf{x}}_1\}; \bar{\mathbf{y}}_1|\mathbf{y}_2), \quad (3.29)$$

such that

$$\mathcal{E} \left\{ \|\mathcal{E}\{\mathbf{s}|\bar{\mathbf{x}}_1\} - \bar{\mathbf{y}}_1\|^2 \right\} \leq D_{N_1} - \mathcal{E} \left\{ \|\mathbf{s} - \mathcal{E}\{\mathbf{s}|\mathbf{x}_1, \mathbf{y}_2\}\|^2 \right\}.$$

Since  $\mathcal{E}\{\mathbf{s}|\bar{\mathbf{x}}_1\}$  is independent of  $\mathbf{y}_2$ , the optimal  $\bar{\mathbf{y}}_1$  does not depend on the particular value of  $\mathbf{y}_2$ . The conditioning in (3.29) can thus be omitted and the problem reduces to a direct encoding of the source  $\mathbf{p}_1 = \mathcal{E}\{\mathbf{s}|\bar{\mathbf{x}}_1\}$  whose covariance matrix can be computed as

$$\mathbf{R}_{p_1} = \mathbf{R}_s - \mathbf{R}_{s|\bar{\mathbf{x}}_1} = \mathbf{R}_{s|\mathbf{y}_2} - \mathbf{R}_{s|x_1, \mathbf{y}_2}. \quad (3.30)$$

The lower bound thus directly follows from the corresponding rate-distortion function (see, e.g., [29, Th. 13.3.3]) and yields the claimed formula.

*Achievability:* Let us consider the following encoding architecture. We first apply to the vector  $\mathbf{x}_1$  the local approximation transform (3.5). The obtained vector is then optimally encoded provided that  $\mathbf{y}_2$  is available at the decoder. Under our jointly Gaussian assumption, the corresponding rate-distortion function is that of the innovation process

$$\mathbf{R}_{s\bar{\mathbf{x}}_1} \mathbf{R}_{\bar{\mathbf{x}}_1}^{-1} \mathbf{x}_1 - \mathcal{E} \left\{ \mathbf{R}_{s\bar{\mathbf{x}}_1} \mathbf{R}_{\bar{\mathbf{x}}_1}^{-1} \mathbf{x}_1 | \mathbf{y}_2 \right\} = \mathbf{R}_{s\bar{\mathbf{x}}_1} \mathbf{R}_{\bar{\mathbf{x}}_1}^{-1} \bar{\mathbf{x}}_1,$$

whose covariance matrix is given by (3.30). The rate achieved by this scheme hence follows from [29, Th. 13.3.3] and corresponds to  $R_1(\theta)$ . Let us denote by  $\mathbf{y}_1$  the vector received at the decoder in this case. By the orthogonality principle, the distortion achieved by this method can be decomposed as

$$\mathcal{E} \left\{ \|\mathbf{s} - \mathcal{E}\{\mathbf{s}|\mathbf{y}_1, \mathbf{y}_2\}\|^2 \right\}$$

$$= \mathcal{E} \left\{ \|\mathbf{s} - \mathcal{E} \{\mathbf{s}|\mathbf{x}_1, \mathbf{y}_2\}\|^2 \right\} + \mathcal{E} \left\{ \|\mathcal{E} \{\mathbf{s}|\mathbf{x}_1, \mathbf{y}_2\} - \mathcal{E} \{\mathbf{s}|\mathbf{y}_1, \mathbf{y}_2\}\|^2 \right\}. \quad (3.31)$$

Moreover,

$$\begin{aligned} \mathcal{E} \{\mathbf{s}|\mathbf{y}_1, \mathbf{y}_2\} &\stackrel{(a)}{=} \mathcal{E} \{ \mathcal{E} \{ \mathbf{s}|\mathbf{x}_1, \mathbf{y}_2 \} | \mathbf{y}_1, \mathbf{y}_2 \} \\ &\stackrel{(b)}{=} \mathcal{E} \{ \mathcal{E} \{ \mathbf{s}|\mathbf{y}_2 \} | \mathbf{y}_1, \mathbf{y}_2 \} + \mathcal{E} \{ \mathcal{E} \{ \mathbf{s}|\bar{\mathbf{x}}_1 \} | \mathbf{y}_1, \mathbf{y}_2 \} \\ &\stackrel{(c)}{=} \mathcal{E} \{ \mathbf{s}|\mathbf{y}_2 \} + \mathcal{E} \{ \mathbf{R}_{s\bar{\mathbf{x}}_1} \mathbf{R}_{\bar{\mathbf{x}}_1}^{-1} \bar{\mathbf{x}}_1 | \mathbf{y}_1, \mathbf{y}_2 \}, \end{aligned}$$

where (a) follows from the successive conditioning property of conditional expectation and the fact that  $\mathbf{y}_1$  is a function of  $\mathbf{x}_1$ , (b) from the fact that  $\mathcal{E} \{ \mathbf{s}|\mathbf{x}_1, \mathbf{y}_2 \} = \mathcal{E} \{ \mathbf{s}|\mathbf{y}_2 \} + \mathcal{E} \{ \mathbf{s}|\bar{\mathbf{x}}_1 \}$  in the jointly Gaussian case and from the linearity of conditional expectation and (c) from the successive conditioning property of conditional expectation and our jointly Gaussian assumption. The second term in the distortion (3.31) can thus be written as

$$\begin{aligned} &\mathcal{E} \left\{ \|\mathcal{E} \{ \mathbf{s}|\mathbf{x}_1, \mathbf{y}_2 \} - \mathcal{E} \{ \mathbf{s}|\mathbf{y}_1, \mathbf{y}_2 \}\|^2 \right\} \\ &= \mathcal{E} \left\{ \|\mathbf{R}_{s\bar{\mathbf{x}}_1} \mathbf{R}_{\bar{\mathbf{x}}_1}^{-1} \bar{\mathbf{x}}_1 - \mathcal{E} \{ \mathbf{R}_{s\bar{\mathbf{x}}_1} \mathbf{R}_{\bar{\mathbf{x}}_1}^{-1} \bar{\mathbf{x}}_1 | \mathbf{y}_1, \mathbf{y}_2 \}\|^2 \right\} \\ &= \mathcal{E} \left\{ \|\mathbf{R}_{s\bar{\mathbf{x}}_1} \mathbf{R}_{\bar{\mathbf{x}}_1}^{-1} \bar{\mathbf{x}}_1 - \mathcal{E} \{ \mathbf{R}_{s\bar{\mathbf{x}}_1} \mathbf{R}_{\bar{\mathbf{x}}_1}^{-1} \bar{\mathbf{x}}_1 | \mathbf{y}_1, \mathbf{y}_2 \}\|^2 \right\}. \end{aligned}$$

It corresponds to the distortion of the source  $\mathbf{p}_1$  and also follows from [29, Th. 13.3.3]. Using (3.31), the achieved distortion directly evaluates as  $D_{N_1}(\theta)$ , demonstrating the optimality of the proposed encoding architecture.

### 3.A.3 Proof of Theorem 3.3

The proof consists of two parts. In the first part (converse), we prove that the minimum achievable distortion is given by (3.16). In the second part (achievability), we show that the filtering strategy (3.15) achieves this distortion. Before we proceed, let us define the function

$$u_\theta(x) = \begin{cases} 1 & \text{if } x \leq \theta, \\ 0 & \text{if } x > \theta. \end{cases}$$

We further denote by  $\mathbf{T}_N(P) \in \mathbb{C}^{N \times N}$  the Toeplitz matrix given by

$$\mathbf{T}_N(P) = \begin{bmatrix} p[0] & p[1] & \cdots & p[N-1] \\ p[-1] & p[0] & \cdots & p[N-2] \\ \vdots & \vdots & \ddots & \vdots \\ p[-N+1] & p[-N+2] & \cdots & p[0] \end{bmatrix},$$

where  $P(\omega)$  is the discrete-time Fourier transform of the generating sequence  $p[n]$ . We assume that  $p[n]$  is absolutely summable such that  $P(\omega)$  exists, is essentially continuous and bounded [59, Sec. 4.1]. With these definitions in mind, we can state the following lemma.

**Lemma 3.3.** Let  $\mathbf{T}_N(P)$  be a sequence of Hermitian Toeplitz matrices where

$P(\omega)$  is such that the limiting eigenvalue distribution  $p(u)$  is continuous. Then, for any function  $g(x)$  continuous on  $[\text{ess inf}_\omega P(\omega), \text{ess sup}_\omega P(\omega)]$ ,

$$\lim_{N \rightarrow \infty} \frac{1}{N} \sum_{n=1}^N g(\lambda_{N,n}) u_\theta(\lambda_{N,n}) = \frac{1}{2\pi} \int_{\omega \in \mathcal{X}} g(P(\omega)) d\omega,$$

where  $\lambda_{N,n}$  denote the eigenvalues of  $\mathbf{T}_N(P)$  and  $\mathcal{X} = \{\omega \in [0, 2\pi] : P(\omega) \leq \theta\}$ .

**Proof:** Let us first prove the assertion for functions  $g(x)$  of the form  $g(x) = x^k$ , where  $k$  is some non-negative integer. We proceed by induction. For  $k = 0$ , we know that the assertion holds true by [59, Th. 4.1], that is,

$$\lim_{N \rightarrow \infty} \frac{1}{N} \sum_{n=1}^N u_\theta(\lambda_{N,n}) = \frac{1}{2\pi} \int_{\omega \in \mathcal{X}} d\omega.$$

Assume it has been proved for  $k - 1$ , we now prove it for  $k$ . We first note that the left hand side of the assertion can be expressed as

$$\begin{aligned} & \frac{1}{N} \sum_{n=1}^N \lambda_{N,n}^k u_\theta(\lambda_{N,n}) \\ &= \frac{1}{N} \sum_{n=1}^N \lambda_{N,n}^{k-1} \min\{\theta, \lambda_{N,n}\} - \frac{\theta}{N} \sum_{n=1}^N \lambda_{N,n}^{k-1} (1 - u_\theta(\lambda_{N,n})) \\ &= \frac{1}{N} \sum_{n=1}^N \lambda_{N,n}^{k-1} \min\{\theta, \lambda_{N,n}\} - \frac{\theta}{N} \sum_{n=1}^N \lambda_{N,n}^{k-1} + \frac{\theta}{N} \sum_{n=1}^N \lambda_{N,n}^{k-1} u_\theta(\lambda_{N,n}). \end{aligned}$$

Since  $\min$  is a continuous function, we can apply the Toeplitz distribution theorem [59, Th. 4.2] to the first and second summations and our induction assumption to the third one to obtain

$$\begin{aligned} & \lim_{N \rightarrow \infty} \frac{1}{N} \sum_{n=1}^N \lambda_{N,n}^k u_\theta(\lambda_{N,n}) \\ &= \frac{1}{2\pi} \int_{\omega \in [0, 2\pi]} P^{k-1}(\omega) \min\{\theta, P(\omega)\} d\omega \\ & \quad - \frac{\theta}{2\pi} \int_{\omega \in [0, 2\pi]} P^{k-1}(\omega) d\omega + \frac{\theta}{2\pi} \int_{\omega \in \mathcal{X}} P^{k-1}(\omega) d\omega \\ &= \frac{1}{2\pi} \int_{\omega \in \mathcal{X}} P^k(\omega) d\omega, \end{aligned}$$

which yields the desired result. Since any polynomial in  $x$  can be expressed as a linear combination of monomials  $x^k$  ( $k \geq 0$ ), the above argumentation can be straightforwardly extended to polynomials. Finally, the case of a continuous function  $g(x)$  follows directly by invoking the Stone-Weierstrass theorem [59, Th. 2.3]. ■

Note that Lemma 3.3 allows us to carry similar computations on functions with a finite number of discontinuities by simply isolating the continuous pieces. Extension to an infinite but countable number of discontinuities may be envi-

sioned but special care has to be taken with the function  $g(x)$  so as to satisfy Lebesgue's theorem assumptions [22, Th. 12]. We can now turn to the proof of the theorem.

*Achievability:* The optimal finite dimensional distortion  $D_N(K_1)$  is computed from Theorem 3.1 as

$$D_N(K_1) = \mathbf{tr}(\mathbf{T}_N(P_{s|x_1, y_2})) + \sum_{n=1}^{N - \lfloor \alpha_1 N \rfloor} \lambda_{N, n},$$

where  $\lambda_{N, n}$  denote the eigenvalues of  $\mathbf{T}_N(P_1)$  arranged in increasing order with  $P_1(\omega) = P_{s|y_2}(\omega) - P_{s|x_1, y_2}(\omega)$ . The first term of  $D_1(\alpha_1)$  directly follows from the limit (3.14) and the Toeplitz distribution theorem [59, Th. 4.2] as

$$\lim_{N \rightarrow \infty} \frac{1}{N} \mathbf{tr}(\mathbf{T}_N(P_{s|x_1, y_2})) = \frac{1}{2\pi} \int_{\omega \in [0, 2\pi]} P_{s|x_1, y_2}(\omega) d\omega.$$

Now using Lemma 3.2, we have that

$$\begin{aligned} P_1(\omega) &= P_{s|y_2}(\omega) - P_{s|x_1, y_2}(\omega) \\ &= P_s(\omega) - P_{s|\bar{x}_1}(\omega) \\ &= P_{s\bar{x}_1}(\omega) P_{\bar{x}_1}^{-1}(\omega) P_{s\bar{x}_1}^H(\omega). \end{aligned}$$

The second term thus follows from the fact that

$$\begin{aligned} \lim_{N \rightarrow \infty} \frac{1}{N} \sum_{n=1}^{N - \lfloor \alpha_1 N \rfloor} \lambda_{N, n} &= \lim_{N \rightarrow \infty} \frac{1}{N} \sum_{n=1}^N \lambda_{N, n} u_\theta(\lambda_{N, n}) \\ &= \frac{1}{2\pi} \int_{\omega \in \mathcal{A}_1^c} P_{s|y_2}(\omega) - P_{s|x_1, y_2}(\omega) d\omega, \end{aligned}$$

where  $\theta$  is chosen such that the fraction of eigenvalues smaller than  $\theta$  is equal to  $1 - \alpha_1$ , that is, such that  $p_1(\theta) = 1 - \alpha_1$ . The last equality follows from Lemma 3.3 with  $g(x) = x$  and  $\mathcal{A}_1 = \{\omega \in [0, 2\pi] : P_1(\omega) > \theta\}$ .

*Converse:* The distortion can be expressed as

$$\begin{aligned} \mathcal{E} \left\{ \|s[n] - \hat{s}[n]\|^2 \right\} &= \mathcal{E} \left\{ \|s[n] - \mathcal{E} \{s[n] | y_1[n], y_2[n]\}\|^2 \right\} \\ &= \frac{1}{2\pi} \int_{\omega \in [0, 2\pi]} P_{s|y_1, y_2}(\omega) d\omega \\ &= \frac{1}{2\pi} \int_{\omega \in \mathcal{A}_1} P_{s|y_1, y_2}(\omega) d\omega + \frac{1}{2\pi} \int_{\omega \in \mathcal{A}_1^c} P_{s|y_1, y_2}(\omega) d\omega. \end{aligned}$$

We now distinguish two cases:

1. When  $\omega \in \mathcal{A}_1$ ,  $K_1(\omega) \neq 0$  is non-zero almost everywhere since we assumed that the involved power spectral densities are non-zero almost everywhere. Thus  $P_{s|\bar{y}_1}(\omega) = P_{s|\bar{x}_1}(\omega)$  almost everywhere, where  $\bar{x}_1[n] = x_1[n] - h_2[n] * y_2[n]$  with  $H_2(\omega) = P_{x_1 y_2}(\omega) P_{y_2}^{-1}(\omega)$ . It follows directly from Lemma 3.2 that  $P_{s|y_1, y_2}(\omega) = P_{s|y_2}(\omega) + P_{s|\bar{y}_1}(\omega) - P_s(\omega)$  almost everywhere. We thus have  $P_{s|y_1, y_2}(\omega) = P_{s|x_1, y_2}(\omega)$  almost everywhere.

2. When  $\omega \in \mathcal{A}_1^c$ ,  $K_1(\omega) = 0$  and  $P_{s|y_1, y_2}(\omega) = P_{s|y_2}(\omega)$ .

We can thus write

$$\begin{aligned} \mathcal{E} \left\{ \|s[n] - \hat{s}[n]\|^2 \right\} &= \frac{1}{2\pi} \int_{\omega \in \mathcal{A}_1} P_{s|x_1, y_2}(\omega) d\omega + \frac{1}{2\pi} \int_{\omega \in \mathcal{A}_1^c} P_{s|y_2}(\omega) d\omega \\ &= \frac{1}{2\pi} \int_{\omega \in [0, 2\pi]} P_{s|x_1, y_2}(\omega) d\omega \\ &\quad + \frac{1}{2\pi} \int_{\omega \in \mathcal{A}_1^c} P_{s|y_2}(\omega) - P_{s|x_1, y_2}(\omega) d\omega, \end{aligned}$$

which proves the achievability, hence the theorem. The term  $P_{s\bar{x}_1}(\omega) P_{\bar{x}_1}^{-1}(\omega)$  in  $K_1(\omega)$  is not needed for optimality since it is assumed to be non-zero almost everywhere. This solution is however provided by analogy to the finite dimensional case.

### 3.A.4 Proof of Theorem 3.4

By assumption, the covariance matrices  $\mathbf{R}_{s|y_2}$  and  $\mathbf{R}_{s|x_1, y_2}$  are of Toeplitz form with power spectral density  $P_{s|y_2}(\omega)$  and  $P_{s|x_1, y_2}(\omega)$ , respectively. It thus follows directly from Theorem 3.2 and the Toeplitz distribution theorem [59, Th. 4.2] that the limits (3.19) evaluate as

$$\begin{aligned} D_1(\theta) &= \lim_{N \rightarrow \infty} \frac{1}{N} D_N(\theta) \\ &= \lim_{N \rightarrow \infty} \frac{1}{N} \text{tr}(\mathbf{T}_N(P_{s|x_1, y_2})) + \frac{1}{N} \sum_{n=1}^N \min\{\theta, \lambda_{N,n}\} \\ &= \frac{1}{2\pi} \int_0^{2\pi} P_{s|x_1, y_2}(\omega) d\omega \\ &\quad + \frac{1}{2\pi} \int_0^{2\pi} \min\{\theta, P_{s|y_2}(\omega) - P_{s|x_1, y_2}(\omega)\} d\omega \end{aligned}$$

and

$$\begin{aligned} R_1(\theta) &= \lim_{N \rightarrow \infty} \frac{1}{N} R_N(\theta) \\ &= \lim_{N \rightarrow \infty} \frac{1}{N} \sum_{n=1}^N \max\left\{0, \frac{1}{2} \log_2 \frac{\lambda_{N,n}}{\theta}\right\} \\ &= \frac{1}{4\pi} \int_0^{2\pi} \max\left\{0, \log_2 \frac{P_{s|y_2}(\omega) - P_{s|x_1, y_2}(\omega)}{\theta}\right\} d\omega, \end{aligned}$$

where  $\lambda_{N,n}$  denote the eigenvalues of the matrix  $\mathbf{T}_N(P_1(\omega))$ , where  $P_1(\omega) = P_{s|y_2}(\omega) - P_{s|x_1, y_2}(\omega)$ . The distortion-rate function is parameterized with  $\theta \in (0, \text{ess sup}_\omega P_1(\omega)]$ .

### 3.A.5 Proof of Proposition 3.1

The distortion in the centralized scenario can be computed using Theorem 3.3 assuming that  $s[n] = x_1[n]$  and  $z_2[n] = 0$ . We can readily check that  $P_s(\omega)$



is positive, symmetric and decreasing in  $[0, \pi]$ . The distortion can thus be expressed using (3.18) and known integration formulas [56, p. 181] as

$$\begin{aligned} D(\alpha) &= \frac{1}{2\pi} \int_{\omega \in \mathcal{A}_1^c} P_s(\omega) d\omega \\ &= \frac{1-\rho^2}{2\pi} \int_{\pi\alpha}^{2\pi-\pi\alpha} \frac{1}{1+\rho^2-2\rho\cos\omega} d\omega \\ &= 1 - \frac{2}{\pi} \arctan\left(\frac{1+\rho}{1-\rho} \tan\left(\frac{\pi\alpha}{2}\right)\right) \end{aligned}$$

and the proof follows.

### 3.A.6 Proof of Proposition 3.2

The centralized scenario amounts to considering  $x_1[n] = s[n]$  and  $y_2[n] = 0$ . Let us define  $\bar{\theta}$  as

$$\bar{\theta} = \min_{\omega} P_s(\omega) = \min_{\omega} \frac{1-\rho^2}{1+\rho^2-2\rho\cos\omega} = \frac{1-\rho}{1+\rho}.$$

For  $0 < \theta \leq \bar{\theta}$ , the distortion (3.9) satisfies  $D_c(\theta) = \theta$  and the rate (3.10) evaluates as

$$\begin{aligned} R_c(\theta) &= \frac{1}{4\pi} \int_0^{2\pi} \max\left\{0, \log_2 \frac{P_s(\omega)}{\theta}\right\} d\omega \\ &= \frac{1}{4\pi} \int_0^{2\pi} \log_2 \frac{1-\rho^2}{1+\rho^2-2\rho\cos\omega} d\omega - \frac{1}{2} \log_2 \theta \\ &= \frac{1}{2} \log_2(1-\rho^2) - \frac{1}{2} \log_2 \theta, \end{aligned}$$

where the last equality follows from known integration formulas [56, p. 560]. Combining  $D_c(\theta)$  and  $R_c(\theta)$  yields the desired result. The rate  $\bar{R}$  simply follows as  $\bar{R} = R_c(\bar{\theta})$ . For  $\theta > \bar{\theta}$  (or  $R < \bar{R}$ ), the rate-distortion function must be left in parametric form since, in this case, no analytical solution of  $R_c(\theta)$  seems to exist.

### 3.A.7 Proof of Proposition 3.3

The distortion in the perfect side information scenario can be obtained by setting  $\mathbf{y}_2 = \mathbf{x}_2$  in Theorem 3.1. Let  $\mathbf{s}^T = [\mathbf{x}_1^T, \mathbf{x}_2^T]$ , we have that  $\mathbf{R}_{\mathbf{s}|x_1, y_2} = \mathbf{R}_{\mathbf{s}|x_1, x_2} = \mathbf{O}_{2N \times 2N}$  and

$$\mathbf{R}_{\mathbf{s}|x_2} = \begin{bmatrix} \mathbf{R}_{x_1|x_2} & \mathbf{O}_{N \times N} \\ \mathbf{O}_{N \times N} & \mathbf{O}_{N \times N} \end{bmatrix}.$$

Thus, the  $N$  largest eigenvalues of  $\mathbf{R}_{\mathbf{s}|x_2}$  are those of  $\mathbf{R}_{x_1|x_2}$ , the  $N$  remaining ones being zero. The matrix  $\mathbf{R}_{x_1|x_2}$  can be computed as

$$\mathbf{R}_{x_1|x_2} = \mathbf{R}_{x_1} - \mathbf{R}_{x_1 x_2} \mathbf{R}_{x_2}^{-1} \mathbf{R}_{x_1 x_2}^H$$

$$= \text{diag} \left( 1 - \rho^2, \frac{1 - \rho^2}{1 + \rho^2}, \dots, \frac{1 - \rho^2}{1 + \rho^2} \right),$$

that is, the non-zero eigenvalues  $\lambda_{N,n}$  of  $\mathbf{R}_{s|x_2}$  are all given by  $(1 - \rho^2) / (1 + \rho^2)$  except the maximum one which is equal to  $1 - \rho^2$ . Since the distortion is not affected by the change of a finite number of eigenvalues, it can be computed from (3.14) as

$$\begin{aligned} D_s(\alpha) &= \lim_{N \rightarrow \infty} \frac{1}{2N} \sum_{n=1}^{N-K} \lambda_{N,n} \\ &= \lim_{N \rightarrow \infty} \frac{1 - \rho^2}{2(1 + \rho^2)} \left( 1 - \frac{K}{N} \right) \\ &= \frac{1 - \rho^2}{2(1 + \rho^2)} (1 - \alpha), \end{aligned}$$

where  $\alpha \sim K/N$ .

### 3.A.8 Proof of Proposition 3.4

Let us consider the (cross) covariance matrices derived in the proof of Proposition 3.3 and define

$$\bar{\theta} = \min_{\omega} P_{x_1|x_2}(\omega) = \min_{\omega} \frac{1 - \rho^2}{1 + \rho^2} = \frac{1 - \rho^2}{1 + \rho^2}.$$

For  $0 < \theta \leq \bar{\theta}$ , the limits (3.19) can be computed from Theorem 3.2 as

$$\begin{aligned} D_s(\theta) &= \lim_{N \rightarrow \infty} D_{p,N}(\theta) \\ &= \lim_{N \rightarrow \infty} \frac{1}{2N} \sum_{n=1}^N \min \{ \theta, \lambda_{N,n} \} \\ &= \frac{1}{4\pi} \int_0^{2\pi} \min \left\{ \theta, \frac{1 - \rho^2}{1 + \rho^2} \right\} d\omega \\ &= \frac{1}{2} \theta, \end{aligned}$$

where  $\lambda_{N,n}$  denote the eigenvalues of the covariance matrix  $\mathbf{R}_{x_1|x_2}$ . Similarly,

$$\begin{aligned} R_s(\theta) &= \lim_{N \rightarrow \infty} R_{p,N}(\theta) \\ &= \lim_{N \rightarrow \infty} \frac{1}{N} \sum_{n=1}^N \max \left\{ 0, \frac{1}{2} \log_2 \frac{\lambda_{N,n}}{\theta} \right\} \\ &= \frac{1}{2\pi} \int_0^{2\pi} \max \left\{ 0, \frac{1}{2} \log_2 \frac{1 - \rho^2}{\theta(1 + \rho^2)} \right\} d\omega \\ &= \frac{1}{2} \log_2 \frac{1 - \rho^2}{1 + \rho^2} - \frac{1}{2} \log_2 \theta. \end{aligned}$$

Combining  $D_s(\theta)$  and  $R_s(\theta)$  yields the desired result. Note that the considered

range for  $\theta$  allows obtaining any rate  $R \geq 0$ .

### 3.A.9 Proof of Proposition 3.5

The distortion in the partial observation scenario is obtained by setting  $\mathbf{y}_2$  as the all-zero vector in Theorem 3.1. In this case, we have

$$\mathbf{R}_{s|x_1, y_2} = \mathbf{R}_{s|x_1} = \begin{bmatrix} \mathbf{R}_{x_2|x_1} & \mathbf{O}_{N \times N} \\ \mathbf{O}_{N \times N} & \mathbf{O}_{N \times N} \end{bmatrix},$$

where  $\mathbf{s}^T = [\mathbf{x}_1^T, \mathbf{x}_2^T]$ . Since  $\mathbf{R}_{x_2|x_1} = \mathbf{R}_{x_1|x_2}$ , the distortion corresponding to the first term in (3.16) is equal to the distortion of the perfect side information scenario with  $\alpha = 0$ , that is,

$$D_p^{(1)}(\alpha) = D_s(0) = \frac{1 - \rho^2}{2(1 + \rho^2)}.$$

The distortion corresponding to the second term can be obtained by noticing that

$$\begin{aligned} \mathbf{R}_{s|y_2} - \mathbf{R}_{s|x_1, y_2} &= \mathbf{R}_s - \mathbf{R}_{s|x_1} \\ &= \mathbf{R}_{(x_1, x_2)} - \mathbf{R}_{(x_1, x_2)|x_1} \\ &= \begin{bmatrix} \mathbf{R}_{x_1} \\ \mathbf{R}_{x_1 x_2}^H \end{bmatrix} \mathbf{R}_{x_1}^{-1} \begin{bmatrix} \mathbf{R}_{x_1} & \mathbf{R}_{x_1 x_2} \end{bmatrix}. \end{aligned}$$

For conforming matrices, we have that  $\det(\mathbf{A}\mathbf{B} + \mathbf{I}) = \det(\mathbf{B}\mathbf{A} + \mathbf{I})$ , where  $\det(\cdot)$  denotes the determinant. Thus, for  $\lambda \neq 0$ , we can write

$$\begin{aligned} &\det(\mathbf{R}_{s|y_2} - \mathbf{R}_{s|x_1, y_2} - \lambda \mathbf{I}_{2N}) \\ &= \det\left(\begin{bmatrix} \mathbf{R}_{x_1} \\ \mathbf{R}_{x_1 x_2}^H \end{bmatrix} \mathbf{R}_{x_1}^{-1} \begin{bmatrix} \mathbf{R}_{x_1} & \mathbf{R}_{x_1 x_2} \end{bmatrix} - \lambda \mathbf{I}_{2N}\right) \\ &= \det\left(\mathbf{R}_{x_1}^{-1} \begin{bmatrix} \mathbf{R}_{x_1} & \mathbf{R}_{x_1 x_2} \end{bmatrix} \begin{bmatrix} \mathbf{R}_{x_1} \\ \mathbf{R}_{x_1 x_2}^H \end{bmatrix} - \lambda \mathbf{I}_N\right) \\ &= \det(\mathbf{R}_{x_1} + \mathbf{R}_{x_1}^{-1} \mathbf{R}_{x_1 x_2} \mathbf{R}_{x_1 x_2}^H - \lambda \mathbf{I}_N). \end{aligned}$$

Hence, the  $N$  largest eigenvalues  $\lambda_{N,n}$  of  $\mathbf{R}_{s|y_2} - \mathbf{R}_{s|x_1, y_2}$  are those of  $\mathbf{R}_1 = \mathbf{R}_{x_1} + \mathbf{R}_{x_1}^{-1} \mathbf{R}_{x_1 x_2} \mathbf{R}_{x_1 x_2}^H$ , the  $N$  remaining ones being zero. The matrix  $\mathbf{R}_1$ , with eigenvalues  $\lambda_{N,n}$ , is easily seen to be asymptotically equivalent to the Toeplitz matrix  $\mathbf{T}_N(P_1)$  with  $P_1(\omega)$  defined as

$$\begin{aligned} P_1(\omega) &= P_{x_1}(\omega) + P_{x_1}^{-1}(\omega) P_{x_1 x_2}(\omega) P_{x_1 x_2}^H(\omega) \\ &= \frac{(1 - \rho^2)(1 + 4\rho^2 + \rho^4 + 2\rho^2 \cos \omega)}{(1 + \rho^2)(1 + \rho^4 - 2\rho^2 \cos \omega)}. \end{aligned}$$

We can readily check that  $P_1(\omega)$  is positive, symmetric and decreasing in  $[0, \pi]$ . The distortion corresponding to the second term of the distortion in (3.16) can thus be evaluated using Lemma 3.3, the integration range (3.18) and integration

formulas from [56, p. 181] as

$$\begin{aligned}
D_p^{(2)}(\alpha) &= \lim_{N \rightarrow \infty} \frac{1}{2N} \sum_{n=1}^{N-K} \lambda_{N,n} \\
&= \frac{1}{4\pi} \int_{\omega \in \mathcal{A}_1^c} P_1(\omega) d\omega \\
&= \frac{1}{4\pi} \int_{\pi\alpha}^{2\pi - \pi\alpha} \frac{(1 - \rho^2)(1 + 4\rho^2 + \rho^4 + 2\rho^2 \cos \omega)}{(1 + \rho^2)(1 + \rho^4 - 2\rho^2 \cos \omega)} d\omega \\
&= 1 - \frac{(1 - \alpha)(1 - \rho^2)}{2(1 + \rho^2)} - \frac{2}{\pi} \arctan \left( \frac{1 + \rho^2}{1 - \rho^2} \tan \left( \frac{\pi\alpha}{2} \right) \right),
\end{aligned}$$

where  $\alpha \sim K/N$ . The result follows by adding  $D_p^{(1)}(\alpha)$  and  $D_p^{(2)}(\alpha)$ .

### 3.A.10 Proof of Proposition 3.6

Similarly to the proof of Proposition 3.5, the first term in the distortion (3.20) is equal to the distortion of the perfect side information scenario with  $R = 0$ , that is,

$$D_p^{(1)}(R) = D_s(0) = \frac{1 - \rho^2}{2(1 + \rho^2)}.$$

The second term in the distortion as well as the rate (3.21) can be computed exactly when  $0 < \theta \leq \bar{\theta}$  with  $\bar{\theta}$  defined as

$$\begin{aligned}
\bar{\theta} &= \min_{\omega} P_1(\omega) \\
&= \min_{\omega} \frac{(1 - \rho^2)(1 + 4\rho^2 + \rho^4 + 2\rho^2 \cos \omega)}{(1 + \rho^2)(1 + \rho^4 - 2\rho^2 \cos \omega)} \\
&= \frac{1 - \rho^2}{1 + \rho^2},
\end{aligned}$$

where  $P_1(\omega)$  is the power spectral density defined in the proof of Proposition 3.5. Using the Toeplitz distribution theorem [59, Th. 4.2], we can write

$$\begin{aligned}
D_p^{(2)}(\theta) &= \lim_{N \rightarrow \infty} \frac{1}{2N} \sum_{n=1}^N \min\{\theta, \lambda_{N,n}\} \\
&= \frac{1}{4\pi} \int_0^{2\pi} \min\{\theta, P_1(\omega)\} d\omega \\
&= \frac{1}{2} \theta,
\end{aligned}$$

where  $\lambda_{N,n}$  are the eigenvalues of the covariance matrix  $\mathbf{R}_1$ . Similarly, using the integration range (3.18) and integration formulas from [56, p. 560], we obtain

$$R_p(\theta)$$

$$\begin{aligned}
&= \lim_{N \rightarrow \infty} \frac{1}{N} \sum_{n=1}^N \max \left\{ 0, \frac{1}{2} \log_2 \frac{\lambda_{N,n}}{\theta} \right\} \\
&= \frac{1}{2\pi} \int_0^{2\pi} \max \left\{ 0, \frac{1}{2} \log_2 \frac{(1-\rho^2)(1+4\rho^2+\rho^4+2\rho^2 \cos \omega)}{\theta(1+\rho^2)(1+\rho^4-2\rho^2 \cos \omega)} \right\} d\omega \\
&= \frac{1}{2} \log_2 \left( \frac{(1-\rho^2)(1+4\rho^2+\rho^4)}{2(1+\rho^2)} + \frac{(1-\rho^2)\sqrt{1+6\rho^2+\rho^4}}{2} \right) - \frac{1}{2} \log_2 \theta.
\end{aligned}$$

Combining  $D_p^{(1)}(\theta)$ ,  $D_p^{(2)}(\theta)$  and  $R_p(\theta)$  yields the desired result. The rate  $\bar{R}$  simply follows as  $\bar{R} = R_p(\bar{\theta})$ . For  $\theta > \bar{\theta}$  (or  $R < \bar{R}$ ), the distortion-rate function must be left in parametric form since, in this case, no analytical expression of  $D_p(\theta)$  and  $R_p(\theta)$  seems to exist.



## Chapter 4

# Gain-rate Optimality

### 4.1 Introduction

We now focus on the problem of binaural hearing aids stated in Section 2.5. Our goal is to compute monaural and binaural gain-rate functions for a simple acoustic scenario. We then wish to compare these results with gain-rate functions obtained using data measured in a realistic acoustic environment.

In Section 4.2, we reformulate the quadratic remote Wyner-Ziv rate-distortion function derived in Theorem 3.4 to take into account a weighted MSE criterion and multiple input channels. As the optimal encoding architecture requires knowledge of statistics that are difficult to compute in a practical setting, we also investigate the optimality of an encoding strategy that does not take into account the side information available at the decoder. In Section 4.3, we then consider a very simple acoustic model for which monaural gain-rate functions can be derived explicitly. In Section 4.4, we present a similar analysis for the binaural scenario. Binaural gain-rate functions are derived and optimal rate allocation strategies are obtained. In Section 4.5, we explore various features of the considered rate-constrained binaural noise reduction system by means of gain-rate functions obtained numerically. For this purpose, we use audio signals recorded using a behind-the-ear hearing aid in a reverberant acoustic environment. The chapter is summarized in Section 4.6.

### 4.2 Coding Strategies

Optimal encoding strategies for the remote Wyner-Ziv problem will be referred to as *side information aware* (SIA) since they require the knowledge of statistics that involve the side information which is only available at the decoder. These statistics may not be computable in practice due to the distributed nature of the communication setup. Moreover, SIA schemes resort to coding techniques (see, e.g., [108]), which often increase significantly the complexity of either the transmitter or the receiver. In a context where low latency and reduced power consumption are of prime interest at both ends of the communication medium, it is worth quantifying the loss incurred by a suboptimal but simpler wireless communication architecture. To this end, we consider the scenario where the data is encoded in a rate-distortion optimal fashion for a decoder that does not

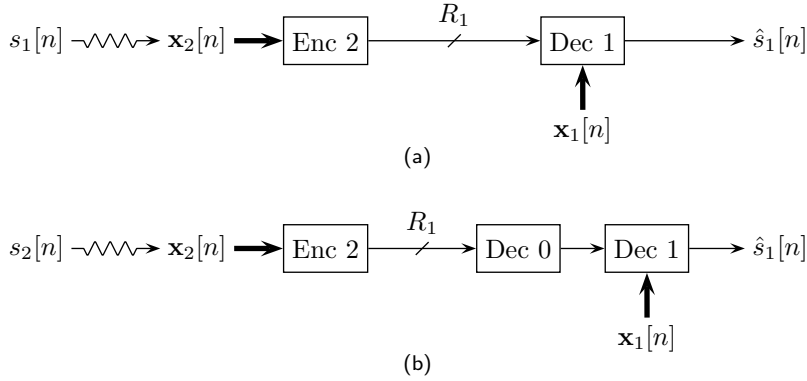


**Figure 4.1:** Block diagram of the two considered coding strategies. (a) SIA coding. (b) SIU coding.

have access to the side information. This second class of encoding strategies will be referred to as *side information unaware* (SIU) since the correlation between the observed signal and the side information does not need to be known at the encoder.

### 4.2.1 Side Information Aware Coding

Let us first reformulate the quadratic remote Wyner-Ziv rate-distortion function derived in Theorem 3.4 to take into account a weighted MSE criterion and multiple microphone inputs. As depicted in Figure 4.1(a), the encoder now observes the vector signal  $\mathbf{x}_2[n]$  corresponding to the remote source  $s_1[n]$  and outputs a bit stream that appears at a rate of  $R_1$  bits per sample. Recall that, in the considered signal model (2.5), the desired source  $s_1[n]$  corresponds to the speech component of the reference microphone, that is,  $s_1[n] = x_{1,0}^s[n]$ . Based on the received data and the side information  $\mathbf{x}_1[n]$ , the decoder computes a reconstruction  $\hat{s}_1[n]$  with weighted MSE [12, Sec. 4.5.4]

$$D_1 = \frac{1}{2\pi} \int_0^{2\pi} |A(\omega)|^2 P_{e_1}(\omega) d\omega, \quad (4.1)$$

where  $A(\omega)$  is the transfer function of the weighting filter  $a[n]$  and  $e_1[n]$  is the reconstruction error process defined as

$$e_1[n] = s_1[n] - \hat{s}_1[n].$$

The optimal rate-distortion trade-off follows directly from Theorem 3.4 by considering vector sequences and an additional weighting operator. For further reference, we record the following theorem.

**Theorem 4.1.** The optimal rate-distortion trade-off with SIA coding is given in parametric form by

$$R_1(\theta) = \frac{1}{4\pi} \int_0^{2\pi} \max \left\{ 0, \log_2 \frac{|A(\omega)|^2 P_1(\omega)}{\theta} \right\} d\omega, \quad (4.2)$$



$$D_1(\theta) = \frac{1}{2\pi} \int_0^{2\pi} |A(\omega)|^2 P_{s_1|x_1, x_2}(\omega) d\omega \quad (4.3)$$

$$+ \frac{1}{2\pi} \int_0^{2\pi} \min\{\theta, |A(\omega)|^2 P_1(\omega)\} d\omega, \quad (4.4)$$

where  $P_1(\omega) = P_{s_1|x_1}(\omega) - P_{s_1|x_1, x_2}(\omega)$  and  $\theta \in (0, \text{ess sup}_\omega |A(\omega)|^2 P_1(\omega)]$ .  $R_1(\theta)$  is expressed in bits per sample and  $D_1(\theta)$  in MSE per sample.

As mentioned in Section 3.4.2, an optimal encoding architecture amounts to first estimating the remote source  $s_1[n]$  as if the innovation process  $\bar{\mathbf{x}}_2[n]$  were available at the encoder (estimation stage), that is, by passing  $\mathbf{x}_2[n]$  through the multichannel Wiener filter with transfer function  $\Phi_{s_1 \bar{x}_2}(\omega) \Phi_{\bar{x}_2}^{-1}(\omega)$ . This estimate is then optimally encoded taking into account the presence of the side information at the decoder (coding stage).

### 4.2.2 Side Information Unaware Coding

We now consider the coding setup illustrated in Figure 4.1(b). The transmitter encodes its observation  $\mathbf{x}_2[n]$  in a rate-distortion optimal fashion for a decoder that does not have access to  $\mathbf{x}_1[n]$ . The decoded signal is then provided to the decoder with side information in order to reconstruct the remote source  $s_1[n]$ . Furthermore, the encoder assumes that the process to be estimated at the other end is  $s_2[n] = x_{2,0}^s[n]$ , that is, the speech component of its own reference microphone. It thus optimizes its coding strategy accordingly. The use of the remote source  $s_2[n]$  in place of  $s_1[n]$  avoids the need, at the encoder, for statistics involving the side information. In this scenario, the encoding strategy reduces to that of a remote source coding problem with a weighted MSE criterion [12, Sec. 4.5.4]. The optimal rate-distortion trade-off under these conditions is given by the following theorem. The normalized frequency  $\omega$  is omitted for conciseness.

**Theorem 4.2.** The optimal rate-distortion trade-off with SIU coding is given in parametric form by

$$\begin{aligned} R_1(\theta) &= \frac{1}{4\pi} \int_0^{2\pi} \max\left\{0, \log_2 \frac{|A|^2 P_1}{\theta}\right\} d\omega, \\ D_1(\theta) &= \frac{1}{2\pi} \int_0^{2\pi} |A|^2 \left( P_{s_1} - \frac{|\Phi_{s_1 x_2} \Phi_{x_2}^{-1} \Phi_{s_2 x_2}^H|^2}{|\Phi_{s_2 x_2} \Phi_{x_2}^{-1} \Phi_{s_2 x_2}^H|^2} P_1 \right) d\omega \\ &\quad + \frac{1}{2\pi} \int_0^{2\pi} \frac{|\Phi_{s_1 x_2} \Phi_{x_2}^{-1} \Phi_{s_2 x_2}^H|^2}{|\Phi_{s_2 x_2} \Phi_{x_2}^{-1} \Phi_{s_2 x_2}^H|^2} \min\{\theta, |A|^2 P_1\} d\omega \\ &\quad - \frac{1}{2\pi} \int_0^{2\pi} |A|^2 \left[ \Phi_{s_1 x_1} - \Phi_1 \max\{0, |A|^2 P_1 - \theta\} \right] \\ &\quad \quad \cdot \left[ \Phi_{x_1} - \Phi_2 \max\{0, |A|^2 P_1 - \theta\} \right]^{-1} \\ &\quad \quad \cdot \left[ \Phi_{s_1 x_1} - \Phi_1 \max\{0, |A|^2 P_1 - \theta\} \right]^H d\omega, \end{aligned}$$

where  $P_1 = P_{s_2} - P_{s_2|x_2}$ ,

$$\Phi_1 = \frac{\Phi_{s_1x_2} \Phi_{x_2}^{-1} \Phi_{s_2x_2}^H \Phi_{s_2x_2} \Phi_{x_2}^{-1} \Phi_{x_1x_2}^H}{|A|^2 P_1^2}$$

and

$$\Phi_2 = \frac{\Phi_{x_1x_2} \Phi_{x_2}^{-1} \Phi_{s_2x_2}^H \Phi_{s_2x_2} \Phi_{x_2}^{-1} \Phi_{x_1x_2}^H}{|A|^2 P_1^2},$$

with  $\theta \in (0, \text{ess sup}_\omega |A|^2 P_1]$ .  $R_1(\theta)$  is expressed in bits per sample and  $D_1(\theta)$  in MSE per sample.

**Proof:** See Appendix 4.A.1. ■

It is important to emphasize that the function  $D_1(R_1)$  described in parametric form by Theorem 4.2 is *not* the result of a variational problem as stated for example in [12, Sec. 2.3]. In particular, it is decreasing but is not necessarily convex. Strictly speaking, we cannot refer to it as a rate-distortion function but more as the optimal rate-distortion trade-off for a particular class of coding strategies. For simplicity of exposure, we however adopt the same notation in Theorems 4.1 and 4.2.

With the SIU scheme, the encoder first computes a weighted MSE estimate of the remote source  $s_2[n]$  using  $\mathbf{x}_2[n]$  (estimation stage) and then encodes it (coding stage). The method is suboptimal in the sense that (i) the remote source does not correspond to the desired source at hearing aid 1 and (ii) the redundancy between  $\mathbf{x}_1[n]$  and  $\mathbf{x}_2[n]$  is not taken into account at the coding stage. It was shown in [37] that, under the considered signal model, the loss incurred at the estimation stage is zero if  $\mathbf{x}_2[n]$  is of dimension one (no dimensionality reduction), or if the power spectral density matrix  $\Phi_{x^s}(\omega)$  of the binaural speech component  $\mathbf{x}^s[n]$  is of rank one, and that the cross correlation between  $\mathbf{x}_1^n[n]$  and  $\mathbf{x}_2^n[n]$  is zero. Therefore, the difference between SIA and SIU coding may not necessarily vanish at high rate. To resolve this asymptotic mismatch, one may combine the estimation stage of the SIA scheme and the coding stage of the SIU scheme. In this case, statistics involving the side information are required for the design of the appropriate multichannel Wiener filter at the encoder. In a bidirectional communication setup, however, an alternating optimization scheme devised by Doclo *et al.* [37] allows to alleviate this problem. This will be discussed in more detail in Chapter 5.

### 4.3 Monaural Gain-rate Trade-offs

Let us apply the optimal rate-distortion trade-offs of Section 4.2 to the problem of binaural noise reduction. We adopt the perspective of hearing aid 1, as depicted in Figure 4.2, and compute the monaural gain-rate function (2.6) for the two coding strategies developed previously. To this end, we consider a very simple scenario which, far from being realistic, allows us to derive explicit formulas which have many of the features of the gain-rate functions computed numerically in a realistic environment (see Section 4.5). It hence provides useful insights about the trade-offs inherent to the problem of rate-constrained binaural noise reduction.

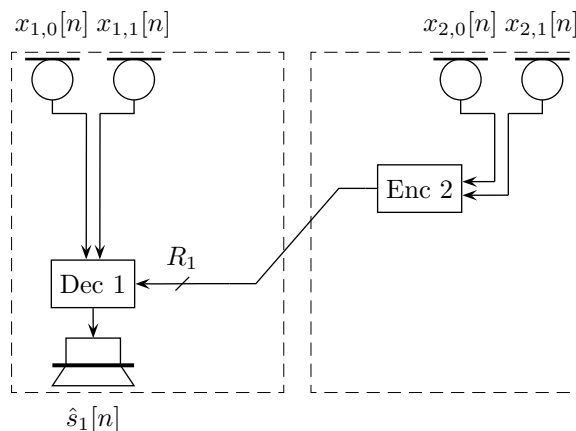


**Figure 4.2:** Monaural communication setup from the perspective of hearing aid 1 with  $L_1 = L_2 = 2$  microphones.

Let us consider the simplified scenario which solely consists of a speech source surrounded by ambient noise. We assume omnidirectional microphones, neglect the head-shadow effect and work under the far-field assumption. The distortion criterion is the MSE, that is, we set  $A(\omega) = 1$  in (4.1). Furthermore, the speech and noise sources have flat power spectral densities. The speech and noise power spectral density matrices of the signals recorded at hearing aid 1 can thus be expressed as

$$\Phi_{x_1^s}(\omega) = \sigma_s^2 \mathbf{H}_1(\omega) \mathbf{H}_1^H(\omega) \quad \text{and} \quad \Phi_{x_1^n}(\omega) = \sigma_{n_1}^2 \mathbf{I}_{L_1},$$

respectively. The quantities  $\sigma_s^2$  and  $\sigma_{n_1}^2$  respectively correspond to the variances of the speech and noise sources. The SNR is denoted by  $\gamma_1$ . The vector  $\mathbf{H}_1(\omega) \in \mathbb{C}^{L_1}$  contains the acoustic transfer functions from the speech source to the microphones and, under our far-field assumption, is given by

$$\mathbf{H}_1(\omega) = [e^{-j\omega\Delta_0}, e^{-j\omega\Delta_1}, \dots, e^{-j\omega\Delta_{L_1-1}}]^T,$$

where  $\Delta_l$  denotes the propagation delay from the source to the  $l$ th microphone ( $l = 0, 1, \dots, L_1 - 1$ ). With these definitions,  $P_{s_1|x_1}(\omega)$  can be computed as

$$\begin{aligned} P_{s_1|x_1}(\omega) &= P_{s_1}(\omega) - \Phi_{s_1x_1}(\omega) \Phi_{x_1}^{-1}(\omega) \Phi_{s_1x_1}^H(\omega) \\ &= \sigma_s^2 - \sigma_s^4 \mathbf{H}_1^H(\omega) [\sigma_s^2 \mathbf{H}_1(\omega) \mathbf{H}_1^H(\omega) + \sigma_{n_1}^2 \mathbf{I}_{L_1}]^{-1} \mathbf{H}_1(\omega) \\ &\stackrel{(a)}{=} \sigma_s^2 [1 + \gamma_1 \mathbf{H}_1^H(\omega) \mathbf{H}_1(\omega)]^{-1} \\ &\stackrel{(b)}{=} \sigma_s^2 (1 + L_1 \gamma_1)^{-1}, \end{aligned} \tag{4.5}$$

where (a) follows from the matrix inversion lemma [69, Sec. 0.7.4] and (b) from the fact that  $\mathbf{H}_1^H(\omega) \mathbf{H}_1(\omega) = L_1$ . Similarly,  $P_{s_1|x_1, x_2}(\omega)$  can be computed as

$$P_{s_1|x_1, x_2}(\omega) = \sigma_s^2 (1 + L_1 \gamma_1 + L_2 \gamma_2)^{-1}, \tag{4.6}$$

where  $\gamma_2$  denotes the SNR at the microphones of hearing aid 2. Using the power spectral densities (4.5) and (4.6) in Theorem 4.1 yields

$$D_1^{(a)}(R_1) = \frac{\sigma_s^2 L_1 L_2 \gamma_1 \gamma_2}{1 + L_1 \gamma_1 + L_2 \gamma_2} \left( 1 + \frac{L_2 \gamma_2}{1 + L_1 \gamma_1} 2^{-2R_1} \right) \quad \text{for } R_1 \geq 0. \quad (4.7)$$

The monaural gain-rate function with SIA coding follows by evaluating the gain-rate function (2.6) using the distortion-rate function (4.7). We find

$$G_1^{(a)}(R_1) = \frac{1 + L_1 \gamma_1 + L_2 \gamma_2}{1 + L_1 \gamma_1} \left( 1 + \frac{L_2 \gamma_2}{1 + L_1 \gamma_1} 2^{-2R_1} \right)^{-1} \quad \text{for } R_1 \geq 0. \quad (4.8)$$

The gain-rate function obtained with the SIU coding scheme can be obtained similarly. Using Theorem 4.2, we obtain

$$D_1^{(u)}(R_1) = \frac{\sigma_s^2}{L_1 \gamma_1} \left[ 1 + \frac{1 + L_2 \gamma_2}{L_1 \gamma_1} (1 + L_2 \gamma_2 2^{-2R_1})^{-1} \right]^{-1} \quad \text{for } R_1 \geq 0. \quad (4.9)$$

The monaural gain-rate function with SIU coding follows by evaluating the gain-rate function (2.6) using the optimal distortion-rate trade-off (4.9). We find

$$G_1^{(u)}(R_1) = \frac{L_1 \gamma_1}{1 + L_1 \gamma_1} + \frac{1 + L_2 \gamma_2}{1 + L_1 \gamma_1} (1 + L_2 \gamma_2 2^{-2R_1})^{-1} \quad \text{for } R_1 \geq 0. \quad (4.10)$$

To get some insights about the gain provided by the wireless link as a function of the communication bitrate, let us consider the case where the hearing aids are both equipped with  $L = 2$  microphones with equal SNR  $\gamma$ . We compare, in Figure 4.3, the gain achieved by the two coding schemes for different signal-to-noise ratios. At 20 dB (see Figure 4.3(a)), we observe that the SIU coding strategy may lead to a significant loss, in terms of noise reduction capability, in comparison to the SIA scheme. However, as the input SNR decreases (see Figures 4.3(b) and 4.3(c)), the spatial correlation between the recorded signals decreases significantly and the gap between the SIA and SIU curves vanishes for all rates. Using the gain-rate functions (4.8) and (4.10), a simple optimization reveals that the maximum loss evaluates as

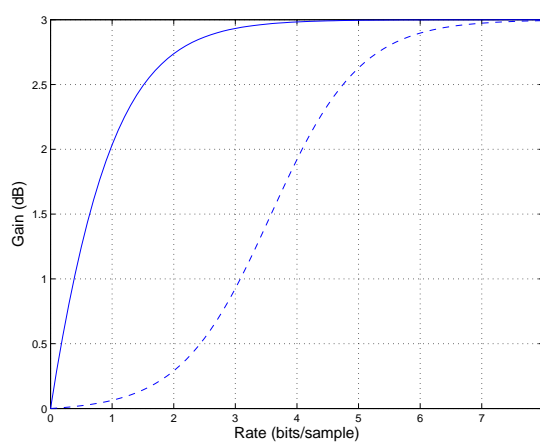
$$\max_{R_1} \frac{G_1^{(a)}(R_1)}{G_1^{(u)}(R_1)} = \frac{(2L\gamma + 1)(L\gamma + 1)}{(L\gamma + \sqrt{L\gamma + 1})^2}, \quad (4.11)$$

and is attained at

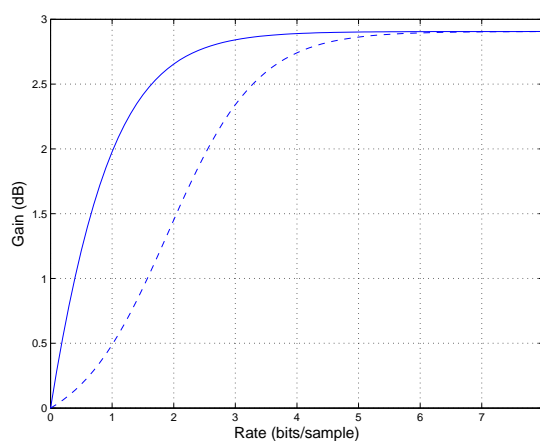
$$\arg \max_{R_1} \frac{G_1^{(a)}(R_1)}{G_1^{(u)}(R_1)} = \frac{1}{2} \log_2 \left( 1 + \sqrt{L\gamma + 1} \right) \quad \text{bits/sample}. \quad (4.12)$$

The maximum loss (4.11) is plotted as a function of the input SNR in Figure 4.4. The result suggests that the use of SIA coding strategies is uninteresting in very noisy scenarios.

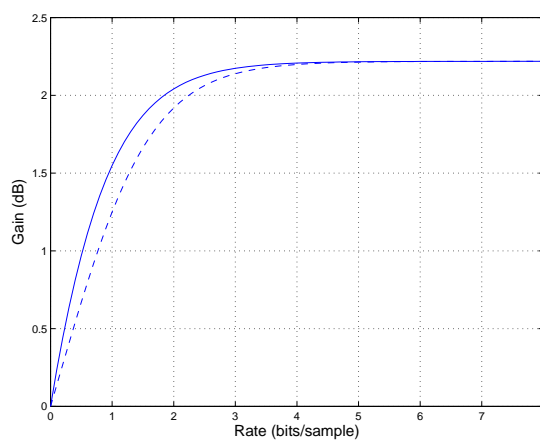
In Figure 4.5, we plot the noise reduction gain provided by the wireless link as a function of the communication bitrate and the input SNR. The following remarks are at hand. At high rates, both gain-rate functions remain bounded



(a)



(b)



(c)

**Figure 4.3:** Monaural gain-rate functions with SIA coding (solid) and SIU coding (dashed) for different input signal-to-noise ratios. (a) 20 dB. (b) 10 dB. (c) 0 dB. We observe that the gain achieved by taking into account the side information may be significant at high SNR but vanishes in very noisy scenarios.

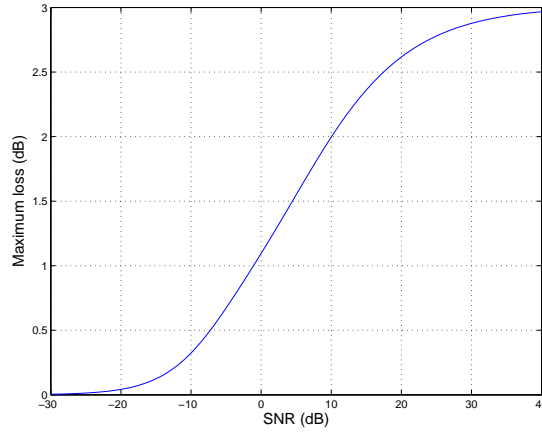
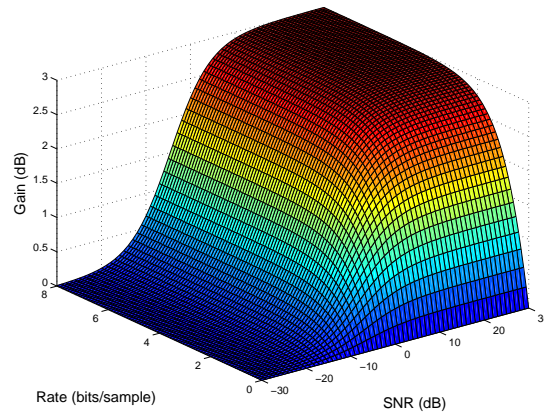


**Figure 4.4:** Maximum loss incurred by the SIU coding strategy over the SIA scheme as a function of the input SNR. We observe that in a highly noisy environment, the gain provided by the SIA approach is rather negligible.

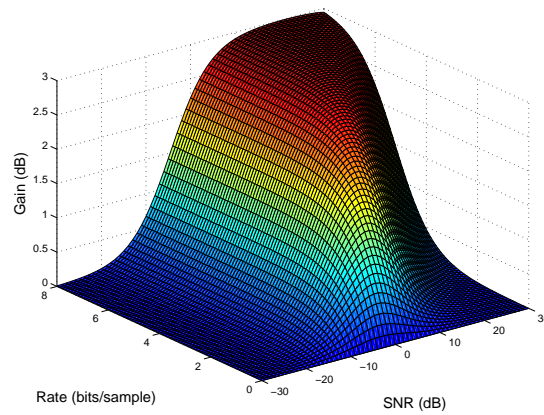
and correspond to the gain obtained when there is no rate constraint. At high SNR, this gain approaches  $10 \log_{10}(2)$  dB where the factor 2 relates to the fact that the wireless link allows doubling the number of available microphones. We also notice that, in this scenario, the results depend neither on the actual position of the source nor on the geometrical properties of the hearing aid setup. This results from the far-field assumption and the fact that the noise is uncorrelated across microphones. While the function gain-rate function with SIA coding is strictly increasing in both  $R_1$  and  $\gamma$ , the gain-rate function with SIU coding behaves slightly differently. It is strictly increasing in  $R_1$  but, for any communication bitrate, there exists a finite SNR which provides maximum gain (see Figure 4.5(b)). This fact may be explained by the following observation. As the SNR increases, the availability of signals recorded from both hearing aids permits a better estimation of the desired source. However, the observed signals also become more correlated. In the scenario where the side information is neglected at the encoder, the communication resources are thus used to transmit redundant information, hence preventing significant noise reduction. The observed “optimum” follows from these two opposite behaviors.

## 4.4 Binaural Gain-rate Trade-offs

Let us now turn our attention to the binaural setup depicted in Figure 4.6. A natural question that arises in this context is that of the optimal rate allocation between the two hearing instruments. More precisely, assume that you are given a total bit budget of  $R$  bits per sample, how should this be allocated to  $R_1$  and  $R_2$  to minimize the sum distortion  $D = D_1 + D_2$ , hence maximizing the binaural gain  $G(R)$  given by (2.7)? To this end, observe that the setup depicted in Figure 4.6 corresponds to two separate source coding problems.



(a)



(b)

**Figure 4.5:** Gain provided by the wireless communication link as a function of the communication bitrate and the input SNR with (a) SIA coding and (b) SIU coding. We observe that the gain-rate function in (a) is strictly increasing in both the rate and SNR while, in case (b), there exists a finite input SNR which provides maximum gain.

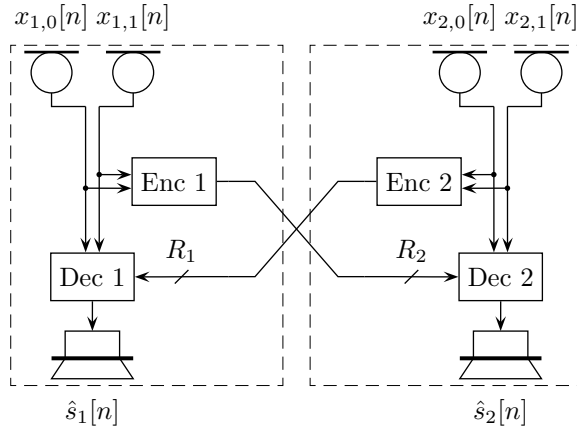


**Figure 4.6:** Binaural communication setup with  $L_1 = L_2 = 2$  microphones.

The optimal distortion-rate trade-off can thus be obtained as

$$D(R) = \min_{R_1, R_2} D_1(R_1) + D_2(R_2), \quad (4.13)$$

$$\text{s.t. } R_1 + R_2 \leq R \text{ and } R_1, R_2 \geq 0.$$

We consider the simple scenario studied in Section 4.3 as a means to obtain a closed-form solution to the above minimization task and to provide the optimal policy for rate allocation between the two hearing aids. In the sequel, we assume, without loss of generality, that  $\gamma_1 \geq \gamma_2$ .

Let us first consider the SIA coding scheme. In this case, the minimization problem (4.13) can be restated as

$$D^{(a)}(R) = \min_{R_1, R_2} f(R_1, R_2),$$

$$\text{s.t. } g_k(R_1, R_2) \leq 0 \text{ for } k = 1, 2, 3,$$

with  $f, g_k : \mathbb{R}^2 \rightarrow \mathbb{R}$  defined by

$$f(R_1, R_2) = D_1^{(a)}(R_1) + D_2^{(a)}(R_2),$$

$$g_1(R_1, R_2) = R_1 + R_2 - R,$$

$$g_2(R_1, R_2) = -R_1 \text{ and}$$

$$g_3(R_1, R_2) = -R_2,$$

where  $D_1^{(a)}(R_1)$  and  $D_2^{(a)}(R_2)$  are computed from (4.7). Since the functions  $f$  and  $g_k$  are convex and differentiable on  $\mathbb{R}^2$ , the optimal solution  $(R_1, R_2)$  follows from the Karush-Kuhn-Tucker conditions [19, Sec. 5.5.3]. We obtain

$$R_1 = \begin{cases} \frac{1}{2}(R - \bar{R}) & \text{if } R \geq \bar{R}^{(a)}, \\ 0 & \text{otherwise,} \end{cases} \quad (4.14)$$



and

$$R_2 = R - R_1, \quad (4.15)$$

where the threshold rate is given by

$$\bar{R}^{(a)} = \bar{R} = \frac{1}{2} \log_2 \frac{L_1 \gamma_1 (L_1 \gamma_1 + 1)}{L_2 \gamma_2 (L_2 \gamma_2 + 1)}. \quad (4.16)$$

The binaural gain-rate function  $G^{(a)}(R)$  follows by substituting the optimal distortion-rate trade-off

$$D^{(a)}(R) = D_1^{(a)}(R_1) + D_2^{(a)}(R_2),$$

computed using (4.7), (4.14) and (4.15) into the definition (2.7). We find

$$G^{(a)}(R) = \begin{cases} C_1 \left[ 2 + \frac{2L_2\gamma_2}{L_1\gamma_1 + 1} 2^{-(R-\bar{R})} \right]^{-1} & \text{if } R \geq \bar{R}^{(a)}, \\ C_1 \left[ 1 + \frac{L_1\gamma_1 + L_2\gamma_2 + 1}{L_1\gamma_1 + 1} + \frac{L_2\gamma_2}{L_1\gamma_1 + 1} 2^{-2(R-\bar{R})} \right]^{-1} & \text{otherwise,} \end{cases}$$

where the constant  $C_1$  is defined as

$$C_1 = 1 + \frac{L_2\gamma_2}{L_1\gamma_1 + 1} + \frac{L_1\gamma_1 + L_2\gamma_2 + 1}{L_2\gamma_2 + 1}.$$

Let us now consider the SIU coding scheme. In this case, the minimization problem (4.13) cannot be solved using the Karush-Kuhn-Tucker conditions since the optimal distortion-rate trade-offs given by (4.9) are not necessarily convex. However, they are strictly decreasing. The inequality  $R_1 + R_2 \leq R$  is thus active at the optimum, otherwise we can always increase  $R_1$  or  $R_2$  and lower the distortion. The optimization task (4.13) thus reduces to

$$\begin{aligned} D^{(u)}(R) &= \min_{R_1} D_1^{(u)}(R_1) + D_2^{(u)}(R - R_1), \\ \text{s.t. } & 0 \leq R_1 \leq R. \end{aligned}$$

A tedious but relatively straightforward functional analysis reveals that the optimal solution  $(R_1, R_2)$  is given by

$$R_1 = \begin{cases} \frac{1}{2} (R - \bar{R}) - \frac{1}{2} \log_2 \frac{1 - C_2 2^{-(R+\bar{R})}}{1 - C_2 2^{-(R-\bar{R})}} & \text{if } R \geq \bar{R}^{(u)}, \\ 0 & \text{otherwise,} \end{cases} \quad (4.17)$$

and

$$R_2 = R - R_1, \quad (4.18)$$

where  $\bar{R}$  is given by (4.16), the constant  $C_2$  is defined as

$$C_2 = \frac{L_1 L_2 \gamma_1 \gamma_2}{L_1 \gamma_1 + L_2 \gamma_2 + 1},$$

and the threshold rate is expressed as

$$\bar{R}^{(u)} = \max \left\{ 0, \bar{R} + \log_2 \frac{C_2 + 1}{2} \left( 1 + \sqrt{1 - \frac{4C_2}{(C_2 + 1)^2} 2^{-2\bar{R}}} \right) \right\}. \quad (4.19)$$

The binaural gain-rate function  $G^{(u)}(R)$  follows by substituting the optimal distortion-rate trade-off

$$D^{(u)}(R) = D_1^{(u)}(R_1) + D_2^{(u)}(R_2),$$

computed using (4.9), (4.17) and (4.18) into the definition (2.7). We find

$$G^{(u)}(R) = \begin{cases} C_3 (L_1 \gamma_1 + L_2 \gamma_2 + 2) \left[ 2^{-2R} - \left( \frac{1}{C_2} \right)^2 \right] \\ \cdot \left[ (L_1 \gamma_1 + L_2 \gamma_2) 2^{-2R} - 2 \sqrt{\frac{1}{C_3}} 2^{-R} - \frac{2}{C_2} \right]^{-1} & \text{if } R \geq \bar{R}^{(u)}, \\ \left[ 1 + \frac{L_1 \gamma_1 + 1}{L_2 \gamma_2 + 1} \right] \\ \cdot \left[ 1 + \frac{(1 + L_1 \gamma_1)(1 + L_1 \gamma_1 2^{-2R})}{(1 + L_1 \gamma_1 + L_2 \gamma_2)(1 + C_2 2^{-2R})} \right]^{-1} & \text{otherwise,} \end{cases}$$

where the constant  $C_3$  is defined as

$$C_3 = \frac{L_1 L_2 \gamma_1 \gamma_2}{(L_1 \gamma_1 + 1)(L_2 \gamma_2 + 1)}.$$

In Figure 4.7(a), we plot an example of binaural gain-rate function for  $\gamma_1 = 10$  dB and  $\gamma_2 = 0$  dB when both hearing aids are equipped with  $L = 2$  microphones. The corresponding rate allocation is depicted in Figure 4.7(b). The rate allocation strategies derived above suggest that the hearing device with smaller SNR does not transmit any data unless the total available bitrate is larger than a given threshold. Below this rate, the noisiest device benefits exclusively from the available bandwidth. At equal SNR, the threshold rate of the SIA coding scheme (4.16) is equal to zero. In other words, the communication link is evenly shared between the two hearing aids for all rates. By contrast, the threshold rate with SIU coding (4.19) reduces to

$$\bar{R}^{(u)} = \max \{0, \log_2 C_2\} = \max \left\{ 0, \log_2 \frac{L^2 \gamma^2}{2L\gamma + 1} \right\},$$

such that it is greater than zero for large enough SNR. Below this threshold rate, the communication bandwidth is fully allocated to one hearing aid. In this case, it can be checked that the hearing device benefiting from the wireless link can be chosen arbitrarily, as expected from the symmetry of the problem. Figure 4.8 depicts the percentage of the total bitrate benefiting to hearing aid 1 for different input signal-to-noise ratios. With SIU coding at equal SNR, we observe a sharp transition between two policies, namely unidirectional communication and equal rate allocation. We also note that the SIU threshold rate is

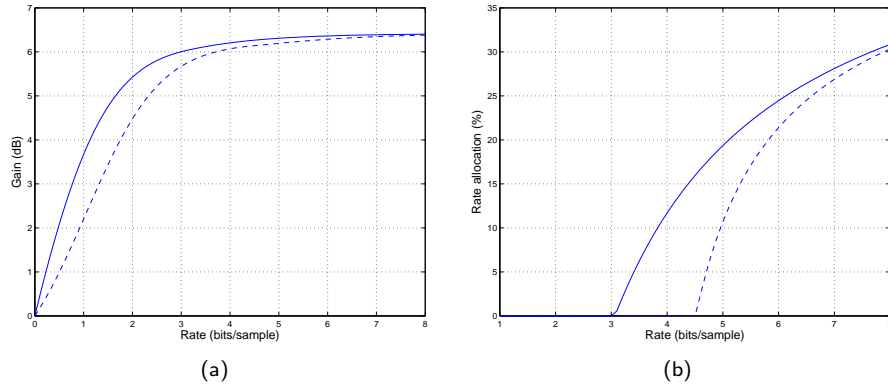


**Figure 4.7:** Binaural communication using SIA coding (solid) and SIU coding (dashed). (a) Binaural gain-rate functions. (b) Percentage of the total bitrate benefitting to hearing aid 1. Here,  $\gamma_1 = 10$  dB and  $\gamma_2 = 0$  dB. We observe that, for small enough rates, the noisiest device benefits exclusively from the wireless link.

larger than that of the SIA coding scheme.

## 4.5 Simulation Results

We present numerical results obtained from acoustic data recorded in a realistic environment. The recording setup is described along with the considered distortion measure. Different noise configurations are then simulated as a means to quantify the real benefit of SIA coding over SIU coding in a practical scenario. We also explore the gain provided by the increased spatial extent enabled by the wireless link. Finally, we discuss optimal rate allocation strategies.

### 4.5.1 Setup

Two hearing aids, each equipped with 2 omnidirectional microphones at a distance of approximately 1 cm, have been mounted on a dummy head in a room with reverberation time [97, Sec. 9.5]  $T_{60} \approx 120$  ms. The head-related transfer functions (HRTF) for the 4 microphones have been measured every  $15^\circ$  in the horizontal plane for a loudspeaker at a distance of 1 m. The angles are measured clockwise and the zero angle corresponds to the front. The sampling frequency is set to 20.48 kHz. The acoustic scene is synthesized using the measured HRTFs. The speech component in (2.5) corresponds to a single speech source at  $0^\circ$ , that is, it is obtained as the convolution of a speech signal with the corresponding head-related impulse response (HRIR). The noise component consists of a stationary white Gaussian ambient noise along with one or more interfering point sources of equal power at different azimuths. The power spectral density of the speech component is estimated using 3 seconds of a sentence of the HINT database [98]. The power spectral density of the interferers are each computed using a 3 second segment of multi-talker babble noise available in the NOISEX-92 database [140]. The HINT database is

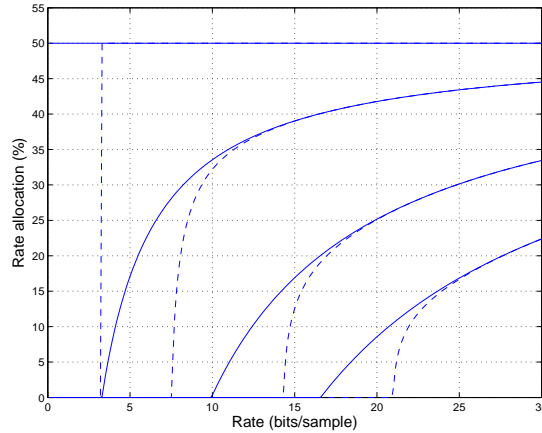


**Figure 4.8:** Percentage of the total bitrate benefiting to hearing aid 1 with SIA coding (solid) and SIU coding (dashed). The different sets of curves correspond to  $(\gamma_1, \gamma_2) \in \{(10, 10), (20, 10), (40, 10), (60, 10)\}$  dB (left to right). We observe that the threshold rate for SIU coding is larger than that for SIA coding.

commonly used for speech intelligibility studies and the NOISEX-92 database contains excerpts from various realistic noisy environments. The power of the involved sources is adjusted such as to meet a desired (broadband) SNR of 0 dB at the front microphone of hearing aid 1.

To assess the noise reduction improvement provided by collaborating hearing aids, the transfer function  $A(\omega)$  used in the weighted MSE (4.1) expresses the relative importance of the frequency  $\omega$  for speech intelligibility, as defined in [1]. Note also that, unless otherwise stated, the results presented in this section are computed from the perspective of hearing aid 1.

#### 4.5.2 Coding Strategies

Figure 4.9 depicts the monaural gain-rate functions for a single interfering source at  $90^\circ$ . In this scenario, the estimation stage of the SIU encoder is strictly suboptimal compared to that of the SIA encoder (more than one microphone and correlated noises between the hearing aids). The loss incurred by the SIU scheme is thus significant, in particular in the high-rate regime. Note that the use of the SIA estimation stage would remedy this asymptotic mismatch. As the number of interfering sources increases, however, the correlation between the signals recorded at the hearing aids decreases. Figure 4.10 plots the maximum loss (4.11) over all rates for different noise configurations. We observe that the performance gap between the two coding strategies is reduced significantly, corroborating the analytical results obtained for the simple acoustic model analyzed in Section 4.3. While SIA coding strategies may provide large gains in simple acoustic environments, their use is rather questionable in more noisy scenarios, for example, a discussion in a very crowded room.

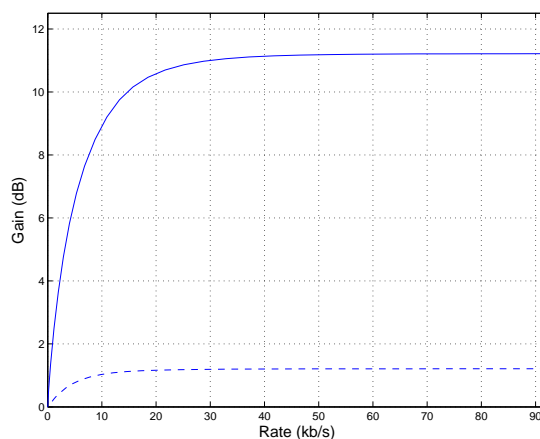


**Figure 4.9:** Monaural gain-rate functions with SIA coding (solid) and SIU coding (dashed) in the presence of one interferer at  $90^\circ$ .

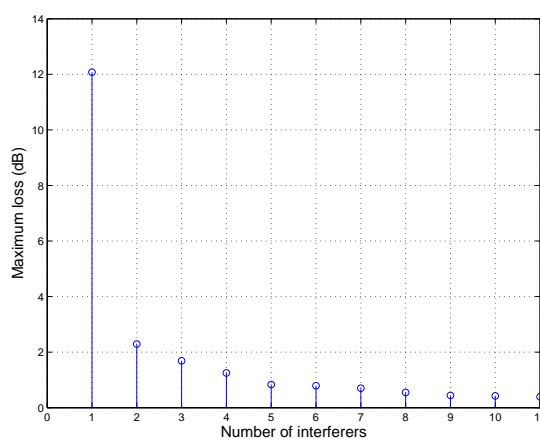


**Figure 4.10:** Maximum loss incurred by the SIU coding strategy over the SIA scheme as a function of the number of interfering point sources. The first interferer is positioned at  $30^\circ$  and the subsequent ones every  $30^\circ$  clockwise. The SNR is kept fixed for all configurations. We observe that the loss associated with the use of the SIU scheme is negligible in a very noisy environment.

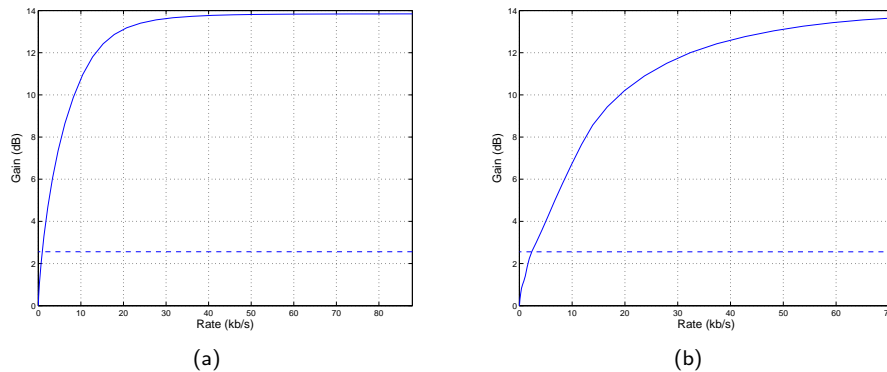


**Figure 4.11:** Comparison of the gains obtained for a monaural (dashed) and binaural (solid) microphone configuration with one interferer at  $15^\circ$ . The coding scheme is (a) SIA and (b) SIU. In the monaural case, we use two microphones of the same hearing device; there is no rate constraint. In the binaural case, we use the first microphone of each hearing aid. We observe that the use of binaural signals provide large beamforming gains.

### 4.5.3 Spatial Extent

The use of a wireless link allows combining signals from microphones that together form an array with greater spatial extent, enabling better beamforming resolution. To illustrate this fact, Figure 4.11 depicts the monaural gain-rate functions obtained using the first microphone of each hearing device (binaural configuration), typically 20 cm apart. We compare these gains with that achieved using the two microphones directly embedded in hearing aid 1 (monaural configuration). We observe that, for large enough communication rates, significant gains can be achieved by exploiting the inter-aural distance. At very low bitrates, however, the quality of the transmitted signal is not sufficient for the binaural configuration to compete with the monaural one, since the latter does not undergo any communication rate constraints. Note that, more generally, the beamforming capability of the system can be evaluated by means of its directivity pattern; the system is optimized for a specific acoustic scenario and the response to a monochromatic source is computed for all possible propagating directions. In the considered rate-constrained setup, however, the computation of such a directivity pattern would require to derive the distortion achieved when the input statistics differ from those used to design the associated encoding and decoding algorithms. Hence, the optimal rate-distortion trade-offs derived in Section 4.2 cannot be used for this purpose.

### 4.5.4 Rate Allocation

As already mentioned previously, the rate-constrained binaural noise reduction problem raises two important questions related to the allocation of the available communication resources. In a binaural setup, how should the total bitrate be shared between the two hearing devices? How should then each hearing aid allocate its own resources across the signal bandwidth?

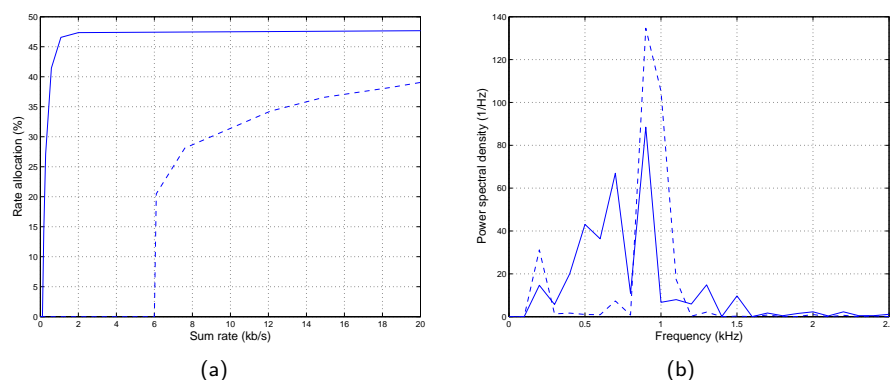


**Figure 4.12:** Rate allocation with one interferer at  $90^\circ$  using SIA coding (solid) and SIU coding (dashed). (a) Percentage of the total bitrate benefiting to hearing aid 1. Hearing aid 1 is subject to less disturbances and thus benefits of less communication resources. (b) Power spectral densities used for the reverse water-filling allocation strategy.

The first issue was addressed in Section 4.4 in a simple, yet insightful, scenario. The intuition is that the hearing device that undergoes the strongest disturbances benefits from the total available bitrate up to a certain threshold, above which the communication resources start being shared. Figure 4.12(a) depicts the rate allocation in the case of an interfering point source at  $90^\circ$ . Owing to the head-shadow effect, the right hearing aid experiences more noise than the left device. This fact is even more apparent in acoustic environment with low reverberation, such as the one considered here. As it can be observed, the percentage of the total available bitrate benefiting to the left hearing aid remains null up to the threshold rate  $\bar{R}^{(a)} \approx 0.1$  kb/s with SIA coding, and  $\bar{R}^{(u)} \approx 6$  kb/s with SIU coding. The rate allocation strategy thus exhibits a behavior similar to that of the scenario analyzed in Section 4.4 for which the optimal rule has been derived.

The second issue pertains to the allocation of the bitrate across the frequency support of the transmitted signal, at one hearing device. The optimal strategy directly follows from Theorems 4.1 and 4.2 which suggest to allocate the available bitrate according to the reverse water-filling principle (see Section 2.3), that is, such that the frequency bands with higher energy are allocated more bitrate. For illustration purpose, we plot in Figure 4.12(b) the one-sided power spectral densities used at hearing aid 1 for rate allocation with SIA and SIU coding in the presence of a single interferer at  $45^\circ$ . In this example, the frequency band with center frequency 700 Hz is significant for the rate allocation with SIA coding, while it has little importance in the SIU scheme.

## 4.6 Summary

The fundamental trade-off between communication bitrate and binaural noise reduction was investigated. We considered two coding strategies: the first one assumes that statistics involving the side information can be computed at the

---

encoder. The second one does not take into account this side information. The optimal rate-distortion trade-offs under these assumptions were derived for a multi-microphone setting and a weighted MSE criterion.

We then applied these results to the computation of gain-rate functions. We considered a very simple model which allowed us to derive explicit formulas and explore the main features of the considered rate-constrained binaural noise reduction system. We first computed monaural gain-rate functions. The main differences between the two coding methods were investigated. We then derived optimal binaural gain-rate trade-offs. A particular emphasis was put on the problem of rate allocation between the hearing aids. We showed that, as intuition suggests, the hearing device experiencing more noise benefits from more communication bandwidth. However, while the resources are evenly shared at equal signal-to-noise ratios with SIA coding, this is not necessarily true with SIU coding. In fact, for low enough bitrates, only one device may benefit from the wireless link.

We then explored various characteristics of the problem using experimental data. In particular, we studied the increase of spatial resolution enabled by a microphone array with greater spatial extent. More importantly, we showed that the insights gained from the simple acoustic model are corroborated with measurements done in a realistic acoustic environment.



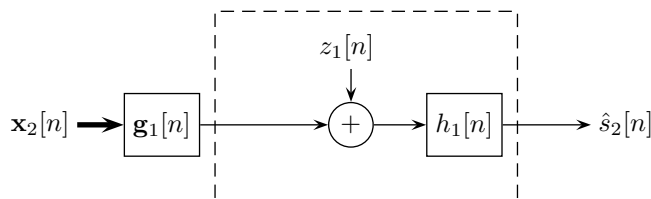


**Figure 4.13:** System describing the optimal reconstruction in the remote source coding problem. The dashed rectangle indicates the optimum forward test channel.

## 4.A Proofs

### 4.A.1 Proof of Theorem 4.2

The optimal encoding strategy reduces to that of a remote source coding problem. The rate  $R_1(\theta)$  hence directly follows from the remote rate-distortion function in [12, Sec. 4.5.4]. Moreover, the signal reconstructed at the decoder DEC 0 (see Figure 4.1(b)), denoted by  $\hat{s}_2[n]$ , can be described by the system depicted in Figure 4.13. The observed process  $\mathbf{x}_2[n]$  is first passed through a linear and time-invariant multichannel filter  $\mathbf{g}_1[n]$  with transfer function

$$\mathbf{G}_1(\omega) = \Phi_{s_2 x_2}(\omega) \Phi_{x_2}^{-1}(\omega),$$

to obtain a process whose power spectral density is given by

$$P_1(\omega) = P_{s_{21}}(\omega) - P_{s_{21}|x_2}(\omega) = \Phi_{s_{21} x_2}(\omega) \Phi_{x_2}^{-1}(\omega) \Phi_{s_{21} x_2}^H(\omega).$$

We then add an independent Gaussian noise  $z_1[n]$  with mean zero and power spectral density

$$P_{z_1}(\omega) = \max \left\{ 0, \frac{\theta P_1(\omega)}{|A(\omega)|^2 P_1(\omega) - \theta} \right\},$$

where  $\theta \in (0, \text{ess sup}_\omega |A(\omega)|^2 P_1(\omega)]$ . Finally, the resulting spectrum is bandlimited by the filter  $h_1[n]$  with frequency response

$$H_1(\omega) = \max \left\{ 0, \frac{|A(\omega)|^2 P_1(\omega) - \theta}{|A(\omega)|^2 P_1(\omega)} \right\}.$$

The filter  $h_1[n]$  is tantamount to an ideal bandlimiting filter with frequency support

$$\left\{ \omega : |A(\omega)|^2 P_1(\omega) \geq \theta \right\}$$

whose output, denoted by  $r[n]$ , is passed through the Wiener filter implementing the optimum MSE decoding rule  $\hat{s}_2[n] = \mathcal{E} \{ s_2[n] | r[n] \}$ . Since  $\mathbf{x}_1[n]$  is available at the decoder DEC 1, and that we are interested in  $s_1[n]$  and not in  $s_2[n]$ , the optimum MSE estimation rule may be replaced by  $\hat{s}_1[n] =$

$\mathcal{E} \{s_1[n]|r[n], \mathbf{x}_1[n]\}$ . The resulting weighted MSE can thus be expressed as

$$\begin{aligned} & \frac{1}{2\pi} \int_0^{2\pi} |A(\omega)|^2 P_{s_1|r, \mathbf{x}_1}(\omega) d\omega \\ &= \frac{1}{2\pi} \int_0^{2\pi} |A(\omega)|^2 P_{s_1|r}(\omega) d\omega \\ & - \frac{1}{2\pi} \int_0^{2\pi} |A(\omega)|^2 \Phi_{s_1 \bar{\mathbf{x}}_1}(\omega) \Phi_{\bar{\mathbf{x}}_1}^{-1}(\omega) \Phi_{s_1 \bar{\mathbf{x}}_1}^H(\omega) d\omega, \end{aligned} \quad (4.20)$$

where  $\bar{\mathbf{x}}_1[n] = \mathbf{x}_1[n] - \mathcal{E} \{\mathbf{x}_1[n]|r[n]\}$ . The first term in (4.20) corresponds to the error made in a remote setup where no side information is available. The second term is the gain provided by the availability of  $\mathbf{x}_1[n]$  for the reconstruction. Evaluating the power spectral densities involved in (4.20) immediately yields the claimed distortion formula.

## Chapter 5

# Multichannel Filtering in the Weighted Overlap-Add Domain

### 5.1 Introduction

A key building block of the distributed coding architectures described in Chapter 4 is a multichannel Wiener filter (MWF). It is applied at each hearing aid to produce the loudspeaker output as well as to compute the signal transmitted over the wireless link. For complexity reasons, filtering is often performed using frequency-domain operations. The signals are analyzed with a filter bank and linearly combined in the transformed domain. The time-domain output is then synthesized. While modification occurs in the frequency domain, it must be kept in mind that the MSE reconstruction error is evaluated using the time-domain signals provided to the ears, that is, using a time-domain MSE criterion.

We consider a weighted overlap-add (WOLA) filter bank, which allows for an efficient realization of a DFT filter bank, and investigate optimal filtering strategies that account for the modifications introduced by the WOLA structure. In Section 5.2, we first study monaural filtering, namely filtering that occurs at each hearing device to produce the loudspeaker output. Three optimization schemes are proposed and their complexity is discussed. Recursive algorithms to compute the filter weights are described. Section 5.3 then addresses binaural filtering, where the signals transmitted over the wireless link must also be computed. We comment on practical implementation issues that arise with this binaural configuration. Section 5.4 presents simulation results to evaluate the performance of the considered optimization methods and Section 5.5 summarizes the chapter.

### 5.2 Monaural Filtering

Let us first consider the multichannel filter that operates on the input signals in order to produce the loudspeaker output. We describe the processing architec-

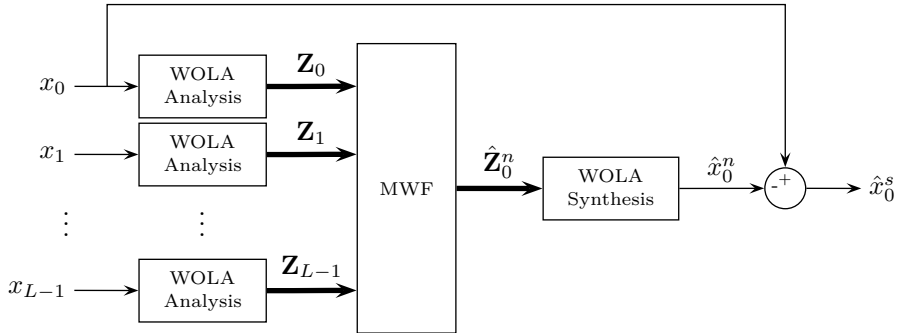


**Figure 5.1:** Block diagram of the monaural WOLA filtering architecture. The time and frame indexes are omitted for conciseness.

ture and define a frequency-domain optimality criterion. As the corresponding optimization problem appears untractable, we derive three suboptimal solutions along with the associated recursive algorithms. We finally discuss some practical considerations related to delay and computational complexity.

## 5.2.1 Processing Architecture

### Overview

Let us consider again the signal model (2.5). We denote by  $x_l[n]$  the discrete-time signal at the  $l$ th input channel. For ease of notation, the index of the hearing aid is omitted. These inputs can be microphone recordings or signals received from the wireless link. As this chapter specifically addresses the estimation part of the distributed source coding problem, we will assume the communication bitrate to be high enough such as to neglect the quantization noise added to the signals transmitted over the communication link. In this case, we decompose the input signals into uncorrelated speech and noise components as

$$x_l[n] = x_l^s[n] + x_l^n[n] \quad \text{for } l = 0, 1, \dots, L - 1.$$

Recall that our goal is to estimate the speech component of the reference microphone (microphone 0). It can be easily shown that, under a MSE criterion, we can equivalently estimate the noise component of the reference signal and subtract it from the original signal as

$$\hat{x}_0^s[n] = x_0[n] - \hat{x}_0^n[n]. \quad (5.1)$$

From an implementation point of view, this has the advantage to provide the loudspeaker with the original (unprocessed) signal if the multichannel filtering module fails, or is simply inactive. The algorithm proceeds as illustrated by the block diagram in Figure 5.1. Each input sequence  $x_l[n]$  is first passed through the analysis part of a WOLA filter bank with  $K$  channels to obtain the short-time Fourier sequences  $Z_{l,k}[m]$  for  $k = 0, 1, \dots, K - 1$ . The index  $m$  denotes the frame index. These sequences are then put into a multichannel Wiener

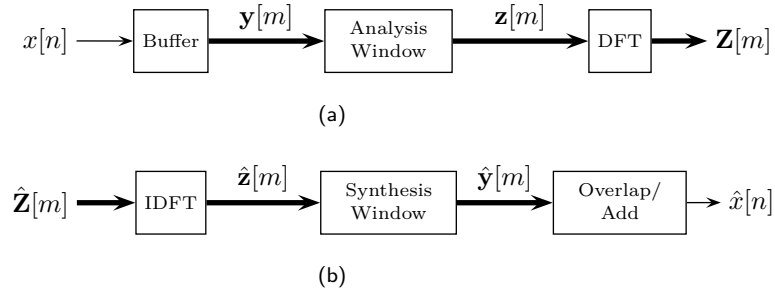


**Figure 5.2:** Block-by-block interpretation of the WOLA filter bank. (a) Analysis part. (b) Synthesis part.

filter which computes an estimate  $\hat{Z}_{0,k}^n[m]$  of the noise present in the reference signal  $Z_{0,k}[m]$ . This estimate is passed through the synthesis part of a WOLA filter bank to obtain the signal  $\hat{x}_0^n[n]$ . The latter is finally subtracted from the reference signal to produce the loudspeaker output (5.1).

To get some insights into the optimization problem at hand, let us assume that the first  $N$  coefficients of  $x_0^n[n]$  are non-zero and denote by  $\mathbf{x}_0^n \in \mathbb{C}^N$  the vector

$$\mathbf{x}_0^n = [x_0^n[0], x_0^n[1], x_0^n[N-1]]^T.$$

Let  $\mathbf{Z}_0^n \in \mathbb{C}^{MK}$  be the corresponding vector of transformed (or filter bank) coefficients

$$\mathbf{Z}_0^n = [Z_{0,0}^n[0], \dots, Z_{0,K-1}^n[0], \dots, Z_{0,0}^n[M-1], \dots, Z_{0,K-1}^n[M-1]]^T.$$

The vectors  $\hat{\mathbf{x}}_0^n \in \mathbb{C}^N$  and  $\hat{\mathbf{Z}}_0^n \in \mathbb{C}^{MK}$  are defined similarly. Under appropriate conditions, the WOLA filter bank implements a tight frame expansion [93, Sec. 5.2] such that

$$\mathcal{E} \left\{ \|\mathbf{x}_0^n - \hat{\mathbf{x}}_0^n\|^2 \right\} = C \mathcal{E} \left\{ \|\mathbf{Z}_0^n - \hat{\mathbf{Z}}_0^n\|^2 \right\} \quad (5.2)$$

for some constant  $C > 0$ . Provided that we have access to the *entire* input sequence, mean square optimality in the time domain can thus be guaranteed in the transformed domain using a standard Wiener approach. In practice, however, coefficients are only observed on a frame-by-frame basis. In this case, an equality of the form (5.2) no longer holds since some of the coefficients are not taken into account. Our goal is thus to provide mean square optimal strategies at this frame level. To this end, we will express the sequence  $x_0^n[n]$  using frequency domain operations, define a frame-based optimality criterion and investigate various filtering architectures. Before we proceed let us first describe in more detail the WOLA analysis and synthesis blocks as well as the multichannel Wiener filter.

### Weighted Overlap-Add Filter Bank

A WOLA filter bank is based on a block-by-block interpretation of a DFT filter bank. As depicted in Figure 5.2, it can be divided into two main parts: the *analysis* part and the *synthesis* part. The analysis part maps a discrete-time

input signal  $x[n]$  into a short-time Fourier transform representation  $Z_k[m]$ . The synthesis part reconstructs a discrete-time output signal  $\hat{x}[n]$  from input sequences  $\hat{Z}_k[m]$ . The filter bank is said to be perfect reconstruction if  $\hat{x}[n]$  is equal to  $x[n]$  when no processing occurs in the transformed domain<sup>1</sup>, that is, when  $\hat{Z}_k[m] = Z_k[m]$  for all  $k \in \{0, 1, \dots, K-1\}$ . Let us now describe each part in detail.

The analysis part consists of the following operations. First, the sample-based input sequence  $x[n]$  is converted to a frame-based sequence by grouping  $K$  consecutive samples with a  $K-S$  sample overlap, such that the frame  $\mathbf{y}[m] \in \mathbb{C}^K$  can be written in vector form as

$$\mathbf{y}[m] = [x[mS], x[mS+1], \dots, x[mS+K-1]]^T.$$

The value  $S$  corresponds to the shift, in samples, from one frame to the next. In the sequel, we assume that  $K$  is a multiple of  $S$ . Every frame is then multiplied by an analysis window  $g[n]$  of size  $K$  with coefficients  $g[0], g[1], \dots, g[K-1]$  such that the windowed frame  $\mathbf{z}[m] \in \mathbb{C}^K$  can be expressed as

$$\mathbf{z}[m] = \mathbf{D}_g \mathbf{y}[m],$$

where  $\mathbf{D}_g \in \mathbb{C}^{K \times K}$  denotes the diagonal matrix whose diagonal elements are given by  $g[0], g[1], \dots, g[K-1]$ . A DFT is applied to the result yielding the short-time Fourier representation

$$\mathbf{Z}[m] = [Z_0[m], Z_1[m], \dots, Z_{K-1}[m]]^T = \mathbf{F} \mathbf{z}[m],$$

where  $\mathbf{F} \in \mathbb{C}^{K \times K}$  denotes the DFT matrix.

The synthesis part can be described as follows. The input frame

$$\hat{\mathbf{Z}}[m] = [\hat{Z}_0[m], \hat{Z}_1[m], \dots, \hat{Z}_{K-1}[m]]^T$$

is first converted to time domain as

$$\hat{\mathbf{z}}[m] = \mathbf{F}^{-1} \hat{\mathbf{Z}}[m],$$

and a synthesis window  $h[n]$  of size  $K$  with coefficients  $h[0], h[1], \dots, h[K-1]$  is applied to obtain

$$\hat{\mathbf{y}}[m] = \mathbf{D}_h \hat{\mathbf{z}}[m]. \quad (5.3)$$

For each index  $n$ , the value of the discrete-time output sequence  $\hat{x}[n]$  is obtained by adding the contribution of  $K/S$  overlapping frames as (backward formula)

$$\hat{x}[n] = \sum_{q=0}^{K/S-1} \mathbf{u}_{n-\lfloor n/S \rfloor S + qS}^T \hat{\mathbf{y}}[\lfloor n/S \rfloor - q], \quad (5.4)$$

---

<sup>1</sup>More generally, the filter bank is said to be perfect reconstruction if the output is a delayed version of the input. Our mathematical derivation assumes noncausal filters, such that this delay can be set to zero.

or equivalently (forward formula)

$$\hat{x}[n] = \sum_{q=0}^{K/S-1} \mathbf{u}_{n-\lfloor n/S \rfloor S + (K/S-1)S - qS}^T \hat{\mathbf{y}}[\lfloor n/S \rfloor - (K/S-1) + q], \quad (5.5)$$

where  $\mathbf{u}_k \in \mathbb{R}^K$  denotes the  $k$ th canonical vector, that is, with a one at position  $k$  and zero elsewhere. If  $k$  is outside the range  $\{0, 1, \dots, K-1\}$ ,  $\mathbf{u}_k$  simply corresponds to the all-zero vector. The index  $\lfloor n/S \rfloor - (K/S-1)$  is that of the first frame that contributes to the output at index  $n$ . The overlap-add formula (5.5) reveals that, once the first frame has been computed, the next  $K/S-1$  frames must also be available to output the value  $\hat{x}[n]$ . In a practical (causal) implementation, the delay required to output the first value that contributes to the reconstruction of  $x[n]$  is  $S-1$ . The overall delay of the WOLA filter bank when no processing occurs in the transformed domain is thus  $S-1 + (K/S-1)S = K-1$  samples.

It should be noted that, in the above WOLA implementation, the length of the analysis and synthesis windows is at the maximum equal to the size  $K$  of the DFT. A more general structure can be obtained by relaxing this constraint but the computational complexity of the corresponding analysis/synthesis block is larger. The interested reader is referred to [30, Sec. 7.2.5] for a more general treatment of the WOLA filter bank and its implementation.

### Multichannel Wiener Filtering

Let us now describe the multichannel filtering block in Figure 5.1. Let

$$\mathbf{Z}_l[m] = [Z_{l,0}[m], Z_{l,1}[m], \dots, Z_{l,K-1}[m]]^T$$

denote the vector input sequence at the  $l$ th channel. The filtering operation aims at providing an estimate

$$\hat{\mathbf{Z}}_0^n[m] = [\hat{Z}_{0,0}^n[m], \hat{Z}_{0,1}^n[m], \dots, \hat{Z}_{0,K-1}^n[m]]^T$$

of the noise present in the reference signal  $\mathbf{Z}_0[m]$ . To this end, the  $L$  input channels are linearly combined as

$$\hat{\mathbf{Z}}_0^n[m] = \sum_{l=0}^{L-1} \mathbf{D}_{Z_l}[m] \mathbf{W}_l[m], \quad (5.6)$$

where  $\mathbf{W}_l[m] \in \mathbb{C}^K$  corresponds to the frequency-domain coefficients of the filter applied at channel  $l$  and frame  $m$ , and  $\mathbf{D}_{Z_l}[m] \in \mathbb{C}^{K \times K}$  is the diagonal matrix with diagonal elements  $Z_{l,0}[m], Z_{l,1}[m], \dots, Z_{l,K-1}[m]$ . Observe that the matrix multiplications in (5.6) are equivalent to circular convolutions in the time domain, that is,

$$\hat{\mathbf{z}}_0^n[m] = \sum_{l=0}^{L-1} \mathbf{z}_l[m] \circledast \mathbf{w}_l[m],$$

where  $\otimes$  denotes the circular convolution operator and  $\mathbf{w}_l[m]$  the time-domain filter coefficients. For convenience, we rewrite the sum in (5.6) with matrix operations as

$$\hat{\mathbf{Z}}_0^n[m] = \mathbf{B}_Z[m]\mathbf{W}[m], \quad (5.7)$$

where  $\mathbf{B}_Z[m] \in \mathbb{C}^{K \times LK}$  and  $\mathbf{W}[m] \in \mathbb{C}^{LK}$  are defined as

$$\mathbf{B}_Z[m] = [\mathbf{D}_{Z_0}[m], \mathbf{D}_{Z_1}[m], \dots, \mathbf{D}_{Z_{L-1}}[m]] \quad (5.8)$$

and

$$\mathbf{W}[m] = [\mathbf{W}_0^T[m], \mathbf{W}_1^T[m], \dots, \mathbf{W}_{L-1}^T[m]]^T,$$

respectively. It is important to emphasize that the above filtering architecture implicitly assumes that the (frequency) components of the input sequence  $Z_l[m]$  are uncorrelated and can thus be processed separately. This assumption is in general violated owing to the correlation introduced by the analysis part of the WOLA filter bank. A more general structure can be obtained by considering general matrices (as opposed to diagonal ones) in the linear combination (5.6). The derivation of optimal filtering strategies and associated recursive algorithms in this context follows along the same line as that of the diagonal case and is thus omitted. Mean square optimal estimation using a general transform matrix is discussed in Appendix A.1.

### Loudspeaker Output

The derivation of the WOLA filter bank and the multichannel filter allows us to express the loudspeaker output signal as

$$\hat{x}_0^s[n] = x_0[n] - \hat{x}_0^n[n], \quad (5.9)$$

where the noise estimate  $\hat{x}_0^n[n]$  is given by

$$\begin{aligned} & \hat{x}_0^n[n] \\ & \stackrel{(a)}{=} \sum_{q=0}^{K/S-1} \mathbf{u}_{n-\lfloor n/S \rfloor S+qS}^T \hat{\mathbf{y}}_0^n[\lfloor n/S \rfloor - q] \\ & \stackrel{(b)}{=} \sum_{q=0}^{K/S-1} \mathbf{u}_{n-\lfloor n/S \rfloor S+qS}^T \mathbf{D}_h \hat{\mathbf{z}}_0^n[\lfloor n/S \rfloor - q] \\ & = \sum_{q=0}^{K/S-1} \mathbf{u}_{n-\lfloor n/S \rfloor S+qS}^T \mathbf{D}_h \mathbf{F}^{-1} \hat{\mathbf{Z}}_0^n[\lfloor n/S \rfloor - q] \\ & \stackrel{(c)}{=} \sum_{q=0}^{K/S-1} \mathbf{u}_{n-\lfloor n/S \rfloor S+qS}^T \mathbf{D}_h \mathbf{F}^{-1} \mathbf{B}_Z[\lfloor n/S \rfloor - q] \mathbf{W}[\lfloor n/S \rfloor - q], \end{aligned}$$

where (a) follows from the overlap-add formula (5.4), (b) from the windowing operation in (5.3), and (c) from the multichannel filtering formula (5.7). From the properties of the DFT, it holds that

$$\mathbf{D}_h \mathbf{F}^{-1} = \frac{1}{K} \mathbf{F}^{-1} \mathbf{C}_H, \quad (5.10)$$



where  $\mathbf{C}_H \in \mathbb{C}^{K \times K}$  denotes the circulant matrix whose first column is given by  $H[0], H[1], \dots, H[K-1]$ , namely, the DFT coefficients of the synthesis window  $h[n]$ . Equation (5.10) simply means that windowing in the time domain corresponds to filtering in the frequency domain. The noise estimate can thus be expressed as

$$\hat{x}_0^n[n] = \frac{1}{K} \sum_{q=0}^{K/S-1} \mathbf{u}_{n-\lfloor n/S \rfloor S + qS}^T \mathbf{F}^{-1} \mathbf{C}_H \mathbf{B}_Z[\lfloor n/S \rfloor - q] \mathbf{W}[\lfloor n/S \rfloor - q]. \quad (5.11)$$

### 5.2.2 Frame-Based Optimality Criterion

We wish to define a frame-based optimality criterion for the optimization of the filter coefficients. To this end, we first rewrite the overlap-add formula in block-form. Let  $p = \lfloor (n - mS) / S \rfloor$  and consider the indexes  $n \in \{mS, mS + 1, \dots, mS + S - 1\}$ . Using (5.11), it holds that

$$\begin{aligned} \hat{x}_0^n[n] &= \frac{1}{K} \sum_{q=0}^{K/S-1} \mathbf{u}_{n-(m+p-q)S}^T \mathbf{F}^{-1} \mathbf{C}_H \mathbf{B}_Z[m+p-q] \mathbf{W}[m+p-q] \\ &\stackrel{(a)}{=} \frac{1}{K} \sum_{q=-p}^{K/S-1-p} \mathbf{u}_{n-(m-q)S}^T \mathbf{F}^{-1} \mathbf{C}_H \mathbf{B}_Z[m-q] \mathbf{W}[m-q] \\ &\stackrel{(b)}{=} \frac{1}{K} \sum_{q=-K/S+1}^{K/S-1} \mathbf{u}_{n-mS+qS}^T \mathbf{F}^{-1} \mathbf{C}_H \mathbf{B}_Z[m-q] \mathbf{W}[m-q], \end{aligned}$$

where (a) follows from a change of variable and (b) from the definition of the canonical vector  $\mathbf{u}_k$  and the fact that  $n \in \{mS, mS + 1, \dots, mS + S - 1\}$ . We now define the matrix  $\mathbf{U} \in \mathbb{R}^{K \times K}$  that contains ones on its first upper diagonal and zero elsewhere. The matrix  $\mathbf{U}$  simply upshifts a post-multiplied vector by one element and replaces the last element by zero. The matrix power  $\mathbf{U}^{qS}$  hence performs a  $qS$ -element upshift ( $q \geq 0$ ). Similarly, the matrix  $\mathbf{U}^T$  downshifts the vector by one element and  $\mathbf{U}^{qS,T}$  by  $qS$  elements ( $q \geq 0$ ). For notational convenience, we define the matrix  $\mathbf{U}_q \in \mathbb{R}^{K \times K}$  as

$$\mathbf{U}_q = \begin{cases} \mathbf{U} & \text{for } q \geq 0 \text{ and} \\ \mathbf{U}^T & \text{for } q < 0, \end{cases}$$

such that the block signal  $\hat{\mathbf{x}}_0^n[m]$  can be expressed as

$$\begin{aligned} \hat{\mathbf{x}}_0^n[m] &= [\hat{x}_0^n[mS], \hat{x}_0^n[mS + 1], \dots, \hat{x}_0^n[mS + K - 1]]^T \\ &= \frac{1}{K} \sum_{q=-K/S+1}^{K/S-1} \mathbf{U}_q^{|q|S} \mathbf{F}^{-1} \mathbf{C}_H \mathbf{B}_Z[m-q] \mathbf{W}[m-q]. \end{aligned}$$

The index  $q$  allows ranging over the frames that overlap with frame  $m$ , namely the  $K/S - 1$  previous and  $K/S - 1$  subsequent ones. In each term of the sum,

the matrix  $\mathbf{U}_q^{|q|S}$  only retains the coefficients that contribute to the current frame. Let us define the matrix  $\mathbf{V} \in \mathbb{C}^{K \times K}$  as

$$\mathbf{V}_q = \mathbf{F}\mathbf{U}_q\mathbf{F}^{-1}.$$

It holds that  $\mathbf{V}_q^{|q|S} = \mathbf{F}\mathbf{U}_q^{|q|S}\mathbf{F}^{-1}$  such that the above reconstruction formula can be rewritten as

$$\hat{\mathbf{x}}_0^n[m] = \frac{1}{K} \mathbf{F}^{-1} \sum_{q=-K/S+1}^{K/S-1} \mathbf{V}_q^{|q|S} \mathbf{C}_H \mathbf{B}_{Z^n}[m-q] \mathbf{W}[m-q].$$

The noise estimate  $\hat{\mathbf{x}}_0^n[m]$  can be further decomposed into the contributions of the noise and speech components of the input signals as

$$\begin{aligned} \hat{\mathbf{x}}_0^n[m] &= \frac{1}{K} \mathbf{F}^{-1} \sum_{q=-K/S+1}^{K/S-1} \mathbf{V}_q^{|q|S} \mathbf{C}_H \mathbf{B}_{Z^n}[m-q] \mathbf{W}[m-q] \\ &\quad + \frac{1}{K} \mathbf{F}^{-1} \sum_{q=-K/S+1}^{K/S-1} \mathbf{V}_q^{|q|S} \mathbf{C}_H \mathbf{B}_{Z^s}[m-q] \mathbf{W}[m-q], \end{aligned}$$

where the matrices  $\mathbf{B}_{Z^n}[m]$  and  $\mathbf{B}_{Z^s}[m]$  are defined similarly as in (5.8). This allows us to write the loudspeaker output (5.9) in block-form as

$$\begin{aligned} \hat{\mathbf{x}}_0[m] &= \mathbf{x}_0[m] - \hat{\mathbf{x}}_0^n[m] \\ &= \mathbf{x}_0^s[m] + \mathbf{x}_0^n[m] - \hat{\mathbf{x}}_0^n[m] \\ &= \mathbf{x}_0^s[m] + \mathbf{e}^n[m] - \mathbf{e}^s[m], \end{aligned} \tag{5.12}$$

where we define

$$\begin{aligned} \mathbf{e}^n[m] &= \mathbf{x}_0^n[m] - \frac{1}{K} \mathbf{F}^{-1} \sum_{q=-K/S+1}^{K/S-1} \mathbf{V}_q^{|q|S} \mathbf{C}_H \mathbf{B}_{Z^n}[m-q] \mathbf{W}[m-q] \\ &= \frac{1}{K} \mathbf{F}^{-1} \sum_{q=-K/S+1}^{K/S-1} \mathbf{V}_q^{|q|S} \mathbf{C}_H (\mathbf{Z}_0^n[m-q] - \mathbf{B}_{Z^n}[m-q] \mathbf{W}[m-q]) \quad \text{and} \\ \mathbf{e}^s[m] &= \frac{1}{K} \mathbf{F}^{-1} \sum_{q=-K/S+1}^{K/S-1} \mathbf{V}_q^{|q|S} \mathbf{C}_H \mathbf{B}_{Z^s}[m-q] \mathbf{W}[m-q]. \end{aligned}$$

The second equality in  $\mathbf{e}^n[m]$  follows from the assumption that the WOLA filter bank is perfect reconstruction, that is,

$$\mathbf{x}_0^n[m] = \frac{1}{K} \mathbf{F}^{-1} \sum_{q=-K/S+1}^{K/S-1} \mathbf{V}_q^{|q|S} \mathbf{C}_H \mathbf{Z}_0^n[m-q].$$

The sequence  $\mathbf{e}^n[m]$  represents the *residual noise* and the quantity  $\mathbf{e}^s[m]$  can be interpreted as a linear *speech distortion*. They both affect the original speech component  $\mathbf{x}_0^s[m]$  in an additive manner, as shown in the decomposition (5.12). The ultimate goal of the multichannel Wiener filter is to limit both  $\mathbf{e}^n[m]$  and  $\mathbf{e}^s[m]$ . The MSE distortion amounts to minimizing the sum of these two terms. In the sequel, we use a slightly more general approach which consists to weight these two terms unequally [34, 42]. More precisely, we define the time-domain cost as a weighted sum of the mean squared residual noise and the mean squared speech distortion, that is,

$$\begin{aligned} J_t[m] &= \mathcal{E} \left\{ \mathbf{e}^{n,H}[m] \mathbf{e}^n[m] \right\} + \frac{1}{\mu} \mathcal{E} \left\{ \mathbf{e}^{s,H}[m] \mathbf{e}^s[m] \right\} \\ &= \mathcal{E} \left\{ \left( \mathbf{e}^n[m] + \frac{1}{\sqrt{\mu}} \mathbf{e}^s[m] \right)^H \left( \mathbf{e}^n[m] + \frac{1}{\sqrt{\mu}} \mathbf{e}^s[m] \right) \right\} \\ &= \mathcal{E} \left\{ \left\| \mathbf{e}^n[m] + \frac{1}{\sqrt{\mu}} \mathbf{e}^s[m] \right\|^2 \right\}, \end{aligned}$$

where the second equality follows from the assumption that the speech and noise components are uncorrelated. The parameter  $\mu$  allows trading off noise reduction and speech distortion [34, 42]. If  $\mu = 1$ , the MSE criterion is obtained. If  $\mu < 1$  speech distortion is reduced at the expense of increased residual noise. On the other hand, if  $\mu > 1$ , residual noise is decreased at the expense of additional speech distortion. Informal listening experiments suggest that  $\mu$  can be typically chosen around 2 without any perceptible speech artifacts. An important observation is that the above criterion assumes that *all* the input signals can be written as the sum of uncorrelated speech and noise components. This is generally not the case with coarsely quantized signals (obtained from the wireless link) since the added quantization noise typically depends on both the signal and noise components. This assumption can however be used as an approximation.

Since processing is done in the frequency domain, we will find it more convenient to express the errors signals in the frequency domain as

$$\begin{aligned} \mathbf{E}^n[m] &= \mathbf{F} \mathbf{e}^n[m] \\ &= \frac{1}{K} \sum_{q=-K/S+1}^{K/S-1} \mathbf{V}_q^{|q|S} \mathbf{C}_H (\mathbf{Z}_0^n[m-q] - \mathbf{B}_{Z^n}[m-q] \mathbf{W}[m-q]), \quad (5.13) \end{aligned}$$

$$\begin{aligned} \mathbf{E}^s[m] &= \mathbf{F} \mathbf{e}^s[m] \\ &= \frac{1}{K} \sum_{q=-K/S+1}^{K/S-1} \mathbf{V}_q^{|q|S} \mathbf{C}_H \mathbf{B}_{Z^s}[m-q] \mathbf{W}[m-q], \quad (5.14) \end{aligned}$$

and to minimize the frequency-domain cost function

$$J_f[m] = \mathcal{E} \left\{ \mathbf{E}^{n,H}[m] \mathbf{E}^n[m] \right\} + \frac{1}{\mu} \mathcal{E} \left\{ \mathbf{E}^{s,H}[m] \mathbf{E}^s[m] \right\}$$

$$\begin{aligned}
&= \mathcal{E} \left\{ \left( \mathbf{E}^n[m] + \frac{1}{\sqrt{\mu}} \mathbf{E}^s[m] \right)^H \left( \mathbf{E}^n[m] + \frac{1}{\sqrt{\mu}} \mathbf{E}^s[m] \right) \right\} \\
&= \mathcal{E} \left\{ \left\| \mathbf{E}^n[m] + \frac{1}{\sqrt{\mu}} \mathbf{E}^s[m] \right\|^2 \right\}. \tag{5.15}
\end{aligned}$$

Since  $\mathbf{F}^H \mathbf{F} = K$ , we have that  $J_f[m] = K J_t[m]$  and the two optimization problems are equivalent. Unfortunately, finding the optimal weights that minimize the cost function  $J_f[m]$  is a tedious task. This is mainly due to the inter-frame dependency introduced by the synthesis part of the WOLA filter bank and mathematically represented by the sum in the error signals (5.13) and (5.14). We thus resort to suboptimal strategies for which conclusive results can be found.

### 5.2.3 Suboptimal Strategies

We present three suboptimal solutions to the general optimization problem formalized previously. The first one (and the simplest one), referred to as *non-weighted* optimization, disregards the effect of the WOLA filter bank. The second one takes into account the fact that the output frame is further multiplied by a synthesis window. We refer to it as *weighted* optimization. Finally, the third method is an attempt to take the complete synthesis part of the WOLA filter bank into account by means of an iterative procedure. It is therefore referred to as *iterative* optimization.

#### Non-Weighted Optimization

The non-weighted optimization scheme considers the error between the input and output signals as observed at the input and output of the multichannel Wiener filter. It is suboptimal in the sense that it disregards both the windowing and the overlap-add procedure of the WOLA filter bank. In this case, the error signals (5.13) and (5.14) reduce to

$$\mathbf{E}_{NW}^n[m] = \mathbf{Z}_0^n[m] - \mathbf{B}_{Z^n}[m] \mathbf{W}[m], \tag{5.16}$$

$$\mathbf{E}_{NW}^s[m] = \mathbf{B}_{Z^s}[m] \mathbf{W}[m], \tag{5.17}$$

and the corresponding cost function (5.15), denoted by  $J_{f,NW}[m]$ , is given by

$$J_{f,NW}[m] = \mathcal{E} \left\{ \left\| \mathbf{Z}_0^n[m] - \left( \mathbf{B}_{Z^n}[m] + \frac{1}{\sqrt{\mu}} \mathbf{B}_{Z^s}[m] \right) \mathbf{W}[m] \right\|^2 \right\}.$$

The weights that minimize the above cost function are the well-known Wiener coefficients given by (see Appendix A.2)

$$\begin{aligned}
\mathbf{W}_{NW}[m] &= \left[ \mathcal{E} \{ \mathbf{B}_{Z^n}^H[m] \mathbf{B}_{Z^n}[m] \} + \frac{1}{\mu} \mathcal{E} \{ \mathbf{B}_{Z^s}^H[m] \mathbf{B}_{Z^s}[m] \} \right]^{-1} \\
&\quad \cdot \mathcal{E} \{ \mathbf{B}_{Z^n}^H[m] \mathbf{Z}_0^n[m] \}
\end{aligned} \tag{5.18}$$

### Weighted Optimization

The weighted optimization scheme takes into account the windowing operation applied in the synthesis part of the WOLA filter bank. Intuitively, the synthesis window weights the output frame such that the residual error is less harmful when the weights are close to zero. Taking this fact into account in the optimization problem leads to better results. In this case, the error signals (5.13) and (5.14) reduce to

$$\mathbf{E}_W^n[m] = \frac{1}{K} \mathbf{C}_H (\mathbf{Z}_0^n[m] - \mathbf{B}_{Z^n}[m] \mathbf{W}[m]), \quad (5.19)$$

$$\mathbf{E}_W^s[m] = \frac{1}{K} \mathbf{C}_H \mathbf{B}_{Z^s}[m] \mathbf{W}[m], \quad (5.20)$$

and the corresponding cost function (5.15), denoted by  $J_{f,W}[m]$ , is given by

$$J_{f,W}[m] = \mathcal{E} \left\{ \left\| \frac{1}{K} \mathbf{C}_H \mathbf{Z}_0^n[m] - \frac{1}{K} \mathbf{C}_H \left( \mathbf{B}_{Z^n}[m] + \frac{1}{\sqrt{\mu}} \mathbf{B}_{Z^s}[m] \right) \mathbf{W}[m] \right\|^2 \right\}.$$

The optimal solution follows directly from the non-weighted case by simply replacing  $\mathbf{B}_{Z^n}[m]$ ,  $\mathbf{B}_{Z^s}[m]$  and  $\mathbf{Z}_0^n[m]$  by  $(1/K) \mathbf{C}_H \mathbf{B}_{Z^n}[m]$ ,  $(1/K) \mathbf{C}_H \mathbf{B}_{Z^s}[m]$  and  $(1/K) \mathbf{C}_H \mathbf{Z}_0^n[m]$ , respectively. We obtain

$$\begin{aligned} \mathbf{W}_W[m] = & \left[ \mathcal{E} \{ \mathbf{B}_{Z^n}^H[m] \mathbf{C}_H^H \mathbf{C}_H \mathbf{B}_{Z^n}[m] \} + \frac{1}{\mu} \mathcal{E} \{ \mathbf{B}_{Z^s}^H[m] \mathbf{C}_H^H \mathbf{C}_H \mathbf{B}_{Z^s}[m] \} \right]^{-1} \\ & \cdot \mathcal{E} \{ \mathbf{B}_{Z^n}^H[m] \mathbf{C}_H^H \mathbf{C}_H \mathbf{Z}_0^n[m] \} \end{aligned}$$

### Iterative Optimization

The overlap-add stage in the synthesis part of the WOLA filter bank introduces a strong dependency between adjacent frames, such that the weights for each frame cannot be optimized *separately* anymore but the weights for all frames must be optimized *jointly*. Even if one has access to the entire frame sequence in advance, the optimal solution remains untractable. Similarly to the terminal-by-terminal perspective considered in Chapter 3 in the context of distributed estimation, a possible suboptimal approach is to optimize the weights on a frame-by-frame basis. In turn, we find the optimal solution at one frame assuming all else is fixed. In this case, the error signals (5.13) and (5.14) can be expressed as

$$\mathbf{E}_I^n[m] = \tilde{\mathbf{Z}}_0^n[m] - \frac{1}{K} \mathbf{C}_H \mathbf{B}_{Z^n}[m] \mathbf{W}[m], \quad (5.21)$$

$$\mathbf{E}_I^s[m] = \frac{1}{K} \mathbf{C}_H \mathbf{B}_{Z^s}[m] \mathbf{W}[m], \quad (5.22)$$

where we define

$$\tilde{\mathbf{Z}}_0^n[m] = \mathbf{Z}_0^n[m]$$

$$- \frac{1}{K} \sum_{\substack{q=-K/S+1 \\ q \neq 0}}^{K/S-1} \mathbf{V}_q^{|q|S} \mathbf{C}_H \left( \mathbf{B}_{Z^n}[m-q] + \frac{1}{\sqrt{\mu}} \mathbf{B}_{Z^s}[m-q] \right) \mathbf{W}[m-q].$$

The corresponding cost function (5.15), denoted by  $J_{f,I}[m]$ , is given by

$$J_{f,I}[m] = \mathcal{E} \left\{ \left\| \tilde{\mathbf{Z}}_0^n[m] - \frac{1}{K} \mathbf{C}_H \left( \mathbf{B}_{Z^n}[m] + \frac{1}{\sqrt{\mu}} \mathbf{B}_{Z^s}[m] \right) \mathbf{W}[m] \right\|^2 \right\}.$$

The solution to this optimization problem is the same as that of the weighted case except that the desired signal  $(1/K) \mathbf{C}_H \mathbf{Z}_0^n[m]$  must be replaced by the residual estimation error  $\tilde{\mathbf{Z}}_0^n[m]$ , that is, the part of  $\mathbf{Z}_0^n[m]$  that has not yet been estimated using the adjacent frames. The optimal solution is thus

$$\begin{aligned} \mathbf{W}_I[m] = & \left[ \mathcal{E} \{ \mathbf{B}_{Z^n}^H[m] \mathbf{C}_H^H \mathbf{C}_H \mathbf{B}_{Z^n}[m] \} + \frac{1}{\mu} \mathcal{E} \{ \mathbf{B}_{Z^s}^H[m] \mathbf{C}_H^H \mathbf{C}_H \mathbf{B}_{Z^s}[m] \} \right]^{-1} \\ & \cdot K \mathcal{E} \{ \mathbf{B}_{Z^n}^H[m] \mathbf{C}_H^H \tilde{\mathbf{Z}}_0^n[m] \} \end{aligned} \quad (5.23)$$

The iterative method then amounts to passing through all the frames in a given order (possibly multiple times) and to update the weights according to (5.23). Since at each step the previous solution lies in the current optimization space, the cost function (5.15) cannot increase and the iterative procedure is guaranteed to converge to a stationary point, which can be either a local minimum or a saddle point. While global convergence cannot be guaranteed, it is clear that the iterative method outperforms the two other schemes since its starting point can be set as the solution of the weighted optimization problem.

In practice, this method is unfortunately not applicable since it relies on the entire frame sequence. A possible alternative is to resort to a *causal* version of the above algorithm where the previous  $K/S - 1$  weights are known and the next  $K/S - 1$  ones are set to zero. In this case, the considered residual noise can be expressed as

$$\begin{aligned} & \tilde{\mathbf{Z}}_0^n[m] \\ = & \mathbf{Z}_0^n[m] - \frac{1}{K} \sum_{q=1}^{K/S-1} \mathbf{V}_q^{|q|S} \mathbf{C}_H \left( \mathbf{B}_{Z^n}[m-q] + \frac{1}{\sqrt{\mu}} \mathbf{B}_{Z^s}[m-q] \right) \mathbf{W}[m-q], \end{aligned} \quad (5.24)$$

and the optimal solution follows directly from (5.23). The current weights are thus optimized to estimate most of the residual error using the current frame, disregarding the fact that some of this error will be estimated using the next  $K/S - 1$  frames. Many other variations are of course possible. With this causality constraint, however, the iterative approach cannot be guaranteed to improve upon the weighted optimization.

### 5.2.4 Recursive Algorithms

We derive recursive algorithms for computing the weights of each of the three optimization methods described in Section 5.2.3.

#### Non-Weighted Optimization

The statistical quantities involved in the computation of the weights (5.18) are estimated using exponentially weighted time averages as

$$\begin{aligned} \mathcal{E} \{ \mathbf{B}_{Z^n}^H[m] \mathbf{B}_{Z^n}[m] \} &\approx \mathbf{Q}_{NW}^n[m] \\ &= (1 - \lambda) \sum_{i=0}^m \lambda^{m-i} \mathbf{B}_{Z^n}^H[i] \mathbf{B}_{Z^n}[i] \\ &= \lambda \mathbf{Q}_{NW}^n[m-1] + (1 - \lambda) \mathbf{B}_{Z^n}^H[m] \mathbf{B}_{Z^n}[m], \end{aligned}$$

$$\begin{aligned} \mathcal{E} \{ \mathbf{B}_{Z^s}^H[m] \mathbf{B}_{Z^s}[m] \} &\approx \mathbf{Q}_{NW}^s[m] \\ &= (1 - \lambda) \sum_{i=0}^m \lambda^{m-i} \mathbf{B}_{Z^s}^H[i] \mathbf{B}_{Z^s}[i] \\ &= \lambda \mathbf{Q}_{NW}^s[m-1] + (1 - \lambda) \mathbf{B}_{Z^s}^H[m] \mathbf{B}_{Z^s}[m] \end{aligned}$$

and

$$\begin{aligned} \mathcal{E} \{ \mathbf{B}_{Z^n}^H[m] \mathbf{Z}_0^n[m] \} &\approx \mathbf{q}_{NW}[m] \\ &= (1 - \lambda) \sum_{i=0}^m \lambda^{m-i} \mathbf{B}_{Z^n}^H[i] \mathbf{Z}_0^n[i] \\ &= \lambda \mathbf{q}_{NW}[m-1] + (1 - \lambda) \mathbf{B}_{Z^n}^H[m] \mathbf{Z}_0^n[m], \end{aligned}$$

where  $\mathbf{Q}_{NW}^n[m]$  and  $\mathbf{Q}_{NW}^s[m]$  are the estimated correlation matrices, and the vector  $\mathbf{q}_{NW}[m]$  is the estimated cross correlation. The parameter  $\lambda$  ( $0 \leq \lambda \leq 1$ ) is an exponential forgetting factor. Along the lines of [36, Sec. 3.3], an update equation for the weights can be found by enforcing (5.18) at frames  $m$  and  $m-1$  using the above estimates. We can write

$$\begin{aligned} &\mathbf{W}_{NW}[m] \\ &= \left[ \mathbf{Q}_{NW}^n[m] + \frac{1}{\mu} \mathbf{Q}_{NW}^s[m] \right]^{-1} \mathbf{q}_{NW}[m] \\ &= \left[ \mathbf{Q}_{NW}^n[m] + \frac{1}{\mu} \mathbf{Q}_{NW}^s[m] \right]^{-1} \left[ \lambda \mathbf{q}_{NW}[m-1] + (1 - \lambda) \mathbf{B}_{Z^n}^H[m] \mathbf{Z}_0^n[m] \right] \\ &= \left[ \mathbf{Q}_{NW}^s[m] + \frac{1}{\mu} \mathbf{Q}_{NW}^s[m] \right]^{-1} \\ &\quad \cdot \left\{ \lambda \left[ \mathbf{Q}_{NW}^n[m-1] + \frac{1}{\mu} \mathbf{Q}_{NW}^s[m-1] \right] \mathbf{W}_{NW}[m-1] \right. \\ &\quad \left. + (1 - \lambda) \mathbf{B}_{Z^n}^H[m] \mathbf{Z}_0^n[m] \right\} \end{aligned}$$

$$\begin{aligned}
&= \left[ \mathbf{Q}_{NW}^n[m] + \frac{1}{\mu} \mathbf{Q}_{NW}^s[m] \right]^{-1} \\
&\cdot \left\{ \left[ \mathbf{Q}_{NW}^n[m] - (1-\lambda) \mathbf{B}_{Z^n}^H[m] \mathbf{B}_{Z^n}[m] \right. \right. \\
&\quad \left. \left. + \frac{1}{\mu} \left( \mathbf{Q}_{NW}^s[m] - (1-\lambda) \mathbf{B}_{Z^s}^H[m] \mathbf{B}_{Z^s}[m] \right) \right] \mathbf{W}_{NW}[m-1] \right. \\
&\quad \left. + (1-\lambda) \mathbf{B}_{Z^n}^H[m] \mathbf{Z}_0^n[m] \right\}.
\end{aligned}$$

Rearranging the last equation yields the update formula

$$\begin{aligned}
\mathbf{W}_{NW}[m] &= \mathbf{W}_{NW}[m-1] + \eta(1-\lambda) \left[ \mathbf{Q}_{NW}^n[m] + \frac{1}{\mu} \mathbf{Q}_{NW}^s[m] \right]^{-1} \\
&\cdot \left[ \mathbf{B}_{Z^n}^H[m] \tilde{\mathbf{E}}_{NW}^n[m] - \frac{1}{\mu} \mathbf{B}_{Z^s}^H[m] \tilde{\mathbf{E}}_{NW}^s[m] \right], \quad (5.25)
\end{aligned}$$

where  $\tilde{\mathbf{E}}_{NW}^n[m]$  and  $\tilde{\mathbf{E}}_{NW}^s[m]$  correspond respectively to the error signals (5.16) and (5.17) evaluated using the weights  $\mathbf{W}_{NW}[m-1]$ . The parameter  $\eta$  is an added step size parameter.

### Weighted Optimization

As mentioned previously, the weighted optimization simply amounts to replacing, in the non-weighted scheme, the quantities  $\mathbf{B}_{Z^n}[m]$ ,  $\mathbf{B}_{Z^s}[m]$  and  $\mathbf{Z}_0^n[m]$  by  $(1/K) \mathbf{C}_H \mathbf{B}_{Z^n}[m]$ ,  $(1/K) \mathbf{C}_H \mathbf{B}_{Z^s}[m]$  and  $(1/K) \mathbf{C}_H \mathbf{Z}_0^n[m]$ , respectively. The correlation matrices are denoted by  $\mathbf{Q}_W^s[m]$  and  $\mathbf{Q}_W^n[m]$  in this case. With these modifications, the update equations for the weighted optimization scheme directly follow from (5.25) as

$$\begin{aligned}
\mathbf{W}_W[m] &= \mathbf{W}_W[m-1] + \eta(1-\lambda) \left[ \mathbf{Q}_W^n[m] + \frac{1}{\mu} \mathbf{Q}_W^s[m] \right]^{-1} \\
&\cdot \frac{1}{K} \left[ \mathbf{B}_{Z^n}^H[m] \mathbf{C}_H^H \tilde{\mathbf{E}}_W^n[m] - \frac{1}{\mu} \mathbf{B}_{Z^s}^H[m] \mathbf{C}_H^H \tilde{\mathbf{E}}_W^s[m] \right], \quad (5.26)
\end{aligned}$$

where  $\tilde{\mathbf{E}}_W^n[m]$  and  $\tilde{\mathbf{E}}_W^s[m]$  correspond respectively to the error signals (5.19) and (5.20) evaluated using the weights  $\mathbf{W}_W[m-1]$ .

### Iterative Optimization

The update equations for the iterative optimization scheme can be straightforwardly obtained from that of the weighted scheme. As pointed out above, the desired signal  $\mathbf{Z}_0^n[m]$  simply needs to be replaced by the residual estimation error  $\tilde{\mathbf{Z}}_0^n[m]$  defined in (5.24). Denoting the covariance matrices by  $\mathbf{Q}_I^n[m]$  and



$f_s$	8 kHz	16 kHz	20.48 kHz	44.1 kHz	48 kHz
$K = 64$	7.88	3.94	3.08	1.43	1.31
$K = 128$	15.88	7.94	6.20	2.88	2.65
$K = 256$	31.88	15.94	12.45	5.78	5.31
$K = 512$	63.88	31.94	24.95	11.59	10.65
$K = 1024$	127.88	63.94	49.95	23.20	21.31
$K = 2048$	255.88	127.94	99.95	46.42	42.65

**Table 5.1:** Delay of the WOLA filter bank, in milliseconds, for different frame lengths  $K$  and sampling frequencies  $f_s$ .

$\mathbf{Q}_I^s[m]$  in this case, the update equations follow as

$$\mathbf{W}_I[m] = \mathbf{W}_I[m-1] + \eta(1-\lambda) \left[ \mathbf{Q}_I^n[m] + \frac{1}{\mu} \mathbf{Q}_I^s[m] \right]^{-1} \cdot \frac{1}{K} \left[ \mathbf{B}_{Z^n}^H[m] \mathbf{C}_H^H \tilde{\mathbf{E}}_I^n[m] - \frac{1}{\mu} \mathbf{B}_{Z^s}^H[m] \mathbf{C}_H^H \tilde{\mathbf{E}}_I^s[m] \right], \quad (5.27)$$

where  $\tilde{\mathbf{E}}_I^n[m]$  and  $\tilde{\mathbf{E}}_I^s[m]$  correspond respectively to the error signals (5.21) and (5.22) evaluated using the weights  $\mathbf{W}_W[m-1]$ .

### 5.2.5 Practical Considerations

Some of the recursive algorithms derived in Section 5.2.4, while being theoretically sound, are of little interest in practice owing to the stringent constraints imposed by digital hearing aids in terms of computational complexity and processing delay. We discuss these issues along with other practical implementation details and select the architectures that are susceptible to be used in practice.

#### Analysis and Synthesis Windows

The WOLA filter bank gives us the freedom to choose the frame size  $K$ , the frame shift  $S$ , an analysis window  $g[n]$  and a synthesis window  $h[n]$  according to specific design criteria. A desirable (and natural) property is that of perfect reconstruction which guarantees that unprocessed signals go through the filter bank undistorted. Also, the frame size should be chosen small enough to ensure affordable processing delays. Table 5.1 summarizes filter bank delays for different frame sizes  $K$  and sampling frequencies  $f_s$ . For our purpose,  $K = 128$  and  $f_s = 20.48$  kHz such that the delay is 6.2 ms.

Regarding the analysis and synthesis windows, many choices are possible. For example,  $g[n]$  can be a periodic Hanning window of size  $K/2 = 64$  samples with  $K/4 = 32$  leading and following zeros, and  $h[n] = 1$  (no synthesis window). The perfect reconstruction property is satisfied if  $S$  is set to 32 samples (50% window overlap). In this case, delays up to a maximum absolute value of  $K/4 = 32$  samples can be synthesized perfectly owing to the presence of zero-padding. The absence of synthesis window, however, does not permit the reduction of artifacts that may arise due to the large delays that occur in

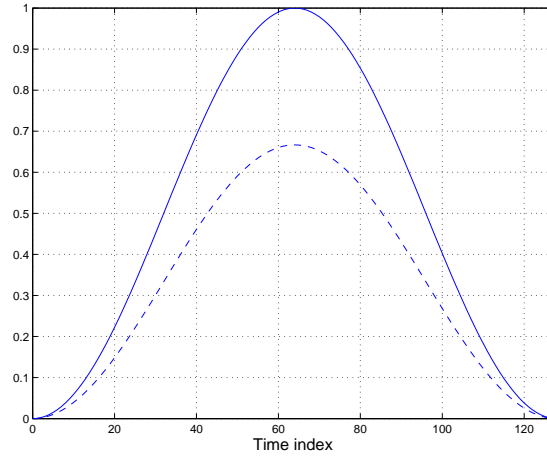


**Figure 5.3:** Analysis window (solid) and synthesis window (dashed) of the considered WOLA filter bank.

reverberant environments. Another alternative is to choose  $g[n]$  to be a periodic Hanning window of size  $K = 128$  (no zero-padding) and  $h[n] = (2/3)g[n]$ . These windows are depicted in Figure 5.3. Using  $S = 32$  samples (75% window overlap), the corresponding filter bank can be shown to be perfect reconstruction. This is the configuration chosen for the simulation results presented in Section 5.4. For a more general discussion of the design of analysis and synthesis windows, we refer to the exposition in [30, Sec. 7.3].

### Computation of the Weights

Let us look more carefully at the computation of the weights in the recursive algorithms described previously. For clarity, the notation adopted is that of the non-weighted optimization scheme. Similar comments apply to the two other optimization methods. The computation of the term  $\mathbf{B}_{Z^n}[m]$  in (5.18), which is required to update the noise correlation matrix  $\mathbf{Q}_{NW}^n[m]$  and the residual noise error  $\mathbf{E}_{NW}^n[m]$ , is only possible during noise-only periods. The algorithm thus requires a voice activity detector that indicates whether a frame contains speech or not (see Section 5.3.3). Moreover, the update of the weights must be performed during noise-only periods. Since the term  $\mathbf{B}_{Z^s}[m]$  cannot be computed, the regularization factor appearing in the weight update (5.25) will be approximated, as in [36, Sec. 3.4], by

$$\begin{aligned} \frac{1}{\mu} \mathbf{B}_{Z^s}^H[m] \tilde{\mathbf{E}}_{NW}^s[m] &= \frac{1}{\mu} \mathbf{B}_{Z^s}^H[m] \mathbf{B}_{Z^s}[m] \mathbf{W}_{NW}[m-1] \\ &\approx \frac{1}{\mu} \mathbf{Q}^n[m] \mathbf{W}_{NW}[m-1], \end{aligned}$$

that is, the instantaneous correlation matrix  $\mathbf{B}_{Z^n}^H[m] \mathbf{B}_{Z^n}[m]$  is approximated by the average correlation matrix  $\mathbf{Q}_{NW}^n[m]$ . We now define the input correla-

tion matrix  $\mathbf{Q}_{NW}[m] \in \mathbb{C}^{LK \times LK}$  through the relation

$$\mathbf{Q}_{NW}[m] = \lambda \mathbf{Q}_{NW}[m-1] + (1 - \lambda) \mathbf{B}_Z^H[m] \mathbf{B}_Z[m],$$

where  $\mathbf{B}_Z[m] = \mathbf{B}_{Z^s}[m] + \mathbf{B}_{Z^n}[m]$  is defined in (5.8). The matrix  $\mathbf{Q}_{NW}[m]$  is updated during speech periods whereas the noise correlation matrix  $\mathbf{Q}_{NW}^n[m]$  is updated during noise-only periods. Using the assumption that speech and noise are uncorrelated, the speech correlation matrix  $\mathbf{Q}_{NW}^s[m]$  can then be computed as  $\mathbf{Q}_{NW}^s[m] \approx \mathbf{Q}_{NW}[m] - \mathbf{Q}_{NW}^n[m]$ . Note that the positive definitiveness of the correlation matrix  $\mathbf{Q}_{NW}^s[m]$  should be ensured in order to avoid convergence issues (see, e.g., [36, Sec. 4.1]).

### Complexity

For complexity reasons, the recursive algorithms derived in Section 5.2.4 are not all amenable to practical implementation. In particular, the  $LK \times LK$ -dimensional matrix inversion involved in the weight updates (5.25)–(5.27) is in general prohibitive as it requires  $\mathcal{O}(K^3L^3)$  operations.

In the non-weighted scheme, the noise (resp. speech) correlation matrix is computed as a weighted sum of terms of the form  $\mathbf{B}_{Z^n}^H[m] \mathbf{B}_{Z^n}[m]$  (resp.  $\mathbf{B}_{Z^s}^H[m] \mathbf{B}_{Z^s}[m]$ ). It thus possesses a *block structure with diagonal blocks* that one can capitalize on in order to reduce the matrix inversion cost. More precisely, the correlation matrix can be permuted into a *block diagonal* matrix whose inversion only requires  $\mathcal{O}(KL^3)$  operations. Details of this complexity reduction can be found in [36, Sec. 4.1].

In the weighted scheme, however, the computation of the noise (resp. speech) correlation matrix involves terms of the form  $\mathbf{B}_{Z^n}^H[m] \mathbf{C}_H^H \mathbf{C}_H \mathbf{B}_{Z^n}[m]$  (resp.  $\mathbf{B}_{Z^s}^H[m] \mathbf{C}_H^H \mathbf{C}_H \mathbf{B}_{Z^s}[m]$ ) such that the blocks in the resulting correlation matrix are not diagonal anymore. In other words, the synthesis window  $h[n]$  (represented by the circulant matrix  $\mathbf{C}_H$ ) correlates the frequency components of an input channel such that frequency bins should now be processed jointly. The weighted optimization scheme (and therefore the iterative scheme) appears to be computationally prohibitive for practical implementation. In a realistic acoustic environment, however, the noise reduction improvement provided by these two methods over the non-weighted case is rather negligible (see Section 5.4).

In order to further reduce the computational cost of the matrix inversion in the non-weighted case, three approximation methods can be considered. They are referred to as *block diagonal*, *diagonal* and *averaged diagonal* approximations and differ in the way the block diagonal correlation matrix is approximated.

- (i) Block-diagonal: the block diagonal structure of the correlation matrix is preserved, that is, no approximation.
- (ii) Diagonal: only the diagonal components are preserved such that inter-channel correlation is neglected in the update of the weights.
- (iii) Averaged diagonal: the diagonal correlation sub-matrix of each input channel is further averaged over all channels such that the power variation across channel is neglected.

For real-time applications, the block diagonal matrix inversion still remains rather costly. A practical implementation should thus rely on the diagonal or averaged diagonal approximations which provide significant computational gains at the expense of slower convergence.

## 5.3 Binaural Filtering

Let us now consider the binaural configuration. It comprises multichannel Wiener filters to produce the loudspeaker outputs as well as filters that compute the signals transmitted over the wireless link. We describe this binaural processing architecture and discuss its optimality. Some practical considerations are then examined.

### 5.3.1 Processing Architecture

#### Overview

As illustrated in Figure 5.4, the binaural estimation system consists of two monaural entities connected by means of a wireless communication link. The microphone signals processed at hearing aid 1 and 2 are respectively denoted by  $x_{1,l}[n]$  and  $x_{2,l}[n]$  for  $l = 0, 1, \dots, L - 1$ . The loudspeaker outputs  $\hat{x}_{1,0}^s[n]$  and  $\hat{x}_{2,0}^s[n]$  are obtained as described in Section 5.2. In the binaural system, however, each hearing aid must also compute the signals transmitted over the wireless link. Let us look at these additional filtering operations.

#### Multichannel Wiener Filtering

The multichannel filters of hearing aid 1 and 2 respectively compute the noise estimates  $\hat{\mathbf{Z}}_{1,0}^n[m]$  and  $\hat{\mathbf{Z}}_{2,0}^n[m]$  by linearly combining their own microphone signals and the signal received over the wireless link. The noise estimates follow from (5.6) and (5.7) as

$$\hat{\mathbf{Z}}_{1,0}^n[m] = \mathbf{B}_{Z_1}[m]\mathbf{K}_1[m] + \mathbf{D}_{R_1}[m]\mathbf{G}_1[m], \quad (5.28)$$

$$\hat{\mathbf{Z}}_{2,0}^n[m] = \mathbf{B}_{Z_2}[m]\mathbf{K}_2[m] + \mathbf{D}_{R_2}[m]\mathbf{G}_2[m], \quad (5.29)$$

where  $\mathbf{R}_1[m]$  and  $\mathbf{R}_2[m]$  denote the signals received over the wireless link by hearing aid 1 and 2, respectively. The vectors  $\mathbf{K}_1[m] \in \mathbb{C}^{LK}$ ,  $\mathbf{K}_2[m] \in \mathbb{C}^{LK}$ ,  $\mathbf{G}_1[m] \in \mathbb{C}^K$  and  $\mathbf{G}_2[m] \in \mathbb{C}^K$  are the frequency-domain coefficients of the filters applied at frame  $m$ . Similarly, the signals transmitted over the wireless link, denoted by  $\mathbf{T}_1[m]$  and  $\mathbf{T}_2[m]$ , are obtained as

$$\mathbf{T}_1[m] = \mathbf{B}_{Z_1}[m]\mathbf{H}_1[m], \quad (5.30)$$

$$\mathbf{T}_2[m] = \mathbf{B}_{Z_2}[m]\mathbf{H}_2[m], \quad (5.31)$$

where the vectors  $\mathbf{H}_1[m] \in \mathbb{C}^{LK}$  and  $\mathbf{H}_2[m] \in \mathbb{C}^{LK}$  are the frequency-domain coefficients of the filters applied at frame  $m$ . In the absence of communication disturbances, the signal transmitted by one hearing aid is received perfectly at the contralateral device, that is,  $\mathbf{R}_1[m] = \mathbf{T}_2[m]$  and  $\mathbf{R}_2[m] = \mathbf{T}_1[m]$ .

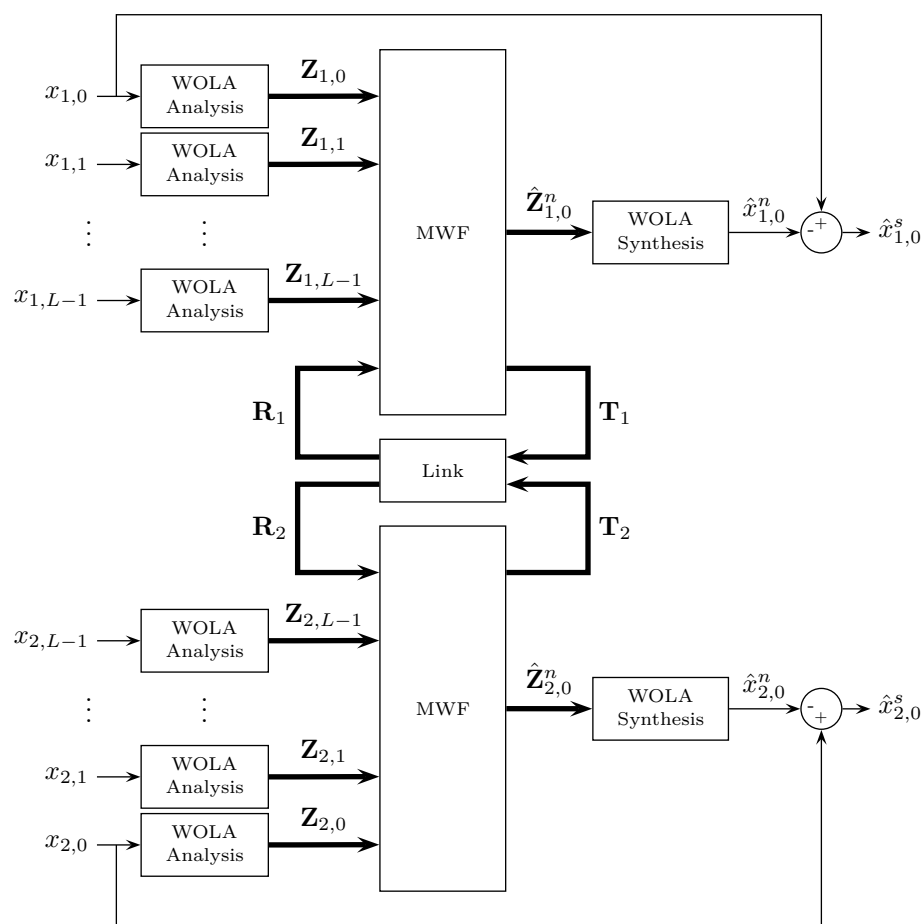


**Figure 5.4:** Block diagram of the binaural WOLA filtering architecture. The time and frame indexes are omitted for conciseness.

### 5.3.2 Binaural Optimality

It can be shown that  $\hat{\mathbf{Z}}_{1,0}^n[m]$  and  $\hat{\mathbf{Z}}_{2,0}^n[m]$ , obtained from (5.28) and (5.29), can be equivalently expressed as

$$\hat{\mathbf{Z}}_{1,0}^n[m] = \mathbf{B}_Z[m] \mathbf{W}_1[m], \quad (5.32)$$

$$\hat{\mathbf{Z}}_{2,0}^n[m] = \mathbf{B}_Z[m] \mathbf{W}_2[m], \quad (5.33)$$

where we define the matrix  $\mathbf{B}_Z[m] \in \mathbb{C}^{K \times 2LK}$  as

$$\mathbf{B}_Z[m] = [\mathbf{B}_{Z_1}[m] \quad \mathbf{B}_{Z_2}[m]],$$

and the vectors  $\mathbf{W}_1[m] \in \mathbb{C}^{2LK}$  and  $\mathbf{W}_2[m] \in \mathbb{C}^{2LK}$  as

$$\mathbf{W}_1[m] = \begin{bmatrix} \mathbf{K}_1[m] \\ (\mathbf{I}_L \otimes \mathbf{D}_{G_1}[m]) \mathbf{H}_2[m] \end{bmatrix} \quad \text{and} \quad \mathbf{W}_2[m] = \begin{bmatrix} \mathbf{K}_2[m] \\ (\mathbf{I}_L \otimes \mathbf{D}_{G_2}[m]) \mathbf{H}_1[m] \end{bmatrix},$$

where  $\otimes$  denotes the Kronecker product.

With the SIU coding strategy (see Section 4.2.2), the optimal filters  $\mathbf{H}_1[m]$  and  $\mathbf{H}_2[m]$  do not depend on the statistics of signals available at the contralateral device. The optimal filter coefficients can thus be computed using one of the optimization methods described in Section 5.2.3. In the SIA coding scheme (see Section 4.2.1), the statistics involved in the computation of the optimal filters  $\mathbf{H}_1[m]$  and  $\mathbf{H}_2[m]$  rely on signals recorded at the contralateral device. Since we only have access to a one-dimensional version of these signals, the statistics cannot be readily computed. However, it was shown in [37] that, under the assumption of a single speech source in each frequency (i.e., the diagonal blocks of the speech correlation matrix  $\mathcal{E} \{ \mathbf{B}_{Z^s}^H[m] \mathbf{B}_{Z^s}[m] \}$  permuted in block diagonal form have all rank one), a simple alternating optimization can nevertheless converge to the optimal solution. The alternating scheme amounts to setting

$$\mathbf{H}_1[m] = \mathbf{K}_1[m-1], \quad (5.34)$$

$$\mathbf{H}_2[m] = \mathbf{K}_2[m-1], \quad (5.35)$$

and to finding the optimal weights  $\mathbf{G}_1[m]$  and  $\mathbf{K}_2[m]$  using the available input signals  $\mathbf{Z}_1[m]$  and  $\mathbf{R}_1[m] = \mathbf{T}_2[m]$  for which statistics can be computed. Similarly, the optimal filter coefficients  $\mathbf{G}_2[m]$  and  $\mathbf{K}_1[m]$  are computed using the available input signals  $\mathbf{Z}_2[m]$  and  $\mathbf{R}_2[m] = \mathbf{T}_1[m]$ . If the assumption of a single speech source is not verified, the algorithm does not converge to the optimal solution but can still be used. Note that the optimality of this procedure is guaranteed for the non-weighted criterion. Nevertheless, the weighted and iterative optimization methods described in Section 5.2.3 can also be used in order to reduce the error present in the final time-domain outputs. In the case of a single speech source in each frequency, the optimal filters of both hearing aids can be shown to be frequency-wise co-linear [37]. The key behind the above algorithm is that this co-linearity can be enforced throughout the iterations, based on a transmitted signal of dimension one. Optimality may be extended to more general scenarios provided that the relationship between the binaural filters is fixed and can be enforced through alternation.

---

### 5.3.3 Practical Considerations

In Section 5.2.5, we discussed a few practical issues related to the implementation of monaural filtering. The binaural scheme described above raises a number of additional questions that we would like to address.

#### Wireless Link

The binaural algorithm described in Section 5.3.2 assumes that one can transmit frequency-domain signals. The main advantage is that the sequences computed by the multichannel Wiener filter in the WOLA-transformed domain can be directly sent over the wireless link. This allows keeping the delay at a bare minimum since no further WOLA synthesis (at the transmitter) or WOLA analysis (at the receiver) is required. However, owing to the WOLA filter bank redundancy, the transmission rate is  $K/S$  times higher (a factor 4 in our case) than the rate needed to code the equivalent time-domain signal. This may be compensated by appropriate source coding at the transmitter at the expense of higher latency.

In order to reduce the transmission bitrate, another alternative is to synthesize the time-domain signal and thus avoid the redundancy introduced by the WOLA filter bank. This strategy, however, doubles the processing delay and is therefore not very practical.

The third option is to process the signal transmitted by the wireless link in the time domain. More precisely, the microphones signals are combined using a time-domain implementation of the multichannel Wiener filter. The output signal is then transmitted to the other device and converted to the WOLA domain. In this case, the receiver needs to compensate for both the transmission delay of the wireless link and that of the time-domain multichannel filter, but no additional WOLA filter bank is required. Ideally, the time-domain filter coefficients should be chosen such that time-domain filtering followed by WOLA analysis is equivalent to WOLA analysis followed by frequency-domain filtering. While this is generally not possible (see Section 5.2), a rough approximation could consist of neglecting the effect of the WOLA analysis block and computing the time-domain coefficients as the inverse DFT of the coefficients applied every other  $K/S$  frames in the frequency-domain. Convergence of the corresponding recursive algorithm should however be insured.

While the alternating optimization scheme of Section 5.3.2 is optimal in the case of a single speech source, the above remarks suggest that its implementation in the WOLA framework may be difficult considering the sharp transmission bitrates and processing delay constraints. Another possibility, considered in [37], consists of simply sending the signal recorded at the reference microphone. While being suboptimal, this strategy has one major advantage which makes it very appealing in practice: the signal is sent unprocessed. The transmission can thus take place in the time domain and avoid the WOLA filter bank redundancy. Furthermore, the signal can be used at the contralateral device to extract true binaural information needed, for example, by a voice activity detector.

### Voice Activity Detection

Voice activity detection is a challenging task, in particular in very noisy environments. Voice activity detectors can be based on various quantities, such as energy [77], likelihood [127] or spectral entropy [95]. The availability of a wireless communication link further allows using binaural signals. For example, detection can be based on the direction of propagation, which may be computed from the peak of the cross correlation between the reference signals. Unfortunately, the binaural scheme presented above does not transmit reference signals but linear combinations of all the microphone inputs. In this case, the cross correlation between the signals transmitted over the wireless link can be expressed as

$$\begin{aligned} \mathcal{E} \{ \mathbf{D}_{T_1}^H[m] \mathbf{D}_{T_2}[m] \} &\stackrel{(a)}{=} \mathbf{B}_{H_2}[m] \mathcal{E} \{ \mathbf{B}_{Z_1}^H[m] \mathbf{B}_{Z_2}[m] \} \mathbf{B}_{H_1}^H[m] \\ &\stackrel{(b)}{\approx} \mathbf{B}_{H_2}[m] \left[ \mathcal{E} \{ \mathbf{D}_{Z_{1,0}}^H[m] \mathbf{D}_{Z_{2,0}}[m] \} \otimes \mathbf{I}_L \right] \mathbf{B}_{H_1}^H[m] \\ &\stackrel{(c)}{=} \mathbf{D}_C[m] \mathcal{E} \{ \mathbf{D}_{Z_{1,0}}^H[m] \mathbf{D}_{Z_{2,0}}[m] \}, \end{aligned}$$

where (a) and (c) follow from the transmitted signals (5.30) and (5.31), and the fact that only additions and multiplications of diagonal matrices are involved. The diagonal matrix  $\mathbf{D}_C[m] \in \mathbb{C}^{K \times K}$  is defined as

$$\mathbf{D}_C[m] = \left( \sum_{l=0}^{L-1} \mathbf{D}_{H_{1,l}}^H[m] \right) \left( \sum_{l=0}^{L-1} \mathbf{D}_{H_{2,l}}[m] \right). \quad (5.36)$$

The approximation in (b) assumes that the cross correlation between any pair of microphones (one microphone of each hearing aid) is similar to that between the reference microphones. This seems like a reasonable assumption considering that the microphones are very closely spaced on each hearing aid. The cross correlation computed using the signals transmitted over the wireless link thus corresponds to a filtered version of the desired cross correlation. The DFT coefficients of this filter at frame  $m$ , denoted by  $\mathbf{C}[m]$ , are the diagonal coefficients of the matrix (5.36). The maximum (in time) of this filtered version will not necessarily correspond to that of the original cross correlation. Furthermore, using the signals computed by the noise reduction algorithm for the purpose of voice activity detection may be hazardous since we end up in a closed-loop system: voice activity detection is based on the outputs of the noise reduction algorithm, and this latter relies on the voice activity detector to compute the output signals. In this context, the strategy of sending the reference (unprocessed) microphone signal is again very appealing. In this case, a cross correlation-based voice activity detector can be implemented without any of the aforementioned limitations.

## 5.4 Simulation Results

The purpose of this simulation section is twofold. First, we compare the WOLA implementations presented in Section 5.2 by means of a simple annihilating experiment. Second, we compute the SNR improvement and the speech dis-



tortion for different values of the parameter  $\mu$  using computationally efficient algorithms.

The simulation setup is the same as that of Section 4.5. The exponential forgetting factor  $\lambda$  is specified through a time-averaging constant  $T_\lambda$  defined as

$$T_\lambda = \frac{1}{1 - \lambda} \frac{S}{f_s}.$$

The parameter  $T_\lambda$  trades off the accuracy of the statistical estimates and the adaptability of the algorithm. The performance of the noise reduction scheme can significantly degrade if this parameter is not chosen properly. In our experiments, we set  $T_\lambda = 0.8$  s. The algorithms are evaluated with a frame size of  $K = 128$  samples and a shift of  $S = 32$  samples (75% overlap). In all cases, the step size  $\eta$  is set to 1. Regarding the iterative scheme, we consider a variation of the causal procedure presented in Section 5.2.3. At each step, instead of considering the current frame and its associated residual error, we consider the last completed frame (i.e., with index  $m - K/S + 1$ ) and propagate the corresponding residual error. The algorithm is thus updated with the error present in the final time-domain output frame.

#### 5.4.1 Annihilating Power

In the considered WOLA framework, a delay cannot be synthesized perfectly since the operations applied in the frequency-domain correspond to a circular (as opposed to a linear) convolution in the time domain. The aliasing that results from this operation is however significantly reduced by the windowing performed in the synthesis part of the WOLA filter bank. Provided that the delay is not too large, this aliasing does not result in any audible artifacts.

In order to assess the capability of the different algorithms to realize a prescribed filtering operation, we perform the following experiment. We simulate, in various acoustic environments, the signals recorded at the reference microphones of both hearing aids for a noise source at different positions. The goal of the noise reduction algorithm is to estimate the signal recorded at the reference microphone of hearing aid 2 using the signal measured at hearing aid 1. If the transfer function between the two reference microphones is perfectly estimated, the difference between the original signal and its estimate is zero (infinite attenuation). If this estimate is not perfect, this attenuation will be smaller. We thus aim at evaluating the annihilating power of the different algorithms.

The parameters of the simulation are as follows. The source signal is a stationary white Gaussian noise sequence with unit power spectral density. Its duration is 10 seconds but the attenuation is computed over the last 5 seconds to ensure that the adaptive algorithm has converged. We consider the following acoustic environments.

- (i) Far field: the microphone signals are simply delayed versions of the original signal. The distance between the microphones is assumed to be 0.2 m and the speed of sound is set to 340 m/s.
- (ii) Head shadow: the microphone signals are synthesized using HRTFs measured on a dummy head in free-field at a distance of 1.5 m.

- (iii) Reverberation: the microphones signals are synthesized using HRTFs measured on a dummy head at a distance of 1 m in a room with reverberation time  $T_{60} \approx 120$  ms.

In Figure 5.5, we plot the attenuation obtained for a noise source at different azimuths. We compare the non-weighted, weighted and iterative optimization methods. Note that the approximation method for the non-weighted scheme (i.e., block diagonal, diagonal or averaged diagonal) only affects the convergence speed and not the optimal solution. Since the attenuation is computed after convergence, the result does not depend on the chosen approximation method. Moreover, the parameter  $\mu$  has no influence on the result since no speech source is present. A general remark is that, as the noise source moves from  $0^\circ$  to  $90^\circ$ , the transfer function between the two microphones is more difficult to synthesize (more head shadow, longer delays). The attenuation hence decreases. A similar comment applies as we go from the far-field environment to an environment with reverberation. In the far-field case, the difference between the iterative and non-weighted methods can be significant. This example is however very synthetic. In a more realistic environment, the gap between the different curves vanishes. This suggests that the gain provided by the iterative and weighted optimization methods is rather negligible in a realistic scenario, and thus, are not worth the added computational complexity.

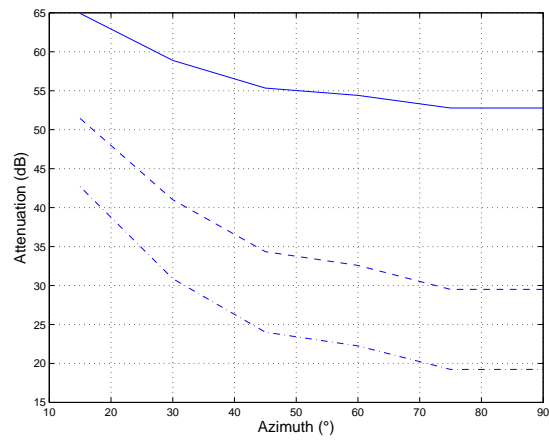
### 5.4.2 Signal-to-Noise Ratio Improvement and Speech Distortion

We evaluate the SNR improvement and speech distortion obtained by the non-weighted optimization scheme using different approximation strategies. Since we chiefly aim at comparing these methods, we will concentrate on the (monaural) noise reduction provided by a single hearing aid equipped with  $L = 2$  microphones, and mounted on the left ear of a dummy head. The desired speech source is at  $0^\circ$  and consists of sentences of the HINT database [98]. The noise consists of five non-stationary multi-talker babble noise sources at  $75^\circ$ ,  $120^\circ$ ,  $180^\circ$ ,  $240^\circ$  and  $285^\circ$ . The microphone signals are synthesized as in Section 5.2.3. The power of the speech source is adjusted such that the (broad-band) SNR at the front microphone is 0 dB. A perfect voice activity detector is used. The SNR improvement and the speech distortion are measured using the intelligibility weighted measures defined in [36, Sec. 6.1].

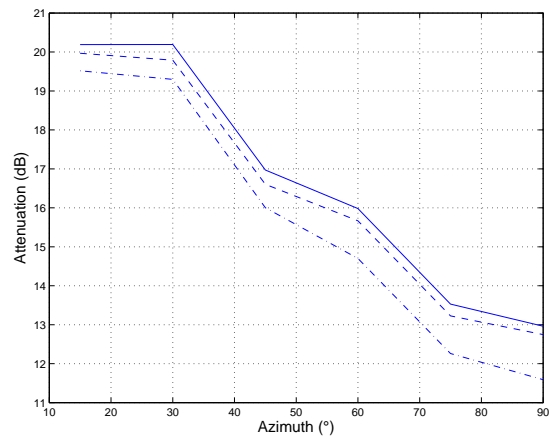
In Figure 5.6, we plot the speech distortion as a function of the SNR improvement obtained by the WOLA algorithms. The curves are obtained by varying the value of the parameter  $\mu$ . For a given SNR improvement, the best method is the one that provides the smallest speech distortion. We observe that the diagonal and averaged diagonal approximations incur a large gap compared to the block diagonal case where no approximation is done. They however allow to significantly reduce the computational complexity and thus are more suitable in a practical setting.

## 5.5 Summary

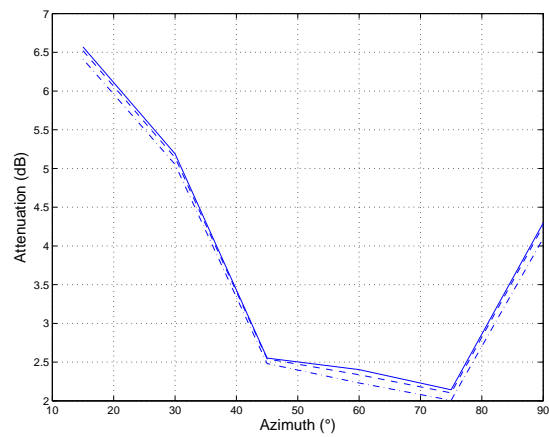
This chapter focused on a key component of the binaural noise reduction scheme, namely a multichannel Wiener filter. For complexity reasons, we



(a)



(b)



(c)

**Figure 5.5:** Attenuation using the non-weighted (dash-dotted), weighted (dashed) and iterative (solid) optimization methods. The acoustic environments are (a) far field, (b) head shadow and (c) reverberation.

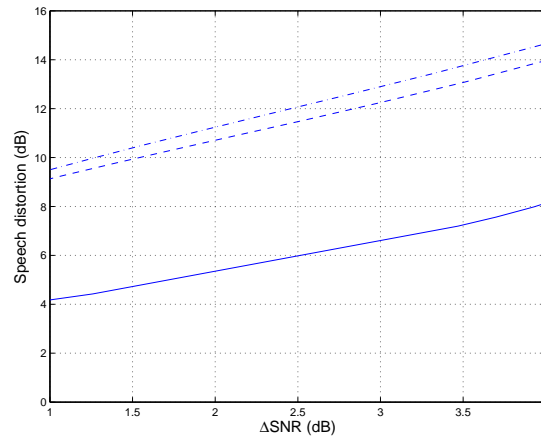


**Figure 5.6:** Speech distortion as a function of the SNR improvement for the non-weighted scheme with block diagonal (solid), diagonal (dashed) and averaged diagonal (dash-dotted) approximations. The curves are obtained by varying the parameter  $\mu$ .

looked at frequency-domain implementations of such filters. More precisely, we studied the optimality of multichannel Wiener filtering in the WOLA domain.

We first looked at monaural filtering for which we defined a frame-based frequency-domain criterion for the computation of the optimal filter weights. This criterion is a generalization of the MSE distortion and allows to conveniently trade off noise reduction and speech distortion through a single parameter. Unfortunately, the optimal solution is difficult to derive because of the strong inter-frame dependency introduced by the WOLA filter bank. We thus resorted to suboptimal solutions for which conclusive results could be found. We proposed three suboptimal schemes. The first one completely neglects the effect of the filter bank. The second one takes into account the weighting operator applied at synthesis. The third one captures some of the inter-frame dependency by means of an iterative procedure. For these three optimization methods, we derived recursive algorithms for the computation of the weights. We discussed their applicability in a practical setting and proposed ways to reduce their computational complexity.

We then looked at binaural filtering strategies for both the SIA and SIU coding schemes. With SIU coding, we pointed out that the optimality results derived in the monaural case are directly relevant for the binaural scenario. With SIA coding, however, these results cannot be readily applied since some of the needed statistics are not available. Nevertheless, we described an alternating optimization method that provides the optimal filter weights under the assumption of a rank-one speech correlation matrix. We then discussed a few practical issues pertaining to the use of a wireless link, in particular in the context of voice activity detection.

Finally, we presented a few simulation results to compare the proposed methods. In a rather synthetic scenario, we showed that significant gains could be obtained by taking into account the WOLA filter bank. However, in a more

---

realistic acoustic environment with reverberation, the advantage provided by the proposed methods over a blind strategy is not worth the added computational complexity.



## Chapter 6

# Distributed Source Coding of Binaural Innovation

### 6.1 Introduction

The information-theoretic analysis presented in Chapter 4 suggests that the correlation between signals recorded at the hearing aids allows reducing the description cost of data transmitted between the two devices. We pointed out that this correlation may be difficult to estimate in practice due to the distributed nature of the setup. With this limitation in mind, the natural question is whether these theoretical concepts are still relevant from a practical point of view. We show that it is indeed the case by designing practical distributed source coding schemes that take advantage of the *a priori* correlation induced by the recording setup in order to recover important binaural parameters. Generally speaking, these parameters allow quantifying the disparity between the binaural signals and may be used in the design of distributed spatial audio coding schemes. We refer to this disparity as the *binaural innovation* and model it in two different ways. The first model, studied in Section 6.2, involves binaural cues. We propose a source coding method that allows recovering these cues in a distributed fashion. The second model, presented in Section 6.3, assumes that the binaural signals are related to each other through a sparse filtering operation. We propose a distributed scheme which permits the recovery of the unknown filter with only few frequency measurements. We also demonstrate how this method can be made robust to model mismatch and evaluate its robustness with respect to additive noise. In Section 6.4, we then show how the estimated binaural innovation can be used to design distributed spatial audio coding schemes. We summarize this chapter in Section 6.5.

### 6.2 Model Based on Auditory Cues

#### 6.2.1 Model Description

Let us consider the binaural signals  $\mathbf{Z}_1[m] \in \mathbb{C}^K$  and  $\mathbf{Z}_2[m] \in \mathbb{C}^K$ . Throughout this chapter, signals are expressed using the frame-based frequency-domain representation obtained from the WOLA filter bank discussed in Chapter 5.

In particular, the  $k$ th component of the signal  $\mathbf{Z}_t[m]$  is denoted  $Z_{t,k}[m]$  for  $t = 1, 2$  and  $k = 0, 1, \dots, K - 1$ . Note that, in the sequel, the frame index  $m$  is omitted for conciseness. We define the *inter channel level difference* (ICLD) at frequency  $k$  as the power ratio between  $Z_{1,k}$  and  $Z_{2,k}$ , that is,

$$\text{ICLD}_k = \frac{\mathcal{E} \left\{ |Z_{1,k}|^2 \right\}}{\mathcal{E} \left\{ |Z_{2,k}|^2 \right\}} \quad \text{for } k = 0, 1, \dots, K - 1.$$

The *inter channel time difference* (ICTD) can be obtained by assuming that the phase difference between  $Z_{1,k}$  and  $Z_{2,k}$  grows linearly with  $k$ . The ICTD corresponds to the slope of this line, namely,

$$\text{ICTD}_k = \frac{K}{2\pi k} \angle \mathcal{E} \left\{ Z_{1,k} Z_{2,k}^* \right\} \quad \text{for } k = 0, 1, \dots, K - 1, \quad (6.1)$$

where  $\angle$  denotes the phase operator which typically returns a value in the interval  $[-\pi, \pi)$ . ICILD and ICTD are referred to as *binaural cues*. It has been shown in [7] that, from a perceptual point of view, the binaural innovation between  $\mathbf{Z}_1$  and  $\mathbf{Z}_2$  can be well captured by a single pair of binaural cues for a group of adjacent frequencies. At each frame  $m$ , the  $K$  frequencies are grouped in frequency sub-bands according to a partition  $\mathcal{B}_l$  ( $l = 1, 2, \dots, L$ ), that is, such that

$$\bigcup_{l=1}^L \mathcal{B}_l = \{0, 1, \dots, K - 1\} \quad \text{and} \quad \mathcal{B}_l \cap \mathcal{B}_{l'} = \emptyset \quad \text{for all } l \neq l'.$$

Typically, the number of sub-bands depends on the amount of assumed redundancy between the binaural signals. If these signals are very redundant (little innovation), only few binaural coefficients are needed. On the contrary, if the binaural signals have very little in common (large innovation), binaural cues should be computed for almost all frequencies. The ICILD in the  $l$ th sub-band is computed as the ratio of the averaged power estimates, that is,

$$\text{ICLD}_l = \frac{\sum_{k \in \mathcal{B}_l} \mathcal{E} \left\{ |Z_{1,k}|^2 \right\}}{\sum_{k \in \mathcal{B}_l} \mathcal{E} \left\{ |Z_{2,k}|^2 \right\}} \quad \text{for } l = 1, 2, \dots, L. \quad (6.2)$$

The ICTD in the  $l$ th sub-band can be obtained by fitting a line through the (unwrapped) phase differences computed in (6.1) for all  $k \in \mathcal{B}_l$ . The slope of the fitted line corresponds to the ICTD. It can be easily checked that optimal fitting in the mean square sense is achieved by setting

$$\text{ICTD}_l = \frac{K}{2\pi} \frac{\sum_{k \in \mathcal{B}_l} k \angle \mathcal{E} \left\{ Z_{1,k} Z_{2,k}^* \right\}}{\sum_{k \in \mathcal{B}_l} k^2} \quad \text{for } l = 1, 2, \dots, L, \quad (6.3)$$

It is important to emphasize that the phase differences should be unwrapped prior to mean square fitting. Optimal unwrapping is computationally expensive as it generally requires a combinatorial search over all possibilities. It can however be addressed using greedy algorithms which typically unwrap the phase



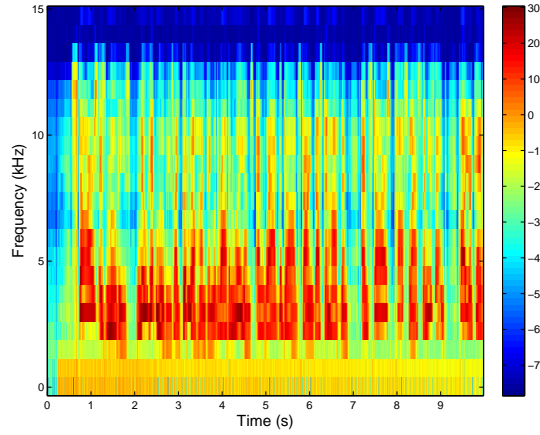


**Figure 6.1:** Power estimates as a function of time and frequency.

differences sequentially. Note also that the statistical quantities involved in the computation of ICLDs and ICTDs are estimated using exponentially weighted time averages, as in Section 5.2.4.

### 6.2.2 Distributed Source Coding of Binaural Cues

In the scenario where an encoder has access to both  $\mathbf{Z}_1$  and  $\mathbf{Z}_2$ , the ICLDs and ICTDs can be easily computed from (6.2) and (6.3), and subsequently quantized to meet a desired bitrate. In the distributed case, however, these signals cannot be processed jointly. In fact, each hearing aid observes one of the signals and transmits data over the wireless link to allow the contralateral device to estimate the binaural cues. We must thus resort to a distributed source coding scheme.

#### Inter Channel Level Differences

Let us first consider the case of ICLDs. Our strategy is as follows. The two hearing aids each compute an estimate of the signal power, expressed in dB, for every critical band  $\mathcal{B}_l$  as

$$P_{t,l} = 10 \log_{10} \left( \frac{1}{|\mathcal{B}_l|} \sum_{k \in \mathcal{B}_l} \mathcal{E} \left\{ |Z_{t,k}|^2 \right\} \right) \quad \text{for } t = 1, 2 \text{ and } l = 1, 2, \dots, L.$$

An example of power estimates as a function of time and frequency is given in Figure 6.1. The ICLD expressed in dB simply corresponds to the power difference given by

$$\Delta P_l = P_{1,l} - P_{2,l}. \quad (6.4)$$

We now explain how hearing aid 2 can efficiently encode the power estimates  $P_{2,l}$  taking into account the specificities of the recording setup and the fact that the powers  $P_{1,l}$  are available at the decoder. These power estimates will be necessary for the computation of ICLDs at hearing aid 1. The key is to observe that, while  $P_{1,l}$  and  $P_{2,l}$  may vary significantly as a function of the

sub-band index  $l$ , the ICLDs given by (6.4) are bounded below (resp. above) by the level difference caused by the head when a source is on the far right (resp. the far left) of the user. We denote this lower and upper bounds by  $\Delta P_l^{\min}$  and  $\Delta P_l^{\max}$ , respectively. This is an example of correlation known a priori which allows us to reduce the transmission bitrate. Note that in the centralized scenario, ICLDs can be quantized by a uniform scalar quantizer with range

$$[\Delta P_l^{\min}, \Delta P_l^{\max}]. \quad (6.5)$$

It can be checked that this strategy is information-theoretic optimal if  $\Delta P_l$  is uniformly distributed within the range (6.5) and that the number of quantization bins is a power of two. In our case, an equivalent bitrate saving can be achieved using a modulo approach. The powers  $P_{1,l}$  and  $P_{2,l}$  are quantized using a uniform scalar quantizer with range  $[P^{\min}, P^{\max}]$  and stepsize  $s$ . The range can be chosen arbitrarily but must be large enough to accommodate all relevant powers. The resulting quantization indices  $i_{1,l}$  and  $i_{2,l}$  satisfy

$$\begin{aligned} i_{1,l} - i_{2,l} &\in \{\Delta i_l^{\min}, \dots, \Delta i_l^{\max}\} \\ &= \left\{ \left\lfloor \frac{\Delta P_l^{\min}}{s} \right\rfloor, \dots, \left\lceil \frac{\Delta P_l^{\max}}{s} \right\rceil \right\}, \end{aligned} \quad (6.6)$$

where  $\lfloor \cdot \rfloor$  and  $\lceil \cdot \rceil$  denote the floor and ceil operations, respectively. Since  $i_{1,l}$  is available at the decoder, hearing aid 2 only needs to transmit a number of bits that allows hearing aid 1 to choose the correct index among the set of candidates whose cardinality is given by

$$\Delta i_l^{\max} - \Delta i_l^{\min} + 1. \quad (6.7)$$

This can be achieved by sending the value of the indices  $i_{1,l}$  modulo the cardinality (6.7), that is, using only  $\log_2(\Delta i_l^{\max} - \Delta i_l^{\min} + 1)$  bits. This strategy thus permits a bitrate saving equal to that of the centralized scenario. Moreover, at low frequencies, the shadowing effect of the head is less important than at high frequencies. The corresponding range is thus smaller and the number of required bits can be reduced. Therefore, the proposed scheme takes full benefit of the characteristics of the recording setup. From an implementation point of view, a single scalar quantizer with stepsize  $s$  is used for all sub-bands. The modulo strategy simply corresponds to an index reuse, as illustrated in Figure 6.2. At the decoder, the index  $i_{2,l}$  is first computed and among all possible indices  $i_{1,l}$  satisfying relation (6.6), the one with the correct modulo is selected. The reconstructed power estimates are denoted  $\hat{P}_{2,l}$  and the ICLDs can be computed at hearing aid 1 using these estimates. Note that the coding scheme for hearing aid 1 is readily obtained by exchanging the roles of the two devices.

It is important to point out that the distributed coding scheme described above assumes that the ICLDs belong to the range given by (6.5). If this condition is violated, then the wrong index will be reconstructed. This may happen, for example, if the ICLD range is chosen too small. The choice of suitable values for the range across sub-bands hence provides a way to trade off the aggressiveness of the coding scheme with the reconstruction accuracy. In particular, we may benefit from the interactive nature of the communication

$$\begin{array}{l}
\begin{array}{c}
+1|2|1|2|1|2|1|2|1|2|1|2|1|2|1|2|1|2|1|2| \\
P^{\min} \qquad \qquad \qquad P^{\max}
\end{array} \quad (l = 1) \\
\begin{array}{c}
+1|2|3|4|1|2|3|4|1|2|3|4|1|2|3|4|1|2|3|4|1|2| \\
P^{\min} \qquad \qquad \qquad P^{\max}
\end{array} \quad (l = 5) \\
\begin{array}{c}
+1|2|3|4|5|6|1|2|3|4|5|6|1|2|3|4|5|6|1|2|3|4| \\
P^{\min} \qquad \qquad \qquad P^{\max}
\end{array} \quad (l = 10)
\end{array}$$

**Figure 6.2:** Illustration of the proposed modulo coding approach. The power  $P$  is always quantized using a scalar quantizer with range  $[P^{\min}, P^{\max}]$  and stepsize  $s$ . Indices, however, are assigned modulo a value specific to each critical band  $l$ . In this example, the index reuse for  $l = 1$  (low frequencies) is more frequent than for  $l = 10$  (high frequencies).

link established between the two hearing aids to adapt the coding scheme dynamically. We might also envision a combined use of standard and distributed coding methods where, from time to time, pilot symbols are transmitted to check the validity of the assumed ICLD range.

### Inter Channel Time Differences

Let us now turn our attention the case of ICTDs. The goal is to compute (6.3) in a distributed fashion. Ideally, each hearing aid should transmit one value per sub-band to allow the contralateral device to estimate the ICTDs. Unfortunately, the computation of (6.3) involves unwrapping operations which are difficult to implement in a distributed fashion. It also relies on the cross correlation between  $Z_{1,k}$  and  $Z_{2,k}$  which cannot be computed in a distributed setup.

As an alternative, a simple approach is to infer the ICTDs from the ICLDs using an HRTF lookup table. More precisely, we assume that the acoustic scene is composed of a single source in the horizontal plane. Using the HRTF lookup table, we find the azimuth that this source should have in order to induce an ICLD as close a possible to the estimate ICLD. The corresponding pair of HRIRs then allows us to compute an ICTD using, for example, a time delay estimation method based on cross correlation. This strategy has the advantage to require no additional information to be transmitted. It is largely based on the assumption that a single source is active in each time-frequency atom. However, owing to its simplicity, it may not always provide satisfactory results, for example, in acoustic environments with long reverberation times. The accuracy of this method will be investigated in Section 6.4 in the context of distributed spatial audio coding.

## 6.3 Model Based on Sparsity Principles

### 6.3.1 Model Description

Another way to model binaural innovation is to consider that the signal  $\mathbf{Z}_2$  can be obtained as a filtered version of  $\mathbf{Z}_1$ . It can thus be expressed as

$$\mathbf{Z}_2 = \mathbf{H} \odot \mathbf{Z}_1, \quad (6.8)$$

where  $\odot$  denotes the element-wise product and  $\mathbf{H} \in \mathbb{C}^K$  is the DFT of the (real-valued) binaural filter  $\mathbf{h} \in \mathbb{C}^K$ . We further assume that  $\mathbf{h}$  has only a few number of non-zero coefficients. In other words, we suppose that it admits a sparse representation in the canonical basis  $\{\mathbf{u}_1, \mathbf{u}_2, \dots, \mathbf{u}_K\}$  of  $\mathbb{R}^K$ . It can thus be decomposed as

$$\mathbf{h} = \sum_{l=1}^L c_l \mathbf{u}_{n_l},$$

where  $n_l \in \{1, 2, \dots, K\}$  denote the indices with non-zero coefficients  $c_l \in \mathbb{R}$ . The sparsity factor  $L$ , chosen between 1 and  $K$ , allows varying the amount of assumed redundancy between the binaural signals. The DFT of  $\mathbf{h}$  can thus be expressed as

$$\mathbf{H} = \sum_{l=1}^L c_l \mathbf{U}_{n_l}, \quad (6.9)$$

where

$$\mathbf{U}_{n_l} = \mathbf{F} \mathbf{u}_{n_l} = \left[ 1, e^{-j\frac{2\pi}{K}n_l}, \dots, e^{-j\frac{2\pi}{K}n_l(K-1)} \right]^T.$$

It is important to emphasize that the binaural signals are not assumed to be themselves sparse, but that they are related to each other through a sparse transformation. The above model is motivated by the simple acoustic scenario studied in Section 4.3. In the presence of a single source in far field, and neglecting reverberation and the head-shadow effect, the signal recorded at hearing aid 2 is simply a delayed version of the one observed at hearing aid 1. Hence, it can be well modeled using a filter with sparsity factor 1. With multiple sources, as well as in the presence of reverberation and head shadowing, the filter is no longer sparse. Despite this model mismatch, it is assumed that the main binaural features can be still well captured with a binaural filter having only few non-zero coefficients.

### 6.3.2 Distributed Source Coding of the Binaural Filter

We wish to retrieve the unknown binaural filter at hearing aid 1 from data transmitted by hearing aid 2. Intuition suggests that, since this filter can be described with fewer than  $K$  real coefficients, the amount of transmitted data can be reduced. In fact, the binaural filter can be perfectly described using only  $2L$  degrees of freedom, namely,  $L$  indices  $n_l$  and  $L$  coefficients  $c_l$ .

Our distributed source coding scheme is based on the concept of annihilating filter which is a well known tool in spectral analysis (see, e.g., [131, Sec. 4.4]). We proceed as follows. Hearing aid 2 transmits only the first  $L+1$  (complex) coefficients of  $\mathbf{Z}_2$ , that is,  $Z_{2,0}, Z_{2,1}, \dots, Z_{2,L}$ . Owing to the conjugate

symmetry property, this corresponds to  $2L + 1$  real coefficients. We consider that these coefficients are quantized finely enough such that quantization noise can be neglected. Based on this data, the binaural filter can be perfectly recovered at hearing aid 1. To see how this can be achieved, observe that the elements of the vector  $\mathbf{H}$  in (6.9), denoted by  $H_0, H_1, \dots, H_{K-1}$ , are given by the first  $K$  coefficients of the sequence

$$H[k] = \sum_{l=1}^L c_l e^{-j \frac{2\pi}{K} k n_l}, \quad (6.10)$$

that is, a linear combination of  $L$  complex exponentials. It can be easily checked that each complex exponential  $U_l[k] = e^{-j \frac{2\pi}{K} k n_l}$  can be annihilated by the filter with impulse response

$$A_l[k] = \delta[k] - e^{-j \frac{2\pi}{K} n_l} \delta[k - 1],$$

that is,

$$A_l[k] * U_l[k] = 0 \quad \text{for } l = 1, 2, \dots, L.$$

The index  $n_l$  can then be retrieved from the root of  $A_l[k]$  given by  $u_l = e^{-j \frac{2\pi}{K} n_l}$ . By linearity of the convolution operator, the signal  $H[k]$  can thus be annihilated using the filter with impulse response

$$A[k] = A_1[k] * A_2[k] * \dots * A_L[k],$$

namely,

$$A[k] * H[k] = 0. \quad (6.11)$$

The annihilating filter  $A[k]$  has  $L + 1$  non-zero coefficients and is of order  $L$  with roots  $u_1, u_2, \dots, u_L$ . It can be arbitrarily scaled such that  $A[0] = 1$ . The condition (6.11) can be rewritten in matrix form as

$$\begin{bmatrix} H[0] & H[-1] & \dots & H[-L] \\ H[1] & H[0] & \dots & H[-L+1] \\ \vdots & \vdots & \ddots & \vdots \\ H[L] & H[L-1] & \dots & H[0] \end{bmatrix} \begin{bmatrix} 1 \\ A[1] \\ \vdots \\ A[L] \end{bmatrix} = \begin{bmatrix} 0 \\ 0 \\ \vdots \\ 0 \end{bmatrix}. \quad (6.12)$$

Since  $H[-k] = H^*[k]$ , only the first  $L + 1$  DFT coefficients of the binaural filter are needed to solve the above system. These coefficients can be directly obtained at hearing aid 1 from the values sent by hearing aid 2 as

$$H[k] = \frac{Z_{2,k}}{Z_{1,k}} \quad \text{for } k = 0, 1, \dots, L.$$

Note that this method requires  $Z_{1,k}$  to be different than zero for all  $k = 0, 1, \dots, L$ , but this happens with probability one. The system (6.12) is a classical Yule-Walker system which is guaranteed to have a unique solution if the indices  $n_l$  are all distinct and the coefficients  $c_l$  are all non-zero. Note that, in this case, the matrix in (6.12) is of rank  $L$ . Once the annihilating filter has been found, its roots  $u_1, u_2, \dots, u_L$  can be computed to retrieve the unknown indices  $n_1, n_2, \dots, n_L$ . The unknown coefficients  $c_1, c_2, \dots, c_L$  are finally evaluated by

means of the linear system of equations

$$\begin{bmatrix} H[0] \\ H[1] \\ \vdots \\ H[L-1] \end{bmatrix} = \begin{bmatrix} 1 & 1 & \cdots & 1 \\ u_1 & u_2 & \cdots & u_L \\ \vdots & \vdots & \ddots & \vdots \\ u_1^{L-1} & u_2^{L-1} & \cdots & u_L^{L-1} \end{bmatrix} \begin{bmatrix} c_1 \\ c_2 \\ \vdots \\ c_L \end{bmatrix}. \quad (6.13)$$

The above system involves a Vandermonde matrix which is invertible if the indices  $n_l$  are all distinct. Given the indices  $n_l$  and coefficients  $c_l$ , the binaural filter can be reconstructed using (6.10).

A couple of remarks are at hand. First, note that any set of  $2L$  consecutive coefficients of  $H[k]$  allows retrieving the annihilating filter using a system of the form (6.12). However, this generally requires  $4L$  real coefficients to be transmitted by hearing aid 2. Due to the conjugate symmetry property, this number can be reduced to  $2L+1$  if the first  $L+1$  coefficients are considered (as above). Second, the computational complexity of the aforementioned approach depends strongly on the assumed sparsity factor. While matrix inversion and polynomial root finding are computational intensive operations ( $\mathcal{O}(L^3)$ ), complexity remains affordable for small values of  $L$ . Moreover, these operations may be approximated using numerical methods that are computationally less demanding.

### 6.3.3 Robustness to Model Mismatch

The above model differs from reality in many respects. First of all, the sparsity assumption is rarely satisfied in practice. Moreover, a filtering operation in the time domain does not exactly correspond to the element-wise product (6.8) due to the problem of circular convolution and the effect of the WOLA filter bank (see Chapter 5). Finally, the coefficients transmitted over the wireless link are subject to quantization error. Measurements that do not follow the assumed model can be considered as noisy. Robustness to model mismatch can thus be achieved using a denoising algorithm. In this work, we resort to an iterative scheme due to Cadzow [25].

Let us assume that hearing aid 1 has access to the frequency coefficients  $H[k]$  for  $k = 0, 1, \dots, P$  where  $P \geq L$ . The number of real coefficients transmitted by hearing aid 2 is now  $2P+1$ . If the values  $H[k]$  perfectly follow the assumed model, it can be checked that the  $(P+1) \times (P+1)$ -dimensional matrix

$$\begin{bmatrix} H[0] & H[-1] & \cdots & H[-P] \\ H[1] & H[0] & \cdots & H[-P+1] \\ \vdots & \vdots & \ddots & \vdots \\ H[P] & H[P-1] & \cdots & H[0] \end{bmatrix} \quad (6.14)$$

has two key properties: (i) it has rank  $L$  and (ii) it is of Toeplitz form. In the noisy case, however, the rank will be larger than  $L$ . The idea behind Cadzow's algorithm is to recover the original properties using an iterative approach. Rank  $L$  is enforced by setting the  $P+1-L$  smallest eigenvalues to zero. The Toeplitz form is obtained by averaging along the diagonals. Alternating between these two operations ultimately leads to a matrix that exhibits the desired proper-

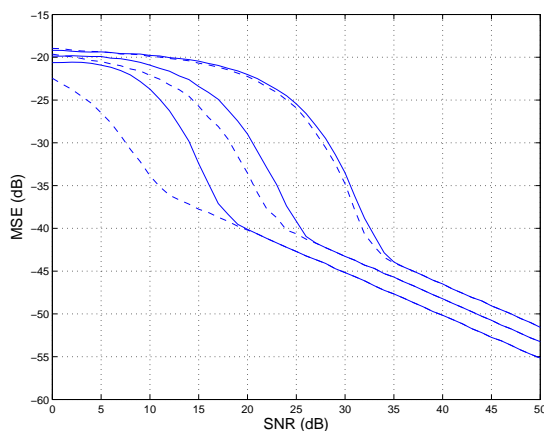


**Figure 6.3:** Mean squared reconstruction error of the binaural filter without (solid) and with (dashed) Cadzow's denoising procedure. The different sets of curves corresponds to  $P = 2, 5, 12$  (right to left). We observe that Cadzow's method allows for significant gains, in particular in the low SNR regime.

ties [25]. The denoised DFT coefficients can then be used in (6.12) and (6.13) to recover the unknown parameters. Note that, in the noisy case, the coefficients of the annihilating filter can be obtained by minimizing the norm of the matrix product (6.12). The solution is given by the right eigenvector corresponding to the smallest singular value [142].

Variations on the above method can be considered [68]. For example, we can take into account multiple consecutive frames for denoising. If the indices  $n_l$  do not vary rapidly as a function of the frame index, the annihilating filter essentially remains the same across frames. The matrix (6.14) can thus be replaced by a matrix obtained by stacking the contribution of each frame. In this case, the rank condition is enforced on the entire matrix but diagonal averaging is performed on each submatrix separately. We thus capitalize on both the intra and inter-frame redundancy to denoise the data.

To illustrate the accuracy of the aforementioned schemes, we present a simple numerical experiment. The vector  $\mathbf{Z}_1$ , chosen of size  $K = 128$ , is obtained as the DFT of  $\mathbf{z}_1 \in \mathbb{C}^K$ . The elements of  $\mathbf{z}_1$  are i.i.d. Gaussian random variables with mean zero and unit variance. The vector  $\mathbf{Z}_2$  follows from (6.8) using a binaural filter with sparsity factor  $L = 1$ . The index  $n_1$  of the non-zero coefficient is chosen uniformly in  $\{1, 2, \dots, K\}$ , and its value  $c_1$  follows a Gaussian distribution with mean zero and unit variance. Model mismatch is simulated by adding independent white Gaussian noise to the binaural filter. The results have been averaged over 20000 realizations. We plot in Figure 6.3 the mean squared reconstruction error of the filter as a function of the SNR for different values of  $P$ . Recall that  $P$  denotes the number of transmitted DFT coefficients. Reconstruction with and without Cadzow's iterative method is considered. We observe that Cadzow's scheme allows reducing the error compared to the case where the properties of the matrix (6.14) are not taken into account. Distortion is also reduced as  $P$  increases. In fact, a significant gain can be achieved with just a few more measurements than the minimum required in the noise-

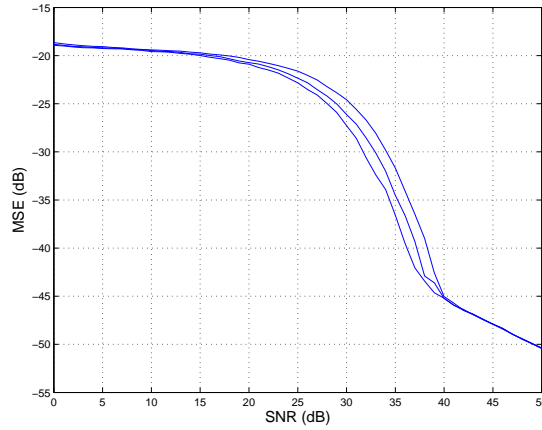


**Figure 6.4:** Mean squared reconstruction error of the binaural filter with Cadzow’s denoising procedure using  $F = 1, 2, 3$  consecutive frames of size  $K = 128$  (right to left). The parameters are  $L = 1$  and  $P = 1$ .

less case. As  $P$  grows, the dimension of the null space of the matrix (6.14) increases such that more noise can be zeroed out when its rank is forced by  $L$ . Hence, the gain provided by Cadzow’s approach becomes larger as  $P$  increases. It can be observed that, above a given SNR, the MSE decreases linearly. This threshold corresponds to the minimum SNR required to perfectly recover  $n_1$ . The remaining distortion corresponds to the error made in estimating  $c_1$  using the linear system (6.13).

In Figure 6.4, we plot the MSE achieved by Cadzow’s method using consecutive frames. The index of the non-zero coefficient is kept fixed for all frames but its value is chosen independently. We observe that taking into account inter-frame dependency allows for a better reconstruction accuracy.

## 6.4 Application: Distributed Spatial Audio Coding

The distributed source coding schemes presented in Sections 6.2 and 6.3 can be applied to the distributed coding of spatial audio content. The general scenario consists of an array of microphones which record a spatio-temporal sound field at different locations. The recorded signals are then transmitted to a fusion center which aims at reconstructing the original multi-channel audio data in a perceptually transparent manner [111]. This multi-terminal configuration has been addressed in Chapter 3. However, for the sake of simplicity and to keep up with the configuration adopted so far, we will concentrate on the scenario of distributed source coding with side information at the decoder. The algorithms proposed in the sequel can be readily extended to the general multi-terminal setup in various ways [68].

The main assumption that we make is that the audio signal  $\mathbf{Z}_2[m]$  to be encoded can be recovered in a perceptually transparent fashion using the signal  $\mathbf{Z}_1[m]$  available at the decoder and the binaural innovation. Therefore, only the data required to estimate this binaural innovation needs to be transmitted. This can be achieved using either of the two schemes proposed above.



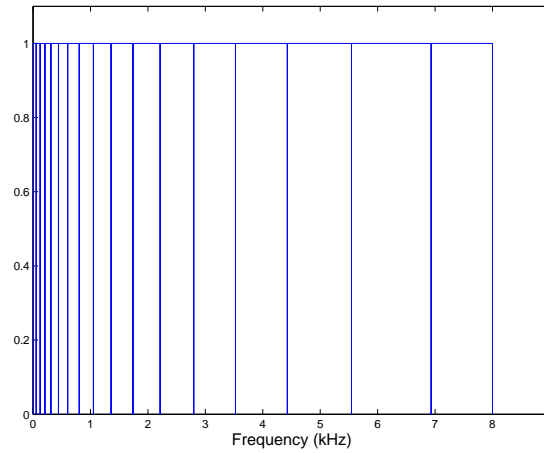


**Figure 6.5:** Partitioning of the frequency band in critical sub-bands with a bandwidth of  $B = 2$  ERB.

Note that this approach is motivated by spatial audio coding applications (see, e.g., [45]) where the aim is to reconstruct signals in a perceptually lossless manner. Therefore, the proposed schemes are not directly relevant for binaural hearing aids where the goal is noise reduction.

### 6.4.1 Model Based on Auditory Cues

Let us look at the first model. It is based on the computation of binaural cues estimated on a sub-band basis. The proposed distributed spatial audio coding scheme uses these cues to recover the unknown signal from the signal available at the decoder [116]. It is motivated by the parametric multichannel audio coding method presented in [7, 8].

Psychoacoustic experiments suggest that spatial perception is most likely based on a frequency sub-band representation with bandwidths proportional to the critical bandwidth of the auditory system [16, Sec. 2.4]. Since this latter can be approximated by the equivalent rectangular bandwidth (ERB) [52], we use a constant bandwidth of  $B$  ERB to obtain a non-uniform partitioning of the frequency band according to the relation

$$B(f) = 21.4 \log_{10}(0.00437f + 1) ,$$

where  $f$  is the frequency measured in Hertz. The partitioning obtained for  $B = 2$  ERB is shown in Figure 6.5. Once the power estimates  $\hat{P}_{2,l}[m]$  of  $\mathbf{Z}_2[m]$  have been computed using the distributed coding scheme described in Section 6.2, we construct a first estimate of  $\mathbf{Z}_2[m]$  using  $\mathbf{Z}_1[m]$  and the estimated ICLDs in each critical band. This is achieved as follows. First, the ICLDs are estimated as

$$\Delta \hat{P}_l[m] = P_{1,l}[m] - \hat{P}_{2,l}[m] \quad \text{for } l = 1, 2, \dots, L.$$

Suitable interpolation is then applied to obtain the ICLDs  $\Delta \hat{P}_k[m]$  for all fre-

quencies [8]. These ICLDs are then applied to the elements of  $\mathbf{Z}_1[m]$  as

$$\hat{Z}'_{2,k}[m] = Z_{1,k}[m] 10^{-\frac{\Delta\hat{P}_k[m]}{20}} \quad \text{for } k = 0, 1, \dots, K-1. \quad (6.15)$$

Phase differences between the two signals are also synthesized. To this end, we compute ICTDs using an HRTF lookup table, as explained in Section 6.2.2. The ICTD obtained for sub-band  $l$  is denoted by  $\Delta\hat{\tau}_l[m]$ . Similarly to the ICLDs, ICTDs  $\Delta\hat{\tau}_k[m]$  are obtained for all frequencies by interpolation [8]. The ICTDs are then applied to the spectrum obtained in (6.15) as

$$\hat{Z}_{2,k}[m] = \hat{Z}'_{2,k}[m] e^{-j\frac{2\pi}{K}k\Delta\hat{\tau}_k[m]}. \quad (6.16)$$

In order to have smoother variations over time and to take into account the power of the signals for time-delay synthesis, improved ICTDs are computed using the above spectrum. More precisely, we treat the signal (6.16) as the true spectrum and compute an exponentially weighted time average of the cross power spectral density between  $Z_{1,k}[m]$  and  $Z_{2,k}[m]$  as

$$Q_k[m] = \lambda Q_k[m-1] + (1-\lambda) Z_{1,k}[m] \hat{Z}_{2,k}^*[m]. \quad (6.17)$$

The improved ICTDs are obtained by substituting the estimate  $Q_k[m]$  in (6.3). Since ICTDs are most important at low frequencies [16, Sec. 2.4], we only synthesize them up to a frequency chosen small enough such that the phase wrapping problem can be neglected. Finally, the interpolated values of the improved ICTDs are used to reconstruct the spectrum  $\hat{Z}_{2,k}[m]$  using (6.16).

To test the proposed scheme, we performed the following simulation. We synthesized a binaural signal using binaural room impulse responses. We then used one signal to recover the other one using the estimated binaural cues, and assessed the reconstruction quality of the binaural output through informal listening experiments. The parameters are chosen as follows. The sampling rate is  $f_s = 32$  kHz and the frame size is  $K = 1024$  samples. The analysis window is a (zero-padded) Hann window of length 896 samples. There is no synthesis window. The frame shift  $S$  is chosen to obtain a 50% window overlap, ensuring the perfect reconstruction property. The partition bandwidth is set to  $B = 2$  ERB which corresponds to  $L = 21$  critical bands spanning frequencies up to 16 kHz. The HRTF lookup table is built from the CIPIC database [2]. It maps ICLDs to ICTDs for 72 uniformly spaced azimuths on the horizontal plane (elevation zero). ICTD synthesis is applied up to 1 kHz. Finally, the exponential forgetting factor  $\lambda$  in (6.17) is specified through the time-averaging constant

$$T_\lambda = \frac{1}{1-\lambda} \frac{S}{f_s}.$$

We set  $T_\lambda = 15$  ms. Regarding the distributed coding scheme, the ICLDs are assumed to take values in intervals of linearly increasing lengths as a function of the critical band index  $l$ , from  $[-5, 5]$  dB when  $l = 1$  to  $[-35, 35]$  dB when  $l = 21$ . The quantizer stepsize  $s$  is chosen such as to meet a desired bitrate of  $R = 8$  kb/s.

We performed various simulations with one and two sources. To synthesize the binaural signals, HRTFs from the CIPIC database [2] were used along with binaural room impulse responses with reverberation time  $T_{60} \approx 120$  ms and

$T_{60} \approx 600$  ms. In the case of no reverberation, informal listening indicates that the proposed algorithm renders the binaural signals with a similar spatial image and only few artifacts. However, the spatial width of the synthesized auditory scene tends to be slightly narrower than the original one, in particular when multiple sources are present. This can be explained by the fact that when two oppositely located sources are concurrently active in a time-frequency atom, the corresponding ICLDs (hence ICTDs) tend to average each other out. While the HRTF lookup table strategy seems satisfactory for simple acoustic scenes, it is not sufficient when multiple sources are present in a reverberant environment. In this case, the synthesized binaural signals are perceptually quite different from the original ones, requiring the transmission of additional phase information.

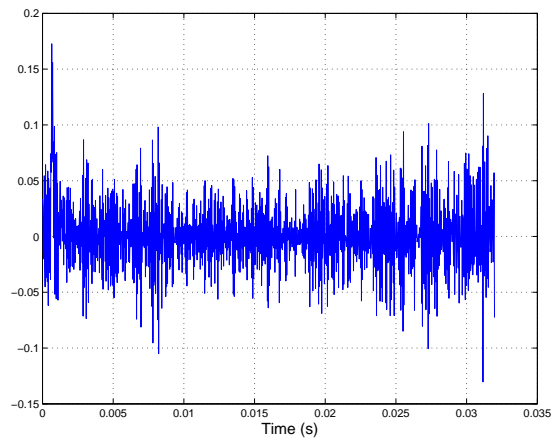
### 6.4.2 Model Based on Sparsity Principles

Let us now turn our attention to the second model. The goal is to compute the binaural filter, as explained in Section 6.3, and to recover the signal  $\mathbf{Z}_2[m]$  from the side information  $\mathbf{Z}_1[m]$  using (6.8). Again, the quality of the binaural reconstruction is assessed through informal listening.

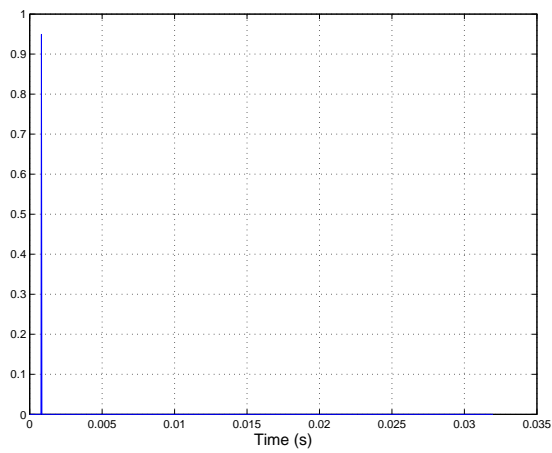
We performed the same simulations as with the model using binaural cues. In order to reduce artifacts due to block processing, the matrix (6.14) was averaged over time using an exponentially weighted time average. The validity of this operation is based on the assumption that the binaural filter does not change too rapidly over time. The averaging constant is set to  $T_\lambda = 50$  ms. The following conclusions can be drawn. In the case of a single source synthesized using HRTFs, the perceptual quality of the reconstruction is acceptable. We used an oversampling factor of  $P/L = 20$  ( $L = 1$  and  $P = 20$ ). This suggests that Cadzow's denoising method is able to properly handle the model mismatch introduced by the filter bank and the fact that the binaural filter has more than  $L = 1$  non-zero coefficient. However, this requires the use of a quite large oversampling ratio. If  $P$  is chosen too small, the spatial auditory scene is distorted. An example of binaural filter impulse response along with its sparse approximation is shown in Figure 6.6. When reverberation is present or when multiple sources are concurrently active, the reconstruction quality degrades quite significantly. This can be expected from the fact that, in this case, the recorded signals deviate strongly from the assumed model. A possible solution is to apply the proposed scheme on a sub-band basis. It was checked that this approach leads to an improved reconstruction of the original auditory image. However, the conjugate symmetry property can no longer be used to obtain twice as many consecutive frequency coefficients. Moreover, the oversampling ratio must be reduced to keep a constant total number of coefficients. This typically leads to audible artifacts in the reconstruction.

## 6.5 Summary

One of the main purposes of establishing a wireless link between two hearing aids is to gain knowledge about important binaural characteristics. In this chapter, these characteristics have been termed binaural innovation. Two parametric models of binaural innovation have been proposed along with methods



(a)



(b)

**Figure 6.6:** Sparse approximation of the binaural filter impulse response. (a) Original version. (b) Sparse approximation using Cadzow's denoising algorithm. The parameters are  $L = 1$  and  $P = 20$ . We observe that the non-zero coefficient is located at the position of the filter tap with largest magnitude.

---

to estimate the unknown parameters in a distributed fashion.

The first model is based on binaural cues, namely, ICLDs and ICTDs. We presented a scheme to estimate these cues using a distributed source coding method. We showed how the proposed algorithm takes into account the specificities of the recording setup in order to reduce the transmission bitrate. Moreover, we proved its optimality by comparing it to the scenario where the input signals can be observed jointly.

The second model is based on the assumption that the binaural signals are related to each other through filtering with a filter having a sparse impulse response. We demonstrated that this sparsity can be used in order to reduce the amount of transmitted information. The reconstruction process involves annihilating filters. We showed how our approach can be made robust to model mismatch using variations on a denoising algorithm by Cadzow.

Finally, we applied the proposed schemes to the distributed coding of spatial audio content. For simple acoustic scenes, we obtained reasonable reconstruction accuracy despite the apparent crudeness of our approximations. However, in scenarios involving multiple sources with reverberation, further research efforts are needed to obtain satisfactory results.



# Chapter 7

## Conclusions

Binaural hearing aids have the potential to significantly improve speech intelligibility in noise and to offer novel solutions to some existing problems. Since the wiring of the two devices is not envisioned for esthetic reasons, inter-aural connectivity must rely on a wireless communication link. The challenges associated with the use of wireless technology are tremendous, most notably due to restricted communication bitrates, processing delays and power consumption limitations. This thesis addressed some of the issues related to binaural processing, from both a theoretical and a practical point of view.

### 7.1 Thesis Summary

After a review of prior art on distributed source coding, the problem of interest was formally stated. We pointed out that binaural noise reduction can be viewed as a distributed estimation problem under communication constraints, and some important assumptions made throughout the dissertation were discussed.

We first looked at a general sensor network scenario for which we derived mean square locally optimal strategies for distributed estimation at a fusion center. Both a linear approximation and a compression framework were considered. We proposed iterative algorithms which improve upon the marginal scenario where each sensor describes its observations independently. The potential of the proposed distributed scheme was illustrated with a simple, yet insightful, correlation model.

Our analysis was then specialized to the setup of binaural hearing aids. We defined the gain-rate function which corresponds to the maximum possible beamforming gain enabled by the wireless link when it operates at a given bitrate. Monaural and binaural gain-rate trade-offs were derived for two coding strategies. The first one assumes that the joint statistics of the recorded signals can be used for the design of encoders and associated decoders. The second one takes the view that such statistics are difficult to compute in a practical setting and do not rely on their availability. For both strategies, optimal policies for rate allocation between the hearing aids were obtained. We also explored numerically various trade-offs inherent to the considered binaural system.

Two practical aspects of binaural noise reduction were then investigated.

The first one considered the practical implementation of the multichannel filters involved in the coding strategies described above. Motivated by computational efficiency, we looked at filtering in the frequency domain using a weighted overlap-add filter bank. We derived three suboptimal methods which take into consideration the influence of the filter bank at different levels. Recursive algorithms for the computation of the filter coefficients were presented and their respective complexity was discussed. We showed through numerical simulations that, in rather synthetic scenarios, large gains can be obtained using the proposed methods. In more realistic acoustic environments, however, taking into account the effect of the filter bank provides only little gains at the expense of a significant increase in complexity. Binaural filtering strategies were then studied. In particular, an alternating optimization method was described and practical considerations related to the wireless link were examined.

The second practical aspect that we considered concerns the use of the wireless link to compute important binaural characteristics. We proposed two ways of modeling these characteristics. The first one involves binaural cues computed on a time-frequency atom basis. A coding scheme to estimate these cues in a distributed fashion was presented. Arguably, the most interesting aspect of the proposed method is that it takes into account the particularities of the recording setup to reduce the transmission bitrate. The second model is based on the assumption that binaural characteristics can be well captured by a filter that is sparse in the time domain. A scheme was proposed to estimate this filter in a distributed fashion. In particular, it was shown how the sparsity assumption allows decreasing the amount of information transmitted from one hearing aid to the contralateral device. Model mismatch was also addressed by means of a composite property mapping algorithm. Finally, application of the two above methods to the distributed coding of spatial audio was presented. Informal listening experiments made under various acoustic environments suggest that the proposed schemes work well for simple cases, but that further research efforts are needed to improve reconstruction quality in more realistic scenarios.

## 7.2 Future Research

The availability of a wireless communication link offers novel perspectives for the design and operation of hearing aid algorithms. This thesis discussed some aspects of binaural processing by solely adopting a source coding perspective, that is, we assumed that the information bits can be reliably transmitted from one hearing aid to the other. Therefore, channel coding, which addresses the problem of reliable communication, also deserves attention [18]. The design of channel codes that work under the stringent constraints imposed by binaural hearing aids would be an interesting topic of investigation. Note that, for the remote Wyner-Ziv scenario considered in this work, a separation theorem can be proved [49, Sec. 1.6.3]. Source and channel codes can thus be designed separately without loss of optimality.

While most of our exposition focused on the problem of noise reduction, tasks such as dynamic compression, acoustic feedback cancelation or scene analysis may also benefit from binaural information. For example, one may determine if feedback occurs at one hearing aid by comparing the character-



---

istics of the signals with those recorded at the contralateral device. In other words, it would be worth studying the binaural feedback problem, where the two feedback paths are estimated jointly rather than separately. Of course, this requires the use of the wireless link and thus entail efficient transmission protocols. Another example is voice activity detection, which is a key component of any Wiener-based multichannel filtering strategy. Detecting the presence of speech in background noise is a challenging task, especially at low SNRs where noise reduction is most useful. In this context, the wireless link may be used to synchronize the voice activity detectors of two hearing aids. For example, a very simple approach would declare speech to occur if detected by at least one hearing aid. This strategy takes advantage of the fact that the two ears may experience different SNRs due to the head shadow effect.

We presented some preliminary results on the distributed coding of spatial audio based either on the computation of binaural cues or on the use of annihilating filters. Further research work are needed to improve the reconstruction accuracy of the proposed schemes. For example, we could design distributed schemes to estimate the true ICTDs, instead of merely relying on a lookup table. For the scheme based on sparsity principles, the computational complexity of Cadzow's procedure could be reduced using low rank approximation methods (see, e.g., [141, Sec. 8.1]). Another problem of interest is the design of a distributed approximation to Cadzow's algorithm. This would allow denoising the data prior to transmission, such that the oversampling factor needed to overcome model mismatch does not impose any rate penalty.



## Appendix A

# Weighted Mean Squared Linear Estimation

We consider the problem of optimal linear estimation under a weighted MSE criterion. In Appendix A.1, the optimal transform matrix is derived in its general form. We then derive the optimal solution subject to an additional diagonal constraint in Appendix A.2.

### A.1 General Transform Matrix

Let  $\mathbf{x} \in \mathbb{C}^M$  and  $\mathbf{y} \in \mathbb{C}^N$  be jointly Gaussian random vectors with mean zero and (cross) covariance matrices

$$\mathbf{R}_x = \mathcal{E} \{ \mathbf{x} \mathbf{x}^H \}, \quad \mathbf{R}_y = \mathcal{E} \{ \mathbf{y} \mathbf{y}^H \} \quad \text{and} \quad \mathbf{R}_{xy} = \mathcal{E} \{ \mathbf{x} \mathbf{y}^H \} .$$

We seek to find the optimal transform matrix  $\mathbf{W} \in \mathbb{C}^{M \times N}$  solution to the weighted MSE minimization problem

$$\min_{\mathbf{W}} \mathcal{E} \left\{ \|\mathbf{A} \mathbf{x} - \mathbf{A} \mathbf{W} \mathbf{y}\|^2 \right\}, \quad (\text{A.1})$$

where  $\mathbf{A} \in \mathbb{C}^{K \times M}$  is a constant weight matrix. Denoting by the superscript  $\dagger$  the pseudoinverse operation, the solution can be stated as follows.

**Theorem A.1.** The optimal transform matrix  $\mathbf{W}$  solution to the optimization problem (A.1) is given by

$$\mathbf{W} = (\mathbf{A}^H \mathbf{A})^\dagger (\mathbf{A}^H \mathbf{A}) \mathbf{R}_{xy} \mathbf{R}_y^\dagger .$$

**Proof:** We can write

$$\begin{aligned} f(\mathbf{W}) &= \mathcal{E} \left\{ \|\mathbf{A} \mathbf{x} - \mathbf{A} \mathbf{W} \mathbf{y}\|^2 \right\} \\ &\stackrel{(a)}{=} \text{tr} \mathcal{E} \left\{ (\mathbf{A} \mathbf{x} - \mathbf{A} \mathbf{W} \mathbf{y}) (\mathbf{A} \mathbf{x} - \mathbf{A} \mathbf{W} \mathbf{y})^H \right\} \\ &\stackrel{(b)}{=} \text{tr} (\mathbf{A} \mathbf{R}_x \mathbf{A}^H) + \text{tr} (\mathbf{A} \mathbf{W} \mathbf{R}_y \mathbf{W}^H \mathbf{A}^H) - 2 \text{Re} \left\{ \text{tr} (\mathbf{A} \mathbf{R}_{xy} \mathbf{W}^H \mathbf{A}^H) \right\}, \end{aligned}$$

where (a) follows from the definition of the Frobenius norm and the fact that expectation and trace commute and (b) from the linearity of expectation. Let us now decompose each variable in its real and imaginary parts as

$$\begin{aligned} \mathbf{R}_x &= \mathbf{R}_{x,r} + j\mathbf{R}_{x,i}, & \mathbf{R}_y &= \mathbf{R}_{y,r} + j\mathbf{R}_{y,i}, & \mathbf{R}_{xy} &= \mathbf{R}_{xy,r} + j\mathbf{R}_{xy,i}, \\ \mathbf{W} &= \mathbf{W}_r + j\mathbf{W}_i & \text{and} & & \mathbf{A} &= \mathbf{A}_r + j\mathbf{A}_i, \end{aligned}$$

such that  $f(\mathbf{W})$  can be written as

$$\begin{aligned} f(\mathbf{W}) &= \text{tr} \left( (\mathbf{A}_r + j\mathbf{A}_i) \left( \mathbf{R}_{x,r} + j\mathbf{R}_{x,i} (\mathbf{A}_r + j\mathbf{A}_i)^H \right) \right) \\ &\quad + \text{tr} \left( (\mathbf{A}_r + j\mathbf{A}_i) (\mathbf{W}_r + j\mathbf{W}_i) (\mathbf{R}_{y,r} + j\mathbf{R}_{y,i}) (\mathbf{W}_r + j\mathbf{W}_i)^H (\mathbf{A}_r + j\mathbf{A}_i)^H \right) \\ &\quad - 2\text{Re} \left\{ \text{tr} \left( (\mathbf{A}_r + j\mathbf{A}_i) (\mathbf{R}_{xy,r} + j\mathbf{R}_{xy,i}) (\mathbf{W}_r + j\mathbf{W}_i)^H (\mathbf{A}_r + j\mathbf{A}_i)^H \right) \right\} \\ &= g(\mathbf{W}_r, \mathbf{W}_i). \end{aligned}$$

Since  $\mathbf{R}_y$  is Hermitian, it holds that its real part is symmetric and its imaginary part is skew-symmetric, that is

$$\mathbf{R}_{y,r}^T = \mathbf{R}_{y,r} \quad \text{and} \quad \mathbf{R}_{y,i}^T = -\mathbf{R}_{y,i}.$$

Using this fact, a straightforward computation reveals that

$$\frac{\partial f(\mathbf{W})}{\partial \mathbf{W}} \stackrel{(a)}{=} \frac{1}{2} \left[ \frac{\partial g(\mathbf{W}_r)}{\partial \mathbf{W}_r} - j \frac{\partial g(\mathbf{W}_i)}{\partial \mathbf{W}_i} \right] \stackrel{(b)}{=} \mathbf{A}^H \mathbf{A} \mathbf{W} \mathbf{R}_y - \mathbf{A}^H \mathbf{A} \mathbf{R}_{xy},$$

where (a) is the generalized complex derivative defined in [20] and (b) follows from matrix trace derivative formulas (see, e.g., [66]). Since  $f(\mathbf{W})$  is convex, a solution to the optimization problem follows by setting the above partial derivative to zero, that is, by solving the system of equations

$$\mathbf{A}^H \mathbf{A} \mathbf{W} \mathbf{R}_y - \mathbf{A}^H \mathbf{A} \mathbf{R}_{xy} = \mathbf{O}_{M \times N}. \quad (\text{A.2})$$

If both matrices  $\mathbf{A}^H \mathbf{A}$  and  $\mathbf{R}_y$  are invertible, the solution is unique and directly follows as

$$\mathbf{W} = \mathbf{R}_{xy} \mathbf{R}_y^{-1}.$$

More generally, when  $\mathbf{A}^H \mathbf{A}$  and  $\mathbf{R}_y$  are of rank  $K_1 \leq M$  and  $K_2 \leq N$ , respectively, we consider their eigenvalue decomposition

$$\begin{aligned} \mathbf{A}^H \mathbf{A} &= \mathbf{U}_1 \mathbf{D}_1 \mathbf{U}_1^H \\ &= [\mathbf{U}_{1,1} \quad \mathbf{U}_{1,2}] \begin{bmatrix} \mathbf{D}_{1,1} & \mathbf{O}_{K_1 \times M - K_1} \\ \mathbf{O}_{M - K_1 \times K_1} & \mathbf{O}_{M - K_1 \times M - K_1} \end{bmatrix} \begin{bmatrix} \mathbf{U}_{1,1}^H \\ \mathbf{U}_{1,2}^H \end{bmatrix} \end{aligned} \quad (\text{A.3})$$

and

$$\begin{aligned} \mathbf{R}_y &= \mathbf{U}_2 \mathbf{D}_2 \mathbf{U}_2^H \\ &= [\mathbf{U}_{2,1} \quad \mathbf{U}_{2,2}] \begin{bmatrix} \mathbf{D}_{2,1} & \mathbf{O}_{K_2 \times N - K_2} \\ \mathbf{O}_{N - K_2 \times K_2} & \mathbf{O}_{N - K_2 \times N - K_2} \end{bmatrix} \begin{bmatrix} \mathbf{U}_{2,1}^H \\ \mathbf{U}_{2,2}^H \end{bmatrix}, \end{aligned} \quad (\text{A.4})$$

where  $\mathbf{D}_{1,1} \in \mathbb{R}^{K_1 \times K_1}$  and  $\mathbf{D}_{2,1} \in \mathbb{R}^{K_2 \times K_2}$  denote the diagonal matrices that contain the (real) non-zero eigenvalues of  $\mathbf{A}^H \mathbf{A}$  and  $\mathbf{R}_y$ , respectively. The unitary matrices  $\mathbf{U}_1$  and  $\mathbf{U}_2$  are partitioned accordingly. Using the decompositions (A.3) and (A.4), the optimality condition (A.2) can be expressed in block-form as

$$\begin{aligned} & \begin{bmatrix} \mathbf{D}_{1,1} \mathbf{U}_{1,1}^H \mathbf{W} \mathbf{U}_{2,1} \mathbf{D}_{2,1} & \mathbf{O}_{K_1 \times N - K_2} \\ \mathbf{O}_{M - K_1 \times K_2} & \mathbf{O}_{M - K_1 \times N - K_2} \end{bmatrix} \\ &= \begin{bmatrix} \mathbf{D}_{1,1} \mathbf{U}_{1,1}^H \mathbf{R}_{xy} \mathbf{U}_{2,1} & \mathbf{D}_{1,1} \mathbf{U}_{1,1}^H \mathbf{R}_{xy} \mathbf{U}_{2,2} \\ \mathbf{O}_{M - K_1 \times K_2} & \mathbf{O}_{M - K_1 \times N - K_2} \end{bmatrix}. \end{aligned} \quad (\text{A.5})$$

Moreover, we note that  $\mathbf{R}_{xy} \mathbf{U}_{2,2}$  is equal to the all-zero matrix. In fact, the elements of the vector  $\mathbf{z} = \mathbf{U}_{2,2}^H \mathbf{y}$  have variance zero. Using Cauchy-Schwarz's inequality [22, Th. C.1.1], it thus holds that

$$0 \leq |\mathcal{E} \{x_m z_n^*\}| \leq \sqrt{\mathcal{E} \{|x_m|^2\} \mathcal{E} \{|z_n|^2\}} = 0,$$

for  $m = 1, 2, \dots, M$  and  $n = 1, 2, \dots, N - K_2$ , such that

$$\mathbf{R}_{xy} \mathbf{U}_{2,2} = \mathcal{E} \{\mathbf{z} \mathbf{z}^H\} = \mathbf{O}_{M \times N - K_2}.$$

The equality (A.5) hence reduces to

$$\mathbf{D}_{1,1} \mathbf{U}_{1,1}^H \mathbf{W} \mathbf{U}_{2,1} \mathbf{D}_{2,1} = \mathbf{D}_{1,1} \mathbf{U}_{1,1}^H \mathbf{R}_{xy} \mathbf{U}_{2,1}. \quad (\text{A.6})$$

The above system has  $K_1 K_2$  equations and  $MN$  unknowns. Since  $K_1 \leq M$  and  $K_2 \leq N$ , it generally has an infinite number of solutions that we can write, without loss of generality, as

$$\mathbf{W} = \mathbf{W}_0 + \mathbf{\Delta}, \quad (\text{A.7})$$

where

$$\mathbf{W}_0 = \mathbf{U}_{1,1} \mathbf{U}_{1,1}^H \mathbf{R}_{xy} \mathbf{U}_{2,1} \mathbf{D}_{2,1}^{-1} \mathbf{U}_{2,1}^H = (\mathbf{A}^H \mathbf{A})^\dagger (\mathbf{A}^H \mathbf{A}) \mathbf{R}_{xy} \mathbf{R}_y^\dagger$$

and  $\mathbf{\Delta} \in \mathbb{C}^{M \times N}$ . Substituting (A.7) into (A.6) reveals that the matrix  $\mathbf{\Delta}$  must satisfy<sup>1</sup>

$$\mathbf{U}_{1,1}^H \mathbf{\Delta} \mathbf{U}_{2,1} = \mathbf{O}_{M \times N}.$$

In this case, it is easily checked that

$$\|\mathbf{W}\|^2 = \|\mathbf{W}_0\|^2 + \|\mathbf{\Delta}\|^2,$$

such that the solution with minimum Frobenius norm is obtained by letting the matrix  $\mathbf{\Delta}$  be the all-zero matrix. This concludes the proof.  $\blacksquare$

Interestingly, when the matrix  $\mathbf{A}^H \mathbf{A}$  is invertible, the optimal solution reduces to  $\mathbf{W} = \mathbf{R}_{xy} \mathbf{R}_y^\dagger$  which does not depend on the chosen weight matrix.

<sup>1</sup>This is the case, for example, if the columns of  $\mathbf{\Delta}$  are in the null space of  $\mathbf{A}^H \mathbf{A}$  or if the columns of  $\mathbf{\Delta}^H$  are in the null space of  $\mathbf{R}_y$ .

## A.2 Diagonal Transform Matrix

Let us consider the minimization in (A.1) with  $M$  equal to  $N$  and the additional requirement that the optimal transform matrix  $\mathbf{W} \in \mathbb{C}^{N \times N}$  be diagonal. We thus look for the solution to the optimization problem

$$\begin{aligned} \min_{\mathbf{W}} \quad & \mathcal{E} \left\{ \|\mathbf{Ax} - \mathbf{AWy}\|^2 \right\}, \\ \text{s.t.} \quad & (\mathbf{W})_{i,j} = 0 \quad \text{for } i \neq j. \end{aligned} \quad (\text{A.8})$$

It is given by the following theorem.

**Theorem A.2.** The optimal transform matrix  $\mathbf{W}$  solution to the optimization problem (A.8) is given by  $\mathbf{W} = \text{diag}(\mathbf{w})$  where

$$\mathbf{w} = \mathcal{E} \left\{ \mathbf{D}_y^H \mathbf{A}^H \mathbf{A} \mathbf{D}_y \right\}^\dagger \mathcal{E} \left\{ \mathbf{D}_y^H \mathbf{A}^H \mathbf{Ax} \right\}. \quad (\text{A.9})$$

**Proof:** It suffices to note that the minimization (A.8) is equivalent to that of finding the vector  $\mathbf{w} \in \mathbb{C}^N$  solution to

$$\min_{\mathbf{w}} \mathcal{E} \left\{ \|\mathbf{Ax} - \mathbf{AD}_y \mathbf{w}\|^2 \right\}.$$

This optimization follows along the same line as that of Theorem A.1 and is easily shown to yield the claimed result.  $\blacksquare$

We observe that here, in contrast to Theorem A.1, the optimal solution always depends on the weight matrix  $\mathbf{A}$ , even when  $\mathbf{A}^H \mathbf{A}$  is non-singular.

# Bibliography

- [1] “ANSI S3.5-1997 American national standard methods for calculation of the speech intelligibility index,” Acoustical Society of America, June 1997.
- [2] V. R. Algazi, R. O. Duda, D. M. Thompson, and C. Avendano, “The cipic hrtf database,” in Proc. *IEEE Workshop on Applications of Signal Processing to Audio and Acoustics*, Oct. 2001, pp. 99–102.
- [3] S. Arimoto, “An algorithm for calculating the capacity and rate-distortion functions,” *IEEE Transactions on Information Theory*, vol. 18, no. 4, pp. 14–20, July 1972.
- [4] Y.-H. Au-Yeung, “A theorem on a mapping from a sphere to the circle and the simultaneous diagonalization of two Hermitian matrices,” *The American Mathematical Society*, vol. 20, no. 2, pp. 545–548, Feb. 1969.
- [5] F. Bacon, *Sylva Sylvarum: Or A Naturall Historie. In Ten Centuries*. London: William Lee, 1627.
- [6] J. Bardeen and W. H. Brattain, “Three-electrode circuit element utilizing semiconductive materials,” U.S. Patent 2,524,035, Oct., 1950.
- [7] F. Baumgarte and C. Faller, “Binaural cue coding – Part I: Psychoacoustic fundamentals and design principles,” *IEEE Transactions on Signal and Audio Processing*, vol. 11, no. 6, pp. 509–519, Nov. 2003.
- [8] F. Baumgarte and C. Faller, “Binaural cue coding – Part II: Schemes and applications,” *IEEE Transactions on Signal and Audio Processing*, vol. 11, no. 6, pp. 520–531, Nov. 2003.
- [9] A. G. Bell, “Improvement in telegraphy,” U.S. Patent 174,465, Mar., 1876.
- [10] E. Bennion, *Antique Hearing Aids*. London: Venier Press, 1994.
- [11] R. A. Bentler and M. Duve, “Comparison of hearing aids over the 20th century,” *Ear and Hearing*, vol. 21, no. 6, pp. 625–639, Dec. 2000.
- [12] T. Berger, *Rate Distortion Theory: A Mathematical Basis for Data Compression*. Englewood Cliffs, NJ: Prentice-Hall, 1971.
- [13] T. Berger, “Multiterminal source coding,” July 1977, Lecture Notes Presented at CISM Summer School on the Information Theory Approach to Communications.

- 
- [14] T. Berger, Z. Zhang, and H. Viswanathan, "The CEO problem," *IEEE Transactions on Information Theory*, vol. 42, no. 3, pp. 887–902, May 1996.
- [15] R. Blahut, "Computation of channel capacity and rate-distortion functions," *IEEE Transactions on Information Theory*, vol. 18, no. 4, pp. 460–473, July 1972.
- [16] J. Blauert, *Spatial Hearing: The Psychophysics of Human Sound Localization*. Cambridge, MA: MIT Press, 1997.
- [17] A. Boothroyd, K. Fitz, J. Kindred, S. Kochkin, H. Levitt, B. Moore, and J. Yantz, "Hearing aids and wireless technology," *Hearing Review*, vol. 14, no. 6, pp. 44–48, June 2007.
- [18] M. Bossert, *Channel Coding for Telecommunications*. New-York, NY: Wiley, 1999.
- [19] S. Boyd and L. Vandenberghe, *Convex Optimization*. Cambridge, MA: Cambridge University Press, 2004.
- [20] D. H. Brandwood, "A complex gradient operator and its application in adaptive array theory," *IEE Proceedings*, vol. 130, Part F, no. 1, pp. 11–16, Feb. 1983.
- [21] A. S. Bregman, *Auditory Scene Analysis: The Perceptual Organization of Sound*. Cambridge, MA: MIT Press, 1990.
- [22] P. Brémaud, *Mathematical Principles of Signal Processing: Fourier and Wavelet Analysis*. New York, NY: Springer-Verlag, 2002.
- [23] M. Büchler, S. Allegro, S. Launer, and N. Dillier, "Sound classification in hearing aids inspired by auditory scene analysis," *EURASIP Journal on Applied Signal Processing*, vol. 2005, no. 18, pp. 2991–3002, Apr. 2005.
- [24] D. Byrne, H. Dillon, T. Ching, R. Katsch, and G. Keidser, "NAL-NL1 procedure for fitting nonlinear hearing aids: Characteristics and comparisons with other procedures," *Journal of the American Academy of Audiology*, vol. 12, no. 1, pp. 37–51, Jan. 2001.
- [25] J. A. Cadzow, "Signal enhancement – A composite property mapping algorithm," *IEEE Transactions on Acoustics, Speech and Signal Processing*, vol. 36, no. 1, pp. 49–62, Jan. 1988.
- [26] "The Hugh Hetherington Hearing Aid Museum," The Center for Hearing Loss Help. [Online]. Available: <http://www.hearingaidmuseum.com/>.
- [27] L. E. Cornelisse, R. C. Seewald, and D. G. Jamieson, "The input/output formula: A theoretical approach to the fitting of personal amplification devices," *The Journal of the Acoustical Society of America*, vol. 97, no. 3, pp. 1854–1864, Mar. 1995.
- [28] T. M. Cover, "A proof of the data compression theorem of Slepian and Wolf for ergodic sources," *IEEE Transactions on Information Theory*, vol. 21, no. 2, pp. 226–228, Mar. 1975.



- 
- [29] T. M. Cover and J. A. Thomas, *Elements of Information Theory*. New-York, NY: Wiley, 1991.
- [30] R. E. Crochiere and L. R. Rabiner, *Multirate Digital Signal Processing*, A. V. Oppenheim, ed. Englewood Cliffs, NJ: Prentice-Hall, 1983.
- [31] J. G. Desloge, W. M. Rabinowitz, and P. M. Zurek, "Microphone-array hearing aids with binaural output – Part I: Fixed-processing systems," *IEEE Transactions on Signal and Audio Processing*, vol. 5, no. 6, pp. 529–542, Nov. 1997.
- [32] R. L. Dobrushin and B. S. Tsybakov, "Information transmission with additional noise," *IEEE Transactions on Information Theory*, vol. 8, no. 5, pp. 293–304, Sept. 1962.
- [33] S. Doclo, T. J. Klasen, T. van den Bogaert, J. Wouters, and M. Moonen, "Theoretical analysis of binaural cue preservation using multi-channel Wiener filtering and interaural transfer functions," in Proc. *International Workshop on Acoustic Echo and Noise Control*, Sept. 2006.
- [34] S. Doclo and M. Moonen, "GSVD-based optimal filtering for single and multimicrophone speech enhancement," *IEEE Transaction on Signal Processing*, vol. 50, no. 9, pp. 2230–2244, Sept. 2002.
- [35] S. Doclo, D. Rong, T. J. Klasen, J. Wouters, S. Haykin, and M. Moonen, "Extension of the multi-channel Wiener filter with ITD cues for noise reduction in binaural hearing aids," *IEEE Workshop on Applications of Signal Processing to Audio and Acoustics*, pp. 70–73, Oct. 2005.
- [36] S. Doclo, A. Spriet, A. Wouters, and M. Moonen, "Frequency-domain criterion for the speech distortion weighted multichannel Wiener filter for robust noise reduction," *Speech Communication, Special Issue on Speech Enhancement*, vol. 49, no. 7-8, pp. 636–656, July-Aug. 2007.
- [37] S. Doclo, T. van den Bogaert, M. Moonen, and J. Wouters, "Reduced-bandwidth and distributed MWF-based noise reduction algorithms for binaural hearing aids," *to appear in IEEE Transactions on Audio, Speech and Language Processing*, 2008.
- [38] M. P. Downs and C. Yoshinaga-Itano, "The efficacy of early identification and intervention for children with hearing impairment," *Pediatric Clinics of North America*, vol. 46, no. 1, pp. 79–87, Feb. 1999.
- [39] S. C. Draper, "Successive structuring of source coding algorithms for data fusion, buffering and distribution in networks," Ph.D. dissertation, Massachusetts Institute of Technology, Cambridge, MA, June 2002.
- [40] S. C. Draper and G. W. Wornell, "Side information aware coding strategies for sensor networks," *IEEE Journal on Selected Areas in Communications*, vol. 22, no. 6, pp. 966–976, Aug. 2004.
- [41] T. A. Edison, "Carbon telephone," U.S. Patent 0,222,390, Dec., 1879.

- 
- [42] Y. Ephraim and H. Van Trees, "A signal subspace approach for speech enhancement," *IEEE Transactions on Signal and Audio Processing*, vol. 3, no. 4, pp. 251–266, July 1995.
- [43] K. Eswaran and M. Gastpar, "Foundations of distributed source coding," in *to appear in Distributed Source Coding: Theory, Algorithms and Applications*, P. L. Dragotti and M. Gastpar, eds. Elsevier, 2009.
- [44] D. Fabry, "In one ear and synchronized with the other: Automatic hearing instruments under scrutiny," *Hearing Review*, vol. 13, no. 12, pp. 36–38, Nov. 2006.
- [45] C. Faller, "Parametric coding of spatial audio," Ph.D. dissertation, Ecole Polytechnique Fédérale de Lausanne, Switzerland, July 2004.
- [46] T. Flynn and R. Gray, "Encoding of correlated observations," *IEEE Transactions on Information Theory*, vol. 33, no. 6, pp. 773–787, Nov. 1987.
- [47] D. J. Freed, "Adaptive feedback cancellation in hearing aids with clipping in the feedback path," *The Journal of the Acoustical Society of America*, vol. 123, no. 3, pp. 1618–1626, Mar. 2008.
- [48] G. Garcia-Frias, "Compression of correlated binary sources using turbo codes," *IEEE Communications Letters*, vol. 5, no. 10, pp. 417–419, Oct. 2001.
- [49] M. Gastpar, "To code or not to code," Ph.D. dissertation, Ecole Polytechnique Fédérale de Lausanne, Switzerland, Nov. 2002.
- [50] M. Gastpar, P. L. Dragotti, and M. Vetterli, "The distributed Karhunen-Loève transform," *IEEE Transactions on Information Theory*, no. 12, pp. 5177–5196, Dec. 2006.
- [51] N. Gehrig and P. L. Dragotti, "Symmetric and asymmetric Slepian-Wolf codes with systematic and non-systematic linear codes," *IEEE Communications Letters*, vol. 9, no. 1, pp. 61–63, Jan. 2005.
- [52] B. R. Glasberg and B. C. J. Moore, "Derivation of auditory filter shapes from notched-noise data," *Hearing Research*, vol. 47, no. 1-2, pp. 103–138, Aug. 1990.
- [53] S. W. Golomb, "Run-length encodings," *IEEE Transactions on Information Theory*, vol. 12, no. 3, pp. 399–401, July 1966.
- [54] V. Goyal, "Theoretical foundations of transform coding," *IEEE Signal Processing Magazine*, vol. 18, pp. 9–21, Sept. 2001.
- [55] V. K. Goyal, "Transform coding with integer-to-integer transforms," *IEEE Transactions on Information Theory*, vol. 46, no. 2, pp. 465–473, Mar. 2000.
- [56] I. S. Gradshteyn and I. M. Ryzhik, *Table of Integrals, Series and Products*, 5th ed. London: Academic Press, 1994.

- 
- [57] R. M. Gray, "Conditional rate-distortion theory," Stanford University, Stanford, CA, Tech. Rep. 6502-2, Oct. 1972.
- [58] R. M. Gray, "On the asymptotic eigenvalue distribution of Toeplitz matrices," *IEEE Transactions on Information Theory*, vol. 18, no. 6, pp. 725–730, Nov. 1972.
- [59] R. M. Gray, "Toeplitz and circulant matrices: A review," *Foundations and Trends in Communications and Information Theory*, vol. 2, no. 3, pp. 155–239, 2006.
- [60] J. E. Greenberg, P. M. Peterson, and P. M. Zurek, "Intelligibility-weighted measures of speech-to-interference ratio and speech system performance," *The Journal of the Acoustical Society of America*, vol. 94, no. 5, pp. 3009–3010, Nov. 1993.
- [61] U. Grenander and G. Szegö, *Toeplitz Forms and Their Applications*, 2nd ed. New-York, NY: Chelsea Publishing Company, 1984.
- [62] V. Hamacher, J. Chalupper, J. Eggers, E. Fischer, U. Kornagel, H. Puder, and U. Rass, "Signal processing in high-end hearing aids: State of the art, challenges and future trends," *EURASIP Journal on Applied Signal Processing*, vol. 18, pp. 2915–2929, 2005.
- [63] T. S. Han and S. Verdù, "Approximation theory of output statistics," *IEEE Transactions on Information Theory*, vol. 39, no. 3, pp. 752–772, May 1993.
- [64] E. C. Hansen, "Telephone apparatus for the deaf," U.S. Patent 1,343,717, June, 1920.
- [65] M. L. Hawley, R. Y. Litovsky, and J. F. Culling, "The benefit of binaural hearing in a cocktail party: Effect of location and type of interferer," *The Journal of the Acoustical Society of America*, vol. 115, no. 2, pp. 833–843, Feb. 2004.
- [66] A. Hjørungnes and D. Gesbert, "Complex-valued matrix differentiation: Techniques and key results," *IEEE Transaction on Signal Processing*, vol. 55, no. 6, pp. 2740–2746, June 2007.
- [67] A. E. Holmes, "Bilateral amplification for the elderly: Are two aids better than one?" *International Journal of Audiology*, vol. 42 (Suppl. 2), pp. 2S63–2S67, 2003.
- [68] A. Hormati, O. Roy, Y. M. Lu, and M. Vetterli, "Distributed compressed sensing based on sparse transforms," *to be submitted to IEEE Transaction on Signal Processing*, 2008.
- [69] R. A. Horn and C. R. Johnson, *Matrix Analysis*. Cambridge, MA: Cambridge University Press, 1985.
- [70] H. Hotelling, "Analysis of a complex of statistical variables into principal components," *Journal of Educational Psychology*, vol. 41, pp. 417–441, 498–520, 1933.

- 
- [71] K. B. Housewright, "Source coding studies for multiterminal systems," Ph.D. dissertation, University of California, Los Angeles, CA, 1978.
- [72] D. A. Huffman, "A method for the construction of minimum-redundancy codes," *Proceedings of the Institute of Radio Engineers*, vol. 40, no. 9, pp. 1098–1101, Sept. 1952.
- [73] A. Hyvärinen, J. Karhunen, and O. Erkki, *Independent Component Analysis*. New-York, NY: Wiley, 2001.
- [74] P. Ishwar, R. Puri, K. Ramchandran, and S. S. Pradhan, "On rate-constrained distributed estimation in unreliable sensor networks," *IEEE Journal on Selected Areas in Communications*, vol. 23, no. 4, pp. 765–775, Apr. 2005.
- [75] D. H. Johnson and D. E. Dudgeon, *Array Signal Processing: Concepts and Techniques*. Englewood Cliffs, NJ: Prentice Hall, 1993.
- [76] E. E. Johnson, "Despite having more advanced features, hearing aids hold line on retail price," *The Hearing Journal*, vol. 61, no. 4, pp. 42–48, Apr. 2008.
- [77] J. C. Junqua, B. Mak, and B. Reaves, "A robust algorithm for word boundary detection in the presence of noise," *IEEE Transactions on Signal and Audio Processing*, vol. 2, no. 3, pp. 406–412, Apr. 1994.
- [78] T. Kailath, A. Sayed, and B. Hassibi, *Linear Estimation*. Englewood Cliffs, NJ: Prentice-Hall, 2000.
- [79] K. Karhunen, "Über lineare Methoden in der Wahrscheinlichkeitsrechnung," *Annales Academiae Scientiarum Fennicae*, vol. 37, pp. 3–79, 1947.
- [80] J. M. Kates, "Constrained adaptation for feedback cancellation in hearing aids," *The Journal of the Acoustical Society of America*, vol. 106, no. 2, pp. 1010–1019, Aug. 1999.
- [81] J. M. Kates and K. H. Arehart, "Multichannel dynamic-range compression using digital frequency warping," *EURASIP Journal on Applied Signal Processing*, vol. 18, no. 1, pp. 3003–3014, Jan. 2005.
- [82] J. M. Kates and M. R. Weiss, "A comparison of hearing-aid array processing techniques," *The Journal of the Acoustical Society of America*, vol. 99, no. 5, pp. 3138–3148, May 1996.
- [83] J. S. Kilby, "Miniaturized electronic circuits," U.S. Patent 3,138,743, June, 1964.
- [84] S. Kirkpatrick, C. D. Gelatt, and M. P. Vecchi, "Optimization by simulated annealing," *Science*, vol. 220, no. 4598, pp. 671–680, May 1983.
- [85] T. Klasen, T. van den Bogaert, M. Moonen, and J. Wouters, "Binaural noise reduction algorithms for hearing aids that preserve interaural time delay cues," *IEEE Transaction on Signal Processing*, vol. 55, no. 4, pp. 1579–1585, Apr. 2007.

- 
- [86] S. Köjbler, U. Rosenhall, and H. Hansson, "Bilateral hearing aids – effects and consequences from a user perspective." *Scandinavian Audiology*, vol. 30, no. 4, pp. 223–235, 2001.
- [87] M. A. Lehr and B. Widrow, "Directional hearing system," U.S. Patent 5,793,875, Nov., 1998.
- [88] A. Lempel and J. Ziv, "Compression of individual sequences via variable-rate coding," *IEEE Transactions on Information Theory*, vol. 24, no. 5, pp. 530–536, Sept. 1978.
- [89] C. Liu, B. C. Wheeler, W. D. O'Brien Jr., C. R. Lansing, R. C. Bilger, D. L. Jones, and A. S. Feng, "A two-microphone dual delay-line approach for extraction of a speech sound in the presence of multiple interferers," *The Journal of the Acoustical Society of America*, vol. 110, no. 6, pp. 3218–3231, Dec. 2001.
- [90] A. Liveris, Z. Xiong, and C. N. Georghiades, "Compression of binary sources with side information at the decoder using LDPC codes," *IEEE Communications Letters*, vol. 6, no. 10, pp. 440–442, Oct. 2002.
- [91] H. Luts, J.-B. Maj, W. Soede, and J. Wouters, "Better speech perception in noise with an assistive multimicrophone array for hearing aids," *Ear and Hearing*, vol. 25, no. 5, pp. 411–420, Oct. 2004.
- [92] J. B. Maj, M. Moonen, and J. Wouters, "SVD-based optimal filtering technique for noise reduction in hearing aids using two microphones," *EURASIP Journal on Applied Signal Processing*, vol. 2002, no. 4, pp. 423–443, Apr. 2002.
- [93] S. Mallat, *A Wavelet Tour of Signal Processing*. London: Academic Press, 1998.
- [94] J. A. Maxwell and P. M. Zurek, "Reducing acoustic feedback in hearing aids," *IEEE Transactions on Signal and Audio Processing*, vol. 3, no. 4, pp. 304–313, July 1995.
- [95] S. McClellan and J. D. Gibson, "Variable-rate CELP based on subband flatness," *IEEE Transactions on Signal and Audio Processing*, vol. 5, no. 2, pp. 120–130, Mar. 1997.
- [96] B. C. Moore, B. R. Glasberg, and M. A. Stone, "Use of a loudness model for hearing aid fitting: III. A general method for deriving initial fittings for hearing aids with multi-channel compression," *British Journal of Audiology*, vol. 33, no. 4, pp. 241–258, Aug. 1999.
- [97] P. M. Morse and K. U. Ingard, *Theoretical Acoustics*. Princeton, NJ: Princeton University Press, 1968.
- [98] M. Nilsson, S. D. Soli, and A. Sullivan, "Development of the Hearing in Noise Test for the measurement of speech reception thresholds in quiet and in noise," *The Journal of the Acoustical Society of America*, vol. 95, no. 2, pp. 1085–1099, Feb. 1994.

- 
- [99] H. Nurdin, R. R. Mazumdar, and A. Bagchi, "On estimation and compression of distributed correlated signals with incomplete observations," in Proc. *Conference on Mathematical Theory of Networks and Systems*, July 2004.
- [100] Y. Oohama, "Gaussian multiterminal source coding," *IEEE Transactions on Information Theory*, vol. 43, no. 7, pp. 1912–1923, Nov. 1997.
- [101] Y. Oohama, "The rate-distortion function for the quadratic Gaussian CEO problem," *IEEE Transactions on Information Theory*, vol. 44, no. 3, pp. 1057–1070, May 1998.
- [102] A. V. Oppenheim and R. W. Schaffer, *Discrete-Time Signal Processing*. Englewood Cliffs, NJ: Prentice-Hall, 1989.
- [103] S. Passerini, B. B. Owens, and F. Coustier, "Lithium-ion batteries for hearing aid applications: I. Design and performance," *Journal of Power Sources*, vol. 89, no. 1, pp. 29–29, July 2000.
- [104] K. Pearson, "On lines and planes of closest fit to systems of points in space," *Philosophical Magazine*, vol. 2, no. 6, pp. 559–572, 1901.
- [105] C. Pirzanski, M. Chasin, M. Klenk, V. Maye, and J. Purdy, "Attenuation variables in earmolds for hearing protection devices," *The Hearing Journal*, vol. 53, no. 6, pp. 44–49, June 2000.
- [106] H. V. Poor, *An Introduction to Signal Detection and Estimation*, 2nd ed. New York, NY: Springer-Verlag, 2001.
- [107] S. S. Pradhan, "On the rate-distortion function of Gaussian sources with memory in the presence of side information at the decoder," University of Illinois, Urbana-Champaign, IL, Project Report, ECE 480, 1998.
- [108] S. S. Pradhan and K. Ramchandran, "Distributed source coding using syndromes (DISCUS): Design and construction," *IEEE Transactions on Information Theory*, vol. 49, no. 3, pp. 626–634, Mar. 2003.
- [109] D. Rebollo-Monedero, S. Rane, A. Aaron, and B. Girod, "High-rate quantization and transform coding with side information at the decoder," *EURASIP Journal on Signal Processing*, vol. 86, no. 11, pp. 3160–3179, 2006.
- [110] J. Rissanen, "Generalized Kraft inequality and arithmetic coding," *IBM Journal of Research and Development*, vol. 20, no. 3, pp. 198–203, May 1976.
- [111] O. Roy, T. Ajdler, R. L. Konsbruck, and M. Vetterli, "Distributed compression in microphone array," in *to appear in Distributed Source Coding: Theory, Algorithms and Applications*, P. L. Dragotti and M. Gastpar, eds. Elsevier, 2009.
- [112] O. Roy and M. Vetterli, "On the asymptotic distortion behavior of the distributed Karhunen-Loève transform," in Proc. *Allerton Conference on Communication, Control and Computing*, vol. 1, Sept. 2005, pp. 406–415.

- 
- [113] O. Roy and M. Vetterli, "Collaborating hearing aids," in Proc. *MSRI Workshop on Mathematics of Relaying and Cooperation in Communication Networks*, Apr. 2006.
- [114] O. Roy and M. Vetterli, "Rate-constrained beamforming for collaborating hearing aids," in Proc. *IEEE International Symposium on Information Theory*, July 2006, pp. 2809–2813.
- [115] O. Roy and M. Vetterli, "Rate-constrained collaborative noise reduction with wireless hearing aids," *submitted to IEEE Transaction on Signal Processing*, 2006.
- [116] O. Roy and M. Vetterli, "Distributed spatial audio coding in wireless hearing aids," in Proc. *IEEE Workshop on Applications of Signal Processing to Audio and Acoustics*, Oct. 2007, pp. 227–230.
- [117] O. Roy and M. Vetterli, "Dimensionality reduction for distributed estimation in the infinite dimensional regime," *IEEE Transactions on Information Theory*, vol. 54, no. 2, pp. 1655–1669, Apr. 2008. [Reproducible]. Available: <http://rr.epfl.ch/16>.
- [118] D. J. Sakrison, "Source encoding in the presence of random disturbance," *IEEE Transactions on Information Theory*, vol. 14, no. 1, pp. 165–167, Jan. 1968.
- [119] C. C. Sarli, E. Dubinsky, B. Halbrook, and P. Skroska, "Deafness in disguise: Concealed hearing devices of the 19th and 20th centuries," Bernard Becker Medical Library, June 2005. [Online]. Available: <http://beckerexhibits.wustl.edu/did/index.htm>.
- [120] C. C. Sarli, R. Uchanski, A. Heidbreder, K. Readmond, and B. Spehar, "19th-century camouflaged mechanical hearing devices," *Otology and Neurotology*, vol. 24, no. 4, pp. 691–698, July 2003.
- [121] I. D. Schizas, G. B. Giannakis, and N. Jindal, "Distortion-rate bounds for distributed estimation using wireless sensor networks," *EURASIP Journal on Advances in Signal Processing*, vol. 2008, 2008.
- [122] I. D. Schizas, G. B. Giannakis, and Z. Q. Luo, "Distributed estimation using reduced-dimensionality sensor observations," *IEEE Transaction on Signal Processing*, vol. 55, no. 8, pp. 4282–4299, Aug. 2007.
- [123] C. E. Shannon, "A mathematical theory of communication," *Bell System Technical Journal*, vol. 27, no. 3, pp. 379–423, 623–656, Oct. 1948.
- [124] A. N. Shiryaev, *Probability*, 2nd ed. New York, NY: Springer-Verlag, 1995.
- [125] W. Shockley, "Circuit element utilizing semiconductive material," U.S. Patent 35,423, Sept., 1951.
- [126] D. Slepian and J. K. Wolf, "Noiseless coding of correlated information sources," *IEEE Transactions on Information Theory*, vol. 19, pp. 471–480, July 1973.

- 
- [127] J. Sohn, N. S. Kim, and W. Sung, "A statistical model-based voice activity detection," *IEEE Signal Processing Letters*, vol. 6, no. 1, pp. 1–3, Jan. 1999.
- [128] P. E. Souza, L. M. Jenstad, and R. Folino, "Using multichannel wide-dynamic range compression in severely hearing-impaired listeners: Effects on speech recognition and quality," *Ear and Hearing*, vol. 26, no. 2, pp. 120–131, Apr. 2005.
- [129] A. Spriet, G. Rombouts, M. Moonen, and J. Wouters, "Adaptive feedback cancellation in hearing aids," *Journal of the Franklin Institute*, vol. 343, pp. 545–573, Sept. 2006.
- [130] V. Stankovic, A. D. Liveris, Z. Xiong, and C. N. Georgiades, "On code design for the Slepian–Wolf problem and lossless multiterminal networks," *IEEE Transactions on Information Theory*, vol. 52, no. 4, pp. 1495–1507, Apr. 2006.
- [131] P. Stoica and R. Moses, *Introduction to Spectral Analysis*. Englewood Cliffs, NJ: Prentice Hall, 2000.
- [132] M. A. Stone and B. C. J. Moore, "Tolerable hearing aids delays. I. Estimation of limits imposed by the auditory path alone using simulated hearing losses," *Ear and Hearing*, vol. 20, no. 3, pp. 182–192, June 1999.
- [133] M. A. Stone, B. C. J. Moore, K. Meisenbacher, and R. P. Derleth, "Tolerable hearing aids delays. V. Estimation of limits for open canal fittings," *Ear and Hearing*, vol. 29, no. 4, pp. 601–617, Aug. 2008.
- [134] S. G. Tanyer and H. Özer, "Voice activity detection in nonstationary noise," *IEEE Transactions on Signal and Audio Processing*, vol. 8, no. 4, pp. 478–482, July 2000.
- [135] S. Y. Tung, "Multiterminal source coding," Ph.D. dissertation, Cornell University, Ithaca, NY, May 1978.
- [136] T. van den Bogaert, S. Doclo, J. Wouters, and M. Moonen, "The effect of multi-microphone noise reduction systems on sound source localization by users of binaural hearing aids," *The Journal of the Acoustical Society of America*, vol. 124, no. 1, pp. 484–497, July 2008.
- [137] T. van den Bogaert, T. J. Klasen, M. Moonen, L. van Deun, and J. Wouter, "Horizontal localization with bilateral hearing aids: Without is better than with," *The Journal of the Acoustical Society of America*, vol. 119, no. 1, pp. 515–526, Jan. 2005.
- [138] H. L. Van Trees, *Optimum Array Processing. Part IV of Detection, Estimation and Modulation Theory*. New-York, NY: Wiley, 2002.
- [139] P. Vandewalle, L. Sbaiz, J. Vandewalle, and M. Vetterli, "Super-resolution from unregistered and totally aliased signals using subspace methods," *IEEE Transaction on Signal Processing*, vol. 55, no. 7, pp. 3687–3703, July 2007. [Reproducible]. Available: <http://rr.epfl.ch/4>.



- 
- [140] A. P. Varga, H. J. M. Steeneken, M. Tomlinson, and D. Jones, "The NOISEX-92 study on the effect of additive noise on automatic speech recognition," Speech Research Unit, Defense Research Agency, Malvern, England, Tech. Rep., 1992.
- [141] S. S. Vempala, *The Random Projection Method*, Series in Discrete Mathematics and Theoretical Computer Science. AMS Bookstore, 2004.
- [142] M. Vetterli, P. Marziliano, and T. Blu, "Sampling signals with finite rate of innovation," *IEEE Transaction on Signal Processing*, vol. 50, no. 6, pp. 1414–1428, June 2002.
- [143] A. Wagner, S. Tavildar, and P. Viswanath, "The rate region of the quadratic Gaussian two-terminal source-coding problem," *IEEE Transactions on Information Theory*, vol. 54, no. 5, pp. 1938–1961, May 2008.
- [144] T. A. Welch, "A technique for high-performance data compression," *Computer*, vol. 17, no. 6, pp. 8–19, June 1984.
- [145] D. P. Welker, J. E. Greenberg, J. G. Desloge, and P. M. Zurek, "Microphone-array hearing aids with binaural output - Part II: A two-microphone adaptive system," *IEEE Transactions on Signal and Audio Processing*, vol. 5, no. 6, pp. 543–551, Nov. 1997.
- [146] B. Widrow, "A microphone array for hearing aids," *IEEE Circuits and Systems Magazine*, vol. 1, no. 2, pp. 26–32, 2001.
- [147] B. Widrow and F.-L. Luo, "Microphone arrays for hearing aids: An overview," *Speech Communication, Special Issue on Speech Processing for Hearing Aids*, vol. 39, no. 1-2, pp. 139–146, Jan. 2003.
- [148] H. S. Witsenhausen, "Indirect rate-distortion problems," *IEEE Transactions on Information Theory*, vol. 26, no. 5, pp. 518–521, Sept. 1980.
- [149] J. K. Wolf and J. Ziv, "Transmission of noisy information to a noisy receiver with minimum distortion," *IEEE Transactions on Information Theory*, vol. 16, no. 4, pp. 406–411, July 1970.
- [150] "Deafness and hearing impairment," World Health Organization, Mar. 2006. [Online]. Available: <http://www.who.int/mediacentre/factsheets/fs300/en/index.html>.
- [151] A. D. Wyner and J. Ziv, "The rate-distortion function for source coding with side information at the decoder," *IEEE Transactions on Information Theory*, vol. 22, no. 1, pp. 1–10, Jan. 1976.
- [152] H. Yamamoto and K. Itoh, "Source coding theory for multiterminal communication systems with a remote source," *IECE Transactions*, vol. E63, no. 10, pp. 700–706, Oct. 1980.
- [153] R. Zamir, "The rate loss in the Wyner-Ziv problem," *IEEE Transactions on Information Theory*, vol. 42, no. 6, pp. 2073–2084, Nov. 1996.

- 
- [154] R. Zamir and T. Berger, "Multiterminal source coding with high resolution," *IEEE Transactions on Information Theory*, vol. 45, no. 1, pp. 106–117, Jan. 1999.
- [155] K. Zhang, "Best linear unbiased estimation fusion with constraints," Ph.D. dissertation, University of New Orleans, New Orleans, LA, Dec. 2003.

# Curriculum Vitae

**Olivier Roy**

Audiovisual Communications Laboratory (LCAV)  
School of Computer and Communication Sciences (I&C)  
Ecole Polytechnique Fédérale de Lausanne (EPFL)  
1015 Lausanne, Switzerland

Email: [olivier.roy@a3.epfl.ch](mailto:olivier.roy@a3.epfl.ch)  
Web: <http://lcavwww.epfl.ch/~oroy>

## Personal

Born in Geneva, Switzerland. Swiss citizen.

## Education

2004 - 2008 **Ph.D.** in Computer and Communication Sciences, LCAV, I&C, EPFL, Switzerland.

1998 - 2004 **M.Sc.** in Communication Systems, I&C, EPFL, Switzerland.

## Professional Experience

2007 **Research Intern**, Phonak, Stäfa, Switzerland.  
Developed binaural noise reduction algorithms for hearing aids.

2004 - 2008 **Teaching Assistant**, EPFL, Switzerland.  
Assisted students in undergraduate and graduate courses.  
Supervised semester and master projects.

2003 - 2004 **Undergrad Research Intern**, Institute for Telecommunications Research, University of South Australia, Australia.  
Completed a master thesis project in the field of multi-antenna communication systems.

2002 **Software Engineer Intern**, Logitech, Fremont CA, USA.  
Joined the Video Unit Group for a 6-month internship.  
Worked on instant messaging based video streaming solutions.

- 
- 2000 - 2004 **Elected Class Representative**, EPFL, Switzerland.  
Represented the student body and worked with the division's leadership.
- 1999 **Exhibition Attendant**, World Telecom '99, Geneva, Switzerland.  
Helped Telenor, a Norwegian telecommunications company, with the logistic of the show.

## Awards and Honors

1. Mike Miller Prize for best student paper at the Australian Communication Theory Workshop, Feb. 2004.

## Publications

### Thesis

1. O. Roy, "Distributed signal processing for binaural hearing aids," PhD thesis, Ecole Polytechnique Fédérale de Lausanne, Switzerland, Oct. 2008.
2. O. Roy, "Optimal estimator-detector receivers for space-time block coding," Master's thesis, Ecole Polytechnique Fédérale de Lausanne, Switzerland, Mar. 2004.

### Book Chapters

1. O. Roy, T. Ajdler, R. L. Konsbruck, and M. Vetterli, "Distributed compression in microphone array," *Distributed Source Coding: Theory and Applications*, P. L. Dragotti and M. Gastpar, eds. Elsevier, 2009.

### Journal Papers

1. A. Hormati, O. Roy, Y. M. Lu, and M. Vetterli, "Distributed sensing of correlated signals linked by sparse filtering," to be submitted to *IEEE Transactions on Signal Processing*.
2. O. Roy and M. Vetterli, "Rate-constrained collaborative noise reduction for wireless hearing aids," to appear in *IEEE Transactions on Signal Processing*, 2009.
3. O. Roy and M. Vetterli, "Dimensionality reduction for distributed estimation in the infinite dimensional regime," *IEEE Transactions on Information Theory*, vol. 54, no. 2, pp. 1655-1669, Apr. 2008. [Reproducible] Available: <http://rr.epfl.ch/16>.

### Conference Papers

1. O. Roy, A. Hormati, Y. M. Lu, and M. Vetterli, "Distributed sensing of signals linked by sparse filtering," submitted to *IEEE International Conference on Acoustic, Speech, and Signal Processing*, 2009.

- 
2. O. Roy and M. Vetterli, "Distributed spatial audio coding in wireless hearing aids," in Proc. *IEEE Workshop on Applications of Signal Processing to Audio and Acoustics*, Oct. 2007, pp. 227-230.
  3. O. Roy and M. Vetterli, "The effective rank: A measure of effective dimensionality," in Proc. *European Signal Processing Conference*, Sep. 2007, pp. 606-610.
  4. T. Ajdler, R. L. Konsbruck, O. Roy, L. Sbaiz, E. Telatar, and M. Vetterli, "Spatio-temporal sampling and distributed compression of the sound field," in Proc. *European Signal Processing Conference*, Sep. 2006.
  5. O. Roy and M. Vetterli, "Rate-constrained beamforming for collaborating hearing aids," in Proc. *International Symposium on Information Theory*, Jul. 2006, pp. 2809-2813.
  6. O. Roy and M. Vetterli, "Distributed compression in acoustic sensor networks using oversampled A/D conversion," in Proc. *IEEE International Conference on Acoustic, Speech, and Signal Processing*, May 2006, vol. 4, pp. 165-168.
  7. O. Roy and M. Vetterli, "Collaborating hearing aids," in Proc. *MSRI Workshop on Mathematics of Relaying and Cooperation in Communication Networks*, Apr. 2006.
  8. O. Roy and M. Vetterli, "On the asymptotic distortion behavior of the distributed Karhunen-Loève transform," in Proc. *Allerton Conference on Communication, Control, and Computing*, Sep. 2005, pp. 406-415.
  9. O. Roy, S. Perreau, and A. Grant, "Optimal estimator-detector receivers for space-time block coding," in Proc. *International Symposium on Information Theory*, June-July 2004, p. 502.
  10. O. Roy, S. Perreau, and A. Grant, "Optimal estimator-detector receivers for space-time block coding," in Proc. *Australian Communication Theory Workshop*, Feb. 2004.